# Development of a Novel 'One-pot' Ethylenediaminetetraacetic Acid (EDTA) Precursor Based Method for Preparation of Hard-Soft Ferrite Nanocomposites and Study of Their Properties

## THESIS

Submitted in partial fulfillment
of the requirements for the degree of
**DOCTOR OF PHILOSOPHY**
**by**
**SUBHENJIT HAZRA**

Under the Supervision of
**Dr. Narendra Nath Ghosh**



# BIRLA INSTITUTE OF TECHNOLOGY AND SCIENCE
# PILANI (RAJASTHAN) INDIA
# 2015

# BIRLA INSTITUTE OF TECHNOLOGY AND SCIENCE
## PILANI (RAJASTHAN)

# CERTIFICATE

This is to certify that the thesis entitled **"Development of a Novel 'One-pot' Ethylenediaminetetraacetic Acid (EDTA) Precursor Based Method for Preparation of Hard-Soft Ferrite Nanocomposites and Study of Their Properties"** and submitted by **Subhenjit Hazra,** ID No. 2010PHXF436G for award of Ph.D. Degree of the Institute, embodies original work done by him under my supervision.

Signature in full of the Supervisor:

Name in capital block letters: **Dr. NARENDRA NATH GHOSH**

Designation: Associate Professor

Date:

# Acknowledgements

# ABSTRACT

Recently, investigations on the "exchange spring systems" have gained profound interest for the development of superior permanent magnets. Theoretically, nanocomposite magnets, which are composed of soft and hard phases possessing high saturation magnetization of soft phase and high coercivity of hard phase, are potential candidates for making next generation permanent magnet and better radar absorbing material. The spring exchange coupling between the hard and soft magnetic phases depends on various factors, including distribution of magnetically soft and hard phases, average grain sizes of the individual phases, particle size and shape, etc. The interaction between the hard and soft magnetic phases significantly influences magnetization, coercivity, and microwave absorption properties of the nanocomposite powders. Microwave-absorbing materials have gained immense interest to the scientists and technologist due to their usage in military application and also commodity markets. These materials also have the potential to address the issues related to environmental pollution caused by the Electromagnetic Interference (EMI) due to extensive use of electronic devices, computer networks, mobile phones etc. The microwave absorbing materials which operate in the frequency range 8.2-12.4 GHz (X-band) regions is also known as radar absorbing material (RAM) and find wide range of applications including electronic devices, military equipment, etc. Researchers are showing their specific concern on development of efficient RAM from last few decades. Ferrites are important class of magnetic materials which exhibit microwave absorption property. However, a single material cannot fulfill the requirements (such as large absorption peak, wide working frequency range and thin absorption layer) of an ideal radar absorber. Nanocomposites consist of hard and soft ferrite phase, could offer to construct combined systems whose properties are complimentary or even mutually exclusive. However, reports on hard-soft ferrite nanocomposites in the literature are very limited. This is because of lack of availability of simple preparation techniques of this type of composites.

In this research work, (i) development of a simple but cost-effective EDTA precursor based 'one-pot' method for synthesis of hard-soft ferrite based nanocomposites (such as

$(BaFe_{12}O_{19})_{1-x}$-$(NiFe_2O_4)_x$, $(SrFe_{12}O_{19})_{1-x}$-$(NiFe_2O_4)_x$, $(BaFe_{12}O_{19})_{1-x}$-$(Ni_{0.65}Zn_{0.35}Fe_2O_4)_x$, $(SrFe_{12}O_{19})_{1-x}$-$(Ni_{0.65}Zn_{0.35}Fe_2O_4)_x$, $(BaFe_{12}O_{19})_{1-x}$-$(Mn_{0.2}Ni_{0.4}Zn_{0.4}Fe_2O_4)_x$, $(SrFe_{12}O_{19})_{1-x}$-$(Mn_{0.2}Ni_{0.4}Zn_{0.4}Fe_2O_4)_x$).has been described. In this synthesis method cheap metal nitrates were used as starting materials, water was used as solvent and there was no need of elaborate reaction set-up.

(ii) Preparation of same nanocomposites using Physical mixing method also been described. For physical mixing method, pure single phase hard ferrites (such as $BaFe_{12}O_{19}$, $SrFe_{12}O_{19}$) and soft ferrites ($NiFe_2O_4$, $Ni_xZn_{(1-x)}Fe_2O_4$, $Mn_{0.2}Ni_xZn_{(0.8-x)}Fe_2O_4$) was prepared separately and then hard-soft ferrite composites was prepared by mixing them in appropriate weight ratio. The synthesized composites using both methods were characterized using thermogravimetric analysis, differential scanning calorimetric analysis, X-ray diffraction, scanning electron microscopy, transmission electron microscopy. The magnetic and microwave absorption properties of these materials have been evaluated.

Nanocomposites prepared by one-pot method showed crystallographically two phase behavior, but magnetically a good single phase exchange spring-coupled behavior with high saturation magnetization as well as high coercivity. This exchange coupling interaction between hard and soft ferrite phase leads to enhance magnetic and microwave absorbing properties compare to pure hard as well as soft ferrite nanoparticles. So, simple and cost-effective preparation technique, superior microwave absorption and magnetic properties make the hard-soft ferrite nanocomposites attractive.

# TABLE OF CONTENTS

# List of Tables

# List of Figures

# List of Abbreviations and Symbols

| Abbreviation | Description |
|---|---|
| EDTA | Ethylenediaminetetraacetic acid |
| MRI | Magnetic resonance imaging |
| CVD | Chemical vapour deposition |
| MOCVD | Metal organic chemical vapor deposition |
| PLD | Pulsed laser deposition |
| CTAC | Cetyltrimethylammonium chloride |
| PVA | Polyvinyl alcohol |
| PEG | Polyethylene glycol |
| TEOS | Tetraethyl orthosilicate |
| APTES | (3-Aminopropyl)triethoxysilane |
| $L_{ex}$ | Exchange length |
| EMI | Electromagnetic Interference |
| RAM | Radar absorbing material |
| Nanocomposite-OP | Nanocomposites synthesized by one-pot method |
| Nanocomposite-PM | Nanocomposites synthesized by physical mixing method |
| DSC | Differential scanning calorimetry |
| TGA | Thermo-gravimetric analysis |
| XRD | X-Ray Diffraction |
| ICDD | International Centre for Diffraction Data |
| SEM | Scanning Electron Microscopy |
| TEM | Transmission Electron Microscope |
| VSM | Vibrating Sample Magnetometer |
| $M_s$ | Saturation magnetization |
| $H_c$ | Coercivity |
| RL | Reflection loss |
| dB | Decibel |

| | |
|---|---|
| $f$ | Frequency of the electromagnetic wave |
| $d$ | Dbsorber thickness |
| c | Velocity of light |
| $Z_0$ | Free space impedance |
| $Z_{in}$ | Absorber impedance |
| $\mu_r$ | Relative complex permeability |
| $\varepsilon_r$ | Relative complex permittivity |
| $\varepsilon'$ | Real part of permittivity |
| $\mu'$ | Real part of permeability |
| $\varepsilon''$ | Imaginary part of permittivity |
| $\mu''$ | Imaginary part of permeability |

_____

<div align="right">

# Chapter 1

</div>

# Introduction

## 1.1 Scope of research work

The focus of this research work is the development of simple and cost-effective Ethylenediaminetetraacetic acid (EDTA) precursor based one-pot chemical methodology in order to synthesize hard-soft ferrite nanocomposites with wide range of composition. Investigations on crystal structure, particle size, magnetic properties and microwave absorption properties of the synthesized nanocomposites. The developed chemical methodology is an attempt in the direction of surmounting the limitations posed by the existing methods of synthesizing these nanopowders.

## 1.2 Introduction to Ferrite

Ferrites are important class of magnetic materials and have gained immense importance for the last few decades due to their wide range of application in communication, electronics, magnetic recording microwave absorption based devices. In the past decade, the nanostructured ferrites have attracted considerable attention because several properties of ferrites such as structural, surface reactivity, electrical, magnetic etc. are greatly influenced by nanostructured phase. The last ten years have witnessed an intensive growth in the activities related to the synthesis and property studies of superparamagnetic ferrite nanoparticles due to their potential use in biotechnology and biomedical applications. The biomedical applications require that the nanoparticles should have high magnetization values, average particle size smaller than 100 nm and a narrow particle size distribution. For this reason though the magnetic property of iron oxides was known to people from ancient times, till date researchers are actively involved in the development of new synthetic strategies for preparation of ferrite nanoparticles. The quest of synthesis of nanostructured ferrite materials, having tailored chemical compositions, high purity, better homogeneity, controlled morphology, microstructure and tunable magnetic and electrical properties led to the development of various preparative methods.[1-12]

_____

## 1.2.1 Historical Development of Ferrites

Magnetite or ferrous ferrites is naturally occurring ferrite and its magnetic nature was known since ancient times. In China more than two millennia ago magnetite was used in mariners compass. However, preparation of various types of ferrites and their industrial applications started in the beginning of 1900. Initially, as magnetic properties of ferrites were inferior to those of ferromagnetic alloys (e.g., Fe-Si alloy), they did not attract much industrial attention. After 1950s, ferrites find applications in radio, television, carrier telephony, computer and microwave devices. From this time scientist, engineers, and technologists of various fields became greatly interested to explore the unique magnetic properties of ferrites, enhancing the properties of existing ferrites and to expand their applications.[13]

Though, reports have been published on the historical development of ferrites that has occurred since about 1940,[14, 15]detailed descriptions on progress and background of ferrites before that period are rarely found. Sugimoto in his centennial feature article in the Journal of the American Ceramic Society described elaborately the past, present and future of ferrites.[13]The first systematic investigations on spinel ferrites were reported by Hilpert in 1909.[16-19] This group had patented the idea of ferrite core.[20, 21] Kato and Takei in 1932 prepared $Fe_3O_4.3CoFe_2O_4$ based magnets, which was commercialized as 'OP magnet'.[22-26] Their investigations on mixed ferrite (mixture of spinel and inverse spinel ferrites) gave the birth of the commercial ferrite core.[27] In 1948 Néel published his theory of anti ferromagnetism of ferrite materials.[28]

Researchers of Philips in Netherland have contributed significantly to the development of science and technology of ferrites. Snoek's[29] work on magnetic properties of Mn-Zn and Ni-Zn ferrites established that ferrites are very important electronic materials, which helped the development of ferrite core industry. In 1950s the invention of hexagonal ferrites (e.g., barium hexaferrite, strontium hexaferrite) by Went et al.[30] and Jonker et al.[31] is a very important event in history of ferrites. During 1950 to 1970, the investigations by US scientists on fundamental science of ferrites as well as their applications influence ferrite industries a lot. Hogan's[32] work on microwave ferrite devices, Albers-Schoenberg's[33] development on Mn-Mg ferrites for magnetic memories, development of magnetic memory devices by Dillon et al.[34] and Camras's[35] pioneering work on acicular fine $\gamma-Fe_2O_3$ particles are some of the outstanding achievements. There is a steady progress of worldwide production of different types of ferrites, since the production of soft ferrite in 1936.

In last 2-3 decades, different ferrites are used in wide range applications namely wide band and pulse transformers, inductors, telecommunication parts, multilayer ferrite chips, microwave ferrites, electromagnetic wave absorber etc. In the last decade when researchers explored the superparamagnetic behavior of ferrites, the field of biomedicine has witnessed a surge of interest in the use of magnetic nanomaterials in early diagnosis and effective treatment of some diseases such as cancer. Muller et al.[9] have published a review article emphasizing the synthesis of superparamagnetic iron oxide and its biomedical applications. The magnetic properties of ferrite nanoparticles are now exploited in various biomedical applications such as biosensors, targeted drug delivery, contrast agents in magnetic resonance imaging (MRI) etc.[4-10]

This review provides an overview of historical development of ferrite science and technology, preparative methods of various types of ferrites and their applications. It includes greater emphasis on various synthetic methodologies. Each synthetic route has been discussed in details with typical examples. We have also discussed different applications of ferrites in conventional industrial applications as well as recently developed advanced research areas.

## 1.3 Classification of Ferrites

The magnetic properties of ferrites arise from the interaction between metallic ions occupying particular positions relative to the oxygen ions in crystal structure of iron oxides.[1] As the crystal structure and magnetic properties of various ferrites are already well documented in several text books and review papers, we are not discussing this aspect of ferrites in details in this review article.[1-4, 10]

### 1.3.1 Spinel Ferrites

Ferrites, having chemical formula $MFe_2O_4$ with spinel crystal structure and $MeFe_{12}O_{19}$ having hexagonal crystal structures are common. Here, M presents divalent metal ion (such as Mn, Fe, Co, Ni, Cu, Zn etc) with an ionic radius approximately between 0.6 to 1Å and Me represents $Ba^{2+}$, $Sr^{2+}$ etc. In case of spinel ferrites a combination of two or more ions is also possible and can be referred as solid solution of two ferrites.[1]

The smallest cell of spinel lattice, having cubic symmetry, contains eight molecules of $MFe_2O_4$ where the relatively large oxygen ions form f.c.c. lattice. In cubic closed packed

structure two types of interstitial sites are present, the tetrahedral and the octahedral sites which are surrounding by 4 and 6 oxygen ion respectively. In this cubic unit cell 64 tetrahedral sites and 32 octahedral sites are present, out of which metal ions occupy only 8 and 16 sites respectively (referred as A and B sites respectively). In $MFe_2O_4$, out of three metal ions one occupies a tetrahedral site and two occupies octahedral site. In normal spinel the divalent M ion occupies in tetrahedral (A) site while trivalent Fe ion occupy the octahedral (B) site. In an inverse spinel structure the divalent M ions occupy one of the B site and trivalent Fe ions occupy other B site and A site.[1]

In a spinel ferrite the metal ions are separated by oxygen ions and the ions in the A sites are antiparallel to those in B sites. In majority of ferrites the two sub lattices are different in number and in the types of ions so there is a resultant magnetization. In case of $MnFe_2O_4$ where both ions have 5 uncompensated spins and the net magnetization is 5 spins per molecule.

### 1.3.2 Hexagonal Ferrites

Hexagonal ferrites (like $BaFe_{12}O_{19}$) possess a complex hexagonal unit cell and belong to magnetoplumbite structures. Magnetoplumbite structures are having general formula $A^{2+}O.6B_2^{3+}O_3$. 12 $Fe^{3+}$ ions in the unit cell of hexagonal structure are arranged as follows: nine ions in the octahedral sites (six nearest $O^{2-}$ neighbors), two ions in the tetrahedral sites (four nearest $O^{2-}$ neighbors), and one ion in the hexagonal site (five nearest $O^{2-}$ neighbors). Materials of this type have a strong uniaxial magnetic direction, which make them suitable candidate for permanent magnets.[36] There are six types of hexagonal ferrite names as (i) M-type ferrites (e.g., $BaFe_{12}O_{19}$, $SrFe_{12}O_{19}$ etc.) (ii) Z-type ferrites (e.g., $Ba_2Co_2Fe_{24}O_{41}$) (iii) Y-type ferrites (e.g., $Ba_2Co_2Fe_{12}O_{22}$) (iv) W-type ferrites (e.g., $BaCo_2Fe_{16}O_{27}$) (v) X-type ferrites (e.g., $Ba_2Co_2Fe_{28}O_{46}$) and (vi) U-type ferrites (e.g., $Ba_2Co_4Fe_{36}O_{60}$).[37]

### 1.3.3 Garnet Ferrites

There is another class of ferrites called garnet ferrites, which is of general formula $3M_2O_3.5Fe_2O_3$ or two units of $Me_3Fe_2(FeO_4)_3$ where Me represents the trivalent rare earth or a magnetic rare earth such as ytterbium. In the orthorhombic crystal structure of garnets, trivalent cations (including rare earth and $Fe^{3+}$) occupying tetrahedral, octahedral or

dodecahedral sites. The net magnetic moment is antiparallel to the rare earth ions on the dodecahedral sites as the interaction between tetrahedral and octahedral sites is antiparallel to each other. The garnet structure is one of the most complex crystal structures as the entire structure is the combination of 4 units of $3M_2O_3.5Fe_2O_3$.[3]

Ferrites are ferromagnetic ceramic materials and they are broadly categorized as soft and hard magnetic material. The word ''soft'' means temporary in the sense that the ferromagnetism emerges only when a magnetic field is applied. In contrast, hard magnets display ferromagnetism in the absence of an external field.

The most common soft ferrites are Mn-Zn ferrite, Ni-Zn ferrite etc. whereas $BaFe_{12}O_{19}$, $SrFe_{12}O_{19}$ are the examples of hard ferrites. It is well established fact that magnetic properties of the ferrites are depends on chemical compositions, crystal structure, particle size, microstructure and surface of the material. Methods of material preparation greatly influence this parameters.[1, 2, 13]

## 1.4 Synthesis of Ferrites

Polycrystalline samples of bulk ferrites are prepared by sintering process as commonly used in the ceramic industries. Ferrite thin films are generally prepared by thin film deposition techniques such as chemical vapour deposition (CVD), metal organic chemical vapor deposition (MOCVD), sputtering laser ablation technique. Numerous wet chemical methods such as co-precipitation, sol-gel, hydrothermal, precursor based method etc. have been developed to meet the demand of synthesis of ferrite nanoparticles having specific size, shape and microstructure for advanced technological applications. Several patents disclose different wet chemical methods which are employed for variety of ferrite for commercial applications. We have reviewed these methods somewhere else.[11]

## 1.4.1 Solid State Method

Bulk iron oxide or ferrites have conventionally been prepared by high temperature solid-state route that involves mechanical mixing of oxides, hydroxide or carbonates (sometimes by using high energy ball mill) followed by calcination at high temperatures (>1000 °C).[38-44]

_____

Hossain et al.[45] have reported synthesis of $Ni_{0.50-x}Mn_xZn_{0.50}Fe_2O_4$ nanopowders using the standard solid-state reaction where $MnCO_3$, NiO, ZnO and $Fe_2O_3$ were used as raw materials. Stoichiometric amounts of starting materials were mixed by ballmilling and then calcined at1100 °C for1h. The calcined powders were then pressed into disk and toroid-shaped samples and sintered at 1250, 1300 and 1350 °C in air for 5h. Synthesis of M-type strontium hexaferrite by conventional solid state method by calcination of hematite ($\alpha$-$Fe_2O_3$) and strontium carbonate ($SrCO_3$) was reported by Yourdkhani et al.[46] The calcination was carried out at 1100 °C for 1 h in air followed by heat treatment in presence of CO with various flow rates. Variety of ferrites can be prepared by using the solid state methods.[47-65]

This method, although capable of producing large-scale bulk ceramic powders, has numerous limitations as far as production of nanostructured ceramics is concerned. High temperatures and long heating schedules, which are the requisites of this method, lead to coarsening of grains. Moreover, volatilization/ melting of the constituent components (such as Zn in Ni-Zn ferrite) may occur during the high temperature processing of some of the multicomponent mixed oxides systems.[66-68] Thus, this method is unsuitable for producing pure, nanostructured ferrite materials.

### 1.4.2 Gas Phase Methods

### 1.4.2.1 Chemical Vapor Deposition (CVD)

In CVD process, a carrier gas stream with precursors is delivered continuously by a gas delivery system to a reaction chamber maintained under vacuum at high temperature (> 900 °C).[69, 70] The CVD reactions take place in the heated reaction chamber and the products combine to form clusters or nanoparticles. Successive heat treatment of the synthesized nanopowders in presence of various high-purity gas streams allows compositional and structural modifications, including purification and crystallization of the particle, as well as transformation to a desirable size, composition, and morphology.[69, 71] The CVD process has been employed to deposit iron oxide by the reaction of iron trichloride, with water at 800-1000 °C.[72] Concentrations of precursor in the carrier gas, rapid expansion and quenching of the nucleated clusters or nanoparticles as they exit from the reactor are the main controlling factors of this method.[69, 70, 73] The CVD process has been employed to deposit iron oxide and ferrite films at 800 to1000 °C.[69, 70, 74]

_____

### 1.4.2.2 Metal Organic Chemical Vapor Deposition (MOCVD)

In MOCVD process, metallo organics are used as precursors that allow reactions to take place at a somewhat lower temperature (300 to 800 °C) and at pressures varying from 1 Torr to ambient. Iron oxide thin films have been prepared via decomposition of acetylacetonate at 400-500 °C and iron trifluoro-acetylacetonate at 300 °C in oxygen.[75, 76] Tris(2,2,6,6 tetramethyl-3,5-heptadionato) Fe(III) , tris(tbutyl-3-oxo-butanoato) Fe(III) and Fe(II) dihydride complexes $H_2Fe[P(CH_3)_3]_4$ act as precursor for synthesis of ferrite thin flim.[77, 78] Films of several other ferrite have also been obtained by employing this technique.[79, 80]

### 1.4.2.3 Laser Ablation Method

Over the past few years, the pulsed laser deposition (PLD) technique has become one of most versatile methods for the deposition of thin films of a wide range of materials. The stoichiometric removals of constituent species from the target during the ablation and relatively less number of controlling parameters are two major advantages of PLD over some of the other physical deposition techniques. Various process parameters including substrate temperature, pressure, ablation yield and deposition rate influence the chemical composition and the crystal structure of the deposited films.[81, 82] Well-crystallized and uniform iron oxide nanoparticles, like nanoparticles of hematite and maghemite, have been obtained in one step using laser pyrolysis.[83] Iron pentacarbonyl is commonly used as a precursor in this method and ethylene is used as the carrier gas to transport the carbonyl vapor to the reaction zone.[84] Series of Ni-Zn ferrite and Zn ferrite thin films have been obtained by laser ablation process on Si substrates.[85] Rafique et al.[82] have reported the preparation of $BaFe_{12}O_{19}$ thin flim using pulse laser deposition technique where an Nd:YAG (1064 nm, 1.1 MW) pulsed laser was used on to the $Al_2O_3$ substrate in a vacuum chamber with controlled atmosphere. Several other research groups have also reported making of ferrite thin film using pulsed laser deposition technique. [86-89]

Some limitations of the gas phase methods are (i) although they are able to deliver high quality products, the yields are usually low and scale-up of the product is challenging (ii) maintaining precise stoichiometry of composition on the product sometimes difficult (iii) variables such as oxygen concentration, gas phase impurities and heating time must be

controlled precisely to obtain pure products (iv) the equipment used in these methods are also expensive and require maintenance.

Generally ferrites are manufactured by conventional ceramic method but its long heating schedule at high temperature restricts the formation of fine particles and limits its purity. As the ferrites are largely used as electronic parts, there are strict requirements in the accuracy of their chemical compositions, dimensions, microstructure and uniformity of the properties. Therefore, extremely high quality control in the manufacturing process of ferrites is necessary. To achieve high quality of ferrite powders, scientists particularly from chemistry, metallurgy and material science are actively involved to develop various solution phase synthetic routes namely co-precipitation, sol-gel, hydrothermal, precursor based methods etc.

### 1.4.3 Solution Phase Methods

### 1.4.3.1 Co-precipitation Method

Co-precipitation method is a very well established and commonly used technique for preparation of iron oxides and ferrites with wide range of compositions.[90-99] In this wet chemical process, ferrites with desired chemical compositions are simultaneously precipitated from aqueous solutions of metal ions using a precipitating agent, generally alkaline solution of carbonates, hydroxides, ammonia or ammines. The resulting solid precipitate contains ferrous and other metal carbonates or hydroxides, which decompose to the oxides when calcined at temperatures ranging from 500 – 800 °C. Final sintering at 1000 – 1200 °C produces the desired ferrites. Precise control over the chemical composition of the product is the main advantage of this technique in comparison with the conventional solid-state technique.

However, the control over the particle size distribution of the materials prepared by co-precipitation method is limited, because growth of the crystal is controlled by kinetic factors. In the co-precipitation process, crystal growth occurs in two stages (i) a short burst of nucleation, which occurs when the concentration of the species reaches critical supersaturation and (ii) a slow growth of the nuclei by diffusion of the solutes to the surface of the crystal.[100-102] The size and shape of the nanoparticles can be tailored to some extent by adjusting pH, ionic strength, temperature, nature of the salts (perchlorates, chlorides, sulfates, and nitrates) or metal ion concentration ratio. As this technique is very simple, it is widely used for

preparation of variety of ferrite nanoparticles. Ferrite having spinel structure such as $NiFe_2O_4$, $ZnFe_2O_4$, $CoFe_2O_4$, $Ni_xZn_{(1-x)}Fe_2O_4$, $MnNiZnFe_2O_4$[95, 96, 103-115] and hexagonal ferrite such as $BaFe_{12}O_{19}$ and $SrFe_{12}O_{19}$[116-130] have been synthesized by several researchers employing co-precipitation method. Here we are discussing the synthesis of $Fe_3O_4$, $CoFe_2O_4$, Mn-Ni-$ZnFe_2O_4$ as typical example.

Co-precipitation is a facile and convenient way to synthesize iron oxides (either $Fe_3O_4$ or $Fe_2O_3$) from aqueous $Fe^{2+}/Fe^{3+}$ salt solutions by the addition of a base under inert atmosphere at room temperature or at elevated temperature.[4] El-Shobaky et al.[131] have reported the synthesis of cobalt ferrites using co-precipitation route using nitrates of cobalt and iron at designated molar ratio (Fe:Co =2). Aqueous solution of NaOH was used as precipitating agent. Co-precipitation was carried out in the pH range of 8-10. After overnight ageing, the precipitate was thoroughly washed with water, dried and then calcined at 400 to 600 °C for 4 h to obtain $CoFe_2O_4$. Synthesis of $Mn_{(0.5-x)}Ni_xZn_{0.5}Fe_2O_4$ nanoparticle (with x = 0.0, 0.1, 0.2, 0.3 and 0.5) using co-precipitation method was reported by Venkataraju et al.[132] $MnCl_2$, $ZnSO_4$, $NiCl_2$ and $FeCl_3$ were starting material and NaOH was used as precipitating agent. The reaction was carried out at constant pH of 11 at 100 °C.

The limitations associated with co-precipitation method are the homogeneity of the product is not always extremely good and sometime reproducibility becomes an issue. Formation of gelatinous precipitate often causes difficulty in separation and retention of impurities in the product might causes formation of undesired crystalline phases, which affects the properties of the final materials. When ammonia is used as precipitating agent, formation of water soluble metal-amine complexes of metal ion occurs, which leaks out during washing and in this situation maintaining the desired stoichiometric of metal ions in the product becomes difficult.[107]

### 1.4.3.2 Sol-Gel Method

In this technique, the organometallic compounds, namely alcoholate, carboxylate or chelate compounds of different metals are generally used as starting materials. In sol-gel method, the acid or base catalyzed hydrolysis followed by condensation reaction of metal alkoxides precursors resulted in dispersions of nanosized oxide particles in a 'sol'. The 'sol' then forms 'gel' by solvent removal or by further condensation or inorganic polymerization in the form of

a three dimensional metal oxide network. The solvents are normally alcohol or water-alcohol mixture. Generally, basic catalysis induces the formation of a colloidal gel, whereas acid catalysis yields a polymeric form of gel.[133-135] The gel, upon calcination at a temperature in the range of ~300- 800 °C in presence of oxygen, produces desired ferrites. The main parameters which influence the structure and properties of the gel are the nature of starting materials, solvent, temperature, concentration of the salt precursors, pH etc.[9, 69,136-138] Mali et al.[139] have reported the synthesis of pure single phase $BaFe_{12}O_{19}$ by using sol-gel combustion method. Citrate complexes of $Ba^{2+}$ and $fe^{3+}$ were prepared by reacting metal nitrates with citric acid. The complexes were hydrolyzed by NaOH. The reaction mixture was dried with continuous stirring to form viscous brown gel. The gel was ignited at 290 °C and finally as-burnt powder was washed and then calcined at various temperatures ranging from 400 to 1100 °C for 1 h in air to obtain $BaFe_{12}O_{19}$ nanoparticles. Sol-gel process was used for synthesis of $NiFe_2O_4$,[140-143] $ZnFe_2O_4$,[144, 145] $CoFe_2O_4$,[146-150] $Ni_xZn_{(1-x)}Fe_2O_4$,[151-155] $BaFe_{12}O_{19}$,[156-164] $SrFe_{12}O_{19}$ [165-168] etc.

Use of expensive metal alkoxides or complex metal compounds as starting material and contamination from byproducts of reactions are the main limitations of this method.

### 1.4.3.3 Hydrothermal Method

Generally in this method, aqueous solutions of metal ions, and/or aqueous slurry containing metal hydroxides are mixed with an alkali solution and the mixture is autoclaved between 100- 400 °C. Processing parameters such as pressure, temperature, reaction time etc. are adjusted to control the nucleation rate which influences the crystal growth.[169, 170] This method is a comparatively low temperature technique, which produces homogeneous multicomponent ferrites with required chemical compositions. Hydrothermal process is found to be superior than conventional high temperature process because it avoids the sintering or agglomeration of ferrite grains.

Khusnir et al.[171] have reported synthesis of $SrFe_{12}O_{19}$ using hydrothermal process where $Fe(NO_3)_3,9H_2O$, $Sr(NO_3)_2,4H_2O$ and NaOH were used as reagents. An aqueous mixture of metal nitrates with excess NaOH was autoclaved in a Teflon cell at 140- 200 °C. Chen et al.[172] have prepared a series of uniform spinel ferrite $MFe_2O_4$ (M=Ni, Co, Mn, and Zn) nanoparticles by direct hydrothermal decomposition of the trinuclear heterometallic

_____

oxocentered acetate cluster of [MFe$_2$O(CH$_3$CO$_2$)$_6$(H$_2$O)$_3$] nH$_2$O in solution. In the first step of the process [MFe$_2$O(CH$_3$CO$_2$)$_6$(H$_2$O)$_3$] nH$_2$O complex was dissolved in water, then the solution was placed in a Teflon-lined stainless steel autoclave for hydrothermal treatment. Hydrothermal process was employed to synthesize wide range of ferrites i.e., both hard and soft ferrite.[173-190]

Although hydrothermal technique is very versatile, the main drawbacks of the conventional hydrothermal method are the slow reaction kinetics at any given temperature and requirement of a high pressure reactor which limits the large scale production of materials.

### 1.4.3.4 Combustion Method

This method is also known as "self-sustaining/propagating high temperature synthesis process." The term 'combustion' covers flaming (gas-phase), smouldering (heterogeneous) as well as explosive reactions. This process is rapid and precursor solution to the final oxide product.[191-202] The process makes use of highly exothermic redox chemical reactions between metals and nonmetals, metathetical (exchange) reaction between reactive compounds or reactions of redox compounds/ mixtures. This method uses the energy produced by the exothermic decomposition of a redox mixture of metal nitrates with an organic compound which acts as fuel to form oxides. The reaction is carried out by dissolving metal nitrates and fuel in minimum amount of water in a pyrex dish and heating the mixture in order to evaporate water to form viscous liquid foams which ignites and undergoes a self-sustained combustion reaction to produce the desire product. Here, due to ignition of organic precursor, which is gas producing self-propagating exothermic reactions, voluminous fine oxides are formed in few minutes. The controlling factor for the method is exothermicity of the combustion reaction which is controlled by the nature of the fuel and the ratio oxidizer/fuel. Gayoso et al.[203] have reported the synthesis of barium ferrite (BaFe$_2$O$_4$ and BaFe$_{12}$O$_{19}$) using nitrates of barium and iron and oxaldihydrazide (ODH, C$_2$H$_6$N$_4$O$_2$) and tetraformaltrisazine (TFTA, C$_4$H$_{12}$N$_6$. 2H$_2$O) as fuels. The combustion reaction was carried out at 300 °C. The disadvantage is that sometimes the exothermic reaction might be difficult to control especially when being performed for a large-scale production. Limited control over particle size and sometimes formation of impurity phases are other drawbacks of this method.

___

### 1.4.3.5 Reverse Micelle and Microimulsion Method

The reverse micelle method is a controlled synthesis route for preparation of ceramic materials and metals having a tailored shape, size and composition.[204, 205] The structure of reverse micelles is characterized by a polar core formed by hydrophilic heads of the surfactant and a non-polar shell formed by hydrophobic tails of the surfactant. The method is employed to synthesize monodispersed nanoparticles with various morphologies. In water-in-oil microemulsions, the aqueous phase is dispersed as microdroplets surrounded by a monolayer of surfactant molecules in the continuous hydrocarbon phase. These microdroplets offer a unique microenvironment for the formation of nanoparticles with limiting size growth. The droplet size of reverse micelles can be readily modulated in the nanometer range by controlling the water- surfactant molar ratios, even though the final size of the nanoparticles may also be influenced by several other factors such as concentration of reactants (especially surfactant) and flexibility of the surfactant film. There are several ways to utilize microemulsion technique to synthesize nanoparticles. In one method, reactants are dissolved in the aqueous phases of two identical water/oil microemulsions and precipitate out upon mixing. The precipitate is confined to the interior of the droplets, thereby nanoparticles with controlled size and shape are formed. In another method, addition of a reducing or precipitating agent to a microemulsion, containing the primary reactants, is used to produce nanosized particle.[206-209]

Han et al.[210] have reported synthesis of $BaFe_{12}O_{19}$ nanoparticles employing microemulsion technique using cetyltrimethylammonium chloride (CTAC) as the surfactant, n-hexanol as cosurfactant, cyclohexane as solvent and $(NH_4)_2CO_3$ and $NH_3.H_2O$ as precipitator. Microemulsion I which conatains CTAC, n hexanol, Hexanol, water, nitrates of barium and iron was added dropwise to microemulsion II which contains CTAC, n-hexanol, hexanol, $(NH_4)_2CO_3$ and $NH_4OH$ at 40 °C with vigorous stirring. Then the reaction mixture was aged for 12 h and the precursor particles formed was washed by centrifuging with anhydrous ethanol and water, dried and calcined at 950 °C for 4h. This technique was also used to synthesize several other ferrites.[211-220] However, this method requires a large amount of solvent and also difficult to scale up.

___

### 1.4.3.6 Precursor based Method

This method involves the preparation of a precursor compound which is complex combinations of metal ions and a chelating agent. The calcination of the precursor at different temperatures gives rise to nanoscale particles of desired mixed oxide system. Various organo-metallic complexes, metal hydroxides/ oxalates/ citrates/ hydrazine carboxylates etc. are some of the commonly used precursor compounds.[221-230]

Mallapur et al. [231]have reported synthesis of spinel ferrite system of $Ni_{0.7-x}Co_xZn_{0.3}Fe_2O_4$ using precursor based method where PVA acts as chelating agent and sucrose acts as fuel. Recently, we have reported synthesis of $Ni_xZn_{1-x}Fe_2O_4$ and $\alpha$-$Fe_2O_3$ using PVA precursor based method and oxalate precursor based method.[232-236] Mohamed et al.[237] have synthesized cobalt ferrite using organic acid precursor method where oxalic acid used as chelating agent. Zinc ferrite nanopowder was synthesized using tartrate precursor method by Yen et al.[229] Tang et al.[238] have synthesize barium hexaferrite nanopowder using sugar as chelating agent. There are some other precursor based methods also available for synthesis of nano ferrites like citrate precursor,[239-241] polymeric precursor route[242,243] etc.

### 1.4.3.7 Other Synthesis Methods

Mechanochemical synthesis is the combination of chemical and mechanical alloying synthesis method. Here, precursors are first prepared by chemical route like sol-gel or co-precipitation method and then these precursors are milled under different conditions using planetary ball mill and finally calcined at 600-900 °C. Manova et al.[244] have synthesized $CoFe_2O_4$ nanopowder using mechanochemical route where cobalt ferrite precursor was prepared using coprecipitation method and then precursor was milled using a Fritsch Planetary mill and calcined at 500 °C to get $CoFe_2O_4$ nanopowder. Ataie et al.[245] have reported synthesis of $BaFe_{12}O_{19}$ nanoparticle using mechanocombustion route where barium hexaferrite precursor was prepared by sol-gel combustion method followed by milling under different conditions using planetary ball mill and finally annealed in air at 700 to 1000 °C for 1 h. Tiwary et al.[246] have synthesized strontium hexaferrite magnets from celestite and blue dust by mechanochemical route. Rod-like and platelet-like nanoparticles of simple-crystalline $BaFe_{12}O_{19}$ have been synthesized employing the molten salt method by Yu et al.[247] S. Maensiri et al.[248] have reported synthesis of $NiFe_2O_4$ nanoparticles by using Ni and Fe nitrates

___

and freshly extracted egg white (ovalbumin) in an aqueous medium. Sonochemical synthesis was reorted for synthesis of ferrites like $NiFe_2O_4$, $SrFe_{12}O_{19}$.[249-251]

Recently, Ghosh and co-workers have developed a simple but cost effective EDTA (Ethylenediaminetetraacetic acid) precursor based synthesis method for synthesis of variety of ferrites nanoparticles.[233, 234, 252-261]

### 1.4.4 Stabilization of ferrite nanoparticles

Stability of magnetic nanoparticles without agglomeration or precipitation is an important issue for application point of view as properties of agglomerated particles differs from monodispersed nanoparticles. Nanoparticles formed by wet chemical methods tend to aggregate in solution in order to reduce their surface energy as surface area to volume ratio for nanoparticle is very large. Therefore, it is required to develop efficient pathways to improve the stability of magnetic nanoparticles for technological as well as biomedical applications. One of the popular attempts to stabilize nanoparticles is dispersing them with anionic surfactants. The nature of the counterions present in the solution, pH and ionic strength play important roles to stabilize the nano particles via interactions between electrical double layers.[10, 262,263] The core–shell structure of magnetic nanoparticle, where bare magnetic nanoparticle acts as a core, is coated by a shell. The shell protects the core against the environment. This approach appears as a promising method for making less agglomerated nanoparticles. Basically, two types of coatings are used to form core shell magnetic nanoparticle (i) coating with organic shells, including surfactant and polymers,[4, 264-269] proteins[270-272] and (ii) coating with inorganic components, including silica,[273-277] precious metals (such as Au,[278-282] Ag,[283] etc.) In general, surfactants or polymers can be chemically attached or physically adsorbed on the surface of magnetic nanoparticles to form a single or double layer,[4, 284] which creates repulsive forces to balance inter particle forces acting on the magnetic nanoparticles. Most common coatings are dextran, carboxymethylated dextran, carboxydextran, starch, arabinogalactan, glycosaminoglycan, sulfonated styrene-divinylbenzene, polyethylene glycol (PEG), polyvinyl alcohol (PVA), chitosan etc. The commonly used surfactants are oleylamine, oleic acid, stearic acid etc.[4-10, 273] Usually, an inert silica coating on the surface of magnetite nanoparticles not only prevents their aggregation in liquid, but also improves their chemical stability and provides better protection against toxicity which is very important for biomedical application. In common synthesis procedure,

silica core shell is used to form *in-situ* through the hydrolysis and condensation of a sol-gel precursor, such as tetraethyl orthosilicate (TEOS).[285-289] The other synthesis methods for silica coating are deposition of silica by using silicic acid solution[290] and microemulsion method, where micelles or inverse micelles are used to control the silica coating.[291] One of the main advantages of having a surface coated by silica is that the silanol groups present on the surface can readily be functionalized by reacting with various coupling agents so that, the magnetic particles can potentially be used in biolabeling, drug targeting, drug delivery. For example, amine groups modified surface of silica-coated magnetite nanoparticles can be prepared by hydrolysis and condensation of aminopropyltriethoxysilane (APTES) on the surface of magnetite nanoparticles.[290-294] Magnetic nanoparticle can be dispersed onto porous silica matrix like SBA-15 and can be used as magnetic separable catalyst for several organic reactions.[295-297]

## 1.5 Applications of Ferrites

### 1.5.1 Conventional Applications of Ferrites

As mentioned in the introduction section, ferrites with various compositions find applications in wide range of technologies.[1-13, 37] Due to interesting electrical and magnetic properties, ferrites are gaining ever-increasing importance in the electronics industry and the electrostatographic arts. Smit and Wijn[2] and Snelling et al.[3] have elaborately discussed the physical properties of various ferrites and their applications. Early commercial ferrites, Mn-Zn ferrite and Ni-Zn ferrite, were developed for the applications where high permeability and low loss were main requirement. By varying compositions these ferrites can be made in a variety of grades for particular applications. The combination of good magnetic properties and high resistivity make these materials suitable as cores for inductors and transformers in carrier telephony technology. These ferrites are used in domestic television receivers as core materials for line time-base transformer. Low loss magnetic material such as Mn-Zn ferrite is used in the manufacture of deflection yoke core for high speed cathode ray tubes. In traditional domestic radio receiver and antennas ferrites are used. High quality magnetic recording tapes have been prepared by using $\gamma$-$Fe_2O_3$, Co doped ferrite, single crystal of Mn-Zn ferrites.

Ferrites having hexagonal crystal structure (e.g., $BaFe_{12}O_{19}$) are characterized by having large coercivity (> 2000 Oe) are used for wide range permanent magnet applications, namely loud speaker magnets, magnetic chunks, small electric motors and focusing magnets.

Spinel ferrites, particularly Mn-Mg ferrite, Mn-Cu ferrite, Li-Ni ferrite, having rectangular hysteresis loops are used in memory cores. These are very small toroids which are used in large number of elements in rapid access data stores. Rectangular loop ferrites are also applied in switching core and multiple-aperature core based devices. Ferrite materials have been used for many microwaves devices such as circulator, isolator, magnetostatic modulator, filter, switches, limiters, tunable electro optic modulator etc. Bulk and thin films of spinel ferrites (e.g., Ni ferrite, Ni-Zn ferrite, Mg-Mn ferrite, Mn-Mg-Zn ferrite etc) and hexagonal ferrite ($BaFe_{12}O_{19}$) and garnet ferrite (YIG) are most often used as microwave ferrites. Recent growth in microwave communication through mobile and satellite communication have enhanced the need for low loss and cost effective microwave devices using ferrite materials. In Table I, we have summarized the claimed applications of different types of ferrites, which have been patented.[11]

Table 1.1 Applications of different ferrite materials

| Composition | Application | Reference |
|---|---|---|
| $(AO_n\{(Fe_{1-X}M_X)_2O_3\}$ where A is Ba or Ba and Sr, M is Zn and Ti, or Zn, Co and Ti, n=6.5-11.0, and x=0.05-0.25 | **High density magnetic recording.** | [293] |
| $MeO_n[Al_XM_YFe_{2-X-(m/3)Y}O_3]$ where, Me is Ba, Sr or Pb, M is Zn, Sc, In, Cr, Ir, Ru, Rh, Ti, Sn or Ge $5 \leq n \leq 6$, $0 < X \leq 0.8$, $0 < Y \leq 0.6$, and m is an ionic valency of M. | **Magneto optical recording medium and a perpendicular magnetic recording medium having the magnetic film.** | [294] |
| $[(MeO_n[Ma_xMb_yCo_zFe_2(x+m/3y+2/3z)O_3]$ where Me is Ba, Sr or Pb Ma is Ga, Al, Cr or Rh Mb is Zn (divalent); Ni, In, Sc, Cr, Sb, Bi, Y or Sm (trivalent), and Mo, Ti, Sn, Ta, V, Mn, Ir, Hf, Pd, Nb, Re, Pt, Os, Zr, Tc, Rh, Ge, Ru, W, Te, Pr or Ce (tetravalent) $x = 0 < x \leq 0.5$ $y = 0 < y \leq 0.5$ $z = 0 < z \leq 0.5$ such that $0 < x+y+z < 1$ m= ionic valency of Mb $5 \leq n \leq 6$ | **Perpendicular magneto optical recording medium.** | [295] |

| | | |
|---|---|---|
| **Magnetic layer comprises of formula MeO$_n$[Ga$_X$M$_Y^I$Fe$_{.2-X-(m/3)Y}$ O$_3$]** <br> **Where Me is Ba, Sr or Pb,** <br> **M$^I$ is Zn, Sc, In, Cr, Ir, Ru, Rh, Ti, Ta, Sn or Ge** <br> **5≤ n≤6,** <br> **0<X≤0.8,** <br> **O<Y≤0.8 and** <br> **m is the ionic valency of M$^I$** | **Magneto optical perpendicular recording medium, which has high recording sensitivity.** | **[296]** |
| **Ferrimagnetic oxide of the formula** <br> **MeGa$_x$ Fe$_{12-x}$O$_{19}$ where Me is Ba, Sr or Pb, x is an integer from 3 to 8.** | **Vertical magnetic-anisotropic magnetic film layer.Magneto-optical recording mediums for recording and reproducing information by application of laser beams.** | **[297]** |
| **Hexagonal ferrite particles of formula** <br> **AO$_n$(Fe$_{1-m}$M$_m$)$_2$O$_3$,** <br> **where n is ~5.0 to 6.0 and m is ~ 0 to 0.2, A is Ba, Sr, Ca or Pb** <br> **M is at least Co, Ti, Ni, Mn, Cu, Zn, In, Ge, and Nb.** | **Magnetic recording medium that is suitable for use in high density recording methods.** | **[298]** |
| **FeFe$_2$O$_4$, NiFe$_2$O$_4$ ZnFe$_2$O$_4$ or NiZnFe$_2$O$_4$** | **Microwave filters and resonators, Radiowave elctronics.** | **[299]** |
| **Ni-Zn-Fe-O films** | **Micro-electronic device manufacturing.** | **[300]** |
| **(i) 2MO.AO.8Fe$_2$O$_3$** <br> **(ii) 2MO.2AO.12Fe$_2$O$_3$** <br> **(iii)2MO.3AO.12Fe$_2$O$_3$** <br> **where M is Mn, Co, Zn, Ni, Mg , Fe and a mixture thereof and A is Ba, Sr, Pb, Ca.** | **The recording medium made, vertical magnetic recording disc, magnetic tape.** | **[301]** |
| **M$^{II}_{0.6}$ Fe$_2$ O$_3$ (M$^{II}$ is Sr or Ba).** | **Anisotropic magnet comprising ferrite particles dispersed in a plastic or rubber binder, shaped in a conventional manner such as calendaring, molding.** | **[302]** |
| **Mn-Zn ferrite with TiO$_2$, SnO$_2$, CuO.** <br> **(Mn-Zn ferrite generally has a composition comprising basic components of more than 50- 55 mol % of Fe$_2$ O$_3$ on the average, 10 to 24 mol % of ZnO and the remainder being MnO).** | **Switching power supply transformer, flyback transformer or deflection yoke, various inductance elements, impedance elements for EMI countermeasure, electromagnetic wave absorbers.** | **[303]** |
| **Fe$_2$O$_3$ (doped with MgO, ZnO, CuO, MnO ,Bi$_2$O$_3$).** | **Deflection yoke care for high speed scanning cathode ray tube.** | **[304]** |
| **AFe$_{12-2x}$Co$_2$M$_x$O$_{19}$ or AFe$_{12-3/2x}$ Co$_x$M$_{1/2x}$O$_{19}$ where A is either Ba, Sr, Pb or Ca, M is either Ti or Ge or V, Nb, Sb or Ta, and x is from 0.5 to 1.1 or where A is either Ba, Sr, Pb or Ca and n is from 5 to 6.** | **High density magnetic recording, having an improved dispersibility in a binder or paint, more particularly to production of a magnetic powder having a high dispersibility suitable for vertical magnetic recording.** | **[305]** |

_____

| | | |
|---|---|---|
| (i) $MeFe_2O_4$<br><br>where Me is either Mn, Ni, Zn, Co or Fe(II).<br><br>(ii) $M_2^1 Me_2^1 Fe_{12} O_{22}$<br><br>where $M^1$ is Ba, Sr, Ca and/or Pb, and $Me^1$ is divalent Mn, Cu, Fe, Co, Ni, Zn, Mg and/or equimolar amounts of Li and trivalent Fe.<br><br>(iii) $M^2(Me^2 Ti)_x Fe_{12-2x}O_{19}$ where $M^2$ is Ba or Sr, $Me^2$ is Zn, Ni and/or Co and x is from 0 to 2.0. | Magnetic ceramics for high frequency technology,<br><br>magnetically soft paint or<br><br>plastoferrites for shielding purposes. | [306] |
| $XFe_2O_4$ where X is either Mg, Zn and Sn. | Yellow pigment capable of withstanding elevated temperatures such as $200^0C$. | [307] |
| Ferrites doped with $Ni^{2+}$, $Zn^{2+}$, $Mn^{2+}$ or $Mg^{2+}$ | Components for telecommunications and higher frequency, filter core. | [308] |
| $AO_n(Fe_{2-x}M_xO_3)$<br><br>where A is at least one of Ba and Sr, n is a molar $(Fe_{2-x}M_xO_3)$/AO ratio in the range of about 5 to about 6, M is more than one substitution element selected from the group of Co, Zn, Ni, Al, Ti, Sn, Si, Nb, and Ta, and x is in a range of 0 to about 3.5. | Magnetic recording media by dispersing the particles in a magnetic paint and coating the paint onto a substrate, or by dispersing the particles in a self-supporting material. | [309] |
| soft ferrites where divalent metal is $Mn^{2+}$, $Ni^{2+}$, $Mg^{2+}$, and $Zn^{2+}$. | Telecommunication circuitry uses, e.g. as channel filters and for switched-mode power supplies in power applications for electronic control and computer uses. | [310] |
| Hexagonal-system ferrite with $Ba^{2+}$, $Sr^{2+}$, $Pb^{2+}$ or $Ca^{2+}$ | Plastic-ferrite composite magnet. | [311] |
| $Zn_xFe_{1-x}O.Fe_2O_3$ where x is from 0.05 to 0.62 | Magnetic cards, magnetic coating. | [312] |
| Magnetite $Fe_2O_3$ particles containing a silicon component inside and a silicon component exposed on the surface of each particle. | Magnetic toner for electrostatic copying and as black pigment powder for coating materials. | [313] |
| Iron oxide which consists of a core of $\gamma$-Fe(III) oxide surrounded by a shell of a magnetite modified with Zn(II) ions and/or Mn(II) ions. | Magnetizable material in the manufacture of magnetic recording media. | [314] |
| $AMe_xFe_{12-x}O_{19}$, where x is from 0.24 to 0.4, A is Ba and/or Sr and Me is In or equimolar amounts of Zn or Co and Ti | Magnetic recording media and plastoferrites, forgery-proof magnetic coding. | [315] |
| Magnetite particles | Magnetic pigment for paints for vehicles, magnetic toner material for electrostatic reproduction. | [316] |
| $(Fe)_a(Co)_b(M^1)_c(M^2)_d(M^3)_e(O)_f$ where $M^1$ is either Ba, Sr, Ca and Pb, $M^2$ is either Ti, Zr, Hf, Si, Ge, Sn, Mn, Mo, W, V, Ce, Nd, Sm, B and Nb, $M^3$ is either Mg, Ni, Cr, Cu, Zn, Cd, In, Ga, Bi, La, Y, P, Sb and Al, a (8-12), b (0-0.5), c (0.3-6), d (0-6), e (0-6) and f respectively represent the numbers of Fe, Co, $M^1$, $M^2$, $M^3$ and O atoms, for example $Ba_{1.1}Fe_{10.8}Co_{0.4}V_{0.6}La_{0.2}$. | Magnetic recording medium. | [317] |

| Co(II) hydroxide enveloped by an outer layer of Fe(II) hydroxide. | Magnetic recording materials. | [318] |
|---|---|---|
| $Y_{3-x}Gd_xFe_{t-2y-z}Co_ySi_yAl_zO_{12}$ <br> where <br> $0.2<x<1.5$, $0.005<y<0.015$, $0<z<1.5$ and $4.75<t<5.0$ | Non-reciprocal circuit elements to reduce losses in high frequency bands such as microwave bands. | [319] |
| Magnetic iron oxide in which the content of silicon element is 0.1-1.5 wt. %, preferably 0.20-1.0 wt. %, more preferably 0.25-0.70 wt. % based on the iron element. | Magnetic recording material, a pigment and a magnetic toner. | [320] |
| Dispersion of magnetic pigment (ferrites, iron particles and nickel alloys) in resin. | Field dependent toner. | [321] |
| $BaFe_{12-x-y}M_xTi_yO_{19}$ where x and y are independently not more than 1.2 and M is Co(II) or Co(II) and a divalent metal other than Co | Magnetic recording. | [322] |
| Plate –like $BaO.6Fe_2O_3$ | Magnetic recording. | [323] |
| $NiO_{0.176}ZnO_{0.45}MgO_{0.3}MnO_{0.05}CuO_{0.06}(Fe_2O_3)_{10}$ | Humidity-insensitive magnetically attractable, semi-conductive, uncoated electrostatographic ferrite carrier material useful for development of electrostatic latent images. | [324] |
| $BaO.6Fe_2O_3$ | Applications in DC motors. | [325] |

During past two decades, when researchers of different disciplines are exploring the various aspects of nanomaterials, it is realized that the unique magnetic properties of ferrite nanoparticles can be exploited in different advanced technologies such as biotechnology, medical science, catalysis, composites, stealth technology etc.

## 1.5.2 Advanced Applications of Ferrite nanoparticles

### 1.5.2.1 Biological application

The use of magnetic nanoparticles has received significant attention in the field of biotechnology and biomedical sciences like immunoassays, cell separation, hyperthermia, magnetic resonance imaging contrast agents, and targeted drug delivery vehicles etc.[4-10] These applications require particles, which exhibit superparamagnetic behavior at room temperature i.e., they can show magnetic property in presence of an external magnetic field and

19

immediately redispersed when the magnetic field is removed. For biomedical applications basic requirement of ferrofluids are (i) they should be stable in water at pH of ~7.2 and physiological conditions[331] and (ii) the size of the particles, which should be relatively small to avoid precipitation due to gravitation forces or agglomeration. Till date Magnetite or maghemite are the most commonly employed ferrite for biomedical applications because of their biocompatibility and low toxicity in the human body.[332, 333]

Magnetic drug delivery is a very promising application of magnetic nanoparticles, where the drug molecules are attached to a functionalized magnetic nanoparticle. These drug carrying nanoparticles are guided to a chosen site using an external magnetic field, continued to stay there until the therapy is complete and after that they removed. Nigam et al.[334] have fabricated citric acid functionalized (citrate-stabilized) $Fe_3O_4$ aqueous colloidal magnetic nanoparticles of size 8–10nm and investigated their potential as a drug carrier system using doxorubicin hydrochloride as a model drug. The anti-tumor activity of mitoxantrone loaded on magnetic nanoparticles was examined by Lee et al.[335] Recently, polymeric nanomaterials embedded with superparamagnetic iron oxide nanoparticles have gained an increasing attention in the field of targeted drug delivery, cell imaging etc.[336-340]

Another interesting application of magnetic nanoparticles is in hyperthermia treatment which is considered as an additional treatment with chemotherapy, radiotherapy and surgery in cancer therapy.[341-346] When superparamagnetic magnetic nanoparticles are exposed to a varying magnetic field, heat is generated by magnetic hysteresis loss, Neel-relaxation and Brown-relaxation effect.[4, 347,348] This generated heat increases the temperature upto ~ 40- 45 $^0$C at which the tumor cells are destroyed as they are more sensitive towards heat than that of normal cells.[349] Herrasti et al.[350] have synthesized biocompatible cobalt ferrite nanoparticle for hyperthermia application.

Magnetic nanoparticles and fluorescent magnetic nanocomposites have been widely used *in-vivo* as magnetic resonance imaging (MRI) contrast agents for molecular and cell imaging.[350-359] Zhang et al.[360] have studied the biological activity and MRI of adipose-derived stem cells by labeling them with superparamagnetic iron oxide nanoparticles and compared them with bone marrow mesenchymal stem cells.

Magnetic separation can be used as a quick and simple method for capturing specific proteins or biomolecules efficiently and reliably. This purification process can take place in one vessel without using expensive liquid chromatography or other techniques.[361,362] Recently Chen et al.[363] have successfully demonstrated the binding of Concanavalin A (Con A) onto $Fe_3O_4$ magnetic nanoparticles via carbodiimide activation. This material acts as a magnetic nano-adsorbent for glycoprotein separation.

## 1.5.2.2 Catalysis

Magnetic separation of catalysts in a liquid-phase reaction is much easier than by filtration and centrifugation, especially when the catalysts are in the sub-micrometer size range. Nanostructured magnetically separable catalysts could offer the advantages of their high catalytic efficiency along with easy separation for expensive reactants. Catalytically active species can be attached with magnetic nanoparticles to prepare this type of catalysts.[364-368] Recently, Astruc et al.[369] have synthesized ruthenium catalyst by immobilizing a pentamethylcyclopentadienyl ruthenium complex on iron oxide nanoparticles for the synthesis of 1,5-disubstituted 1,2,3-trizoles via cycloaddition of alkynes and organic azides. Magnetically seperable superparamagnetic solid catalyst has been synthesized by loading Pd(0) species on zinc ferrite nanoparticles for Suzuki and Heck coupling reactions under ligand free condition by Singh et al.[370] Park et al.[371] have reported one-pot synthesis method to prepare a magnetically separable Au nanoparticle catalyst for the reduction of functionalized nitroarenes with hydrosilanes. Pramanik et al.[372] have synthesized magnetically separable $MnFe_2O_4$-silica nanocomposites for decolourisation of synthetic dyes pollutant. Synthesis of $Fe_3O_4@SBA-15$ and their catalytic activity for synthesis of 3,4-dihydropyrimidin-2(1H)-ones via the Biginelli Reaction was reported by Bhaumik et al.[373]

## 1.5.2.3 Polymer nanocomposites

Although, ferrite-based ceramic materials exhibit exciting magnetic and electrical properties along with high thermal stability but their use in complex structured devices is limited due to their brittleness and lack of structural flexibility. Apart from that, a high sintering temperature (> 1200 °C) is generally required for the processing of sintered ferrite bodies. Therefore, it is very complicated to prepare complex structures for specific high-tech applications with pure ferrite nanopowders. To prepare materials with improved mechanical flexibility and easier

processibility hybridization of ceramic materials with organic polymers recently becomes an attractive concept. In the literature there are certain reports available based on the study of nanoparticles of $Fe_2O_3$ and Mn-Zn ferrite, Ni-Zn ferrite, $BaFe_{12}O_{19}$, $CoFe_2O_4$ dispersed in polymeric matrix. Kim et al.[374] have reported the electromagnetic wave absorption of $Ni_{0.5}Zn_{0.4}Cu_{0.1}Fe_2O_4$ ferrite nanoparticles embedded in the poly (methyl methacrylate) matrix. The efficiency of magnetic polymer composites with multicomponent fillers has been studied by Lopatin et al.[375] for their application as radio-absorbing materials. Magnetic nanocomposites containing $\gamma$-$Fe_2O_3$ embedded in a polymer matrix of sulphonated polystyrene and divinyl benzene prepared by an ion exchange method have been reported by Malini et al.[376]. Kiskan et al.[377] have reported carboxylic acid functional benzoxazine that is easily coated on neat magnetite and forms polybenzoxazine-nanomagnetite nanocomposites via thermally activated ring opening polymerization. These nanoparticles showed typical ferromagnetic characteristics and the magnetic properties were preserved after curing. Rubber ferrite composites, containing different mixed ferrites with various loading levels, have been studied by Anantharaman et al.[378] Jiang et al.[379] have studied a novel poly (aniline-co-o-toluidine)/ $BaFe_{12}O_{19}$ composite, which was successfully synthesized by *in-situ* polymerization method. Ting et al.[380] have reported the microwave absorption of the polyaniline/ $BaFe_{12}O_{19}$ and noticed that microwave absorbing properties can be modulated simply by controlling the content of polyaniline on the samples for the required frequency bands. Deng et al.[381] have studied the synthesis of magnetic and conducting $Fe_3O_4$-crosslinked polyaniline nanoparticles with core-shell structure by using a precipitation-oxidation technique. Xu et al.[382] have reported an in-situ polymerization process to obtain polyaniline/ $BaFe_{12}O_{19}$ nanocomposites and their microwave absorption properties were investigated. We have recently reported ferrite nanoparticle-polybenzoxazine-linear low density Polyethylene (LLDPE) based magnetic nanocomposites.[383-385] These composites are prepared by using a simple melt blending method. Here, ferrite nanoparticles (e.g., $NiFe_2O_4$, $Ni_{0.8}Zn_{0.2}Fe_2O_4$, $CoFe_2O_4$, and $BaFe_{12}O_{19}$) were uniformly dispersed within the polymeric matrix composed of LLDPE and polybenzoxazine. Investigations on mechanical properties and magnetic properties of the nanocomposites revealed that the sheet and the films of these composites possess structural flexibility as well as magnetic properties. Both of these properties can be tuned by judicious choice of ferrite nanoparticle and their loading level in the composition of the composites. These composites have capability of being used in complex device application and coating.

## 1.6 Hard-soft ferrite nanocomposites

Based on magnetic property, ferrites are classified as hard ferrite (e.g. $BaFe_{12}O_{19}$, $SrFe_{12}O_{19}$, $CoFe_2O_4$ etc) and soft ferrite ($NiFe_2O_4$, $NiZnFe_2O_4$ etc). Ferrite material in which the ferromagnetism emerges only when a magnetic field is applied (means temporary) is called the soft ferrite. The general formula is $MOFe_2O_3$, where M is a divalent metal ion like Mn, Ni, Fe, Mg etc. These ferrites have good magnetic properties with extremely high electrical resistivity, so they can operate with almost no eddy current loss at high frequencies.

Ferrite materials exhibit ferromagnetism even in the absence of an external magnetic field is called hard ferrites. Hard ferrites have hexagonal crystal structure. The general formula is $MO6Fe_2O_3$, where M is a divalent metal ion like Ba, Sr and Pb. In the group of hard ferrites, magnetoplumbites or M-type hexagonal ferrites ($MO6Fe_2O_3$) are extensively used in many technological applications due to their superior magnetic properties. Hard-soft ferrite nanocomposites are the materials composed of hard ferrite (e.g. $BaFe_{12}O_{19}$, $SrFe_{12}O_{19}$, $CoFe_2O_4$ etc) and soft ferrite ($NiFe_2O_4$, $NiZnFe_2O_4$ etc).

### 1.6.1 Spring exchange coupling behavior of hard-soft ferrite nanocomposites

Recently, there has been immense attention on the materials having good spring exchange coupling behaviour. According to the exchange spring theory proposed by Kneller and Hawig,[386] nanocomposite magnets consist of soft and hard phases, having sufficiently exchanged coupling between both the phases are known as exchange spring magnet. Here, the high saturation magnetization of the soft phase and the high coercivity of the hard phase contribute for the superior magnetic property of the composite compared to the individual soft/hard phases, thus provide high magnetic energy product. The hard ferrite possesses a high magnetocrystalline anisotropic energy compare to soft ferrite. If the hard ferrite grains are sufficiently exchange-coupled with the neighbouring soft ferrite grains, then the exchange-coupled interaction will not only help to align the magnetization in the soft ferrite phases but also helps to arrange magnetic moments of the hard and soft ferrite phases parallel to each other in hard soft ferrite nanocomposites. This leads to higher energy product and enhances the Reflection Loss (RL) in microwave absorption i.e. hard-soft ferrite nanocomposites exhibited improved microwave absorbing property.[387-391]

_____

In a hard-soft ferrite system, three types of magnetic interactions are present. The most important one is the exchange-coupling interaction between soft and hard phase, the remaining are dipolar interactions between the hard-hard and soft-soft ferrite phases.[387,392] According to the three-dimensional model proposed (as shown in Fig. 1.1), the hard and soft grains are in contact with each other, which can be divided into two parts: an inner part without exchange-coupling interaction (uncoupled) and an interfacial part with exchange-coupling interaction (coupled). Therefore, the exchange-coupling interaction only influences the interface layer which is basically equal to the exchange-length, and there is no exchange-coupling interaction in the inner part of grains.
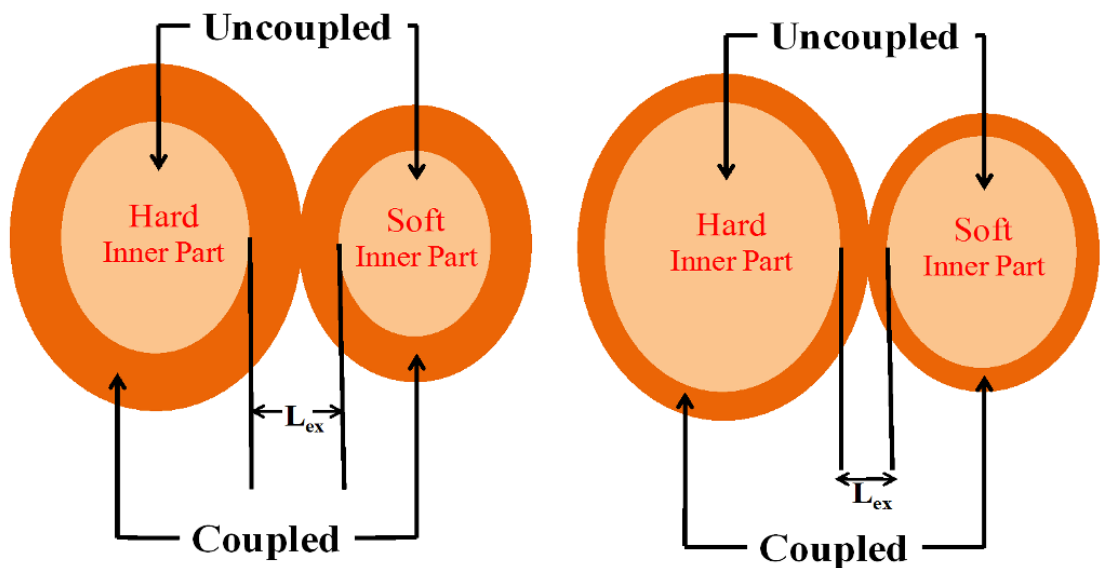
Fig. 1.1 Representation of the three-dimensional model of exchange coupling interactions for hard-soft magnetic grains.

There will be stronger exchange coupling interaction at the interface if the grain size is smaller.[388,390] The range of the exchange–coupling interaction between the grains of hard and soft magnetic phases, i.e., the exchange length, $L_{ex}$, can be expressed as [392]

$$L_{ex} = \left(\frac{A}{K}\right)^{1/2} \qquad (1.1)$$

Where, A and K signify the exchange stiffness and the mean amplitude of the random effective anisotropy constant, respectively. The value of K could be related to the ratio of the grain size to the exchange length by the following equation:

$$K = K1 \left(\frac{D}{L_{ex}}\right)^{3/2} \qquad (1.2)$$

Where, K1 is the first common anisotropy constant of material, D is the diameter of grain. Combination of equation (1.1) and (1.22) results in the following relation:

$$L_{ex} = \frac{A^2}{K^2 D^3} \qquad (1.3)$$

So, larger grain size reduces the exchange length and as a result the coupled regions. In this situation, there is no efficient exchange coupling between hard and soft grains and magnetic properties are controlled mostly by dipolar interaction among soft and hard grains leading to decrement in the remanence and coercive fields. This is due to an inner part for both hard and soft grains without exchange-coupling interaction, which dipolar interaction plays a major role in these uncoupled areas.

## 1.6.2 Applications of hard-soft ferrite nanocomposite

Recently, technologists are exploiting Ferrites as an important class of magnetic materials which exhibit microwave absorption property.[11, 393-405] Microwave-absorbing materials have gained immense interest to the scientists and technologists due to their usage in military application and also commodity markets. Microwave-absorbing materials could be used in stealth defence system because they can effectively reduce the radar cross-section of targets. These materials also have the potential to address the issues related to environmental pollution caused by the Electromagnetic Interference (EMI) due to extensive use of electronic devices, computer networks, mobile phones etc.[387, 388, 406-410] Hence, reduction of interference of electromagnetic radiation, mainly microwave radiation, is highly desirable in current scenario. Therefore, there has been a great deal of interest to develop microwave radiation absorbing materials. The microwave absorbing materials which operate in the frequency range 8.2- 12.4 GHz (X-band) region is also known as radar absorbing material (RAM) and find wide range of applications including electronic devices, military equipment, etc. Researchers are showing their specific concern on development of efficient RAM from last few decades. Various types of materials such as dielectric, magnetic, conducting polymer or composites have been investigated by the scientists to achieve RAMs with desired properties.[411-422]

There is a great demand of radar absorbing material which can offer (i) stability of high temperature (ii) light weight (iii) easy fabrication into various shapes (iv) resistance to corrosion (v) flexibility (vi) can be used as coating materials. However, it is difficult for a single material to fulfil the requirements (such as large absorption peak, wide working frequency range and thin absorption layer) of an ideal radar absorber. Spinel ferrites are used in megahertz range due to their Snoek limitation and hexaferrites exhibit microwave absorption in gigahertz range though band width is narrow.[13, 423, 424] Nanocomposites consist of hard and soft ferrite phase, can offer to construct unified systems whose properties are complimentary or even mutually exclusive. In the hard-soft ferrite nanocomposites, hard ferrite phase and soft ferrite phase are coupled to each other by an exchange through interfacial interaction which influences the relative complex permeability of the materials.[388] Interfacial interaction between the two phases is one of the important factors for the microwave absorption in the GHz frequency range.[387] The interfacial multipoles in nanocomposite causes the surface spin of ferrite nanoparticles disordered, which leads to high magnetic loss i.e. better microwave absorption. According to Maeda et al.[391] the exchange interaction between hard and soft ferrite phases can enhance the microwave absorption properties.

The exchange spring behaviours of some metal alloy systems and multilayer systems (such as $Pr_2Fe_{12}B$,[425] Nd-Fe-B,[426] Sm-Co/Fe,[427] $SmCo_x$-Co,[428] $BaCo_2Fe_{16}O_{27}$ or $Ba_2Co_2Fe_{12}O_{22}$ -FeCo alloy,[429] $BaFe_{12}O_{19}/\alpha$-Fe.[430] etc.) have been reported by researchers. Compare to metallic systems, nanocomposites composed of soft spinel ferrite and hard hexagonal ferrite, have shown their potential to be a promising candidate for superior permanent magnet, because of their low cost, excellent corrosion resistance behaviour and high electrical resistivity. However, best of our knowledge reports on soft- hard ferrite nanocomposites are very limited in the literature,[261, 387, 388, 431-435] due to lack of availability of simple preparation techniques. Most of the reported methods are complex in nature and require high sintering temperatures. Roy et al. have reported preparation of NiZn ferrite-barium ferrite composite, where NiZn ferrite and barium ferrite were prepared separately by coprecipitation method and high temperature solid state method (sintered at 1200 °C) respectively. NiZn ferrite and barium ferrite powders were then mixed in appropriate weight ratios and heat treated at different temperatures ranging from 400 to 800 °C.[433] They have also reported the preparation of $BaCa_2Fe_{16}O_{27}$- $Fe_3O_4$ composites, where $BaCa_2Fe_{16}O_{27}$ was prepared by citrate method and commercial grade $Fe_3O_4$ was procured.[432] Chen et al.[390] have employed citrate based sol-gel

technique to synthesize composite powders with different weight ratios of strontium hexaferrite to zinc ferrite and studied their microwave absorption properties. Song et al.[431] have reported a sol-gel citrate route for preparation of $SrFe_{12}O_{19}$/ $Ni_{0.5}Zn_{0.5}Fe_2O_4$ hollow microfiber at 900 °C. Synthesis and microwave absorbing properties of nanocomposites consist of $BaFe_{12}O_{19}$ (BFO)/$Ni_{0.5}Zn_{0.5}Fe_2O_4$ (NZFO) ferrite microfibers with different mass ratios was investigated by Shen et al.[387] Xie et al.[435] have investigated Sr-Zn ferrite composites which were synthesized by chemical coprecipitation with two step sintering process at 700 °C for 6h and then 1000 °C for 2h. Tyagi et al.[388] have reported composite consists of strontium ferrite/Ni-Zn ferrite powders prepared by co-precipitation method and they have also studied its microwave absorption properties in X-band.

## 1.7 Gaps in existing research

Though, the concept of the exchange spring behavior has been experimentally investigated for a variety of systems in the form of bulk and multilayer films, the desire properties are still far from the prediction. Moreover, most of the investigations involve the study of magnetic spring exchange behavior of metallic systems, but this concept has not yet well explored for hard and soft ferrite nanocomposites. One of the major reasons is the non availability of simple chemical methodology to prepare hard and soft ferrite nanocomposites.

Moreover, the magnetic properties of the magnetic materials are determined by both intrinsic magnetic property as well as micro-structural properties. So, grain size, particle shape, grain boundary type, etc. are important parameters. As far as composites are concerned, in addition to these properties, the distribution of magnetic hard and soft phases determines the magnetic property of the composites. So, synthesis route plays an important role in determining the magnetic properties of the synthesized nanocomposites. For the fabrication of exchange spring magnet, it is required to achieve high level of homogenous mixing of the hard and soft ferrite phase.

To the best of our knowledge from literature survey, not many reports are available on synthesis of hard-soft ferrite composites. Most of the researchers, have prepared hard ferrites (e.g., $BaFe_{12}O_{19}$, $SrFe_{12}O_{19}$ etc.) and soft ferrite ($Ni_xZn_{(1-x)}Fe_2O_4$, $ZnFe_2O_4$ etc.) separately and then mixed these two ferrites by using physical mixing method (such as ball milling) and sintered the mixture at a very high temperature (> 1200 °C). However, nanocomposites,

prepared by this method, suffer from lack of homogeneous mixing of ferrite phases. So, quite often poor exchange spring coupling between hard and soft magnetic phase was observed. High level of homogenous mixing of the hard and soft ferrite phases is possible when both the phases can be grown together from the same reaction mixture. Thus, there is a need to develop a simple 'one-pot' synthesis method for preparation of hard-soft ferrite nanocomposites, where soft ferrite phase and hard ferrite phase can be formed together from the same reaction mixture. As the two ferrite phases form in the same time from the same reaction mixture, better homogeneous mixing of hard and soft ferrite is expected and for this reason, the synthesized nanocomposites should exhibit good single phase magnetic spring coupled behavior with superior magnetic and microwave absorption properties.

Recently, we have reviewed different synthetic methods, which are employed for the preparation of different ferrites and various applications of ferrites.[395] Based on literature survey, it has also been found that, though conventional wet chemical methods are capable of producing ferrite nanoparticles but they are also associated with some inherent limitations such as (i) use of expensive metal alkoxides or complex metal compounds, (ii) use of delicate reagents which are difficult to handle, (iii) frequent use of strong acids/bases and organic solvents, (iv) formation of heterogeneous/undesirable crystalline phases (v) requirement of elaborate experimental setup and time consuming processes.

A synthesis method becomes highly effective if it is versatile in terms of producing nanomaterials with wide range of compositions at relatively lower temperature in a cost-effective and time-efficient manner without using any elaborate experimental set up. Therefore, development of a technically simple but cost-effective synthetic methodology for preparation hard-soft ferrite nanocomposites is the objective for the present research work.

_____

## 1.8 Objectives

(1) Development of a simple but cost-effective Ethylenediamine tetraacetic acid (EDTA) precursor based 'one-pot' method for synthesis of hard-soft ferrite nanocomposites having various compositions (such as $(BaFe_{12}O_{19})_{1-x}$-$(NiFe_2O_4)_x$, $(SrFe_{12}O_{19})_{1-x}$-$(NiFe_2O_4)_x$, $(BaFe_{12}O_{19})_{1-x}$-$(Ni_{0.65}Zn_{0.35}Fe_2O_4)_x$, $(SrFe_{12}O_{19})_{1-x}$-$(Ni_{0.65}Zn_{0.35}Fe_2O_4)_x$, $(BaFe_{12}O_{19})_{1-x}$-$(Mn_{0.2}Ni_{0.4}Zn_{0.4}Fe_2O_4)_x$, $(SrFe_{12}O_{19})_{1-x}$-$(Mn_{0.2}Ni_{0.4}Zn_{0.4}Fe_2O_4)_x$).

(2) Structural characterization of the synthesized nanocomposites by using X-Ray Diffraction (XRD), Thermogravimetric Analysis (TGA), Differential Scanning Calorimetry (DSC), Scanning Electron Microscopy (SEM) and Transmission Electron Microscopy (TEM).

(3) Preparation and structural characterizations of the above mentioned composites by employing "Physical Mixing" method.

(4) Investigations on magnetic (e.g., saturation magnetization, coercivity) and microwave absorption properties of the prepared nanocomposites.

(5) Comparison of magnetic and microwave absorption properties of the composites, prepared by one-pot and physical mixing method.

## 1.9 Characterization Details

The as synthesized nanocomposites were characterized by the following techniques:

**a) Thermal Analysis**:

Thermogravimetric analysis (TGA) and differential scanning calorimetric (DSC) analysis were carried out on the precursor using a DTG-60 and a DSC-60 (Shimaduzu, Japan) respectively in air flow at a heating rate of 10 °C/ min between 30 to 550 °C. Aluminium and Platinum sample pans were used for DSC and TGA respectively.

**b) X-Ray Diffraction (XRD) Analysis:**

Room temperature X-ray diffraction spectra of the precursors and the calcined powders were recorded by using a powder X-Ray diffractometer (Mini Flex II, Rigaku, Japan) with Cu Kα ($\lambda$ = 0.15405 nm) radiation. The sampling speed was 2°/minute and sampling width was 0.01°. The slow scans were performed with a sampling speed of 1.2°/min and a sampling width of 0.02°.

_____

**c) Transmission Electron Microscopy (TEM) Analysis:**

Transmission Electron Microscopic (HRTEM) (JEOL JEM 1400, Japan) images of samples was employed to analyze the shape and size of the synthesized nanocomposites.

**d) Scanning Electron Microscopy (SEM) Analysis:**

Morphology of the nanocomposites, prepared by one-pot method and physical method, was studied using Scanning Electron Microscope (SEM) (JSM-6360LV, JEOL, Japan) using an accelerating voltage of 15 kV. Elemental analysis of the composites was performed using Energy Dispersive X-Ray analysis (EDX) which was attached with SEM.

**e) Magnetization Measurement:**

Room temperature magnetization with respect to external magnetic field was measured for the synthesized composites by using a vibrating sample magnetometer (EV5, ADE Technology, USA). The applied field varied between -15kOe to +15kOe.

**f) Microwave absorption Measurement:**

For measurement of the microwave absorption of the synthesized nanocomposites in X-band (8.2-12.4 GHz range), HP 8510 vector Network Analyzer (USA) was used and reflection loss (RL) was calculated using the measured values of complex permittivity and permeability. For this purpose nanocomposite powders were mixed with a binder (aqueous solution of 10 wt. % polyvinyl alcohol (PVA)) and the mixture was dried. This mixture was further ground and was compressed under a pressure of 10 tons and shaped into rectangular pellets with size of 10.16 mm x 22.86 mm x 2mm, so as to fit exactly into a rectangular waveguide of X-band.

The reflection loss (RL) was calculated from the complex relative permeability and permittivity at a given frequency and specimen thickness using a model of single-layered plane wave absorber, proposed by Naito and Sutake.[436]

$$Z_{in} = Z_0 (\mu_r / \varepsilon_r)^{1/2} \tan h \left[ j \left( \frac{2\pi f d}{c} \right) (\mu_r . \varepsilon_r)^{1/2} \right] \qquad (1.4)$$

$$RL = 20 \log \left| \frac{Z_{in} - Z_0}{Z_{in} + Z_0} \right| \qquad (1.5)$$

Where, $\mu_r = \mu' - j\mu''$ and $\varepsilon_r = \varepsilon' - j\varepsilon''$ are the relative complex permeability and permittivity of the absorber medium, respectively, $f$ is the frequency of the electromagnetic wave, $d$ is the

absorber thickness, c is the velocity of light, $Z_0$ is the free space impedance, and $Z_{in}$ is the absorber impedance.

In order to analyze the change of microwave absorption properties with thickness of the absorber, the reflection loss was calculated using equations (1.4) and (1.5) for different absorber thickness.

**1.10 Outlay of thesis**

The thesis is divided into eight chapters and each chapter is followed by a summary.

In Chapter 1, the subject of synthesis and applications of ferrite, hard-soft ferrite nanocomposites and spring exchange coupling, identification of research gaps based on literature review and the objective of the present research work have been discussed.

Chapter 2, Synthesis and characterization of $(BaFe_{12}O_{19})_{1-x}$-$(NiFe_2O_4)_x$ nanocomposites and study of their magnetic and microwave absorption properties.

Chapter 3, Synthesis and characterization of $(SrFe_{12}O_{19})_{1-x}$-$(NiFe_2O_4)_x$ nanocomposites and study of their magnetic and microwave absorption properties.

Chapter 4, Synthesis and characterization of $(BaFe_{12}O_{19})_{1-x}$-$(Ni_{0.65}Zn_{0.35}Fe_2O_4)_x$ nanocomposites and study of their magnetic and microwave absorption properties.

Chapter 5, Synthesis and characterization of $(SrFe_{12}O_{19})_{1-x}$-$(Ni_{0.65}Zn_{0.35}Fe_2O_4)_x$ nanocomposites and study of their magnetic and microwave absorption properties.

Chapter 6, Synthesis and characterization of $(BaFe_{12}O_{19})_{1-x}$-$(Mn_{0.2}Ni_{0.4}Zn_{0.4}Fe_2O_4)_x$ nanocomposites and study of their magnetic and microwave absorption properties.

Chapter 7, Synthesis and characterization of $(SrFe_{12}O_{19})_{1-x}$-$(Mn_{0.2}Ni_{0.4}Zn_{0.4}Fe_2O_4)_x$ nanocomposites and study of their magnetic and microwave absorption properties.

In Chapter 8, the conclusions and future scope of research work have been presented.

# Chapter 2

# Synthesis and characterization of (BaFe$_{12}$O$_{19}$)$_{1-x}$-(NiFe$_2$O$_4$)$_x$ nanocomposites and study of their magnetic and microwave absorption properties

## 2.1 Experimental procedure

### 2.1.1 Materials required

BaCO$_3$, Ni(NO$_3$)$_2$.6H$_2$O, Fe(NO$_3$)$_3$.9H$_2$O, Nitric Acid and Ethylene diamine tetra acetic acid (EDTA) were purchased from Merck, India and used without further purification. Ba(NO$_3$)$_2$ was prepared by dissolving BaCO$_3$ in aqueous nitric acid.

### 2.1.2 Synthesis of (BaFe$_{12}$O$_{19}$)$_{1-x}$-(NiFe$_2$O$_4$)$_x$ nanocomposites by one-pot method (OP Method) [261]

To prepare (BaFe$_{12}$O$_{19}$)$_{1-x}$-(NiFe$_2$O$_4$)$_x$ nanocomposites (with x= 0.85, 0.75, 0.5 and 0.25) using one-pot method stoichiometric amount of aqueous solutions of Ba(NO$_3$)$_2$, Ni(NO$_3$)$_2$.6H$_2$O, Fe(NO$_3$)$_3$.9H$_2$O and ethylene diamine tetra acetic acid (EDTA) were mixed in a beaker (Table 2.1) and stirred for 2 h. This reaction mixture was then dried at ~110 $^0$C for 2 h. Black colour floppy carbonaceous material was formed after drying, which we refer as precursor powder. The precursor powders thus formed were calcined at 800 °C for 4 h in air atmosphere to obtain (BaFe$_{12}$O$_{19}$)$_{1-x}$-(NiFe$_2$O$_4$)$_x$ nanocomposites.

### 2.1.3 Synthesis of (BaFe$_{12}$O$_{19}$)$_{1-x}$-(NiFe$_2$O$_4$)$_x$ nanocomposites by physical mixing method (PM Method)

A set of composite samples with various composition (with x= 0.85, 0.75, 0.5 and 0.25) was prepared by using 'physical mixing' method where pure NiFe$_2$O$_4$ and BaFe$_{12}$O$_{19}$ powders were mixed with appropriate weight ratio (Table 2.1) using a mortar pestle. Pure BaFe$_{12}$O$_{19}$ and NiFe$_2$O$_4$ nanopowders were prepared separately by using the EDTA-precursor method which has been developed by us.[254, 255] For synthesis of BaFe$_{12}$O$_{19}$, stoichiometric amounts of barium nitrate and ferric nitrate were dissolved in distilled water according to the molar ratio of 1:12, as shown in Table 2.1. An aqueous solution of EDTA was prepared by dissolving

EDTA in hot water with drop wise addition of NH$_4$OH. After complete dissolution of EDTA, the solution was boiled to remove the excess NH$_3$. The pH of the solution was ~6. Aqueous solutions of metal nitrates and EDTA were mixed in a molar ratio of 1: 4 and stirred for 1 h at room temperature using a magnetic stirrer. pH of the resulting mixture was ~2. Black colored precursor was formed when the mixture was evaporated to dryness on a hot plate at ~110 °C. The precursor powder was then calcined in air for 4 h at 800 °C to obtain BaFe$_{12}$O$_{19}$ nanopowder. To prepare NiFe$_2$O$_4$ nanopowders, we have used Fe(NO$_3$)$_3$.9H$_2$O, Ni(NO$_3$)$_2$.6H$_2$O as starting materials and water as solvent. Stoichiometric amounts of metal nitrates were dissolved in distilled water according to the molar compositions as shown in Table 2.1. The aqueous solutions of metal nitrates and EDTA were mixed in a molar ratio of 1:1 and stirred for 1 h at room temperature using a magnetic stirrer. The pH of the reaction mixture was found to be ~2. Dark brown colored precursors were formed when the reaction mixtures were evaporated to dryness on a hot plate at 125 °C. Partial decomposition of the precursors was observed during drying. The precursor powders were then calcined in air for 4h at 550 °C to obtain pure NiFe$_2$O$_4$ nanopowders.

Table 2.1 Starting materials required for preparation of (BaFe$_{12}$O$_{19}$)$_{1-x}$-(NiFe$_2$O$_4$)$_x$ nanocomposites

| Composition | *Ba-carbonate (g) | *Ni$^{II}$-nitrate (g) | *Fe$^{III}$-nitrate (g) | *EDTA (g) | **NiFe$_2$O$_4$ (g) | **BaFe$_{12}$O$_{19}$ (g) |
|---|---|---|---|---|---|---|
| NiFe$_2$O$_4$- pure | - | 1.24 | 3.45 | 3.93 | -- | -- |
| (BaFe$_{12}$O$_{19}$)$_{0.15}$-(NiFe$_2$O$_4$)$_{0.85}$ | 0.08 | 0.675 | 3.86 | 14.38 | 0.544 | 0.466 |
| (BaFe$_{12}$O$_{19}$)$_{0.25}$-(NiFe$_2$O$_4$)$_{0.75}$ | 0.109 | 0.481 | 4.01 | 17.80 | 0.387 | 0.613 |
| (BaFe$_{12}$O$_{19}$)$_{0.50}$-(NiFe$_2$O$_4$)$_{0.50}$ | 0.147 | 0.216 | 4.20 | 17.45 | 0.178 | 0.822 |
| (BaFe$_{12}$O$_{19}$)$_{0.75}$-(NiFe$_2$O$_4$)$_{0.25}$ | 0.166 | 0.082 | 4.30 | 17.28 | 0.065 | 0.935 |
| BaFe$_{12}$O$_{19}$- pure | 0.177 | - | 4.365 | 17.17 | -- | -- |

* One-pot method

** Physical mixing method

From now onwards, nanocomposites prepared by one-pot method and physical mixing method will be referred as 'nanocomposites-OP' and 'nanocomposites-PM' respectively.

_____

## 2.2 Results and Discussion

### 2.2.1 Thermal analysis

To find out the thermal decomposition behavior of precursors, prepared by OP method, TGA and DSC analysis were used. Thermogram of precursor powder (Fig. 2.1) revealed that a total weight loss of ~95 % occurred when the precursor powder was heated from 30 to 550 °C in air. Initially, ~2 % weight loss occurred in the region of 40 to 100 °C due to loss of moisture from the sample. Then, ~93 % weight loss was observed in the temperature range of 250 to 450 °C. This might be due to the oxidative decomposition of precursor and evolution of $CO_2$ and $NO_x$ gases. This decomposition was also observed in DSC thermogram as an exothermic peak at 445 °C. No weight loss was observed in TGA when the sample was heated beyond 450 °C. This confirmed the full decomposition of carbonaceous mass of the precursor occurred within 450 °C.
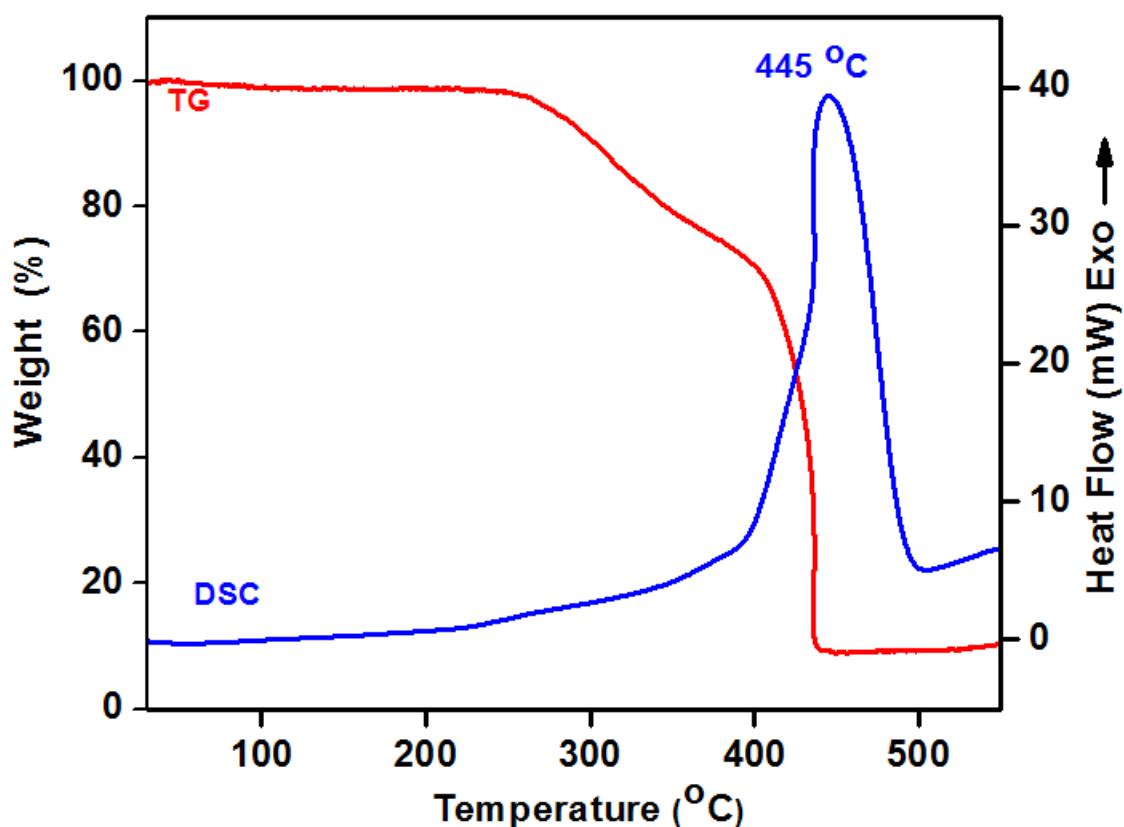


Fig. 2.1 TGA- DSC thermogram of (BaFe$_{12}$O$_{19}$)$_{0.5}$-(NiFe$_2$O$_4$)$_{0.5}$ precursor.

_____

**2.2.2 X-Ray Diffraction analysis**

The XRD spectra of the calcined powders of $(BaFe_{12}O_{19})_{1-x}$-$(NiFe_2O_4)_x$ nanocomposites, obtained by calcining the precursors (prepared by OP method) at 800 °C for 4 h exhibited diffraction peaks corresponding to both $NiFe_2O_4$ [ICDD card number 54-0964] and $BaFe_{12}O_{19}$ [ICDD card number 84-0757] phase (Fig. 2.2 (A) and (B)). XRD patterns indicated the coexistence of both the phases in the synthesized composite powders. We did not observe any impurity peak within the resolution of the technique. It was also observed that the highest intensity peak of $NiFe_2O_4$ at $2\theta = 35.6°$ (corresponding to (311) plane) has increased with increasing the amount of $NiFe_2O_4$ in the composite (i.e., with increasing the value of x). Same observation was also found for $BaFe_{12}O_{19}$ (Fig. 2.2 (B)). XRD patterns of composites, prepared by physical mixing, also showed the presence of both the phases. However, difference in relative intensities of the diffraction peaks for these two types of samples was observed. This might be because of difference in growth of $NiFe_2O_4$ and $BaFe_{12}O_{19}$ phase, crystallite size and their distribution in these two types of composite samples, which were prepared by two different methods. The average crystallite sizes of $NiFe_2O_4$ and $BaFe_{12}O_{19}$ phases in the $(BaFe_{12}O_{19})_{1-x}$-$(NiFe_2O_4)_x$ nanocomposites were calculated by X-ray peak-broadening method using Scherrer's equation[437] and listed in Table 2.2. For this purpose the diffraction peaks for (311) plane for $NiFe_2O_4$ and (114) plane for $BaFe_{12}O_{19}$ were used. The notable feature was that, in $(BaFe_{12}O_{19})_{1-x}$-$(NiFe_2O_4)_x$ nanocomposites (prepared by one-pot method), the crystallite size of $NiFe_2O_4$ phase was increased from 10.2 to 38 nm with increasing amount of $NiFe_2O_4$ phase (from 0.25 to 1) in the composite. The same trend was observed for $BaFe_{12}O_{19}$ phase and its crystallite size was found to be increased from 24 to 43 nm. On the contrary, in case of the $(BaFe_{12}O_{19})_{1-x}$-$(NiFe_2O_4)_x$ nanocomposites (synthesized by physical-mixing method) the crystallite sizes of both $NiFe_2O_4$ and $BaFe_{12}O_{19}$ phase did not change with changing amount of $NiFe_2O_4$ and $BaFe_{12}O_{19}$ phases in the composites and was found to be ~38 and~43 nm for $NiFe_2O_4$ and $BaFe_{12}O_{19}$ respectively for all compositions. These values were almost same in comparison with the crystallite sizes of pure $NiFe_2O_4$ and $BaFe_{12}O_{19}$ nanopowders. These values were almost same in comparison with the crystallite sizes of pure $NiFe_2O_4$ and $BaFe_{12}O_{19}$ nanopowders which imply that the pure phases retain their individual crystalline behaviours in the composites.
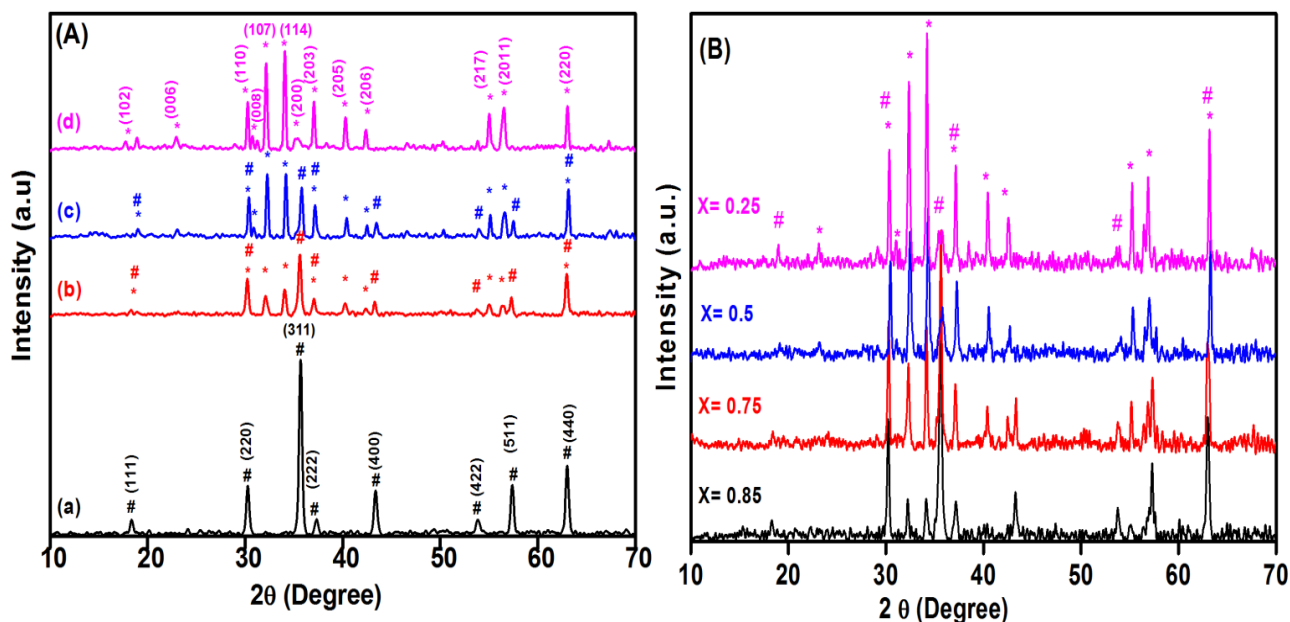
Fig. 2.2 (A) XRD spectra of the (a) pure $NiFe_2O_4$, $(BaFe_{12}O_{19})_{0.25}$-$(NiFe_2O_4)_{0.75}$ nanocomposites prepared by (b) one-pot, (c) physical mixing methods and (d) $BaFe_{12}O_{19}$ nanopowders, (B) XRD spectra of $(BaFe_{12}O_{19})_{1-x}$-$(NiFe_2O_4)_x$ nanocomposites synthesized by one-pot method (#$NiFe_2O_4$ and *$BaFe_{12}O_{19}$).

Table 2.2 Average crystalline size of $(BaFe_{12}O_{19})_{1-x}$-$(NiFe_2O_4)_x$ nanocomposites prepared by one-pot and physical mixing method

| Sample | Crystallite size (nm) | | | |
|---|---|---|---|---|
| | One-pot synthesis | | Physical mixing synthesis | |
| | *(114)plane | #(311)plane | *(114)plane | #(311)plane |
| $NiFe_2O_4$- pure | -- | 38 | --- | 38 |
| $(BaFe_{12}O_{19})_{0.15}$-$(NiFe_2O_4)_{0.85}$ | 24 | 26 | 44 | 39 |
| $(BaFe_{12}O_{19})_{0.25}$-$(NiFe_2O_4)_{0.75}$ | 27 | 22 | 42 | 40 |
| $(BaFe_{12}O_{19})_{0.50}$-$(NiFe_2O_4)_{0.50}$ | 38 | 12.8 | 45 | 38 |
| $(BaFe_{12}O_{19})_{0.75}$-$(NiFe_2O_4)_{0.25}$ | 40 | 10.2 | 43 | 38 |
| $BaFe_{12}O_{19}$- pure | 43 | -- | 43 | -- |

*For $BaFe_{12}O_{19}$
#For $NiFe_2O_4$

_____

## 2.2.3 TEM and SEM analysis

During investigations on morphology of two different types of nanocomposites (prepared by PM and OP method) by HRTEM (Fig. 2.3) two distinct types of microstructures were observed.
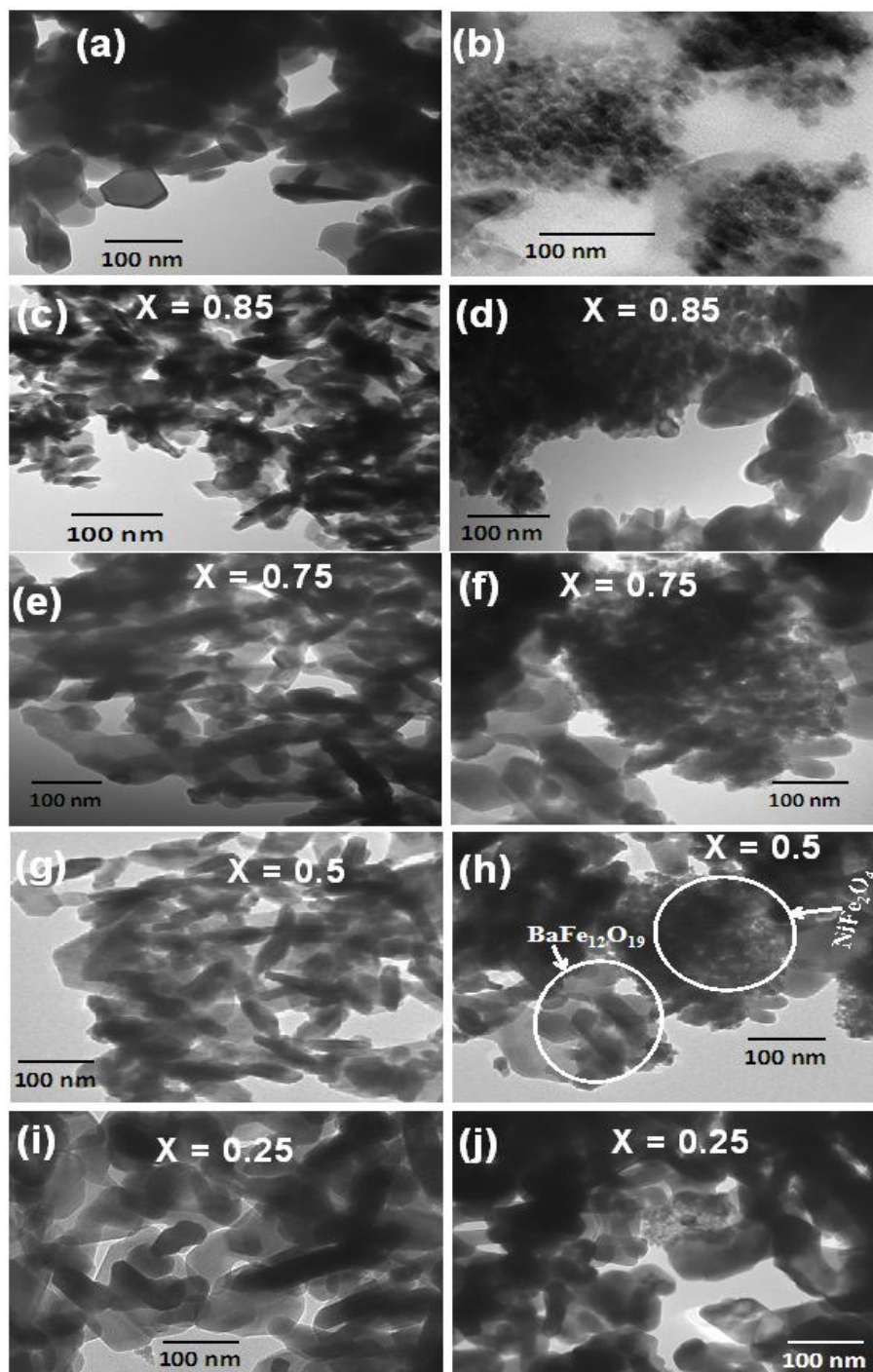


Fig. 2.3 TEM micrographs of (a) pure BaFe$_{12}$O$_{19}$, (b) pure NiFe$_2$O$_4$ nanopowders and (BaFe$_{12}$O$_{19}$)$_{1-x}$-(NiFe$_2$O$_4$)$_x$ nanocomposites synthesis by (c, e, g, i) one-pot and (d, f, h, j) physical mixing method.

_____

In case of the nanocomposites-PM ((Fig. 2.3 (d, f, h, j)), clear segregation of spherical agglomerated NiFe$_2$O$_4$ nanoparticles (~20 nm average particle size, Fig. 2.3 (a)) and hexagonal BaFe$_{12}$O$_{19}$ nanoparticles (~50-70 nm average particle size, Fig 2.3 (b)) were observed. On the contrary, when nanocomposites were prepared by one-pot method, almost uniform shaped nanoparticles with average particle size ~60-70 nm were formed (Fig. 2.3 (c, e, g, i)).

SEM micrographs of the composites also revealed the intimate coexistence of NiFe$_2$O$_4$ and BaFe$_{12}$O$_{19}$ particles in the nanocomposites-OP (Fig. 2.4 (c)) and presence of large BaFe$_{12}$O$_{19}$ (Fig. 2.4 (b)) and small NiFe$_2$O$_4$ (Fig. 2.4 (a)) particles in the nanocomposites prepared by physical mixing method (Fig. 2.4(d)).
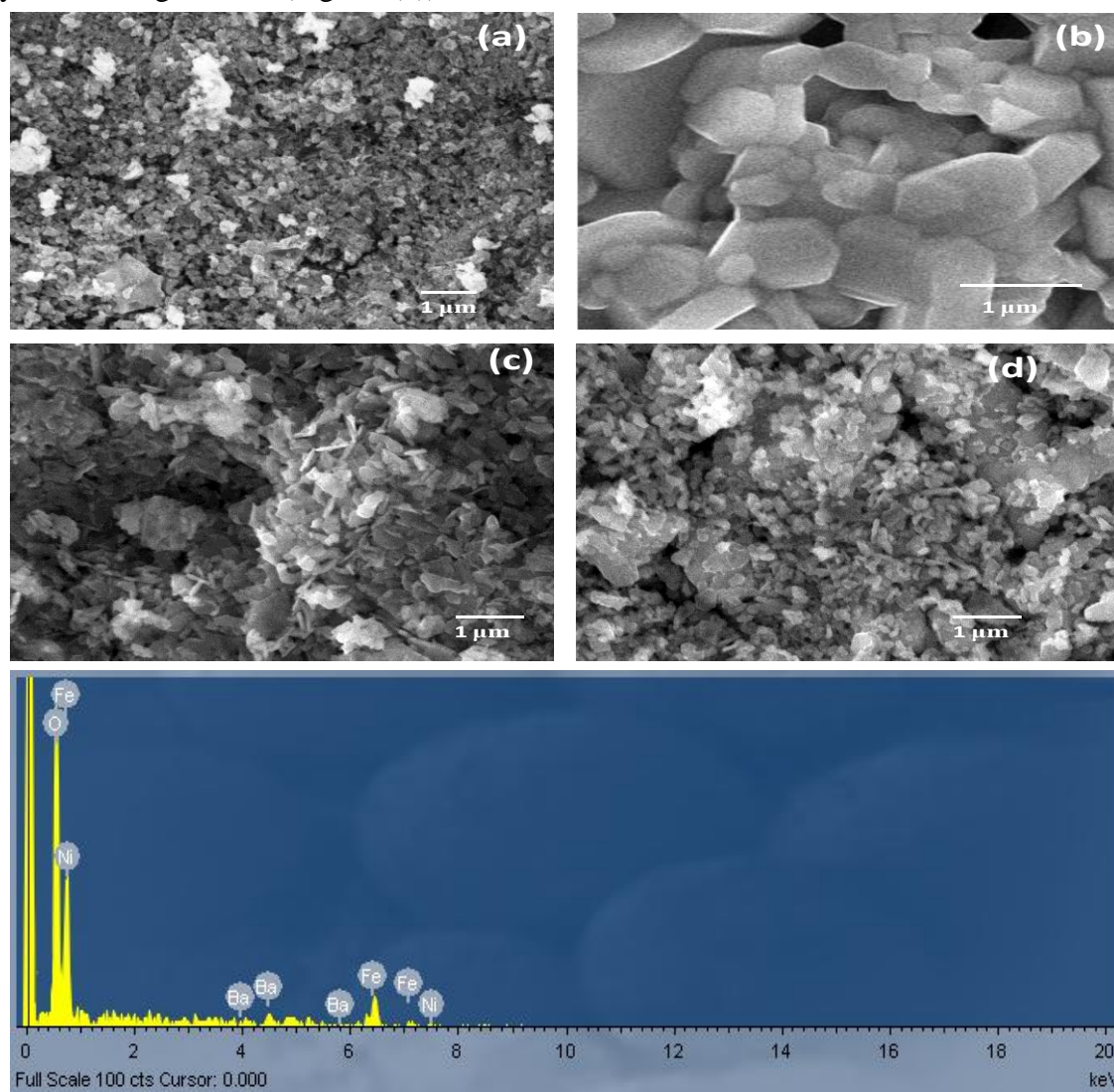


Fig. 2.4 SEM micrographs of (a) pure NiFe$_2$O$_4$, (b) Pure BaFe$_{12}$O$_{19}$ and (BaFe$_{12}$O$_{19}$)$_{0.5}$-(NiFe$_2$O$_4$)$_{0.5}$ nanocomposites prepared by (c) one-pot, (d) physical mixing method and (e) EDX spectra of (BaFe$_{12}$O$_{19}$)$_{0.5}$-(NiFe$_2$O$_4$)$_{0.5}$ nanocomposite prepared by one-pot method.

Electron microscopic analysis confirmed that, the nanocomposites synthesized by one-pot method possess high level of homogeneous mixing of NiFe$_2$O$_4$ and BaFe$_{12}$O$_{19}$ phase than the composites prepared by physical mixing method. This difference in morphology of the samples may influence the magnetic and microwave absorption properties of the nanocomposites.

From thermal, XRD, and microscopic analysis it was confirmed that, in one-pot synthesis route calcination of precursor powder leads to formation of (BaFe$_{12}$O$_{19}$)$_{1-x}$-(NiFe$_2$O$_4$)$_x$ nanocomposites. Precursor powders are prepared by mixing aqueous solution of metal nitrate with EDTA followed by drying of reaction mixture. EDTA, which is a strong multidentate chelating agent, plays a critical role in formation nanocomposites. It not only prevents the segregation or intermittent precipitation of metal ions from solution during evaporation but also helps the formation of a fluffy, voluminous, porous carbon-rich precursor. During decomposition of precursor, nascent metal oxides form which are basically small atomic cluster with proper chemical homogeneity, imbedded into the precursor. These nascent metal oxides finally produce desired composite powders[259, 438] when heat treated at 800 °C. Moreover, in any step of this synthesis method filtration or washing was not involved so, there was no chance to lose any metal ions from the composites. EDX analysis of the final nanocomposites also revealed that all the metal ions are present in the composites (Fig. 2.4 (e)). Hence, the final compositions of the composites are according to the molar compositions of the metal ions taken in the first step of the synthetic method.

### 2.2.4 Magnetic measurements

The room temperature magnetization behaviours of (BaFe$_{12}$O$_{19}$)$_{1-x}$-(NiFe$_2$O$_4$)$_x$ nanocomposites prepared by two different methods (OP and PM method) were measured using VSM with an applied field of 15000 Oe and shown in Fig. 2.5.
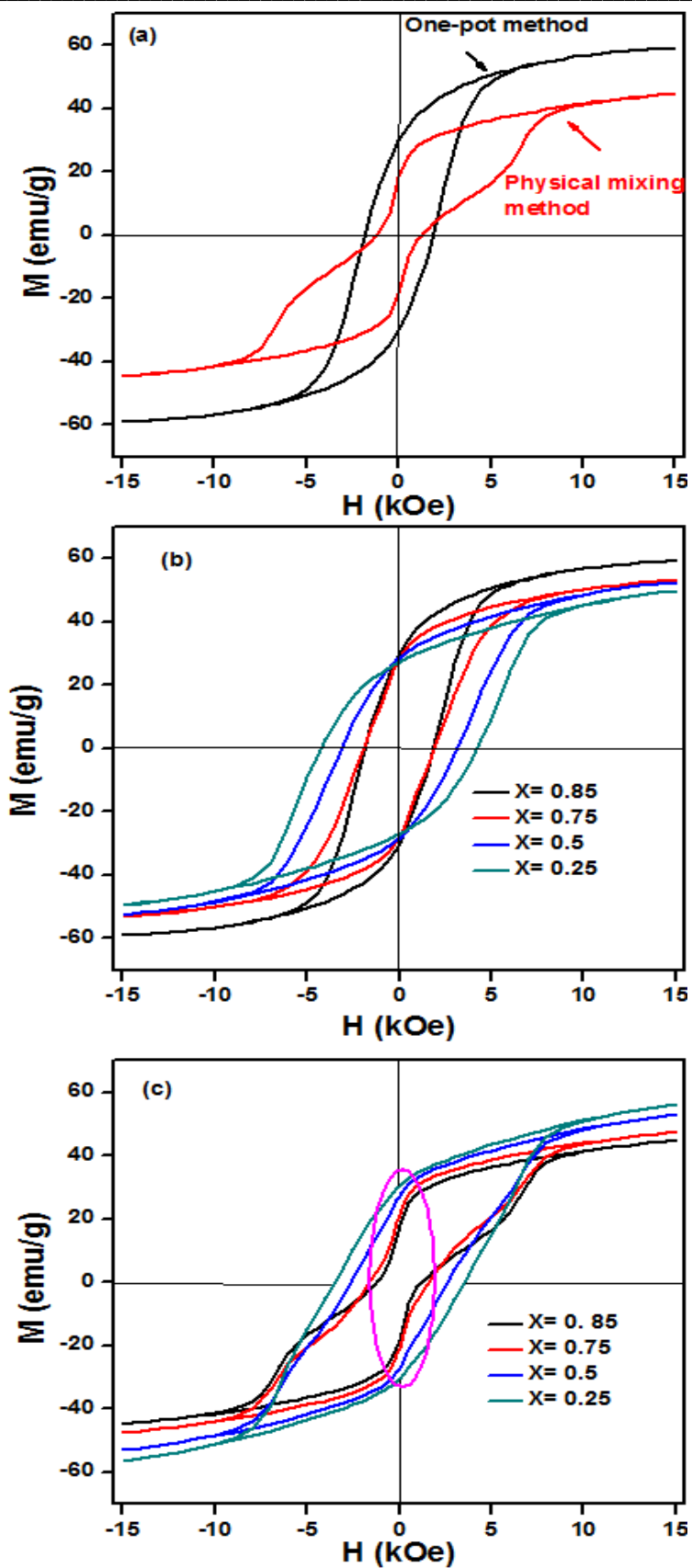
Fig. 2.5 Room temperature hysteresis loops for (a) (BaFe$_{12}$O$_{19}$)$_{0.15}$-(NiFe$_2$O$_4$)$_{0.85}$ nanocomposite prepared by one-pot and physical mixing method and (BaFe$_{12}$O$_{19}$)$_{1-x}$-(NiFe$_2$O$_4$)$_x$ nanocomposite prepared by (b) one-pot, (c) physical mixing method.

The most important observation from magnetic measurement was that, nanocomposites-OP showed single hysteresis loop, indicating hard and soft phases were well exchanged coupled to each other. Whereas, a typical two loop "bee waist" type hysteresis loop was observed in nanocomposites-PM (Fig. 2.5 (a)), suggesting the absence of exchange coupling between hard and soft phase.[387, 431-433] Hence, (BaFe$_{12}$O$_{19}$)$_{1-x}$-(NiFe$_2$O$_4$)$_x$ nanocomposites, prepared by one-pot method, though exhibited crystallographycally two phase behaviour but possessed magnetically good single phase behaviour. Fig. 2.5 (b) also reflects that all the composition of (BaFe$_{12}$O$_{19}$)$_{1-x}$-(NiFe$_2$O$_4$)$_x$ showed single hysteresis loop for composites synthesized by OP-method whereas two loop hysteresis behavior for nanocomposites-PM (Fig. 2.5 (c)).

It was observed that coercivity (H$_c$) values of the samples, prepared by both the methods, increased with increasing BaFe$_{12}$O$_{19}$ content in the sample (Table 2.3). For the saturation magnetization (M$_s$) values it was observed that, initially incorporation of BaFe$_{12}$O$_{19}$ phase caused enhancement of M$_s$, which is quite obvious due to the spring exchange coupling between hard and soft magnetic phases. However, with subsequent increase of BaFe$_{12}$O$_{19}$ phase in the (BaFe$_{12}$O$_{19}$)$_{1-x}$-(NiFe$_2$O$_4$)$_x$ nanocomposites (i.e., with increasing (1-x) values) M$_s$ remained almost same. But H$_c$ values of 'one-pot' samples were found to be larger than those of the samples prepared by physical mixing method.

According to Moon et al.[434] saturation magnetization of composites containing hard ferrite and soft ferrite without exchange coupling can be expressed as

$$M_s = M_{s,h}(1-f_s) + M_{s,s}.f_s \qquad (2.1)$$

Where, M$_{s,h}$ and M$_{s,s}$ corresponds to saturation magnetization of hard and soft ferrite respectively. f$_s$ = weight fraction (percentage) of soft ferrite phases. Theoretically calculated values of M$_s$ of the composites (when hard and soft phases are not exchange coupling) were almost matching with the experimentally obtained values of the composites prepared by physical mixing method (Table 2.3) which proves the absence of spring exchange coupling in the nanocomposite-PM.

_____

Table 2.3 $M_s$ and $H_c$ values of the $(BaFe_{12}O_{19})_{1-x}$-$(NiFe_2O_4)_x$ nanocomposites prepared by one-pot and physical mixing method

| Sample | One-pot synthesis | | Physical mixing synthesis | | Theoretical $M_s$ Without exchange coupling (emu/g) |
|---|---|---|---|---|---|
| | $H_c$ (Oe) | $M_s$ (emu/g) | $H_c$ (Oe) | $M_s$ (emu/g) | |
| $NiFe_2O_4$- pure | 158 | 30.7 | -- | -- | |
| $(BaFe_{12}O_{19})_{0.15}$-$(NiFe_2O_4)_{0.85}$ | 1646 | 59 | 1211 | 44.6 | 43 |
| $(BaFe_{12}O_{19})_{0.25}$-$(NiFe_2O_4)_{0.75}$ | 1916 | 53 | 1602 | 47.5 | 48.2 |
| $(BaFe_{12}O_{19})_{0.50}$-$(NiFe_2O_4)_{0.50}$ | 3136 | 52.6 | 2604 | 53 | 43.6 |
| $(BaFe_{12}O_{19})_{0.75}$-$(NiFe_2O_4)_{0.25}$ | 4251 | 50 | 3516 | 56.5 | 52.3 |
| $BaFe_{12}O_{19}$- pure | 4914 | 56.5 | -- | -- | |

## 2.2.5 Microwave absorption study

Microwave absorption behavior of $(BaFe_{12}O_{19})_{1-x}$-$(NiFe_2O_4)_x$ nanocomposites with different compositions (x= 0.85, 0.75, 0.5, 0.25) synthesized by one-pot method were investigated. Loss tangent vs. frequency were plotted to understand the particular loss mechanism for each nanocomposite and shown in Fig. 2.6 (a) and (b). The dielectric and magnetic loss tangents can be defined as $\tan\delta_\varepsilon = \varepsilon''/ \varepsilon'$ and $\tan\delta_\mu= \mu''/ \mu'$, respectively. Fig. 2.6 (b) shows that these composites are having only magnetic loss parameter whereas the dielectric loss parameter is negligible (Fig. 2.6 (a)).

Reflection loss (RL) was calculated using equations (1.4 and 1.5) and plotted against frequency for different $(BaFe_{12}O_{19})_{1-x}$-$(NiFe_2O_4)_x$ nanocomposites (x= 0.85, 0.75, 0.5, 0.25) synthesized by OP method for thickness 3 mm (Fig. 2.6 (c)). In RL vs frequency plot, the dip of the curves was designated for minimum RL indicating maximum absorption. It was observed that, with decreasing the value of x (i.e. increasing $BaFe_{12}O_{19}$ content in the nanocomposite) maximum absorption was decreases. As the composite having composition $(NiFe_2O_4)_{0.85}$-$(BaFe_{12}O_{19})_{0.15}$ exhibited minimum reflection loss (~ -10 dB) i.e. maximum absorption compare to other composites, so we have chosen this composition for further studies and the microwave absorption properties are compared with the nanocomposite prepared by PM method as well as pure $NiFe_2O_4$ and $BaFe_{12}O_{19}$.
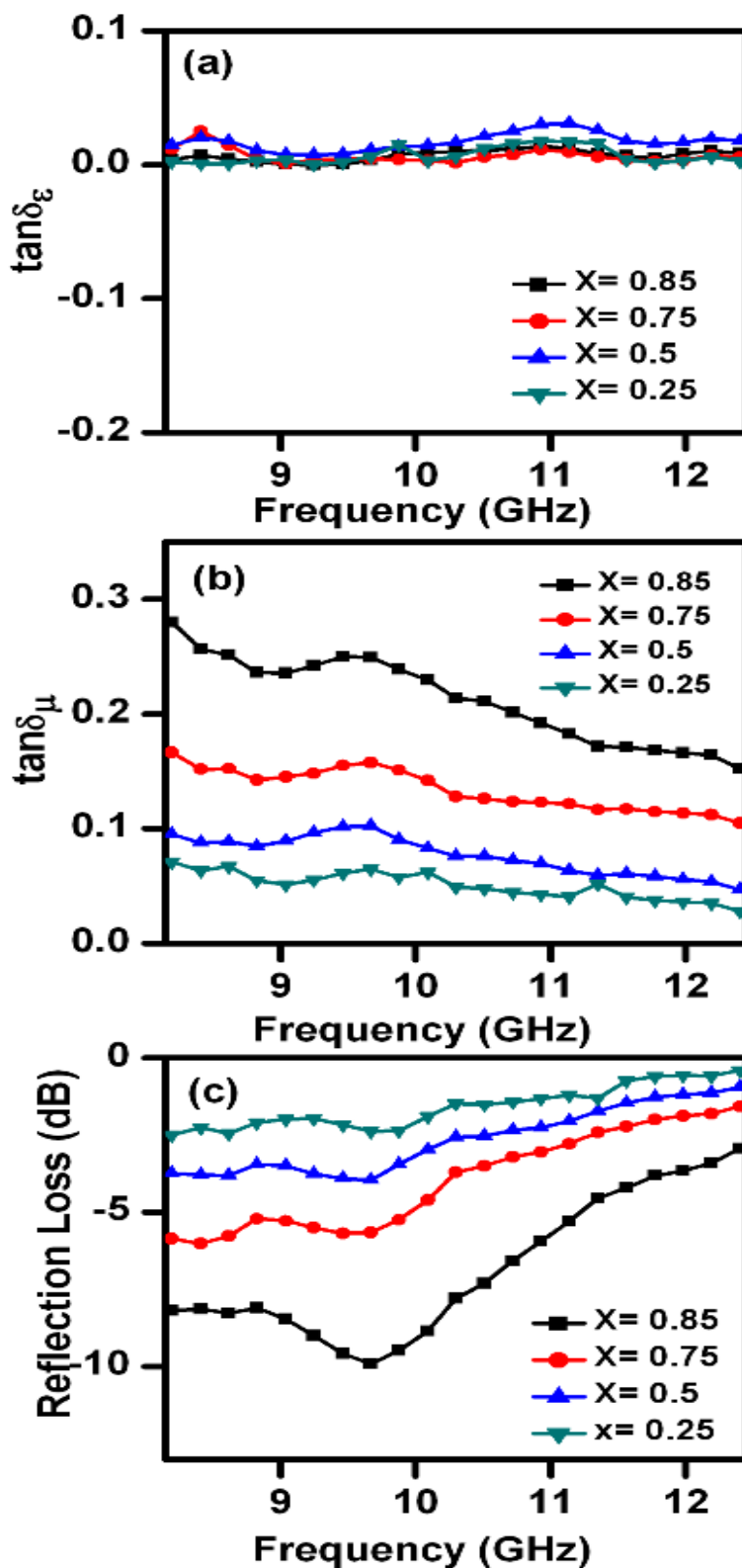
Fig. 2.6 (a) Loss Tangent of relative complex permittivity (tan$\delta_\varepsilon$), (b) Loss Tangent of relative complex permeability (tan$\delta_\mu$) and (c) Reflection loss vs. frequency plot (BaFe$_{12}$O$_{19}$)$_{1-x}$-(NiFe$_2$O$_4$)$_x$ nanocomposites synthesized by one-pot method.

The real and imaginary permittivity (Fig. 2.7 (a). and (b)) and permeability (Fig. 2.7 (c) and (d)) for the nanocomposites synthesized by both the methods, pure BaFe$_{12}$O$_{19}$ and NiFe$_2$O$_4$ nanopowders were plotted as a function of frequency in the X-band range (8.2- 12.4 GHz). It was observed that, $\varepsilon'$ values remained nearly constant over the entire frequency range. Both nanocomposites $\varepsilon'$ value was in between the pure BaFe$_{12}$O$_{19}$ and NiFe$_2$O$_4$ nanopowders (Fig. 2.7 (a)). For the nanocomposite-OP, the imaginary dielectric parameter ($\varepsilon''$) was almost remained constant throughout the entire X-band range (Fig. 2.7 (b)). The real permeability ($\mu'$) values of both the composite and pure nanopowders remained almost constant in the entire frequency range of X-band (Fig.2.7 (c)). The imaginary permeability ($\mu''$) values (Fig. 2.7 (d)) showed a decreasing tendency from 8.2 GHz to 12.4 GHz for both the nanocomposites and pure ferrites, however, maximum imaginary permeability was observed for the composite synthesized by OP-method.
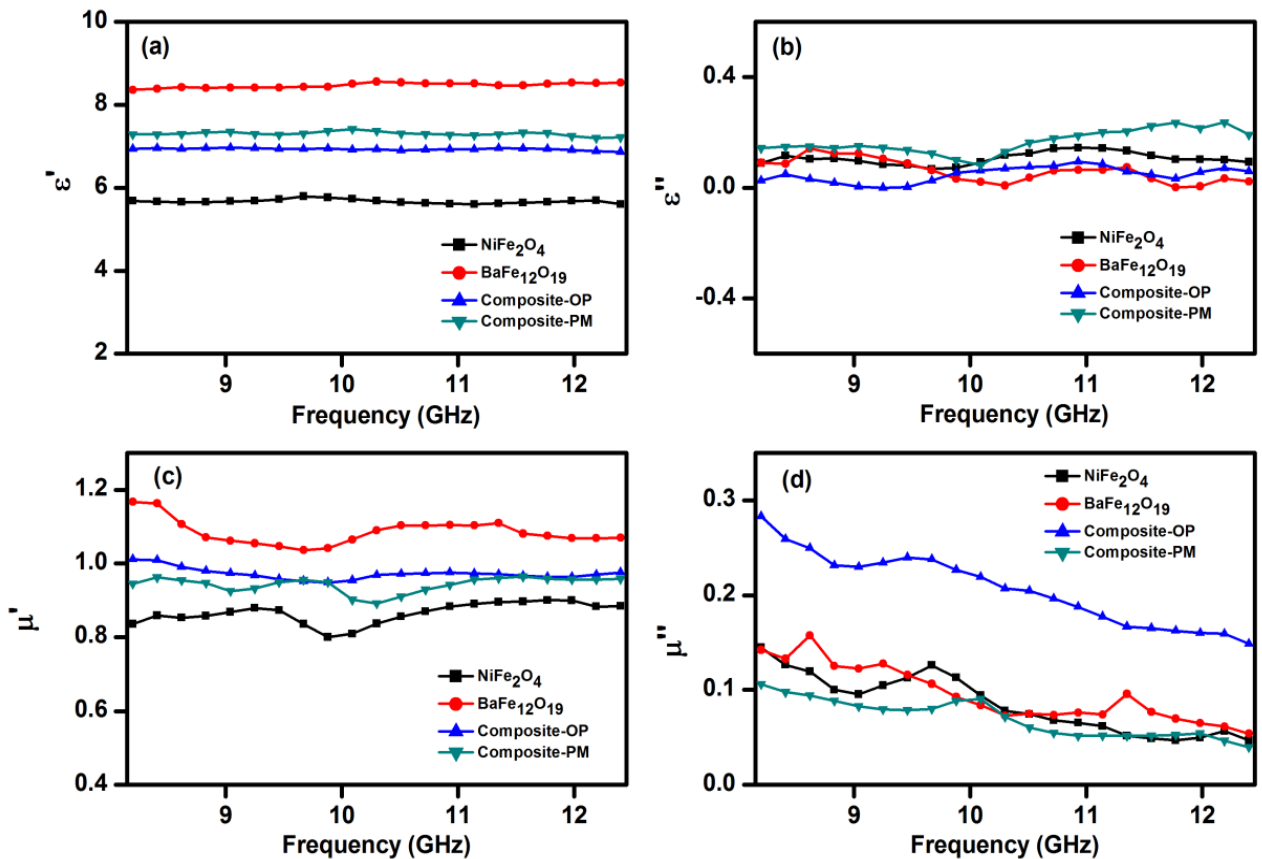


Fig. 2.7 (a) Real ($\varepsilon'$), (b) imaginary ($\varepsilon''$) parts of relative complex permittivity and (c) real ($\mu'$), (d) imaginary ($\mu''$) parts of relative complex permeability of pure BaFe$_{12}$O$_{19}$, NiFe$_2$O$_4$ nanopowders and (BaFe$_{12}$O$_{19}$)$_{0.15}$-(NiFe$_2$O$_4$)$_{0.85}$ nanocomposites prepared by one-pot and physical mixing method.

Refection Loss for nanocomposites as well as pure ferrite nanopowders was calculated for absorber thickness 3 mm and shown in Fig. 2.8 (a). The estimated electromagnetic wave absorption values are listed in Table 2.4. From Fig. 2.8 (a), it was observed that the nanocomposite-OP showed greater reflection loss (-10 dB at 9.67 GHz corresponds to 90% absorption) compare to the composite-PM (-4.3 dB at 10.09GHz). Pure hard and soft ferrite nanopowders showed negligible reflection loss (~-5.8 dB for BaFe$_{12}$O$_{19}$ and ~-3.6 dB for NiFe$_2$O$_4$ nanopowders). Fig. 2.8 (b) illustrates the reflection loss vs. frequency for one-pot synthesized nancomposite with different thickness of the absorber. The reflection loss was increased with increasing thickness of the sample till 3.5 mm with the shifting of the frequency matching to maximum loss towards lower frequency. Reflection loss of ~ -12 dB i.e. ~94% absorption was observed at 8.2 GHz for absorber thickness of 3.5 mm.
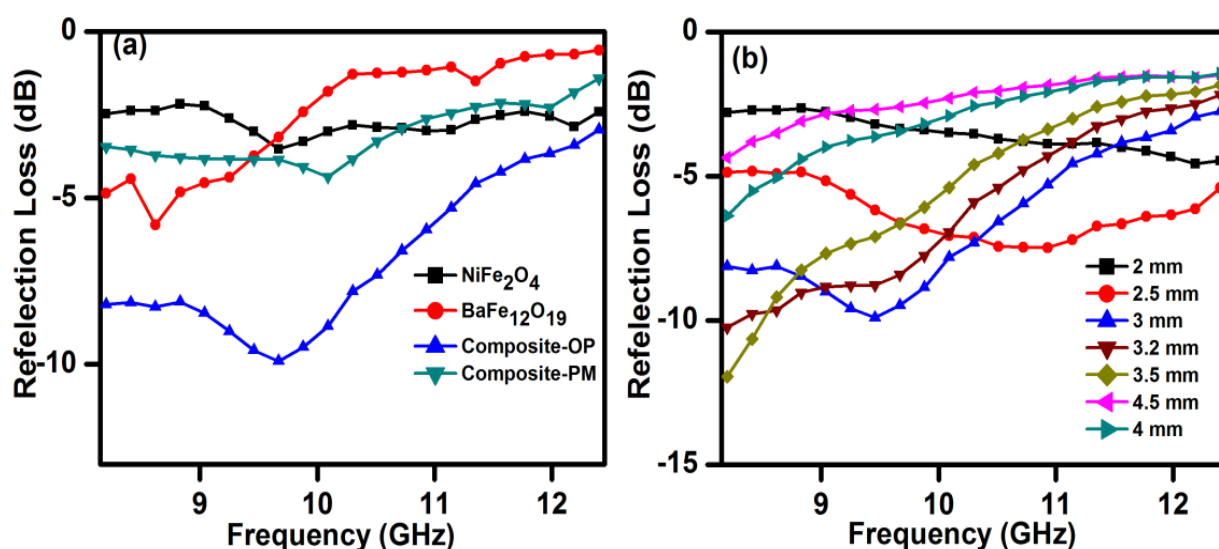


Fig. 2.8 Reflection loss vs. frequency plot for (a) pure BaFe$_{12}$O$_{19}$, NiFe$_2$O$_4$ nanopowders and (BaFe$_{12}$O$_{19}$)$_{0.15}$-(NiFe$_2$O$_4$)$_{0.85}$ nanocomposites prepared by one-pot and physical mixing method and (b) Reflection loss vs. frequency plot for (BaFe$_{12}$O$_{19}$)$_{0.15}$-(NiFe$_2$O$_4$)$_{0.85}$ nanocomposites prepared by one-pot method at different specimen thickness.

The improved microwave absorption property of hard-soft ferrite nanocomposites was attributed due to the exchange spin coupling interaction existing between hard and soft ferrite phases.[387, 388, 390, 435] In the composites (OP method), hard ferrite phase and soft ferrite phase are coupled to each other by an exchange through interfacial interaction which influences the relative complex permeability of the materials.[388] Interfacial interaction between the two

phases is one of the important factors for the microwave absorption in the GHz frequency range.[387]

The interfacial multipoles in nanocomposite causes the surface spin of ferrite nanoparticles disordered, which leads to high magnetic loss. Therefore, the microwave absorption improves.[387] There will be stronger exchange coupling interaction at the interface if the grain size is smaller.[2,26] In addition, the nanocomposites, prepared by OP method, are made of nanoparticles and both NiFe$_2$O$_4$ and BaFe$_{12}$O$_{19}$ nanoparticles are homogeneously mixed, which would have a small size effect and enhanced spring exchange coupling interaction. In a hard-soft ferrite system, three types of magnetic interactions are present. The most important one is the exchange-coupling interaction between soft and hard phase, the remaining are dipolar interactions between the hard-hard and soft-soft ferrite phases.[387, 392]

The hard ferrite possesses a high magnetocrystalline anisotropic energy compare to soft ferrite. If the hard ferrite grains are sufficiently exchange-coupled with the neighbouring soft ferrite grains, then the exchange-coupled interaction will not only help to align the magnetization in the soft ferrite phases but also helps to arrange magnetic moments of the hard and soft ferrite phases parallel to each other in hard soft ferrite nanocomposites. This leads to higher energy product and enhances the Reflection Loss in microwave absorption.[387, 391]

In one-pot synthesis method, as both the phases are grown together from a single reaction mixture, intimate co-existence of nanosized hard and soft ferrite phases were observed in these nanocomposites (Fig. 3 (c, e, g, i)). This fact leads to sufficient exchange coupling between hard and soft ferrite phases, and supply marvellous opportunities for absorbing microwave and dissipating energy

_____

Table 2.4 Microwave absorption characteristics of pure $BaFe_{12}O_{19}$, $NiFe_2O_4$ nanopowders and $(BaFe_{12}O_{19})_{0.15}$-$(NiFe_2O_4)_{0.85}$ nanocomposites prepared by one-pot and physical mixing method

| Sample | Minimum RL (dB) | Frequency (GHz) |
|---|---|---|
| $BaFe_{12}O_{19}$-pure | -5.8 | 8.62 |
| $(BaFe_{12}O_{19})_{0.15}$-$(NiFe_2O_4)_{0.85}$ (one-pot method) | -10 | 9.67 |
| $(BaFe_{12}O_{19})_{0.15}$-$(NiFe_2O_4)_{0.85}$ (physical mixing method) | -4.3 | 10.09 |
| $NiFe_2O_4$-pure | -3.5 | 9.67 |

## 2.3 Summary of Results

(i)    $(BaFe_{12}O_{19})_{1-x}$-$(NiFe_2O_4)_x$ nanocomposites were successfully synthesized using EDTA precursor based one-pot method where precursor was calcined at 800 °C for 4 h.

(ii)   Thermal decomposition of the precursor was completed at ~450 °C.

(iii)  XRD patterns of $(BaFe_{12}O_{19})_{1-x}$-$(NiFe_2O_4)_x$ nanocomposites, prepared by one-pot method as well as physical mixing method exhibited the diffraction peaks corresponding to both spinel $NiFe_2O_4$ and hexagonal $BaFe_{12}O_{19}$ phase.

(iv)   In $(BaFe_{12}O_{19})_{1-x}$-$(NiFe_2O_4)_x$ nanocomposites synthesized by OP method, the crystallite size of $NiFe_2O_4$ phase was increased from 10.2 to 38 nm with increasing amount of $NiFe_2O_4$ phase in the composite. The same trend was observed for $BaFe_{12}O_{19}$ phase and its crystallite size was found to be increased from 24 to 43 nm.

(v)    $(BaFe_{12}O_{19})_{1-x}$-$(NiFe_2O_4)_x$ nanocomposites synthesized by PM method, the crystallite sizes of both spinel and hexagonal phase did not change much with varying amount of $NiFe_2O_4$ and $BaFe_{12}O_{19}$ phases in the composites and were found to be ~38 nm for $NiFe_2O_4$ and ~43 nm for $BaFe_{12}O_{19}$. These values were almost same in comparison with the crystallite sizes of pure $NiFe_2O_4$ and $BaFe_{12}O_{19}$.

(vi)   $(BaFe_{12}O_{19})_{1-x}$-$(NiFe_2O_4)_x$ nanocomposites synthesized by PM method, clear segregation of hexagonal $BaFe_{12}O_{19}$ nanoparticles and spherical shaped agglomerated $NiFe_2O_4$ nanoparticles were observed. Nanocomposites, prepared

_____

by one-pot method, almost uniform shaped nanoparticles (average particle size ~60-70 nm) were observed.

(vii)    (BaFe$_{12}$O$_{19}$)$_{1-x}$-(NiFe$_2$O$_4$)$_x$ nanocomposites synthesized by one-pot method, showed single hysteresis loop, signifying hard and soft phases were well exchanged coupled to each other. Whereas, composites-PM exhibited a typical two loop "bee waist" type hysteresis loop, indicating the absence of exchange coupling between hard and soft phase. $M_s$ and $H_c$ values of all the composites prepared by one-pot method were higher than those of the composites prepared by physical mixing method.

(viii)    Nanocomposites synthesized by one-pot method are having only magnetic loss parameter whereas dielectric loss parameter is negligible.

(ix)    (BaFe$_{12}$O$_{19}$)$_{1-x}$-(NiFe$_2$O$_4$)$_x$ nanocomposites synthesized by one-pot method showed greater reflection loss (~ -10 dB at 9.67 GHz corresponds to 90% absorption) than composite-PM method (~ -4.3 dB at 8.62 GHz) for absorber thickness of 3 mm. Pure soft and hard ferrite nanopowders showed reflection loss lower than -10 dB (~-4 dB and ~-6 dB respectively).

(x)    (BaFe$_{12}$O$_{19}$)$_{0.15}$-(NiFe$_2$O$_4$)$_{0.85}$ nanocomposite synthesized by OP method exhibited reflection loss of ~ -12 dB (i.e. ~94% absorption) at 8.2 GHz for absorber thickness of 3.5 mm.

$$\text{Chapter 3}$$

# Synthesis and characterization of $(SrFe_{12}O_{19})_{1-x}$-$(NiFe_2O_4)_x$ nanocomposites and study of their magnetic and microwave absorption properties

## 3.1 Experimental procedure

### 3.1.1 Materials required

$Sr(NO_3)_2$, $Ni(NO_3)_2.6H_2O$, $Fe(NO_3)_3.9H_2O$ and Ethylene diamine tetra acetic acid (EDTA) were purchased from Merck, India and used without further purification.

### 3.1.2 Synthesis of $(SrFe_{12}O_{19})_{1-x}$-$(NiFe_2O_4)_x$ nanocomposites by one-pot method (OP Method) [441]

To prepare $(SrFe_{12}O_{19})_{1-x}$-$(NiFe_2O_4)_x$ nanocomposites (with x= 0.85, 0.75, 0.5 and 0.25) using one-pot method stoichiometric amount of aqueous solutions of $Sr(NO_3)_2$, $Ni(NO_3)_2.6H_2O$, $Fe(NO_3)_3.9H_2O$ and EDTA were mixed in a beaker (Table 3.1) and stirred for 2 h. This reaction mixture was then dried at ~110 °C for 2 h. Black colour floppy carbonaceous material was formed after drying, which is referred as precursor powder. Then the precursor powders were calcined at 800 °C for 4 h in air atmosphere to obtain desire $(SrFe_{12}O_{19})_{1-x}$-$(NiFe_2O_4)_x$ nanocomposites.

### 3.1.3. Synthesis of $(SrFe_{12}O_{19})_{1-x}$-$(NiFe_2O_4)_x$ nanocomposites by physical mixing method (PM Method)

A set of composite samples with various composition (with x= 0.85, 0.75, 0.5 and 0.25) was prepared by using 'physical mixing' method where pure $NiFe_2O_4$ and $SrFe_{12}O_{19}$ powders were mixed with appropriate weight ratio (Table 3.1) using a mortar pestle. Pure $SrFe_{12}O_{19}$ and $NiFe_2O_4$ nanopowders were prepared separately by using the EDTA-precursor method which has been developed by us.[254,441] For synthesis of $SrFe_{12}O_{19}$ nanoparticles, stoichiometric amounts of $Sr(NO_3)_2$ and $Fe(NO_3)_3.9H_2O$ were dissolved in distilled water according to the molar ratio of 1:12, as shown in Table 3.1. An aqueous solution of EDTA was prepared by dissolving EDTA in hot water with drop wise addition of $NH_4OH$. After complete dissolution of EDTA, the solution was boiled to remove the excess $NH_3$. The pH of

the solution was ~6. Aqueous solutions of metal nitrates and EDTA were mixed in a molar ratio of 1: 4 and stirred for 1 h at room temperature using a magnetic stirrer. pH of the resulting mixture was ~2. Black colored precursor was formed when the mixture was evaporated to dryness on a hot plate at ~110 °C. The precursor powder was then calcined in air for 4 h at 800 °C to obtain SrFe$_{12}$O$_{19}$ nanopowder. Detail synthesis procedure for NiFe$_2$O$_4$ nanoparticles have already been discussed in Chapter 2, Section 2.1.3

Table 3.1 Starting materials required for preparation of (SrFe$_{12}$O$_{19}$)$_{1-x}$-(NiFe$_2$O$_4$)$_x$ nanocomposites

| Composition | *Sr$^{II}$-Nitrate (g) | *Ni$^{II}$-nitrate (g) | *Fe$^{III}$-nitrate (g) | *EDTA (g) | **NiFe$_2$O$_4$ (g) | **SrFe$_{12}$O$_{19}$ (g) |
|---|---|---|---|---|---|---|
| NiFe$_2$O$_4$- pure | - | 1.24 | 3.45 | 3.93 | -- | -- |
| (SrFe$_{12}$O$_{19}$)$_{0.15}$-(NiFe$_2$O$_4$)$_{0.85}$ | 0.089 | 0.69 | 3.94 | 14.67 | 0.555 | 0.445 |
| (SrFe$_{12}$O$_{19}$)$_{0.25}$-(NiFe$_2$O$_4$)$_{0.75}$ | 0.12 | 0.49 | 4.13 | 14.59 | 0.398 | 0.602 |
| (SrFe$_{12}$O$_{19}$)$_{0.50}$-(NiFe$_2$O$_4$)$_{0.50}$ | 0.163 | 0.22 | 4.35 | 14.40 | 0.180 | 0.820 |
| (SrFe$_{12}$O$_{19}$)$_{0.75}$-(NiFe$_2$O$_4$)$_{0.25}$ | 0.186 | 0.08 | 4.49 | 14.36 | 0.069 | 0.931 |
| SrFe$_{12}$O$_{19}$- pure | 0.199 | - | 4.57 | 14.38 | -- | -- |

* One-pot method

** Physical mixing method

_____

## 3.2 Results and Discussion

### 3.2.1 Thermal analysis

To investigate the thermal decomposition behavior of precursors, prepared by OP method, TGA and DSC analysis were used. Thermogram of precursor powder (Fig. 3.1) revealed that a total weight loss of ~88 % occurred when the precursor powder was heated from 30 to 550 °C in air. Initially, ~6 % weight loss occurred in the region of 40 to 100 °C due to loss of moisture from the sample. ~8% weight loss was observed from 100 to 250 °C. Then finally, ~74 % weight loss was observed in the temperature range of 250 to 415 °C. This might be due to the oxidative decomposition of precursor and evolution of $CO_2$ and $NO_x$ gases. This decomposition was also reflected in DSC thermogram as an exothermic peak at 430 °C. No weight loss was observed in TGA when the sample was heated beyond 430 °C. This confirmed the full decomposition of carbonaceous mass of the precursor occurred within 430 °C.
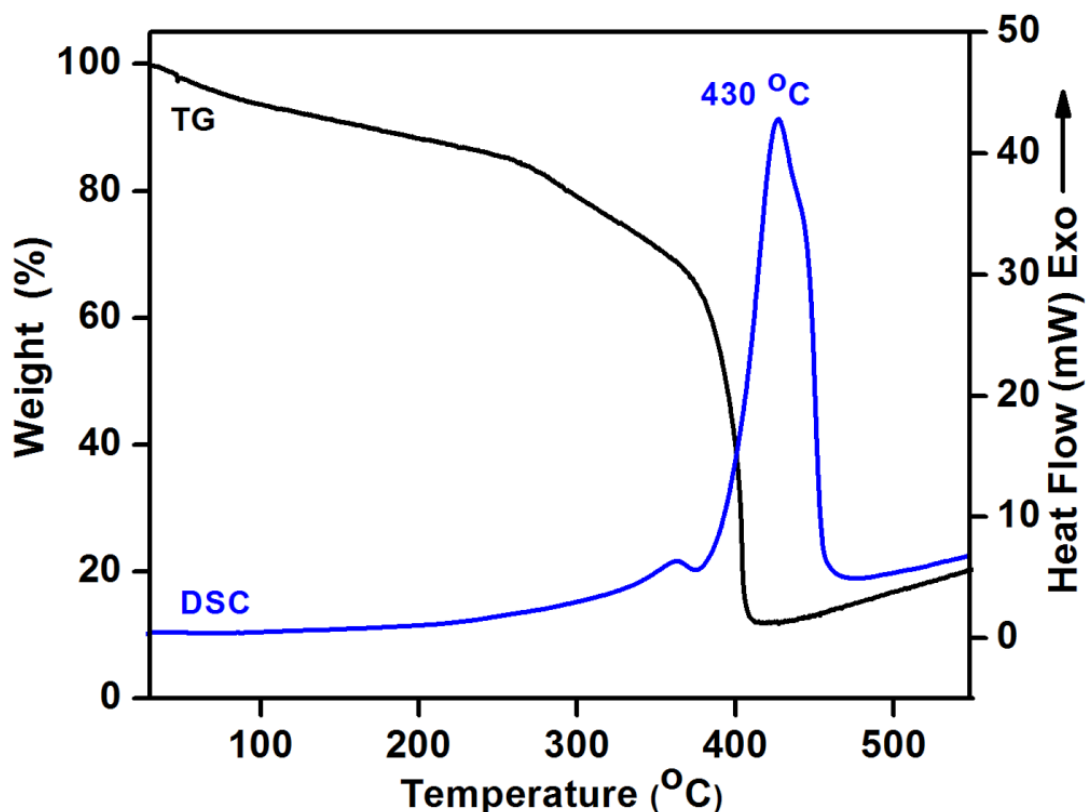


Fig. 3.1 TGA-DSC thermogram of (SrFe$_{12}$O$_{19}$)$_{0.5}$-(NiFe$_2$O$_4$)$_{0.5}$ precursor.

_____

### 3.2.2 X-Ray Diffraction analysis

Room temperature wide angle powder X-ray diffraction (XRD) was carried out to identify the phases present in the nanocomposites. XRD patterns of $(SrFe_{12}O_{19})_{1-x}$-$(NiFe_2O_4)_x$ nanocomposites, which were obtained by calcining the precursors (one-pot), exhibited the diffraction peaks corresponding to both spinel $NiFe_2O_4$ [ICDD 54-0964] and hexagonal $SrFe_{12}O_{19}$ [ICDD 80-1198] phase (Fig. 3.2 (A) and (B)). The XRD patterns indicated the coexistence of both the phases in the composite powders. Any impurity such as NiO, SrO, $SrCO_3$, $\alpha$-$Fe_2O_3$ etc. within the resolution of the technique was not detected. It was also noticed that the highest intensity peak of $NiFe_2O_4$ at $2\theta = 35.6°$ (corresponding to (311) plane) has increased with increasing the amount of $NiFe_2O_4$ in the composite (i.e., with increasing the value of x). Same observation was also found for $SrFe_{12}O_{19}$ (Fig. 2.2 (B)). XRD patterns of nanocomposites-PM also showed the presence of both the phases. However, variation in relative intensities of the diffraction peaks was observed for these two types of composites. This might because of, crystallite size and homogeneity of the $NiFe_2O_4$ and $SrFe_{12}O_{19}$ phases, present in the nanocomposites, vary with the preparation methodology. The average crystallite sizes of $NiFe_2O_4$ and $SrFe_{12}O_{19}$ phases in $(SrFe_{12}O_{19})_{1-x}$-$(NiFe_2O_4)_x$ nanocomposites were calculated by X-ray peak-broadening method using Scherrer's equation[437] and listed on Table 3.2. For $NiFe_2O_4$, the diffraction peak at $2\theta = 35.6°$, which corresponds to (311) plane and for $SrFe_{12}O_{19}$, diffraction peak at $2\theta = 34.2°$, i.e. (114) plane were used. The important feature was that, in $(SrFe_{12}O_{19})_{1-x}$-$(NiFe_2O_4)_x$ nanocomposites-OP, the crystallite size of $NiFe_2O_4$ phase was increased from 23 to 38 nm with increasing amount of $NiFe_2O_4$ phase in the composite. The same trend was observed for $SrFe_{12}O_{19}$ phase and its crystallite size was increased from 30 to 40 nm. On the other hand, in case of $(SrFe_{12}O_{19})_{1-x}$-$(NiFe_2O_4)_x$ nanocomposites-PM, the crystallite sizes of both spinel and hexagonal phase did not vary with varying amount of $NiFe_2O_4$ and $SrFe_{12}O_{19}$ phases in the composites and was found to be ~38 nm for $NiFe_2O_4$ and ~40 nm for $SrFe_{12}O_{19}$. These values were almost same in comparison with the crystallite sizes of pure $NiFe_2O_4$ and $SrFe_{12}O_{19}$ nanopowders which imply that the pure phases retain their crystallinity in the composites.
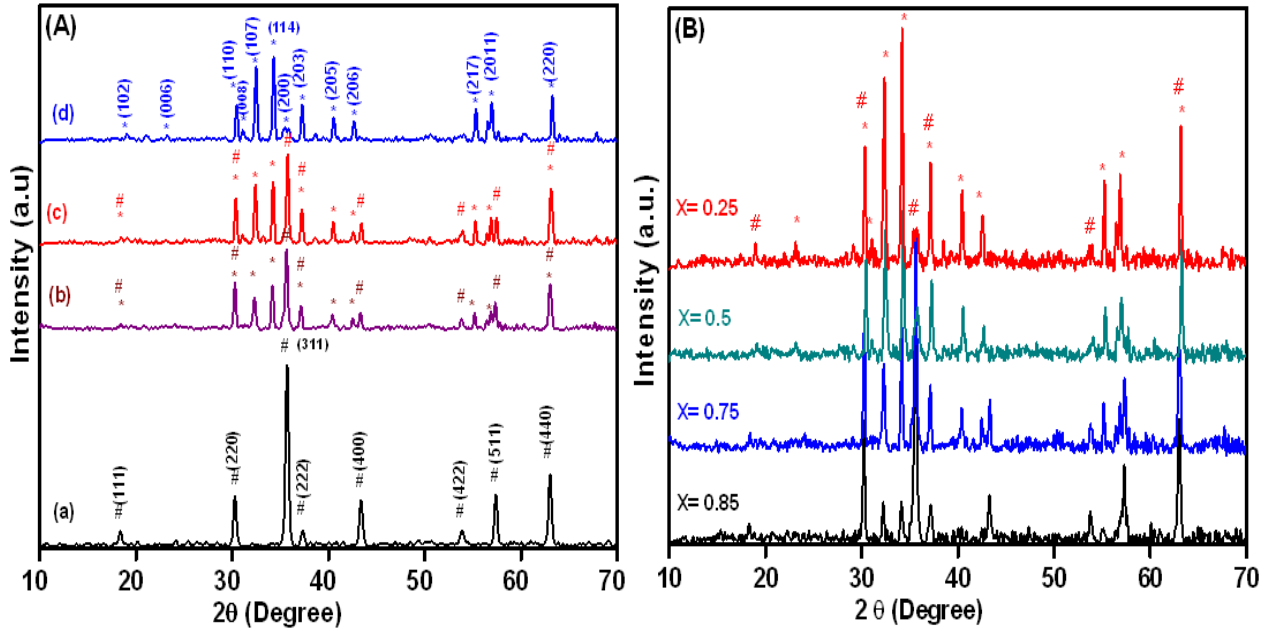
Fig. 3. 2 (A) XRD spectra of the (a) pure $NiFe_2O_4$ nanopowders, $(SrFe_{12}O_{19})_{0.25}$-$(NiFe_2O_4)_{0.75}$ nanocomposites prepared by (b) one-pot and (c) physical mixing methods and (d) $SrFe_{12}O_{19}$ nanopowders, (B) XRD spectra of $(SrFe_{12}O_{19})_{1-x}$-$(NiFe_2O_4)_x$ nanocomposites synthesized by one-pot method (#$NiFe_2O_4$ and *$SrFe_{12}O_{19}$).

Table 3.2 Average crystalline size of $(SrFe_{12}O_{19})_{1-x}$-$(NiFe_2O_4)_x$ nanocomposites prepared by one-pot and physical mixing method

| Sample | Crystallite size (nm) | | | |
|---|---|---|---|---|
| | One-pot synthesis | | Physical mixing synthesis | |
| | *(114) plane | #(311) plane | *(114) plane | #(311) plane |
| $NiFe_2O_4$- pure | -- | 38 | -- | 38 |
| $(SrFe_{12}O_{19})_{0.15}$-$(NiFe_2O_4)_{0.85}$ | 30 | 35 | 41 | 39 |
| $(SrFe_{12}O_{19})_{0.25}$-$(NiFe_2O_4)_{0.75}$ | 32 | 33 | 40 | 38 |
| $(SrFe_{12}O_{19})_{0.50}$-$(NiFe_2O_4)_{0.50}$ | 35 | 30 | 40 | 37 |
| $(SrFe_{12}O_{19})_{0.75}$-$(NiFe_2O_4)_{0.25}$ | 38 | 23 | 42 | 37 |
| $SrFe_{12}O_{19}$- pure | 40 | --- | 40 | -- |

* $SrFe_{12}O_{19}$

# $NiFe_2O_4$

### 3.2.3 TEM and SEM analysis

During investigations on morphology of two different types of nanocomposites (prepared by PM and OP method) by HRTEM (Fig. 3.3) two distinct types of microstructures were observed.
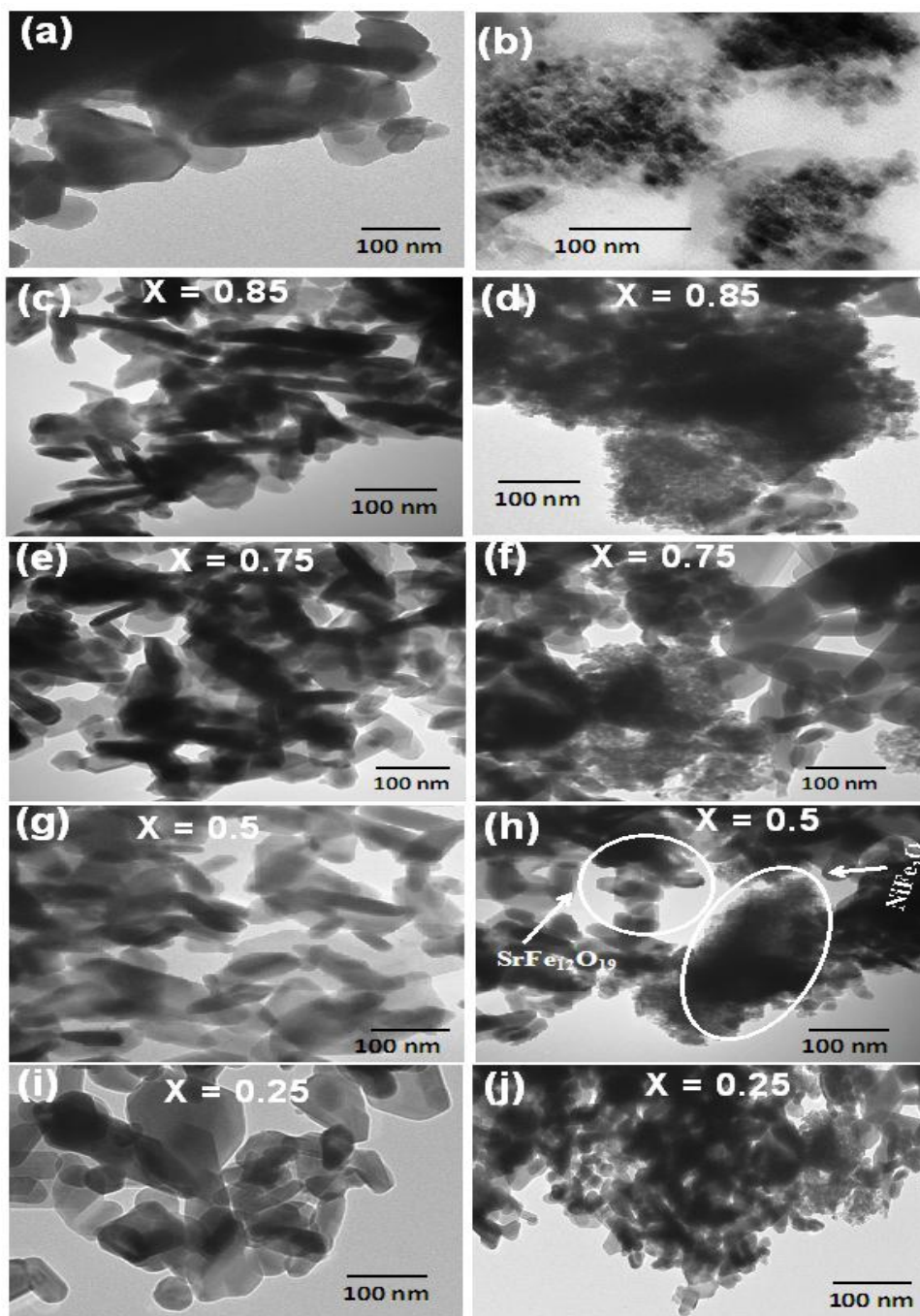


Fig. 3.3 TEM micrographs of (a) pure $SrFe_{12}O_{19}$, (b) pure $NiFe_2O_4$ nanopowders and $(SrFe_{12}O_{19})_{1-x}$-$(NiFe_2O_4)_x$ nanocomposites synthesis by (c, e, g, i) one-pot and (d, f, h, j) physical mixing method.

In case of the nanocomposites-PM (Fig. 3.3 (d, f, h, j), clear segregation of spherical agglomerated $NiFe_2O_4$ nanoparticles (~20 nm average particle size, Fig. 3.3 (a)) and hexagonal $SrFe_{12}O_{19}$ nanoparticles (~50-70 nm average particle size, Fig. 3.3 (b)) were observed. On the other hand, when nanocomposites were prepared by one-pot method, almost uniform shaped nanoparticles with average particle size ~60-70 nm were formed (Fig. 3.3 (c, e, g, i)).

SEM micrographs (Fig. 3.4 (c)) of the composites also revealed the intimate coexistence of $NiFe_2O_4$ and $SrFe_{12}O_{19}$ particles in the nanocomposites-OP. in the nanocomposites prepared by physical mixing method (Fig. 2.4(d)), presence of large $SrFe_{12}O_{19}$ (Fig. 3.4 (b)) and small $NiFe_2O_4$ particles (Fig. 3.4 (a)) was observed. EDX analysis of the final nanocomposites also revealed that all the metal ions are present in the composites (Fig. 3.4 (e)).
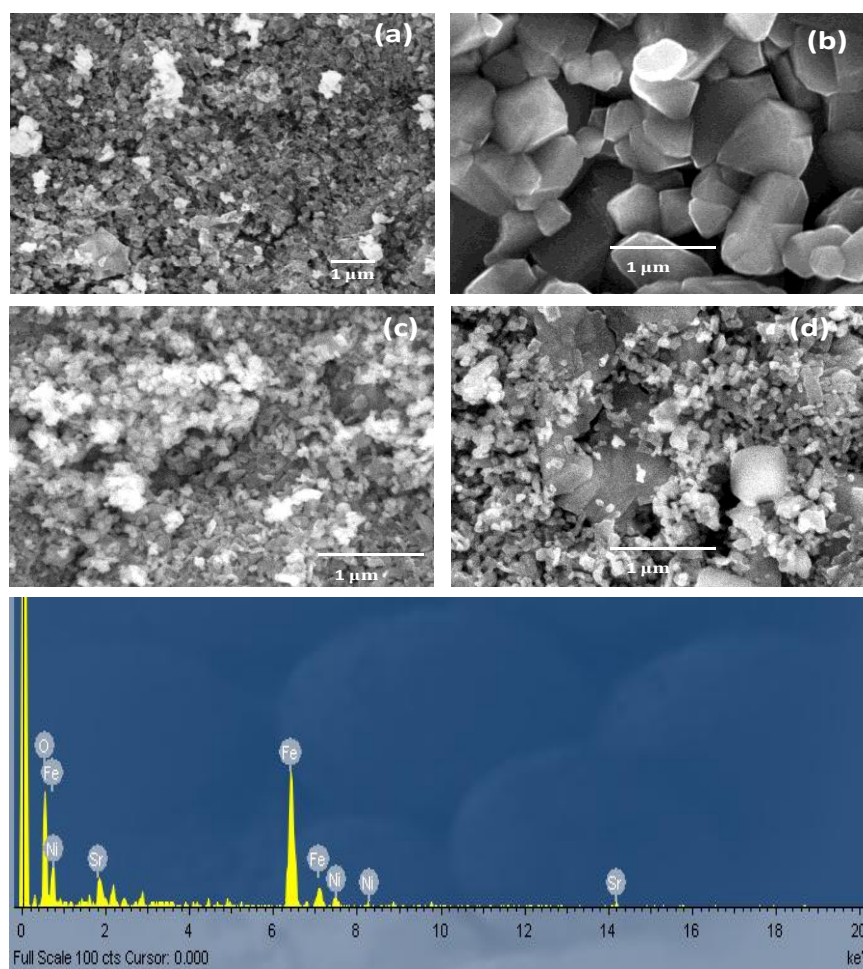


Fig. 3.4 SEM micrographs of (a) pure $NiFe_2O_4$, (b) pure $SrFe_{12}O_{19}$ and $(SrFe_{12}O_{19})_{0.5}$-$(NiFe_2O_4)_{0.5}$ nanocomposites prepared by (c) one-pot, (d) physical mixing method and (e) EDX spectra of $(NiFe_2O_4)_{0.5}$-$(SrFe_{12}O_{19})_{0.5}$ nanocomposite prepared by one-pot method.

Electron microscopic analysis confirmed that, the nanocomposites synthesized by one-pot method possess high level of homogeneous mixing of $NiFe_2O_4$ and $SrFe_{12}O_{19}$ phase than the composites prepared by physical mixing method. This difference in morphology of the samples may influence the magnetic and microwave absorption properties of the nanocomposites.

### 3.2.4 Magnetic measurements

The room temperature magnetization behaviours of $(SrFe_{12}O_{19})_{1-x}$-$(NiFe_2O_4)_x$ nanocomposites prepared by two different methods (OP and PM method) were measured using VSM with an applied field of 15000 Oe and shown in Fig. 3.5. The most important observation was that, nanocomposites-OP showed single hysteresis loop, indicating hard and soft phases were well exchanged coupled to each other. Whereas, a typical two loop "bee waist" type hysteresis loop was observed in nanocomposites-PM (Fig. 3.5 (a)), suggesting the absence of exchange coupling between hard and soft phase. [387, 431-433] Hence, $(SrFe_{12}O_{19})_{1-x}$-$(NiFe_2O_4)_x$ nanocomposites, prepared by one-pot method, though exhibited crystallographycally two phase behaviour but possessed magnetically good single phase behaviour. Fig. 3.5 (b) also reflects that, all the composition of $(SrFe_{12}O_{19})_{1-x}$-$(NiFe_2O_4)_x$ showed single hysteresis loop for composites synthesized by OP-method whereas two loop hysteresis behavior for nanocomposites-PM (Fig. 3.5 (c)).

It was also observed that, coercivity ($H_c$) values of the nanocomposites prepared by both the methods increased with increasing hard ferrite phase (i.e. $SrFe_{12}O_{19}$) content in the nanocomposites and listed in Table. 3.3. In case of nanocomposites-OP, initial incorporation of $SrFe_{12}O_{19}$ phase caused enhancement of saturation magnetization ($M_s$) values. This was due to the spring exchange coupling between hard and soft magnetic phases. However, subsequent increase of $SrFe_{12}O_{19}$ content in the $(SrFe_{12}O_{19})_{1-x}$-$(NiFe_2O_4)_x$ nanocomposites (i.e., with increasing (1-x) values) did not influence much on $M_s$ value. Whereas, in case of nanocomposites-PM, $M_s$ increased with increasing amount of $SrFe_{12}O_{19}$. $M_s$ and $H_c$ values of the composites prepared by 'one-pot' method were found to be higher than those of the composites prepared by physical mixing method. These facts indicate that hard and soft ferrite phases are well exchanged coupled to each other in the composites prepared by one-pot method.

Theoretically calculated values of $M_s$ of the composites (when hard and soft phases are not exchange coupling) by using equation 2.1, were almost matching with the experimentally obtained values of the composites prepared by physical mixing method (Table 3.3) which proves the absence of spring exchange coupling in the nanocomposite-PM.
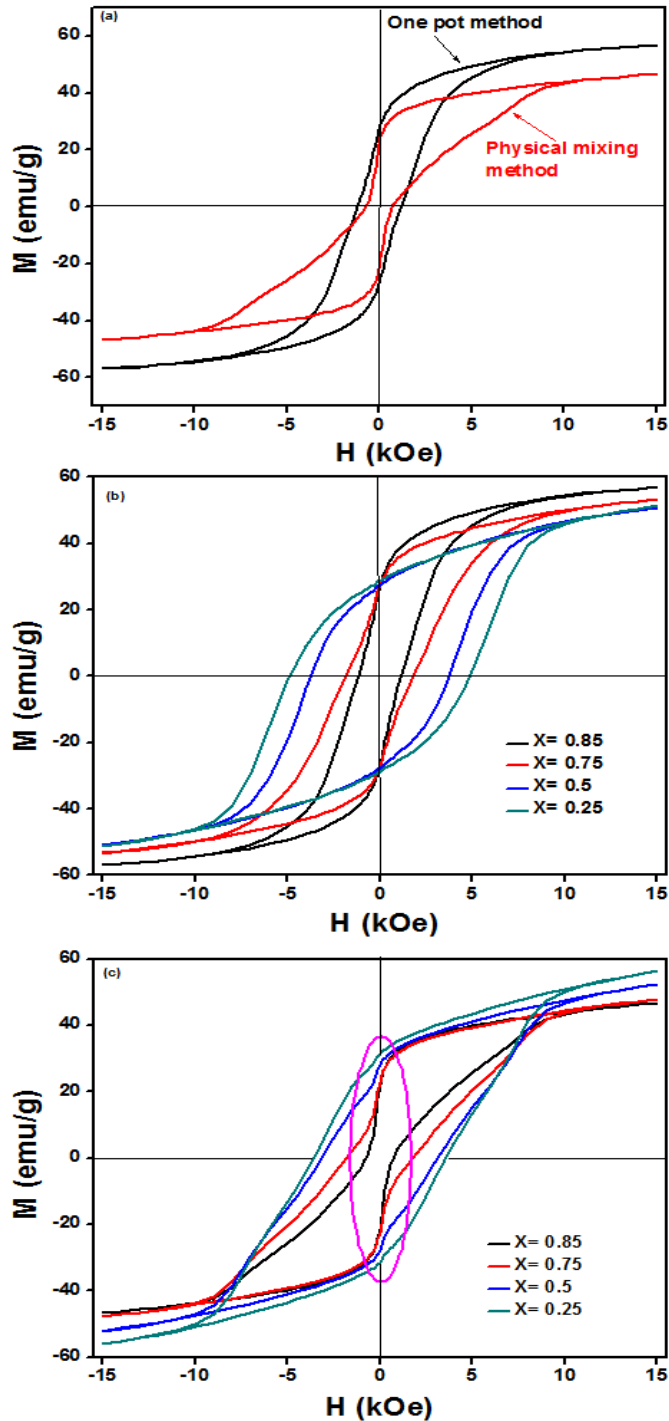


Fig. 3.5 Room temperature hysteresis loops for (a) $(SrFe_{12}O_{19})_{0.15}$-$(NiFe_2O_4)_{0.85}$ nanocomposite prepared by one-pot and physical mixing method and $(SrFe_{12}O_{19})_{1-x}$-$(NiFe_2O_4)_x$ nanocomposite prepared by (b) one-pot, (c) physical mixing method.

Table 3.3 $M_s$ and $H_c$ values of the $(SrFe_{12}O_{19})_{1-x}$-$(NiFe_2O_4)_x$ nanocomposites prepared by one-pot and physical mixing method

| Sample | One-pot synthesis | | Physical mixing synthesis | | Theoretical $M_s$ without exchange coupling (emu/g) |
|---|---|---|---|---|---|
| | $H_c$ (Oe) | $M_s$ (emu/g) | $H_c$ (Oe) | $M_s$ (emu/g) | |
| $NiFe_2O_4$- pure | 158 | 30.7 | -- | -- | -- |
| $(SrFe_{12}O_{19})_{0.15}$-$(NiFe_2O_4)_{0.85}$ | 1170 | 56.9 | 742 | 46.7 | 42.7 |
| $(SrFe_{12}O_{19})_{0.25}$-$(NiFe_2O_4)_{0.75}$ | 1830 | 53.3 | 1805 | 47.7 | 46.9 |
| $(SrFe_{12}O_{19})_{0.50}$-$(NiFe_2O_4)_{0.50}$ | 3746 | 50.7 | 3134 | 52.1 | 52.7 |
| $(SrFe_{12}O_{19})_{0.75}$-$(NiFe_2O_4)_{0.25}$ | 4864 | 51.3 | 3569 | 56.3 | 55.8 |
| $SrFe_{12}O_{19}$- pure | 5866 | 57.6 | -- | -- | -- |

## 3.2.5 Microwave absorption study

Microwave absorption behavior of $(SrFe_{12}O_{19})_{1-x}$-$(NiFe_2O_4)_x$ nanocomposites with different compositions (x= 0.85, 0.75, 0.5, 0.25) synthesized by one-pot method were investigated. Loss tangent vs. frequency were plotted to understand the particular loss mechanism for each nanocomposite and shown in Fig. 3.6 (a) and (b). The dielectric and magnetic loss tangents can be defined as $\tan\delta_\varepsilon = \varepsilon''/\varepsilon'$ and $\tan\delta_\mu = \mu''/\mu'$, respectively. Fig. 3.6 (b) shows that these composites are having only magnetic loss parameter whereas the dielectric loss parameter is negligible (Fig. 3.6 (a)).

Reflection loss (RL) was calculated using equations (1.4 and 1.5) and plotted against frequency for different $(SrFe_{12}O_{19})_{1-x}$-$(NiFe_2O_4)_x$ nanocomposites (x= 0.85, 0.75, 0.5, 0.25) synthesized by OP method for thickness 2.8 mm (Fig. 3.6 (c)). In RL vs frequency plot, the dip of the curves was designated for minimum RL indicating maximum absorption. It was observed that, with decreasing the value of x (i.e. increasing $SrFe_{12}O_{19}$ content in the nanocomposite) maximum absorption was decreases. As the composite having composition $(SrFe_{12}O_{19})_{0.15}$-$(NiFe_2O_4)_{0.85}$ exhibited minimum reflection loss (~ -11 dB) i.e. maximum absorption compare to other composites, so we have chosen this composition for further

_____

studies and the microwave absorption properties are compared with the nanocomposite prepared by PM method as well as pure $NiFe_2O_4$ and $SrFe_{12}O_{19}$.
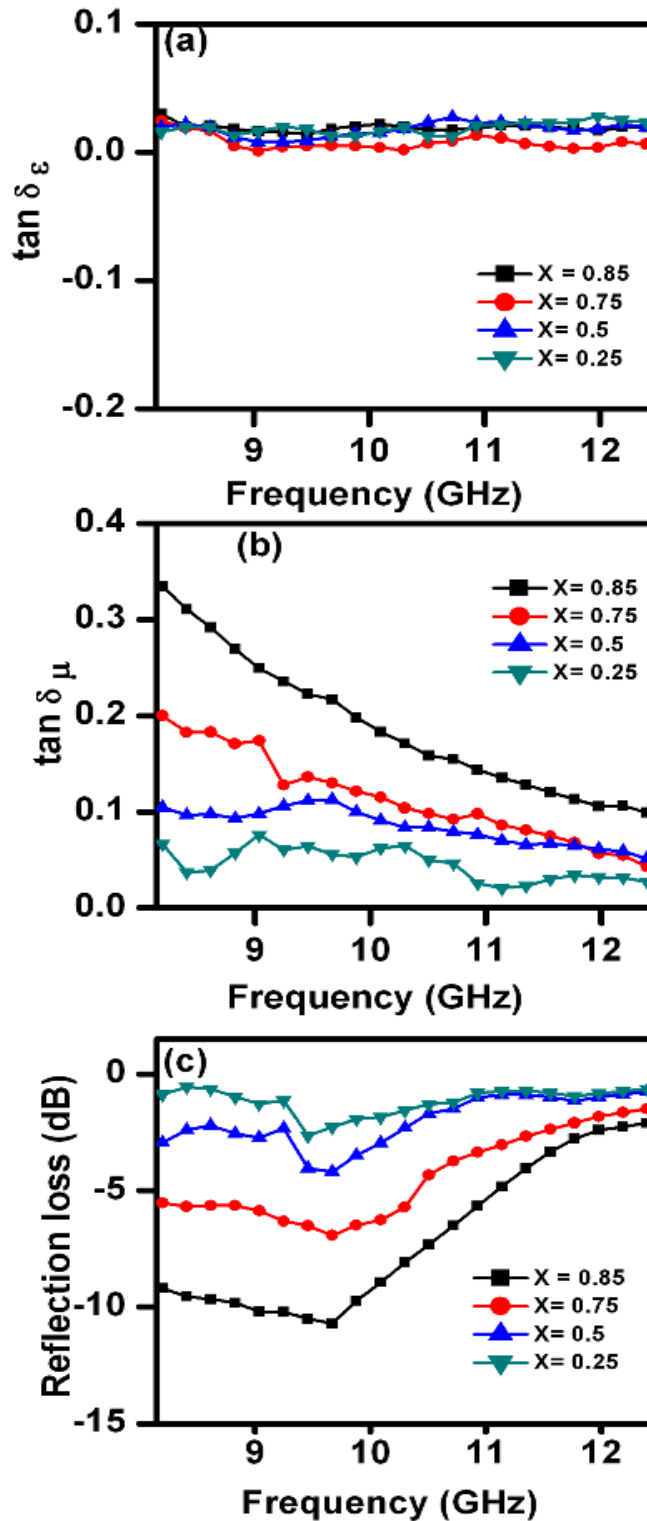


Fig. 3.6 (a) Loss Tangent of relative complex permittivity (tan$\delta_\varepsilon$), (b) Loss Tangent of relative complex permeability (tan$\delta_\mu$) and (c) Reflection loss vs. frequency plot (SrFe₁₂O₁₉)₁₋ₓ-(NiFe₂O₄)ₓ nanocomposites synthesized by one-pot method.

The real and imaginary permittivity (Fig. 3.7(a). and (b)) and permeability (Fig. 3.7 (c) and (d)) for the nanocomposites synthesized by both the methods, pure SrFe$_{12}$O$_{19}$ and NiFe$_2$O$_4$ nanopowders were plotted as a function of frequency in the X-band range (8.2- 12.4 GHz). It was observed that, $\varepsilon'$ values remained nearly constant over the entire frequency range. Nanocomposites prepared by one-pot method showed higher $\varepsilon'$ value than the composite synthesized by physical mixing method as well as pure SrFe$_{12}$O$_{19}$ and NiFe$_2$O$_4$ nanopowders (Fig. 3.7 (a)). For the nanocomposite-OP, the imaginary dielectric parameter ($\varepsilon''$) was almost remained constant throughout the entire X-band range except two broad peaks from 9.4 GHz to 10.7 GHz and 10.7 to 12 GHz. Similarly a broad peak was observed 9.6 GHz to 11.3 GHz for composite prepared by physical mixing method (Fig. 3.7 (b)). Such kind of behaviour can be mostly ascribed due to the intrinsic, electric dipole and interfacial polarization.[387]
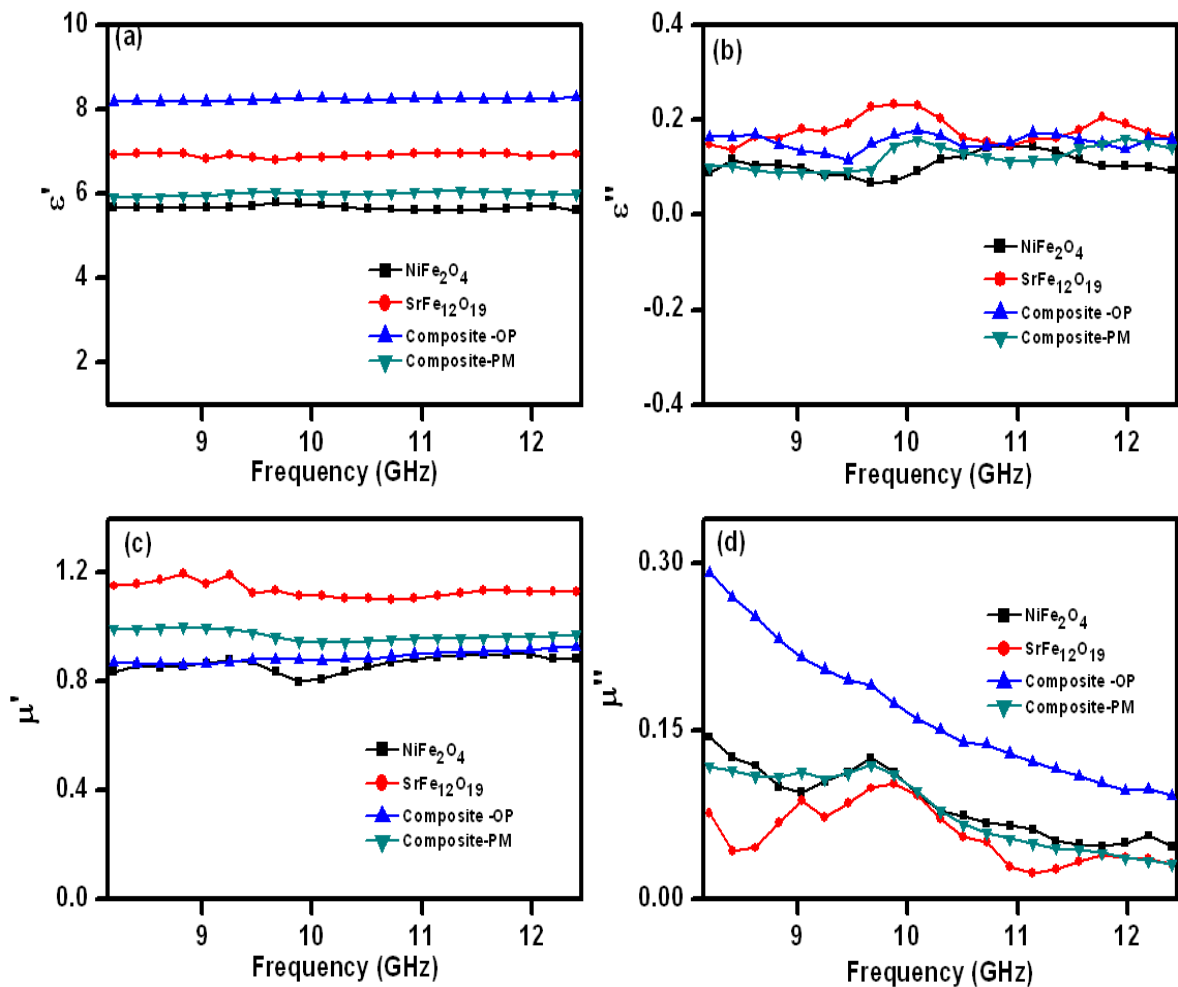


Fig. 3.7 (a) Real ($\varepsilon'$), (b) imaginary ($\varepsilon''$) parts of relative complex permittivity and (c) real ($\mu'$), (d) imaginary ($\mu''$) parts of relative complex permeability of pure SrFe$_{12}$O$_{19}$, NiFe$_2$O$_4$ nanopowders and (SrFe$_{12}$O$_{19}$)$_{0.15}$-(NiFe$_2$O$_4$)$_{0.85}$ nanocomposites prepared by one-pot and physical mixing method.

The real permeability ($\mu'$) values of both the composite and pure nanopowders remained almost constant in the entire frequency range of X-band (Fig. 3.7 (c)). The imaginary permeability ($\mu''$) values (Fig. 3.7 (d)) showed a decreasing tendency from 8.2 GHz to 12.4 GHz for both the nanocomposites and pure ferrites, however, maximum imaginary permeability was observed for the composite synthesized by one-pot method.

Refection Loss for nanocomposites as well as pure ferrite nanopowders was calculated for absorber thickness 2.8 mm and shown in Fig. 3.8 (a). The estimated electromagnetic wave absorption values are listed in Table 3.4. From Fig. 3.8 (a), it was observed that the nanocomposite-OP showed greater reflection loss (-10.7 dB at 9.67 GHz corresponds to ~91% absorption) compare to the composite-PM (-3.46 dB at 9.88 GHz). Pure hard and soft ferrite nanopowders showed negligible reflection loss (~-6 dB for SrFe$_{12}$O$_{19}$ and ~-4 dB for NiFe$_2$O$_4$ nanopowders). For composite-OP showed >10 dB reflection loss (i.e. > 90% absorption) over frequency range of 8.9 GHz to 9.8 GHz. Fig. 3.8 (b) illustrates the reflection loss vs. frequency for one-pot synthesized nancomposite with different thickness of the absorber. The reflection loss was increased with increasing thickness of the sample till 3.2 mm with the shifting of the frequency matching to maximum loss towards lower frequency. Reflection loss of ~ -17 dB i.e. 98% absorption was observed at 8.2 GHz for absorber thickness of 3.2 mm.
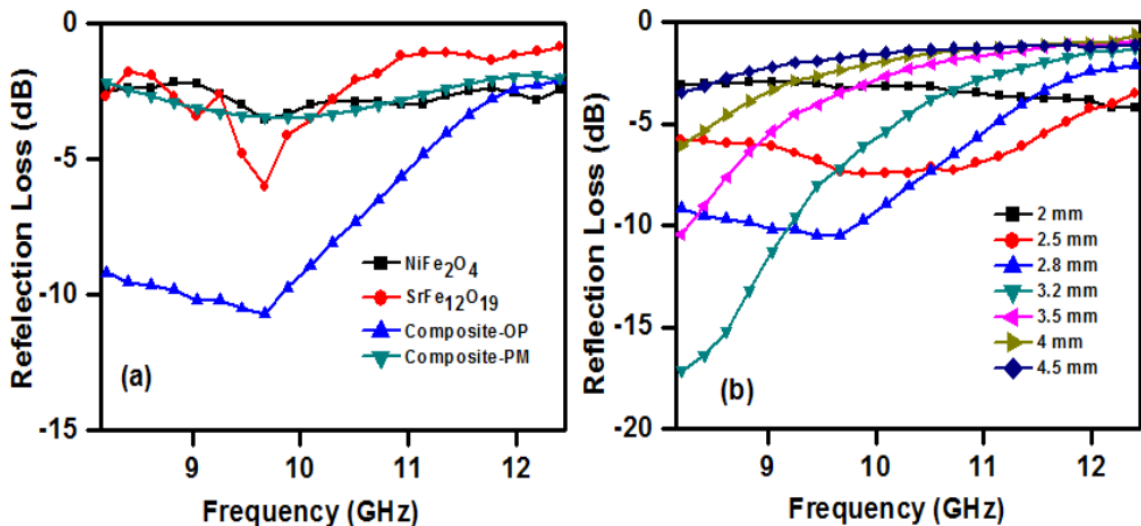


Fig. 3.8 Reflection loss vs. frequency plot for (a) pure SrFe$_{12}$O$_{19}$, NiFe$_2$O$_4$ nanopowders and (SrFe$_{12}$O$_{19}$)$_{0.15}$-(NiFe$_2$O$_4$)$_{0.85}$ nanocomposites prepared by one-pot and physical mixing method and (b) Reflection loss vs. frequency plot for (SrFe$_{12}$O$_{19}$)$_{0.15}$-(NiFe$_2$O$_4$)$_{0.85}$ nanocomposites prepared by one-pot method at different absorber thickness.

_____

Table 3.4 Microwave absorption characteristics of pure SrFe$_{12}$O$_{19}$, NiFe$_2$O$_4$ nanopowders and (SrFe$_{12}$O$_{19}$)$_{0.15}$-(NiFe$_2$O$_4$)$_{0.85}$ nanocomposites prepared by one-pot and physical mixing method

| Sample | Minimum RL (dB) | Frequency (GHz) |
|---|---|---|
| SrFe$_{12}$O$_{19}$-pure | -6.01 | 9.67 |
| (SrFe$_{12}$O$_{19}$)$_{0.15}$-(NiFe$_2$O$_4$)$_{0.85}$ (one-pot method) | -10.7 | 9.67 |
| (SrFe$_{12}$O$_{19}$)$_{0.15}$-(NiFe$_2$O$_4$)$_{0.85}$ (physical mixing method) | -3.46 | 9.88 |
| NiFe$_2$O$_4$-pure | -3.52 | 9.67 |

## 3.3 Summary of Results

(i) (SrFe$_{12}$O$_{19}$)$_{1-x}$-(NiFe$_2$O$_4$)$_x$ nanocomposites were successfully synthesized using EDTA precursor based one-pot method where precursor was calcined at 800 °C for 4 h.

(ii) Thermal decomposition of the precursor was completed at ~430 °C.

(iii) XRD patterns of (SrFe$_{12}$O$_{19}$)$_{1-x}$-(NiFe$_2$O$_4$)$_x$ nanocomposites, prepared by one-pot method as well as physical mixing method exhibited the diffraction peaks corresponding to both spinel NiFe$_2$O$_4$ and hexagonal SrFe$_{12}$O$_{19}$ phase.

(iv) In (SrFe$_{12}$O$_{19}$)$_{1-x}$-(NiFe$_2$O$_4$)$_x$ nanocomposites synthesized by OP method, the crystallite size of NiFe$_2$O$_4$ phase was increased from 23 to 38 nm with increasing amount of NiFe$_2$O$_4$ phase in the composite. The same trend was observed for SrFe$_{12}$O$_{19}$ phase and its crystallite size was found to be increased from 30 to 40 nm.

(v) (SrFe$_{12}$O$_{19}$)$_{1-x}$-(NiFe$_2$O$_4$)$_x$ nanocomposites synthesized by PM method, the crystallite sizes of both spinel and hexagonal phase did not change much with varying amount of NiFe$_2$O$_4$ and SrFe$_{12}$O$_{19}$ phases in the composites and were found to be ~38 nm for NiFe$_2$O$_4$ and ~40 nm for SrFe$_{12}$O$_{19}$. These values were almost same in comparison with the crystallite sizes of pure NiFe$_2$O$_4$ and SrFe$_{12}$O$_{19}$.

(vi) (SrFe$_{12}$O$_{19}$)$_{1-x}$-(NiFe$_2$O$_4$)$_x$ nanocomposites synthesized by PM method, clear segregation of hexagonal SrFe$_{12}$O$_{19}$ nanoparticles and spherical shaped agglomerated NiFe$_2$O$_4$ nanoparticles were observed. Nanocomposites, prepared

by one-pot method, almost uniform shaped nanoparticles (average particle size ~60-70 nm) were observed.

(vii)   (SrFe$_{12}$O$_{19}$)$_{1-x}$-(NiFe$_2$O$_4$)$_x$ nanocomposites synthesized by one-pot method, showed single hysteresis loop, signifying hard and soft phases were well exchanged coupled to each other. Whereas, a typical two loop "bee waist" type hysteresis loop was observed in case of composites-PM, indicating the absence of exchange coupling between hard and soft phase. M$_s$ and H$_c$ values of all the composites prepared by one-pot method were higher than those of the composites prepared by physical mixing method.

(viii)  Nanocomposites synthesized by one-pot method are having only magnetic loss parameter whereas dielectric loss parameter is negligible.

(ix)    (SrFe$_{12}$O$_{19}$)$_{1-x}$-(NiFe$_2$O$_4$)$_x$ nanocomposites synthesized by one-pot method showed greater reflection loss (~ -11 dB at 9.67 GHz corresponds to 91% absorption) than composite-PM method (~ -4 dB at 8.62 GHz) for absorber thickness of 2.8 mm. Pure hard and soft ferrite nanopowders showed reflection loss lower than -10 dB (~-6 dB and ~-4 dB respectively).

(x)     (SrFe$_{12}$O$_{19}$)$_{0.15}$-(NiFe$_2$O$_4$)$_{0.85}$ nanocomposite synthesized by OP method exhibited reflection loss of ~ -17 dB (i.e. ~98% absorption) at 8.2 GHz for absorber thickness of 3.2 mm.

<div align="right">

**Chapter 4**

</div>

# Synthesis and characterization of (BaFe$_{12}$O$_{19}$)$_{1-x}$-(Ni$_{0.65}$Zn$_{0.35}$Fe$_2$O$_4$)$_x$ nanocomposites and study of their magnetic and microwave absorption properties

## 4.1 Experimental procedure

### 4.1.1 Materials required

BaCO$_3$, Ni(NO$_3$)$_2$.6H$_2$O, Fe(NO$_3$)$_3$.9H$_2$O, Zn dust, Nitric Acid and Ethylene diamine tetra acetic acid (EDTA) were purchased from Merck, India and used without further purification. Zn(NO$_3$)$_2$ and Ba(NO$_3$)$_2$ were prepared by dissolving Zn dust and BaCO$_3$ respectively in aqueous nitric acid.

### 4.1.2 Synthesis of (BaFe$_{12}$O$_{19}$)$_{1-x}$-(Ni$_{0.65}$Zn$_{0.35}$Fe$_2$O$_4$)$_x$ nanocomposites by one-pot method (OP Method) [442]

To prepare (BaFe$_{12}$O$_{19}$)$_{1-x}$-(Ni$_{0.65}$Zn$_{0.35}$Fe$_2$O$_4$)$_x$ nanocomposites (with x= 0.85, 0.75, 0.5, and 0.25) using one-pot method stoichiometric amount of aqueous solutions of BaNO$_3$, Ni(NO$_3$)$_2$.6H$_2$O, Zn(NO$_3$)$_2$ Fe(NO$_3$)$_3$.9H$_2$O, and EDTA were mixed in a beaker (Table 4.1) and stirred for 2 h. This reaction mixture was then dried at ~110 °C for 2 h. Black colour floppy carbonaceous material was formed after drying, which referred as precursor powder. Then the precursor powders were calcined at 800 °C for 4 h in air atmosphere to obtain pure (BaFe$_{12}$O$_{19}$)$_{1-x}$-(Ni$_{0.65}$Zn$_{0.35}$Fe$_2$O$_4$)$_x$ nanocomposites.

### 4.1.3 Synthesis of (BaFe$_{12}$O$_{19}$)$_{1-x}$-(Ni$_{0.65}$Zn$_{0.35}$Fe$_2$O$_4$)$_x$ nanocomposites by physical mixing method (PM Method)

A set of composite samples with various composition (with x= 0.85, 0.75, 0.5, and 0.25) was prepared by using 'physical mixing' method where pure Ni$_{0.65}$Zn$_{0.35}$Fe$_2$O$_4$ and BaFe$_{12}$O$_{19}$ powders were mixed with appropriate weight ratio (Table. 4.1) using a mortar pestle. Pure

$BaFe_{12}O_{19}$ and $Ni_{0.65}Zn_{0.35}Fe_2O_4$ nanopowders were prepared separately by using the EDTA-precursor method developed by us.[255, 257] Detail synthesis procedure of $BaFe_{12}O_{19}$ has already been discussed in Chapter 2, Section 2.1.3. For Synthesis of $Ni_{0.65}Zn_{0.35}Fe_2O_4$, stoichiometric amounts of metal nitrates were dissolved in distilled water as shown in Table 4.1. Aqueous solutions of metal nitrates and EDTA were mixed in a molar ratio of 1:1 and stirred for 1 h at room temperature using a magnetic stirrer. pH of the resulting mixtures was found to be ~2. Dark brown coloured precursors were formed when the mixtures were evaporated to dryness on a hot plate at ~110 °C. The precursor powder was then calcined in air at 450 °C for 2.30 h to obtain $Ni_{0.65}Zn_{0.35}Fe_2O_4$ nanopowders.

Table 4.1 Starting materials required for preparation of $(BaFe_{12}O_{19})_{1-x}$-$(Ni_{0.65}Zn_{0.35}Fe_2O_4)_x$ nanocomposites

| Composition | *Zn dust (g) | *Ni$^{II}$-nitrate (g) | *Fe$^{III}$-nitrate (g) | Ba-Carbonate (g) | *EDTA (g) | #Ni$_{0.65}$Zn$_{0.35}$Fe$_2$O$_4$ (g) | #BaFe$_{12}$O$_{19}$ (g) |
|---|---|---|---|---|---|---|---|
| $Ni_{0.65}Zn_{0.35}Fe_2O_4$-pure | 0.097 | 0.798 | 3.42 | -- | 3.73 | -- | -- |
| $(BaFe_{12}O_{19})_{0.15}$-$(Ni_{0.65}Zn_{0.35}Fe_2O_4)_{0.85}$ | 0.053 | 0.437 | 3.84 | 0.08 | 14.29 | 0.5487 | 0.453 |
| $(BaFe_{12}O_{19})_{0.25}$-$(Ni_{0.65}Zn_{0.35}Fe_2O_4)_{0.75}$ | 0.038 | 0.311 | 3.99 | 0.108 | 14.12 | 0.389 | 0.611 |
| $(BaFe_{12}O_{19})_{0.5}$-$(Ni_{0.65}Zn_{0.35}Fe_2O_4)_{0.5}$ | 0.017 | 0.139 | 4.18 | 0.217 | 13.84 | 0.176 | 0.824 |
| $(BaFe_{12}O_{19})_{0.75}$-$(Ni_{0.65}Zn_{0.35}Fe_2O_4)_{0.25}$ | 0.007 | 0.053 | 4.29 | 0.165 | 13.75 | 0.066 | 0.934 |
| $BaFe_{12}O_{19}$-pure | -- | -- | 4.365 | 0.177 | 13.74 | -- | -- |

* For One-pot method.

# For Physical Mixing method.

_____

## 4.2 Results and Discussion

### 4.2.1 Thermal analysis

To find out the thermal decomposition behavior of precursors, prepared by OP method, TGA and DSC analysis were used. Thermogram of precursor powder (Fig. 4.1) revealed that a total weight loss of ~95 % occurred when the precursor powder was heated from 30 to 550 °C in air. Initially, ~7 % weight loss occurred in the region of 40 to 100 °C due to loss of moisture from the sample. Then, ~88 % weight loss was observed in the temperature range of 250 to 420 °C. This might be due to the oxidative decomposition of precursor and evolution of $CO_2$ and $NO_x$ gases. This decomposition was also observed in DSC thermogram as an exothermic peak at 433 °C. No weight loss was observed in TGA when the sample was heated beyond 440 °C. This confirmed the full decomposition of carbonaceous mass of the precursor occurred within 440 °C.
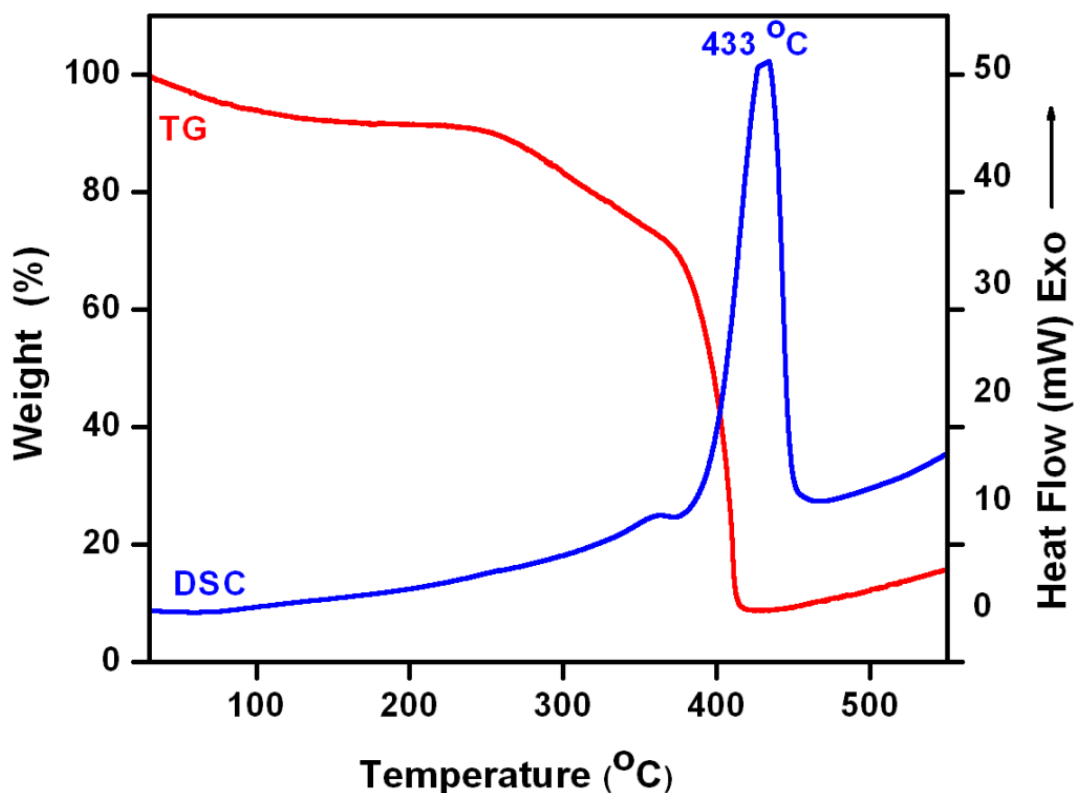


Fig. 4.1 TGA- DSC thermogram of $(BaFe_{12}O_{19})_{0.5}$-$(Ni_{0.65}Zn_{0.35}Fe_2O_4)_{0.5}$ precursor.

_____

**4.2.2 X-Ray Diffraction analysis**

Room temperature wide angle powder X-ray diffraction (XRD) was carried out to investigate the phases present in the nanocomposites. XRD patterns of (BaFe$_{12}$O$_{19}$)$_{1-x}$-(Ni$_{0.65}$Zn$_{0.35}$Fe$_2$O$_4$)$_x$ nanocomposites which were obtained by calcining the precursors (one-pot), exhibited the diffraction peaks corresponding to both spinel Ni$_{0.65}$Zn$_{0.35}$Fe$_2$O$_4$ [ICDD 08-0234] and hexagonal BaFe$_{12}$O$_{19}$ [ICDD 84-0757] phase (Fig. 4.2 (A) and (B)). The XRD patterns indicated the coexistence of both the phases in the composite powders. Any impurity peak, such as NiO, ZnO, BaO, BaCO$_3$, α-Fe$_2$O$_3$ etc. within the resolution of the technique was not observed. It was also observed that the highest intensity peak of soft ferrite phase at 2θ= 35.6° (corresponding to (311) plane) has increased with increasing the amount of Ni$_{0.65}$Zn$_{0.35}$Fe$_2$O$_4$ in the composite (i.e., with increasing the value of x). Same observation was also found for BaFe$_{12}$O$_{19}$ (Fig. 2.2 (B)).XRD patterns of composites-PM also showed the presence of both the phases. However, variation in relative intensities of the diffraction peaks was observed for these two types of composites. This might be due to the fact that, homogeneity of the spinel and hexagonal phases, present in the nanocomposites, vary with the synthesis route. The average crystallite sizes of Ni$_{0.65}$Zn$_{0.35}$Fe$_2$O$_4$ and BaFe$_{12}$O$_{19}$ phases in (BaFe$_{12}$O$_{19}$)$_{1-x}$-(Ni$_{0.65}$Zn$_{0.35}$Fe$_2$O$_4$)$_x$ nanocomposites were calculated by X-ray peak-broadening method using Scherrer's equation[437] and listed on Table 4.2. For Ni$_{0.65}$Zn$_{0.35}$Fe$_2$O$_4$, the diffraction peak at 2θ= 35.6°, which corresponds to (311) plane and for BaFe$_{12}$O$_{19}$, diffraction peak at 2θ= 34.2°, i.e. (114) plane were used. The important feature was that, in (BaFe$_{12}$O$_{19}$)$_{1-x}$-(Ni$_{0.65}$Zn$_{0.35}$Fe$_2$O$_4$)$_x$ nanocomposites-OP method, the crystallite size of Ni$_{0.65}$Zn$_{0.35}$Fe$_2$O$_4$ phase was increased from 12 to 33 nm with increasing amount of Ni$_{0.65}$Zn$_{0.35}$Fe$_2$O$_4$ phase in the composite. The same trend was observed for BaFe$_{12}$O$_{19}$ phase and its crystallite size was found to be increased from 21 to 43 nm. On the other hand, in case of (BaFe$_{12}$O$_{19}$)$_{1-x}$-(Ni$_{0.65}$Zn$_{0.35}$Fe$_2$O$_4$)$_x$ nanocomposites-PM method, the crystallite sizes of both spinel and hexagonal phase did not vary with varying amount of Ni$_{0.65}$Zn$_{0.35}$Fe$_2$O$_4$ and BaFe$_{12}$O$_{19}$ phases in the composites and were found to be ~33 nm and ~43 nm for Ni$_{0.65}$Zn$_{0.35}$Fe$_2$O$_4$ and BaFe$_{12}$O$_{19}$ respectively. These values were almost same in comparison with the crystallite sizes of pure Ni$_{0.65}$Zn$_{0.35}$Fe$_2$O$_4$ and BaFe$_{12}$O$_{19}$ nanopowders which imply that the pure phases retain their individual behaviours in the composites.
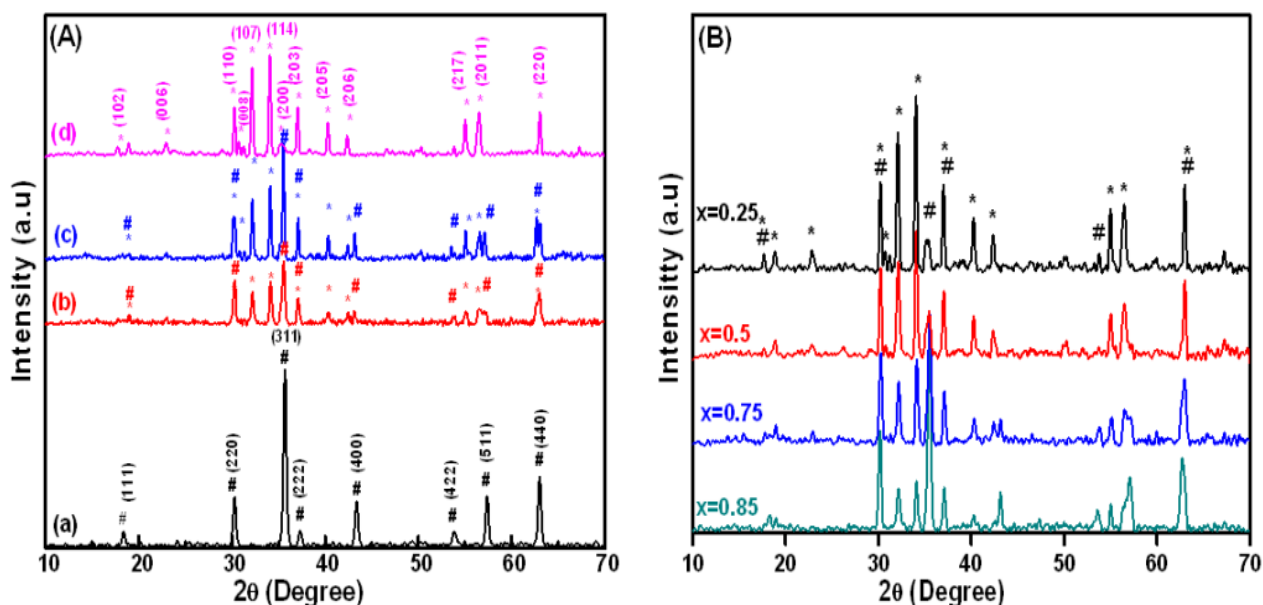
Fig. 4.2 (A) XRD spectra of the (a) pure Ni$_{0.65}$Zn$_{0.35}$Fe$_2$O$_4$ nanopowders, (BaFe$_{12}$O$_{19}$)$_{0.15}$-(Ni$_{0.65}$Zn$_{0.35}$Fe$_2$O$_4$)$_{0.85}$ nanocomposites prepared by (b) one-pot and (c) physical mixing methods and (d) BaFe$_{12}$O$_{19}$ nanopowders, (B) XRD spectra of (BaFe$_{12}$O$_{19}$)$_{1-x}$-(Ni$_{0.65}$Zn$_{0.35}$Fe$_2$O$_4$)$_x$ nanocomposites synthesized by one-pot method (#Ni$_{0.65}$Zn$_{0.35}$Fe$_2$O$_4$ and *BaFe$_{12}$O$_{19}$).

Table 4.2 Average crystalline size of (BaFe$_{12}$O$_{19}$)$_{1-x}$-(Ni$_{0.65}$Zn$_{0.35}$Fe$_2$O$_4$)$_x$ nanocomposites prepared by one-pot and physical mixing method

| Sample | Crystallite Size (nm) | | | |
|---|---|---|---|---|
| | One-Pot synthesis | | Physical mixing synthesis | |
| | *(114)plane | #(311)plane | *(114)plane | #(311)plane |
| Ni$_{0.65}$Zn$_{0.35}$Fe$_2$O$_4$-pure | -- | 33 | -- | -- |
| (BaFe$_{12}$O$_{19}$)$_{0.15}$-(Ni$_{0.65}$Zn$_{0.35}$Fe$_2$O$_4$)$_{0.85}$ | 21 | 26 | 43 | 31 |
| (BaFe$_{12}$O$_{19}$)$_{0.25}$-(Ni$_{0.65}$Zn$_{0.35}$Fe$_2$O$_4$)$_{0.75}$ | 29 | 22 | 44 | 35 |
| (BaFe$_{12}$O$_{19}$)$_{0.5}$-(Ni$_{0.65}$Zn$_{0.35}$Fe$_2$O$_4$)$_{0.5}$ | 33 | 14 | 42 | 34 |
| (BaFe$_{12}$O$_{19}$)$_{0.75}$-(Ni$_{0.65}$Zn$_{0.35}$Fe$_2$O$_4$)$_{0.25}$ | 38 | 12 | 42 | 33 |
| BaFe$_{12}$O$_{19}$-pure | 43 | -- | -- | -- |

* BaFe$_{12}$O$_{19}$

# Ni$_{0.65}$Zn$_{0.35}$Fe$_2$O$_4$

### 4.2.3 TEM and SEM analysis

During investigations on morphology of two different types of nanocomposites (prepared by PM and OP method) by HRTEM (Fig. 4.3) two distinct types of microstructures were observed.
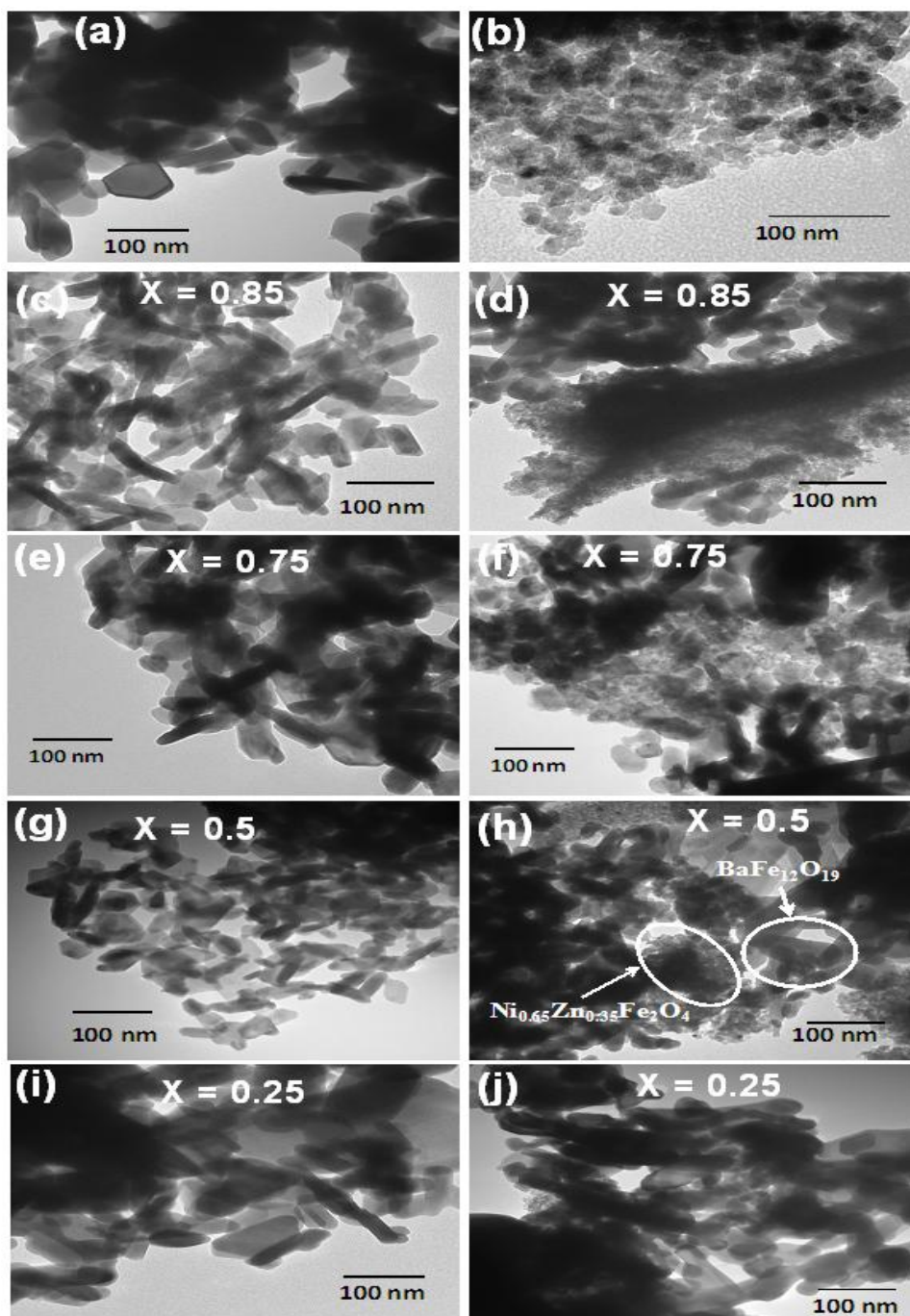


Fig. 4.3 TEM micrographs of (a) pure BaFe$_{12}$O$_{19}$, (b) pure Ni$_{0.65}$Zn$_{0.35}$Fe$_2$O$_4$ nanopowders and (BaFe$_{12}$O$_{19}$)$_{1-x}$-(Ni$_{0.65}$Zn$_{0.35}$Fe$_2$O$_4$)$_x$ nanocomposites synthesis by (c, e, g, i) one-pot and (d, f, h, j) physical mixing method.

_____

In case of the nanocomposites-PM method (Fig. 4.3 (d, f, h, j), clear separation of Ni$_{0.65}$Zn$_{0.35}$Fe$_2$O$_4$ phase, having spherical shaped agglomerated nanoparticles (Fig. 4.3 (a), ~10- 20 nm average particle size) and hexagonal BaFe$_{12}$O$_{19}$ nanoparticles (Fig. 4.3 (a), ~50-70 nm average particle size) were observed. On the contrary, when nanocomposites were prepared by one-pot method, almost uniform shaped nanoparticles (average particle size ~60-70 nm) were observed (Fig. 4.3 (c, e, g, i)).

SEM micrographs (Fig. 4.4) of the samples also revealed the intimate coexistence of Ni$_{0.65}$Zn$_{0.35}$Fe$_2$O$_4$ and BaFe$_{12}$O$_{19}$ particles in the nanocomposites-OP method (Fig. 4.4 (c)) and presence of large BaFe$_{12}$O$_{19}$ (Fig. 4.4 (b)) and small Ni$_{0.65}$Zn$_{0.35}$Fe$_2$O$_4$ (Fig. 4.4 (a)) particles in the nanocomposites prepared by physical mixing method (Fig. 4.4 (d)). EDX analysis of the final nanocomposites also revealed that all the metal ions are present in the composites (Fig. 4.4 (e)).
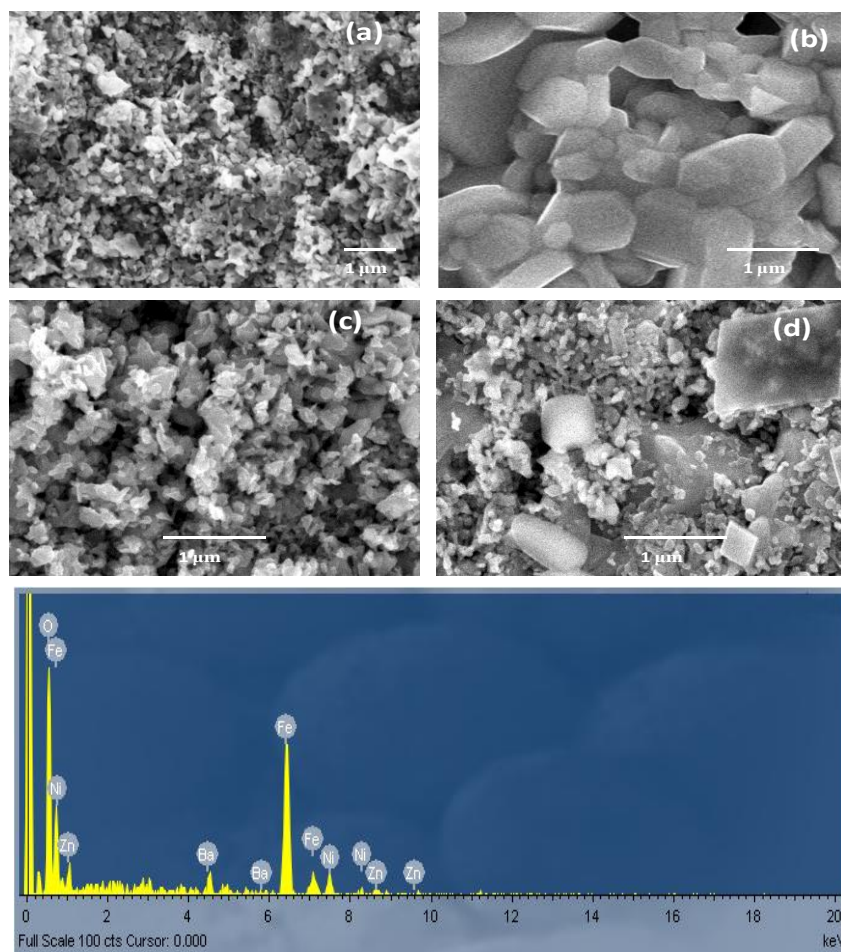


Fig. 4.4 SEM micrographs of (a) pure Ni$_{0.65}$Zn$_{0.35}$Fe$_2$O$_4$, (b) Pure BaFe$_{12}$O$_{19}$, (BaFe$_{12}$O$_{19}$)$_{0.5}$-(Ni$_{0.65}$Zn$_{0.35}$Fe$_2$O$_4$)$_{0.5}$ nanocomposites prepared by (a) one-pot, (b) physical mixing method and (c) EDX spectra of (BaFe$_{12}$O$_{19}$)$_{0.5}$-(Ni$_{0.65}$Zn$_{0.35}$Fe$_2$O$_4$)$_{0.5}$ nanocomposite prepared by one-pot method.

So, from microscopic analysis, it was obvious that the nanocomposites synthesized by one-pot method possess greater homogeneity, whereas composite prepared by physical mixing method, the hexagonal hard phase and spinel soft ferrite phases remain as segregated phases. This difference in morphology of the samples may influence the magnetic and microwave absorption properties of the nanocomposites.

### 4.2.4 Magnetic measurements

The room temperature magnetization behaviours of (BaFe$_{12}$O$_{19}$)$_{1-x}$-(Ni$_{0.65}$Zn$_{0.35}$Fe$_2$O$_4$)$_x$ nanocomposites prepared by two different methods (OP and PM method) were measured using VSM with an applied field of 15000 Oe and shown in Fig. 4.5 The most important observation was that, nanocomposites-OP method, showed single hysteresis loop, indicating hard and soft phases were well exchanged coupled to each other. Whereas, nanocomposites-PM method exhibited a typical two loop "bee waist" type hysteresis loop, suggesting the absence of exchange coupling between hard and soft phase (Fig. 4.5 (a)). [387, 431-433] Fig. 4.5 (b) also revealed that, all the composition of (BaFe$_{12}$O$_{19}$)$_{1-x}$-(Ni$_{0.65}$Zn$_{0.35}$Fe$_2$O$_4$)$_x$ showed single hysteresis loop for composites synthesized by OP-method whereas two loop hysteresis behavior for nanocomposites-PM (Fig. 4.5 (c)). Hence, (BaFe$_{12}$O$_{19}$)$_{1-x}$-(Ni$_{0.65}$Zn$_{0.35}$Fe$_2$O$_4$)$_x$ nanocomposites, prepared by one-pot method, though exhibited crystallographycally two phase behaviour but possessed magnetically good single phase behaviour.

It was also observed that, coercivity (H$_c$) values of the nanocomposites prepared by both the methods increased with increasing hard ferrite phase (i.e. BaFe$_{12}$O$_{19}$) content in the sample (Table 4.3). For the nanocomposites-OP method, initial incorporation of BaFe$_{12}$O$_{19}$ phase caused enhancement of saturation magnetization (M$_s$) values which was due to the spring exchange coupling between hard and soft magnetic phases. However, subsequent increase of BaFe$_{12}$O$_{19}$ content in the (BaFe$_{12}$O$_{19}$)$_{1-x}$-(Ni$_{0.65}$Zn$_{0.35}$Fe$_2$O$_4$)$_x$ nanocomposites (i.e., with increasing (1-x) values) did not affect much on M$_s$ value. Whereas, in case of nanocomposites-PM method, M$_s$ value increased with increasing amount of BaFe$_{12}$O$_{19}$. M$_s$ and H$_c$ values of all the composites prepared by one-pot method were found to be higher than those of the composites prepared by physical mixing method. These facts indicate that hard and soft ferrite phases are well exchanged coupled to each other in the composites prepared by one-pot method. Theoretically calculated values of M$_s$ of the composites (when hard and

___

soft phases are not exchange coupling) by using equation 2.1, were almost matching with the experimentally obtained values of the composites prepared by physical mixing method (Table 4.3).
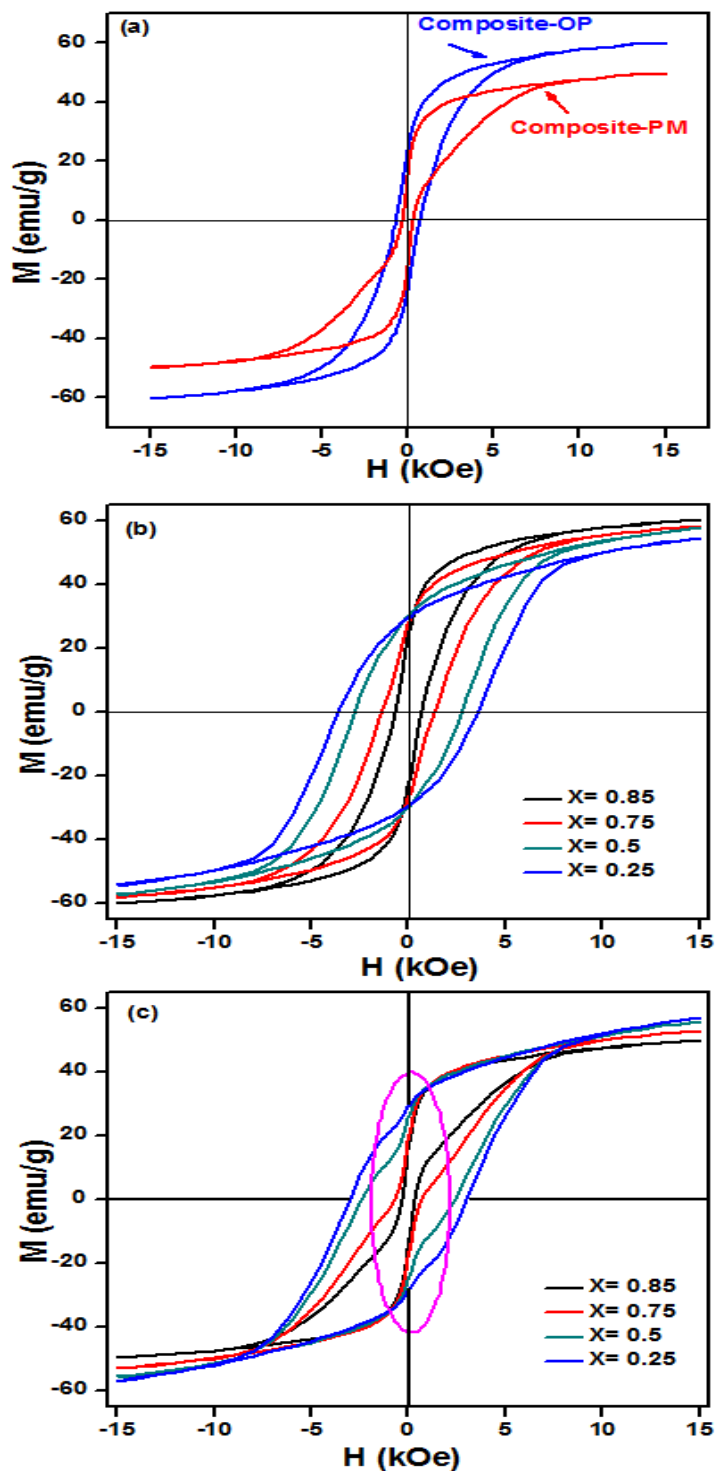


Fig. 4.5 Room temperature magnetic hysteresis loops for (a) $(BaFe_{12}O_{19})_{0.15}$-$(Ni_{0.65}Zn_{0.35}Fe_2O_4)_{0.85}$nanocomposite prepared by one-pot and physical mixing method and $(BaFe_{12}O_{19})_{1-x}$-$(Ni_{0.65}Zn_{0.35}Fe_2O_4)_x$ nanocomposite prepared by (b) one-pot, (c) physical mixing method.

Table 4.3 $M_s$ and $H_c$ values of the $(BaFe_{12}O_{19})_{1-x}$-$(Ni_{0.65}Zn_{0.35}Fe_2O_4)_x$ nanocomposites prepared by one-pot and physical mixing method

| Composition | One-pot synthesis | | Physical mixing synthesis | | Theoretical $M_s$ without exchange coupling (emu/g) |
|---|---|---|---|---|---|
| | $H_c$ (Oe) | $M_s$ (emu/g) | $H_c$ (Oe) | $M_s$ (emu/g) | |
| $Ni_{0.65}Zn_{0.35}Fe_2O_4$-pure | 103 | 41.2 | -- | -- | -- |
| $(BaFe_{12}O_{19})_{0.15}$-$(Ni_{0.65}Zn_{0.35}Fe_2O_4)_{0.85}$ | 681 | 60.2 | 299 | 49.8 | 48.1 |
| $(BaFe_{12}O_{19})_{0.25}$-$(Ni_{0.65}Zn_{0.35}Fe_2O_4)_{0.75}$ | 1357 | 58.2 | 710 | 52.9 | 50.5 |
| $(BaFe_{12}O_{19})_{0.5}$-$(Ni_{0.65}Zn_{0.35}Fe_2O_4)_{0.5}$ | 2822 | 57.5 | 2385 | 55.6 | 53.7 |
| $(BaFe_{12}O_{19})_{0.75}$-$(Ni_{0.65}Zn_{0.35}Fe_2O_4)_{0.25}$ | 3568 | 54.4 | 2997 | 57.0 | 55.6 |
| $BaFe_{12}O_{19}$-pure | 4914 | 56.5 | -- | -- | -- |

## 4.2.5 Microwave absorption study

The complex permittivity and permeability are usually used to analyze the dielectric and magnetic properties of absorber materials. Generally, the real parts ($\varepsilon'$ and $\mu'$) signify the storage capability of electric and magnetic energy, whereas the imaginary parts ($\varepsilon''$ and $\mu''$) stand for the loss of electric and magnetic energy[387, 388]

Microwave absorption behavior of $(BaFe_{12}O_{19})_{1-x}$-$(Ni_{0.65}Zn_{0.35}Fe_2O_4)_x$ nanocomposites with different compositions (x= 0.85, 0.75, 0.5, 0.25) synthesized by one-pot method were investigated. To understand the particular loss mechanism for each composite, the loss tangent vs. frequency were plotted and shown in Fig. 4.6 (a) and (b). The dielectric and magnetic loss tangents can be expressed as $\tan\delta_\varepsilon = \varepsilon''/\varepsilon'$ and $\tan\delta_\mu = \mu''/\mu'$, respectively. Fig. 4.6 (b) shows that these composites are having only magnetic loss parameter whereas the dielectric loss parameter is negligible (Fig. 4.6 (a)). Reflection loss (RL) was calculated using equation (1.4 and 1.5) and plotted against frequency for different $(BaFe_{12}O_{19})_{1-x}$-$(Ni_{0.65}Zn_{0.35}Fe_2O_4)_x$ nanocomposites (x= 0.85, 0.75, 0.5, 0.25) synthesized by OP method for thickness 2.9 mm (Fig. 4.6 (c)). In RL vs frequency plot, the dip of the curves were designated for minimum RL indicating maximum absorption. It was observed that, with decreasing the value of x (i.e. increasing $BaFe_{12}O_{19}$ content in the composite) maximum

absorption was decreases. As the composite having composition $(BaFe_{12}O_{19})_{0.15}$-$(Ni_{0.65}Zn_{0.35}Fe_2O_4)_{0.85}$ exhibited minimum reflection loss ($\sim$ -17dB) i.e. maximum absorption compare to other composites, so we have chosen this composition for further studies and the absorption properties are compared with the composite prepared by PM method as well as pure $Ni_{0.65}Zn_{0.35}Fe_2O_4$ and $BaFe_{12}O_{19}$.
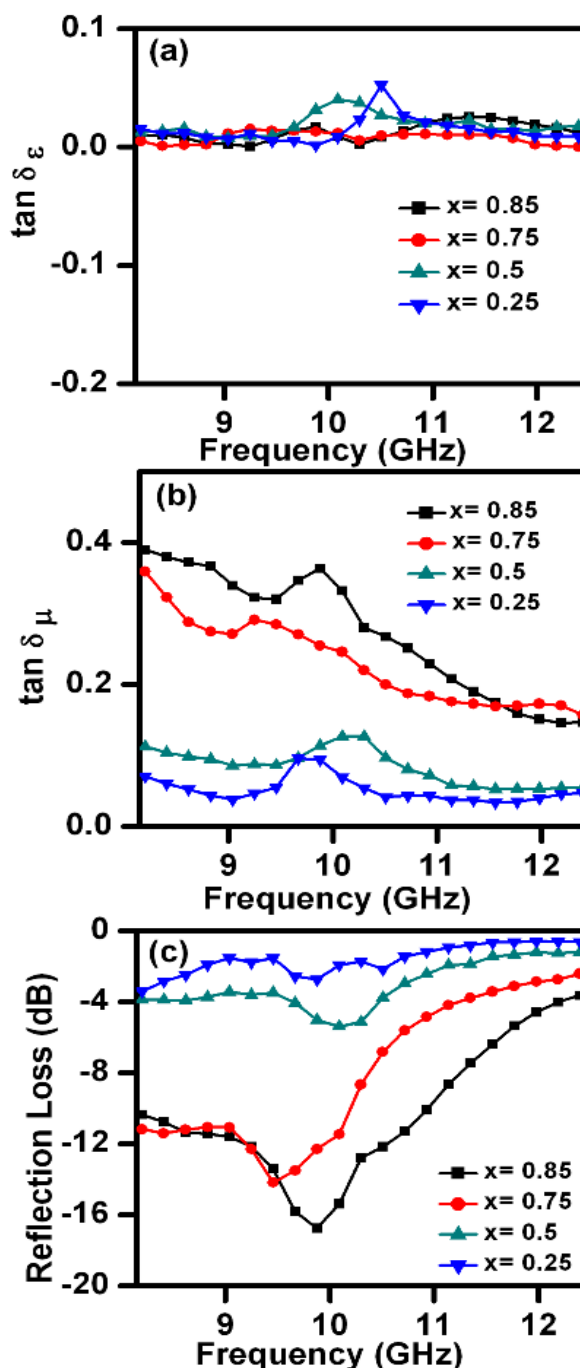


Fig. 4.6 (a) Loss Tangent of relative complex permittivity ($\tan\delta_\varepsilon$), (b) Loss Tangent of relative complex permeability ($\tan\delta_\mu$) and (c) Reflection loss vs. frequency plot $(BaFe_{12}O_{19})_{1-x}$-$(Ni_{0.65}Zn_{0.35}Fe_2O_4)_x$ nanocomposites synthesized by one-pot method.

The real and imaginary permittivity (Fig. 4.7 (a). and (b)) and permeability (Fig. 4.7 (c) and (d)) for the nanocomposites synthesized by both the methods, pure BaFe$_{12}$O$_{19}$ and Ni$_{0.65}$Zn$_{0.35}$Fe$_2$O$_4$ nanopowders were plotted as a function of frequency in the X-band range (8.2-12.4 GHz). It was observed that, $\varepsilon'$ values remained almost constant over the entire frequency range. Both nanocomposites samples showed almost same $\varepsilon'$ value which was in between the values of pure BaFe$_{12}$O$_{19}$ and Ni$_{0.65}$Zn$_{0.35}$Fe$_2$O$_4$. The imaginary dielectric parameter ($\varepsilon''$) values remained almost constant except two broad peaks appeared in the range of 9.2 GHz to 10.3 GHz and 10.3 to 12.4 GHz for the nanocomposite synthesized by one-pot method (Fig. 4.7 (b)). The intrinsic, electric dipole polarization and interfacial polarization are mainly responsible for this kind of behavior.[387]
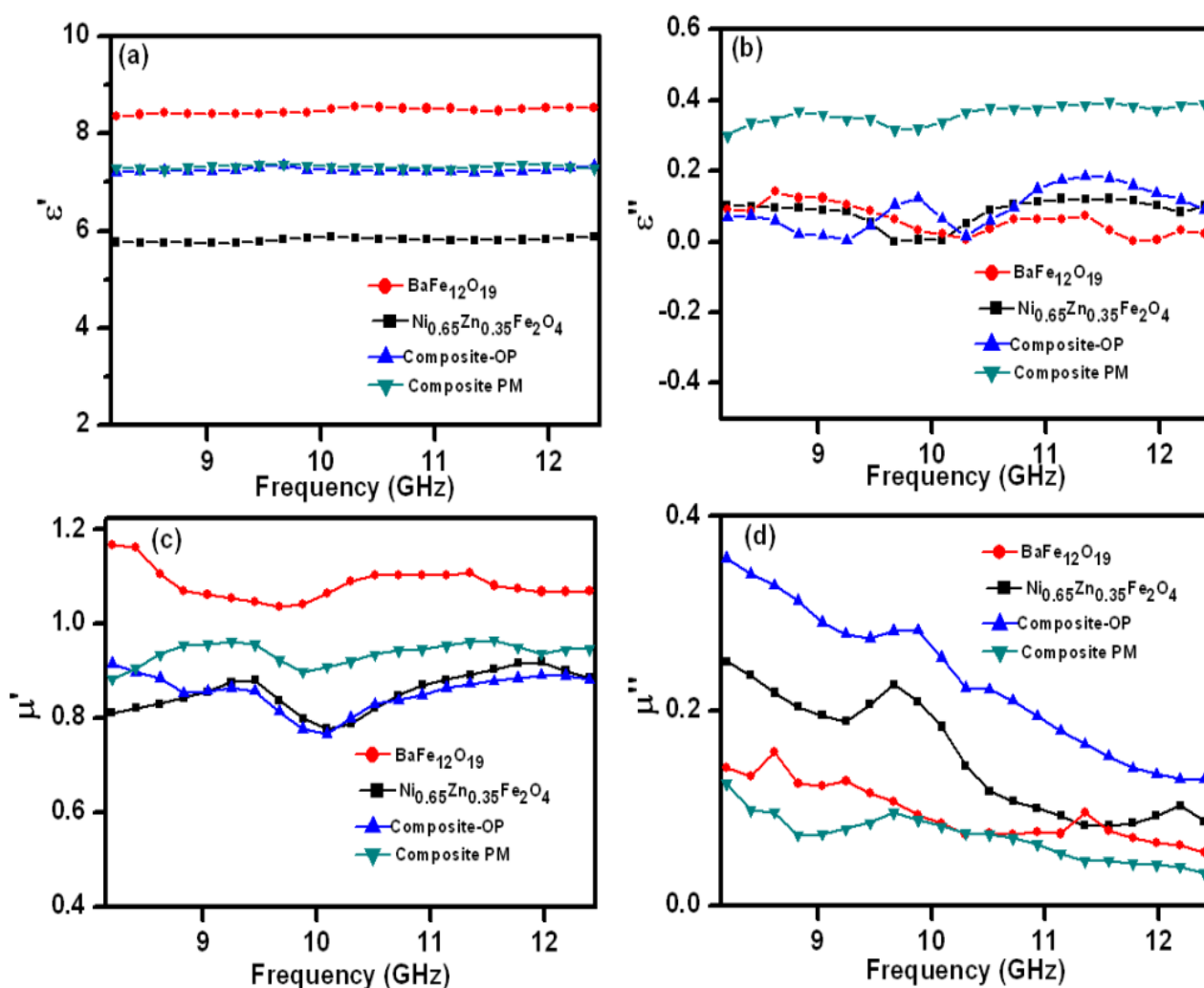


Fig. 4.7 (a) Real ($\varepsilon'$), (b) imaginary ($\varepsilon''$) parts of relative complex permittivity and (c) real ($\mu'$), (d) imaginary ($\mu''$) parts of relative complex permeability of pure BaFe$_{12}$O$_{19}$, Ni$_{0.65}$Zn$_{0.35}$Fe$_2$O$_4$ nanopowders and (BaFe$_{12}$O$_{19}$)$_{0.15}$-(Ni$_{0.65}$Zn$_{0.35}$Fe$_2$O$_4$)$_{0.85}$ nanocomposites prepared by one-pot and physical mixing method.

The real permeability ($\mu'$) values of composite-OP method initially showed a decreasing tendency in the range of 8.2- 10 GHz and then increased for the remaining frequency range of X-band whereas, pure nanopowders and composite-PM method remained almost constant throughout the entire frequency range (Fig. 4.7 (c)). The imaginary permeability ($\mu''$) values (Fig. 7.4 (d)) showed a decreasing tendency from 8.2 GHz to 12.4 GHz for both the nanocomposites and pure ferrites, however, maximum imaginary permeability was observed for the composite synthesized by one-pot method.

Refection Loss for nanocomposites as well as pure ferrite nanopowders was calculated for absorber thickness 2.9 mm and shown in Fig. 4.8 (a). The estimated electromagnetic wave absorption values are listed in Table 4.4. From Fig. 4.8 (a), it was observed that the nanocomposite-OP method showed greater reflection loss (~ -17dB at 9.88GHz corresponds to ~98% absorption) compare to the composite-PM method (~ -7dB at 9.67 GHz). Pure hard and soft ferrite nanopowders showed almost negligible reflection loss. For composite-OP method showed >10 dB reflection loss (i.e. > 90% absorption) over frequency range of 8.2 GHz to 10.85 GHz. Fig. 4.8 (b) illustrates the reflection loss vs. frequency for one-pot synthesized nancomposite with different thickness of the absorber. The reflection loss was found to be increased with increasing thickness of the sample upto 3.05 mm and then decreased. The minimum reflection loss ~ -21dB (maximum absorption, ~ 99.2%) was observed at 9.86 GHz for absorber thickness of 3.05 mm. However, band width of absorption corresponds to reflection loss > 10 dB becomes narrower in comparison to the absorber thickness of 2.9 mm. The RL value of -20 dB is equivalent to 99% absorption, which is considered as the satisfactory microwave absorption.

The improved microwave absorption property of hard-soft ferrite nanocomposites synthesized by One-pot method was attributed due to the exchange spin coupling interaction existing between hard and soft ferrite phases.[387, 388, 390, 435]
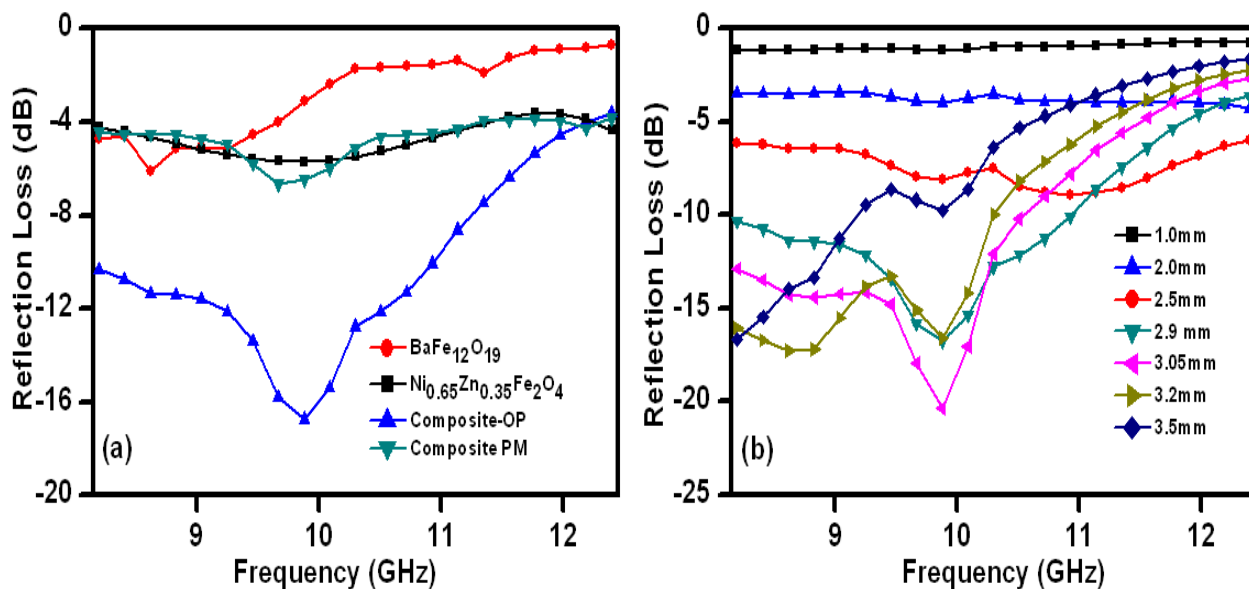
Fig. 4.8 Reflection loss vs. frequency plot for (a) pure $BaFe_{12}O_{19}$, $Ni_{0.65}Zn_{0.35}Fe_2O_4$ nanopowders and $(BaFe_{12}O_{19})_{0.15}$-$(Ni_{0.65}Zn_{0.35}Fe_2O_4)_{0.85}$ nanocomposites prepared by one-pot and physical mixing method and (b) Reflection loss vs. frequency plot for $(BaFe_{12}O_{19})_{0.15}$-$(Ni_{0.65}Zn_{0.35}Fe_2O_4)_{0.85}$ nanocomposites prepared by one-pot method at deferent specimen thickness.

Table 4.4 Microwave absorption characteristics of pure $BaFe_{12}O_{19}$, $Ni_{0.65}Zn_{0.35}Fe_2O_4$ nanopowders and $(BaFe_{12}O_{19})_{0.15}$-$(Ni_{0.65}Zn_{0.35}Fe_2O_4)_{0.85}$ nanocomposites prepared by one-pot and physical mixing method

| Sample | Minimum RL (dB) | Frequency (GHz) |
|---|---|---|
| $BaFe_{12}O_{19}$-pure | -6.1 | 8.62 |
| $(BaFe_{12}O_{19})_{0.15}$-$(Ni_{0.65}Zn_{0.35}Fe_2O_4)_{0.85}$ (one-pot method) | -16.8 | 9.88 |
| $(BaFe_{12}O_{19})_{0.15}$-$(Ni_{0.65}Zn_{0.35}Fe_2O_4)_{0.85}$ (physical mixing method) | -6.65 | 9.67 |
| $Ni_{0.65}Zn_{0.35}Fe_2O_4$-pure | -5.7 | 9.88 |

## 4.3 Summary of Results

(i)    $(BaFe_{12}O_{19})_{1-x}$-$(Ni_{0.65}Zn_{0.35}Fe_2O_4)_x$ nanocomposites were successfully synthesized using EDTA precursor based one-pot method where precursor was calcined at 800 °C for 4 h.

(ii)    Thermal decomposition of the precursor was completed at ~440 °C.

(iii)    XRD patterns of $(BaFe_{12}O_{19})_{1-x}$-$(Ni_{0.65}Zn_{0.35}Fe_2O_4)_x$ nanocomposites, prepared by one-pot method as well as physical mixing method exhibited the diffraction peaks corresponding to both spinel $Ni_{0.65}Zn_{0.35}Fe_2O_4$ and hexagonal $BaFe_{12}O_{19}$ phase.

(iv)    In $(BaFe_{12}O_{19})_{1-x}$-$(Ni_{0.65}Zn_{0.35}Fe_2O_4)_x$ nanocomposites synthesized by OP method, the crystallite size of $Ni_{0.65}Zn_{0.35}Fe_2O_4$ phase was increased from 12 to 33 nm with increasing amount of $Ni_{0.65}Zn_{0.35}Fe_2O_4$ phase in the composite. The same trend was observed for $BaFe_{12}O_{19}$ phase and its crystallite size was found to be increased from 21 to 43 nm.

(v)    $(BaFe_{12}O_{19})_{1-x}$-$(Ni_{0.65}Zn_{0.35}Fe_2O_4)_x$ nanocomposites synthesized by PM method, the crystallite sizes of both spinel and hexagonal phase did not change much with varying amount of $Ni_{0.65}Zn_{0.35}Fe_2O_4$ and $BaFe_{12}O_{19}$ phases in the composites and were found to be ~33 nm for $Ni_{0.65}Zn_{0.35}Fe_2O_4$ and ~43 nm for $BaFe_{12}O_{19}$. These values were almost same in comparison with the crystallite sizes of pure $Ni_{0.65}Zn_{0.35}Fe_2O_4$ and $BaFe_{12}O_{19}$.

(vi)    $(BaFe_{12}O_{19})_{1-x}$-$(Ni_{0.65}Zn_{0.35}Fe_2O_4)_x$ nanocomposites synthesized by PM method, clear segregation of hexagonal $BaFe_{12}O_{19}$ nanoparticles and spherical shaped agglomerated $Ni_{0.65}Zn_{0.35}Fe_2O_4$ nanoparticles were observed. Nanocomposites, prepared by one-pot method, almost uniform shaped nanoparticles (average particle size ~60-70 nm) were observed.

(vii)    $(BaFe_{12}O_{19})_{1-x}$-$(Ni_{0.65}Zn_{0.35}Fe_2O_4)_x$ nanocomposites synthesized by one-pot method, showed single hysteresis loop, signifying hard and soft phases were well exchanged coupled to each other. Whereas, composites-PM exhibited a typical two loop "bee waist" type hysteresis loop, indicating the absence of exchange coupling between hard and soft phase. $M_s$ and $H_c$ values of all the composites prepared by one-pot method were higher than those of the composites prepared by physical mixing method.

_____

(viii)   Nanocomposites synthesized by one-pot method are having only magnetic loss parameter whereas dielectric loss parameter is negligible.

(ix)   $(BaFe_{12}O_{19})_{1-x}$-$(Ni_{0.65}Zn_{0.35}Fe_2O_4)_x$ nanocomposites synthesized by one-pot method showed greater reflection loss (~ -17 dB at 9.88 GHz corresponds to 98% absorption) than composite-PM method (~ -7 dB at 9.67 GHz) for absorber thickness of 2.9 mm. Pure soft and hard ferrite nanopowders showed reflection loss lower than -10 dB (~-6 dB and ~-6 dB respectively).

(x)   $(BaFe_{12}O_{19})_{0.15}$-$(Ni_{0.65}Zn_{0.35}Fe_2O_4)_{0.85}$ nanocomposite synthesized by OP method exhibited reflection loss of ~ -21 dB (i.e. ~99.2% absorption) at 9.86 GHz for absorber thickness of 3.05 mm.

_____

**Chapter 5**

# Synthesis and characterization of (SrFe$_{12}$O$_{19}$)$_{1-x}$-(Ni$_{0.65}$Zn$_{0.35}$Fe$_2$O$_4$)$_x$ nanocomposites and study of their magnetic and microwave absorption properties

## 5.1 Experimental procedure

### 5.1.1 Materials required

Sr(NO$_3$)$_2$, Ni(NO$_3$)$_2$.6H$_2$O, Fe(NO$_3$)$_3$.9H$_2$O, Zn dust, Nitric Acid and Ethylene diamine tetra acetic acid (EDTA) were purchased from Merck, India and used without further purification. Zn(NO$_3$)$_2$ was prepared by dissolving Zn dust in aqueous nitric acid.

### 5.1.2 Synthesis of (SrFe$_{12}$O$_{19}$)$_{1-x}$-(Ni$_{0.65}$Zn$_{0.35}$Fe$_2$O$_4$)$_x$ nanocomposites by one-pot method (OP Method)[443]

To prepare (SrFe$_{12}$O$_{19}$)$_{1-x}$-(Ni$_{0.65}$Zn$_{0.35}$Fe$_2$O$_4$)$_x$ nanocomposites (with x = 0.85, 0.75, 0.5 and 0.25) using one-pot method stoichiometric amount of aqueous solutions of Sr(NO$_3$)$_2$, Ni(NO$_3$)$_2$.6H$_2$O, Zn(NO$_3$)$_2$, Fe(NO$_3$)$_3$.9H$_2$O, and EDTA were mixed in a beaker (Table 5.1) and stirred for 2 h. This reaction mixture was then dried at ~110 °C for 2 h. Black colour floppy carbonaceous material formed after drying, which is referred as precursor powder. Precursor powders were then calcined at 800 °C for 4 h in air atmosphere to obtain pure (SrFe$_{12}$O$_{19}$)$_{1-x}$-(Ni$_{0.65}$Zn$_{0.35}$Fe$_2$O$_4$)$_x$ nanocomposites.

### 5.1.3 Synthesis of (SrFe$_{12}$O$_{19}$)$_{1-x}$-(Ni$_{0.65}$Zn$_{0.35}$Fe$_2$O$_4$)$_x$ nanocomposites by physical mixing method (PM Method)

A set of composite samples with various composition (with x = 0.85, 0.75, 0.5 and 0.25) was prepared by using 'physical mixing' method where pure Ni$_{0.65}$Zn$_{0.35}$Fe$_2$O$_4$ and SrFe$_{12}$O$_{19}$ powders were mixed with appropriate weight ratio (Table 5.1) using a mortar pestle. Pure SrFe$_{12}$O$_{19}$ and Ni$_{0.65}$Zn$_{0.35}$Fe$_2$O$_4$ nanopowders were prepared separately by using the EDTA-precursor method, which has been developed by us.[257, 441] Detail synthesis procedure of pure SrFe$_{12}$O$_{19}$ and Ni$_{0.65}$Zn$_{0.35}$Fe$_2$O$_4$ nanopowders has already been discussed in Chapter 3, Section 3.1.3 and Chapter 4, Section 4.1.3 respectively.

Table 5.1 Starting materials required for preparation of (SrFe$_{12}$O$_{19}$)$_{1-x}$-(Ni$_{0.65}$Zn$_{0.35}$Fe$_2$O$_4$)$_x$ nanocomposites

| Composition | *Zn dust (g) | *Ni$^{II}$-nitrate (g) | *Fe$^{III}$-nitrate (g) | Sr$^{II}$-nitrate (g) | *EDTA (g) | #Ni$_{0.65}$Zn$_{0.35}$Fe$_2$O$_4$ (g) | #SrFe$_{12}$O$_{19}$ (g) |
|---|---|---|---|---|---|---|---|
| Ni$_{0.65}$Zn$_{0.35}$Fe$_2$O$_4$-pure | 0.097 | 0.798 | 3.42 | -- | 3.73 | -- | -- |
| (SrFe$_{12}$O$_{19}$)$_{0.15}$-(Ni$_{0.65}$Zn$_{0.35}$Fe$_2$O$_4$)$_{0.85}$ | 0.053 | 0.446 | 3.92 | 0.088 | 14.62 | 0.558 | 0.442 |
| (SrFe$_{12}$O$_{19}$)$_{0.25}$-(Ni$_{0.65}$Zn$_{0.35}$Fe$_2$O$_4$)$_{0.75}$ | 0.039 | 0.322 | 4.11 | 0.119 | 14.51 | 0.4 | 0.6 |
| (SrFe$_{12}$O$_{19}$)$_{0.5}$-(Ni$_{0.65}$Zn$_{0.35}$Fe$_2$O$_4$)$_{0.5}$ | 0.018 | 0.146 | 4.35 | 0.163 | 14.41 | 0.182 | 0.818 |
| (SrFe$_{12}$O$_{19}$)$_{0.75}$-(Ni$_{0.65}$Zn$_{0.35}$Fe$_2$O$_4$)$_{0.25}$ | 0.007 | 0.055 | 4.48 | 0.186 | 14.35 | 0.069 | 0.931 |
| SrFe$_{12}$O$_{19}$-pure | -- | -- | 4.57 | 0.199 | 14.38 | -- | -- |

* For One-pot method.

# For Physical Mixing method.


## 5.2 Results and Discussion


### 5.2.1 Thermal analysis


To investigate the thermal decomposition behavior of precursors, prepared by OP method, TGA and DSC analysis were used. Thermogram of precursor powder (Fig. 5.1) revealed that, a total weight loss of ~92 % occurred when the precursor powder was heated from 30 to 550 °C in air. Initially, ~3 % weight loss occurred in the region of 40 to 100 °C due to loss of moisture from the sample. In the second stage, ~89 % weight loss was observed in the temperature range of 255 to 440 °C. This might be due to the oxidative decomposition of precursor and evolution of $CO_2$ and $NO_x$ gases. This decomposition was also reflected in DSC thermogram as an exothermic peak at 426 °C. No weight loss was observed in TGA when the sample was heated beyond 450 °C. This confirmed the full decomposition of carbonaceous mass of the precursor occurred within 450 °C.
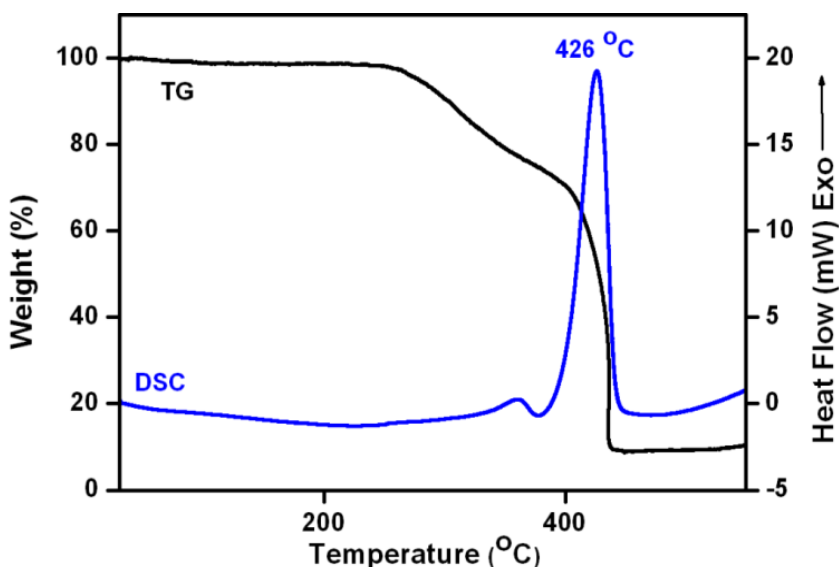
Fig. 5.1 TGA- DSC thermogram of $(SrFe_{12}O_{19})_{0.5}$-$(Ni_{0.65}Zn_{0.35}Fe_2O_4)_{0.5}$ precursor.

## 5.2.2 X-Ray Diffraction analysis

XRD patterns of $(SrFe_{12}O_{19})_{1-x}$-$(Ni_{0.65}Zn_{0.35}Fe_2O_4)_x$ nanocomposites prepared by OP method, exhibited the diffraction peaks corresponding to both spinel $Ni_{0.65}Zn_{0.35}Fe_2O_4$ [ICDD 08-0234] and hexagonal $SrFe_{12}O_{19}$ [ICDD 80-1198] phase (Fig. 5.2 (a) and (b)). XRD patterns indicated the coexistence of both the phases (i.e. $SrFe_{12}O_{19}$ and $Ni_{0.65}Zn_{0.35}Fe_2O_4$) in the composite powders. Any peak for impurity phases, such as NiO, ZnO, SrO, $SrCO_3$, $\alpha$-$Fe_2O_3$ etc. was not observed within the resolution of the technique. XRD patterns of the composites-PM also showed the existence of both the phases. However, variation in relative intensities of the diffraction peaks was observed for these two types of composites. This might be due to the fact that, homogeneous distribution of the spinel and hexagonal phases, in the nanocomposites vary with the synthesis route. The average crystallite sizes of $Ni_{0.65}Zn_{0.35}Fe_2O_4$ and $SrFe_{12}O_{19}$ phases in $(SrFe_{12}O_{19})_{1-x}$-$(Ni_{0.65}Zn_{0.35}Fe_2O_4)_x$ nanocomposites were calculated by X-ray peak-broadening method using Scherrer's equation[437] and listed on Table 5.2. For $Ni_{0.65}Zn_{0.35}Fe_2O_4$, the diffraction peak at $2\theta= 35.6°$, which corresponds to (311) plane and for $SrFe_{12}O_{19}$, diffraction peak at $2\theta= 34.2°$, i.e. (114) plane were used. It was noticed that, in $(SrFe_{12}O_{19})_{1-x}$-$(Ni_{0.65}Zn_{0.35}Fe_2O_4)_x$ nanocomposites-OP, the crystallite size of $Ni_{0.65}Zn_{0.35}Fe_2O_4$ phase was increased from 11 to 33 nm with increasing amount of $Ni_{0.65}Zn_{0.35}Fe_2O_4$ phase in the composite. Similarly for $SrFe_{12}O_{19}$ phase, crystallite size was also increased from 22 to 40 nm with increasing $SrFe_{12}O_{19}$ content in the composite. On the

83

other hand, in case of $(SrFe_{12}O_{19})_{1-x}$-$(Ni_{0.65}Zn_{0.35}Fe_2O_4)_x$ nanocomposites-PM, the crystallite sizes of both spinel and hexagonal phase did not vary with the variation of $Ni_{0.65}Zn_{0.35}Fe_2O_4$ and $SrFe_{12}O_{19}$ content in the composites and was found to be ~33 nm and ~40 nm for $Ni_{0.65}Zn_{0.35}Fe_2O_4$ and $SrFe_{12}O_{19}$ respectively. These values were almost same in comparison with the crystallite sizes of pure $Ni_{0.65}Zn_{0.35}Fe_2O_4$ and $SrFe_{12}O_{19}$ nanopowders, which suggest that the pure phases retain their individual crystallite size in the composites.
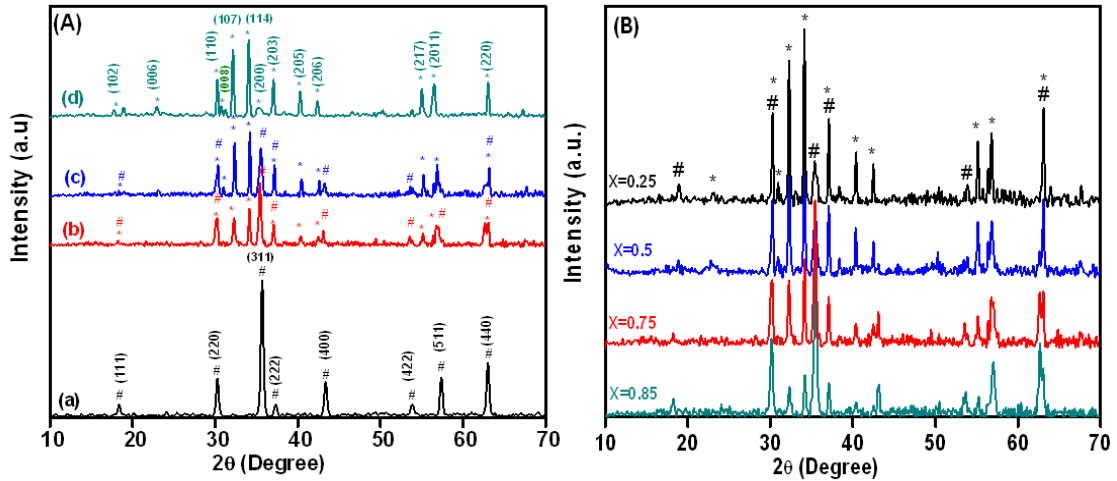


Fig. 5.2 (A) XRD spectra of the (a) pure $Ni_{0.65}Zn_{0.35}Fe_2O_4$ nanopowders, $(SrFe_{12}O_{19})_{0.15}$-$(Ni_{0.65}Zn_{0.35}Fe_2O_4)_{0.85}$ nanocomposites prepared by (b) one-pot and (c) physical mixing methods and (d) $SrFe_{12}O_{19}$ nanopowders, (B) XRD spectra of $(SrFe_{12}O_{19})_{1-x}$-$(Ni_{0.65}Zn_{0.35}Fe_2O_4)_x$ nanocomposites synthesized by one-pot method ($\#Ni_{0.65}Zn_{0.35}Fe_2O_4$ and $*SrFe_{12}O_{19}$).

Table 5.2 Average crystalline size of $(SrFe_{12}O_{19})_{1-x}$-$(Ni_{0.65}Zn_{0.35}Fe_2O_4)_x$ nanocomposites prepared by one-pot and physical mixing method

| Sample | Crystallite size (nm) | | | |
|---|---|---|---|---|
| | One-pot synthesis | | Physical mixing synthesis | |
| | *(114)plane | #(311)plane | *(114)plane | #(311)plane |
| $Ni_{0.65}Zn_{0.35}Fe_2O_4$-pure | -- | 33 | -- | 33 |
| $(SrFe_{12}O_{19})_{0.15}$-$(Ni_{0.65}Zn_{0.35}Fe_2O_4)_{0.85}$ | 22 | 27 | 39 | 31 |
| $(SrFe_{12}O_{19})_{0.25}$-$(Ni_{0.65}Zn_{0.35}Fe_2O_4)_{0.75}$ | 27 | 22 | 41 | 32 |
| $(SrFe_{12}O_{19})_{0.5}$-$(Ni_{0.65}Zn_{0.35}Fe_2O_4)_{0.5}$ | 31 | 17 | 40 | 34 |
| $(SrFe_{12}O_{19})_{0.75}$-$(Ni_{0.65}Zn_{0.35}Fe_2O_4)_{0.25}$ | 37 | 11 | 39 | 33 |
| $SrFe_{12}O_{19}$-pure | 40 | -- | 40 | -- |

* $SrFe_{12}O_{19}$

# $Ni_{0.65}Zn_{0.35}Fe_2O_4$

_____

### 5.2.3 TEM and SEM analysis

TEM micrographs (Fig. 5.3) revealed that nanocomposites, synthesized by using one-pot method, contained hexagonal shaped particles with average particle size of ~60-70 nm (Fig. 5.3 (c, e, g, i). Whereas, composites, prepared via physical mixing route consist of hexagonal SrFe$_{12}$O$_{19}$ particles (average size ~50-60 nm, Fig (5.3 (a)) and agglomerated spherical Ni$_{0.65}$Zn$_{0.35}$Fe$_2$O$_4$ particles (average size ~20 nm, Fig (5.3(b)).
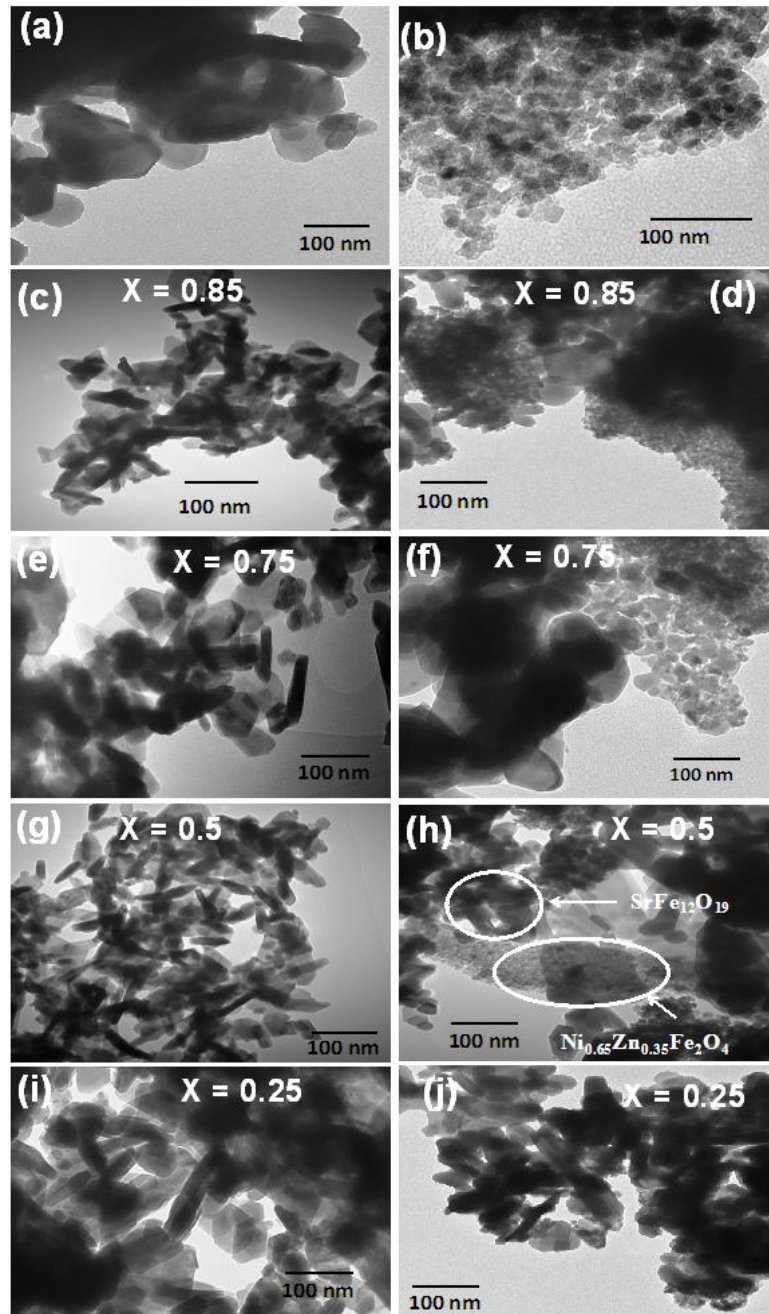


Fig. 5.3 TEM micrographs of (a) pure SrFe$_{12}$O$_{19}$, (b) pure Ni$_{0.65}$Zn$_{0.35}$Fe$_2$O$_4$ nanopowders and (SrFe$_{12}$O$_{19}$)$_{1-x}$-(Ni$_{0.65}$Zn$_{0.35}$Fe$_2$O$_4$)$_x$ nanocomposites synthesis by (c, e, g, i) one-pot and (d, f, h, j) physical mixing method.

SEM micrographs of the nanocomposites-OP showed almost regular shaped particle with loose agglomeration which proved the intimate presence of both hexagonal and spinel phases in the (SrFe$_{12}$O$_{19}$)$_{1-x}$-(Ni$_{0.65}$Zn$_{0.35}$Fe$_2$O$_4$)$_x$ nanocomposites (Fig. 5.4 (c)). On the other hand, composites-PM (Fig. 5.4 (d)) exhibited the mixture of larger and smaller particles with irregular shape which confirm the separate existence of SrFe$_{12}$O$_{19}$ (Fig. 5.4 (b)) and Ni$_{0.65}$Zn$_{0.35}$Fe$_2$O$_4$ (Fig. 5.4 (a)) nanoparticle in the nanocomposites.
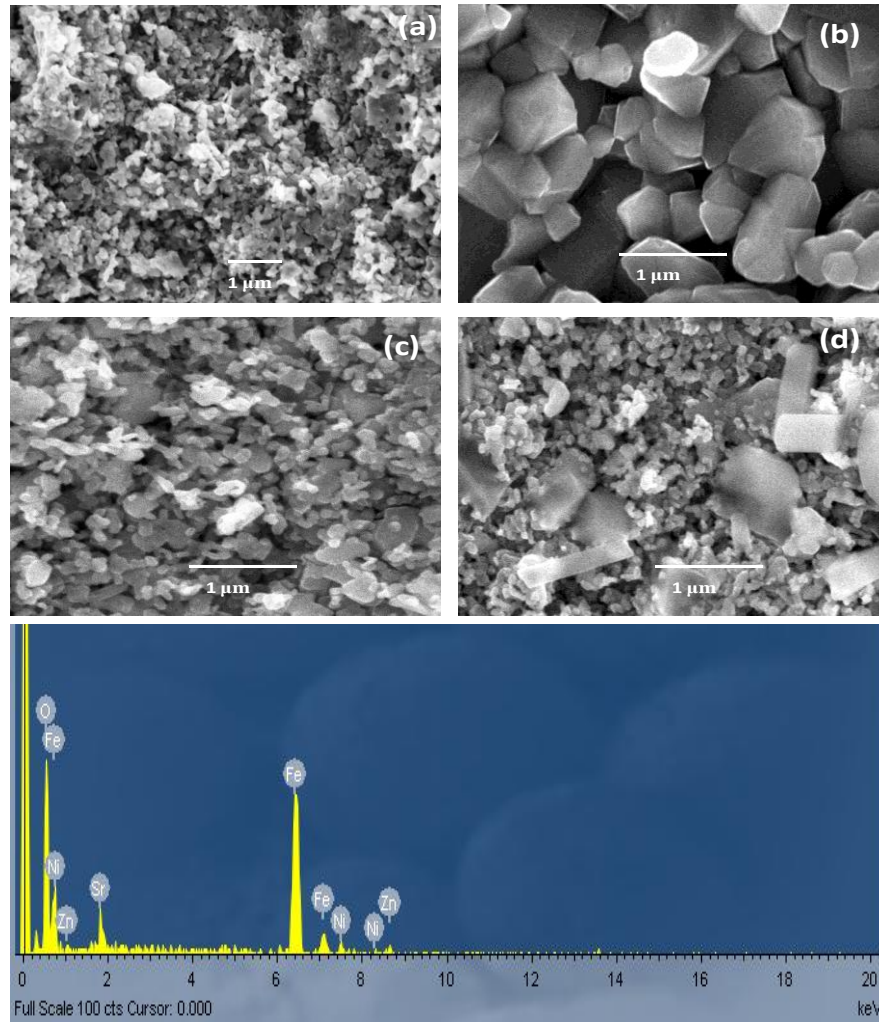


Fig. 5.4 SEM micrographs of (a) pure Ni$_{0.65}$Zn$_{0.35}$Fe$_2$O$_4$, (b) Pure SrFe$_{12}$O$_{19}$, (SrFe$_{12}$O$_{19}$)$_{0.5}$-(Ni$_{0.65}$Zn$_{0.35}$Fe$_2$O$_4$)$_{0.5}$ nanocomposites prepared by (a) one-pot, (b) physical mixing method and (c) EDX spectra of (SrFe$_{12}$O$_{19}$)$_{0.5}$-(Ni$_{0.65}$Zn$_{0.35}$Fe$_2$O$_4$)$_{0.5}$ nanocomposite prepared by one-pot method.

Electron microscopic analysis clearly shows that, the nanocomposites synthesized by one-pot method possess greater homogeneity whereas, in the composites prepared by physical mixing method, SrFe$_{12}$O$_{19}$ phase and Ni$_{0.65}$Zn$_{0.35}$Fe$_2$O$_4$ phase remain as segregated phases. This

difference in morphology of the samples may influence the magnetic and microwave absorption properties of the nanocomposites.

### 5.2.4 Magnetic measurements

Room temperature magnetization behaviours of (SrFe$_{12}$O$_{19}$)$_{1-x}$-(Ni$_{0.65}$Zn$_{0.35}$Fe$_2$O$_4$)$_x$ nanocomposites prepared OP and PM method, shown in Fig. 5.5.
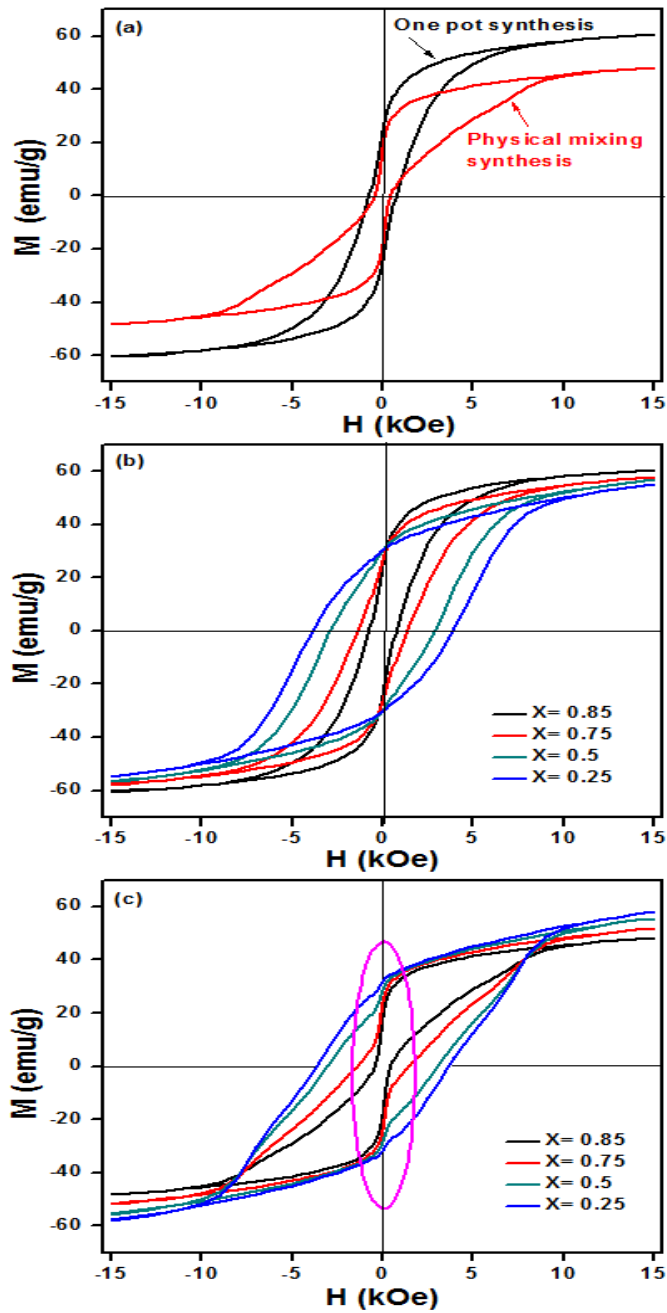


Fig. 5.5 Room temperature hysteresis loops for (a) (SrFe$_{12}$O$_{19}$)$_{0.15}$-(Ni$_{0.65}$Zn$_{0.35}$Fe$_2$O$_4$)$_{0.85}$ nanocomposite prepared by one-pot and physical mixing method and (SrFe$_{12}$O$_{19}$)$_{1-x}$-(Ni$_{0.65}$Zn$_{0.35}$Fe$_2$O$_4$)$_x$ nanocomposite prepared by (b) one-pot, (c) physical mixing method.

_____

The most important observation was that, nanocomposites-OP, showed single hysteresis loop, indicating hard and soft phases were well exchanged coupled to each other. Whereas, nanocomposites-PM exhibited a typical two loop "bee waist" type hysteresis loop, suggesting the absence of exchange coupling between hard and soft phase (Fig 5.5(a)). [387, 431-433] So, (SrFe$_{12}$O$_{19}$)$_{1-x}$-(Ni$_{0.65}$Zn$_{0.35}$Fe$_2$O$_4$)$_x$ nanocomposites, prepared by one-pot method, though exhibited crystallographycally two phase behaviour but possessed magnetically good single phase behaviour. Fig. 5.5 (b) also suggested that, all the composition of (SrFe$_{12}$O$_{19}$)$_{1-x}$-(Ni$_{0.65}$Zn$_{0.35}$Fe$_2$O$_4$)$_x$ showed single hysteresis loop for composites synthesized by OP-method whereas two loop hysteresis behavior for nanocomposites-PM (Fig. 5.5 (c)). M$_s$ and H$_c$ values of the composites prepared by 'one-pot' method were found to be higher than those of the composites prepared by physical mixing method. These facts indicate that hard and soft ferrite phases are well exchanged coupled to each other in the composites prepared by one-pot method. Theoretically calculated values of M$_s$ of the composites (when hard and soft phases are not exchange coupling) using equation 2.1, were almost similar with the experimentally obtained values of the composites prepared by physical mixing method, which also reflects that the hard and soft ferrite phases are not exchange coupled to each other (Table 5.3).

Table 5.3 M$_s$ and H$_c$ values of the (SrFe$_{12}$O$_{19}$)$_{1-x}$-(Ni$_{0.65}$Zn$_{0.35}$Fe$_2$O$_4$)$_x$ nanocomposites prepared by one-pot and physical mixing method

| Composition | One-pot synthesis | | Physical mixing synthesis | | Theoretical M$_s$ without exchange coupling (emu/g) |
|:---:|:---:|:---:|:---:|:---:|:---:|
| | H$_c$ (Oe) | M$_s$ (emu/g) | H$_c$ (Oe) | M$_s$ (emu/g) | |
| Ni$_{0.65}$Zn$_{0.35}$Fe$_2$O$_4$-pure | 103 | 41.2 | -- | -- | -- |
| (SrFe$_{12}$O$_{19}$)$_{0.15}$-(Ni$_{0.65}$Zn$_{0.35}$Fe$_2$O$_4$)$_{0.85}$ | 749 | 60.2 | 469 | 48.2 | 48.4 |
| (SrFe$_{12}$O$_{19}$)$_{0.25}$-(Ni$_{0.65}$Zn$_{0.35}$Fe$_2$O$_4$)$_{0.75}$ | 1441 | 57.6 | 1379 | 51.6 | 51.0 |
| (SrFe$_{12}$O$_{19}$)$_{0.5}$-(Ni$_{0.65}$Zn$_{0.35}$Fe$_2$O$_4$)$_{0.5}$ | 3035 | 56.7 | 2868 | 55.4 | 54.6 |
| (SrFe$_{12}$O$_{19}$)$_{0.75}$-(Ni$_{0.65}$Zn$_{0.35}$Fe$_2$O$_4$)$_{0.25}$ | 387 | 54.9 | 3649 | 57.8 | 56.5 |
| SrFe$_{12}$O$_{19}$-pure | 5866 | 57.6 | -- | -- | -- |

_____

### 5.2.5 Microwave absorption study

The complex permittivity and permeability are usually used to analyze the dielectric and magnetic properties of absorber materials. Generally, the real parts ($\varepsilon'$ and $\mu'$) stand for storage capability of electric and magnetic energy, whereas the imaginary parts ($\varepsilon''$ and $\mu''$) signify the loss of electric and magnetic energy.

Microwave absorption behavior of $(SrFe_{12}O_{19})_{1-x}$-$(Ni_{0.65}Zn_{0.35}Fe_2O_4)_x$ nanocomposites with different compositions (x= 0.85, 0.75, 0.5, 0.25) synthesized by one-pot method were investigated. Loss tangent vs. frequency were plotted to understand the particular loss mechanism for each composite and shown in Fig. 5.6 (a) and (b).
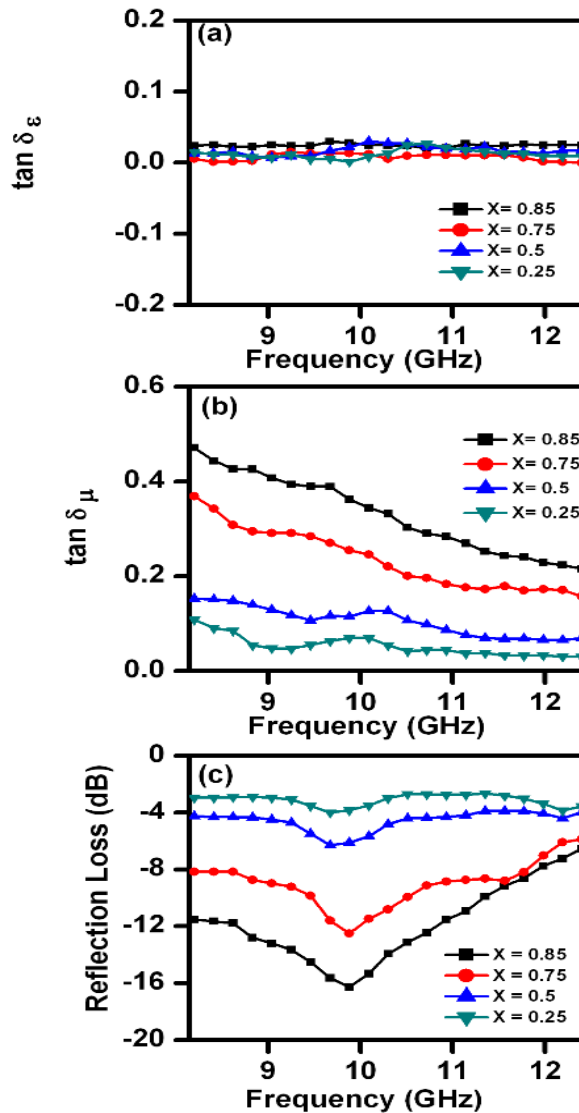


Fig. 5.6 (a) Loss Tangent of relative complex permittivity ($\tan\delta_\varepsilon$), (b) Loss Tangent of relative complex permeability ($\tan\delta_\mu$) and (c) Reflection loss vs. frequency plot $(SrFe_{12}O_{19})_{1-x}$-$(Ni_{0.65}Zn_{0.35}Fe_2O_4)_x$ nanocomposites synthesized by one-pot method.

_____

The dielectric and magnetic loss tangents can be expressed as $\tan\delta_\varepsilon = \varepsilon''/\varepsilon'$ and $\tan\delta_\mu = \mu''/\mu'$, respectively. Fig. 5.6 (b) shows that these composites are having only magnetic loss parameter whereas the dielectric loss parameter is negligible (Fig. 5.6 (a)). Reflection loss was calculated using equations (1.4 and 1.5) and plotted against frequency for (SrFe$_{12}$O$_{19}$)$_{1-x}$-(Ni$_{0.65}$Zn$_{0.35}$Fe$_2$O$_4$)$_x$ nanocomposites synthesized by one-pot method for thickness of 3 mm (Fig. 5.6 (c)). In RL vs. frequency plot, the dip of the curves was designated for minimum RL indicating maximum absorption. This figure illustrates that with decreasing value of x (i.e. increasing SrFe$_{12}$O$_{19}$ content in the composite) maximum absorption decreases. As the composite having composition (SrFe$_{12}$O$_{19}$)$_{0.15}$-(Ni$_{0.65}$Zn$_{0.35}$Fe$_2$O$_4$)$_{0.85}$ exhibited minimum reflection loss (~ -16 dB) i.e. maximum absorption compare to other composites, so we have chosen this composition for further studies and its microwave absorption properties were compared with composite prepared by PM method as well as pure Ni$_{0.65}$Zn$_{0.35}$Fe$_2$O$_4$ and SrFe$_{12}$O$_{19}$.

The real and imaginary permittivity (Fig. 5.7 (a). and (b)) and permeability (Fig. 5.7 (c) and (d)) for the nanocomposites synthesized by both the methods, pure SrFe$_{12}$O$_{19}$ and Ni$_{0.65}$Zn$_{0.35}$Fe$_2$O$_4$ nanopowders were plotted as a function of frequency in the X-band range (8.2-12.4 GHz). It was observed that, $\varepsilon'$ values remained almost constant over the entire frequency range. Both nanocomposites showed almost same $\varepsilon'$ value, which was in between the values of pure SrFe$_{12}$O$_{19}$ and Ni$_{0.65}$Zn$_{0.35}$Fe$_2$O$_4$ (Fig. 5.7(a)). The imaginary dielectric parameter ($\varepsilon''$) values remained almost constant for both composites as well as pure SrFe$_{12}$O$_{19}$ and Ni$_{0.65}$Zn$_{0.35}$Fe$_2$O$_4$ nanopowders (Fig. 5.7 (b)). The real permeability ($\mu'$) values of composite-OP method showed a decreasing trend over the complete frequency range of X-band whereas, pure nanopowders and composite-PM method remained almost constant throughout the entire frequency range (Fig. 5.7 (c)). The imaginary permeability ($\mu''$) values (Fig. 5.7 (d)) showed a decreasing tendency from 8.2 GHz to 12.4 GHz for both the nanocomposites and pure ferrites but the maximum imaginary permeability was observed for the composite synthesized by one-pot method.
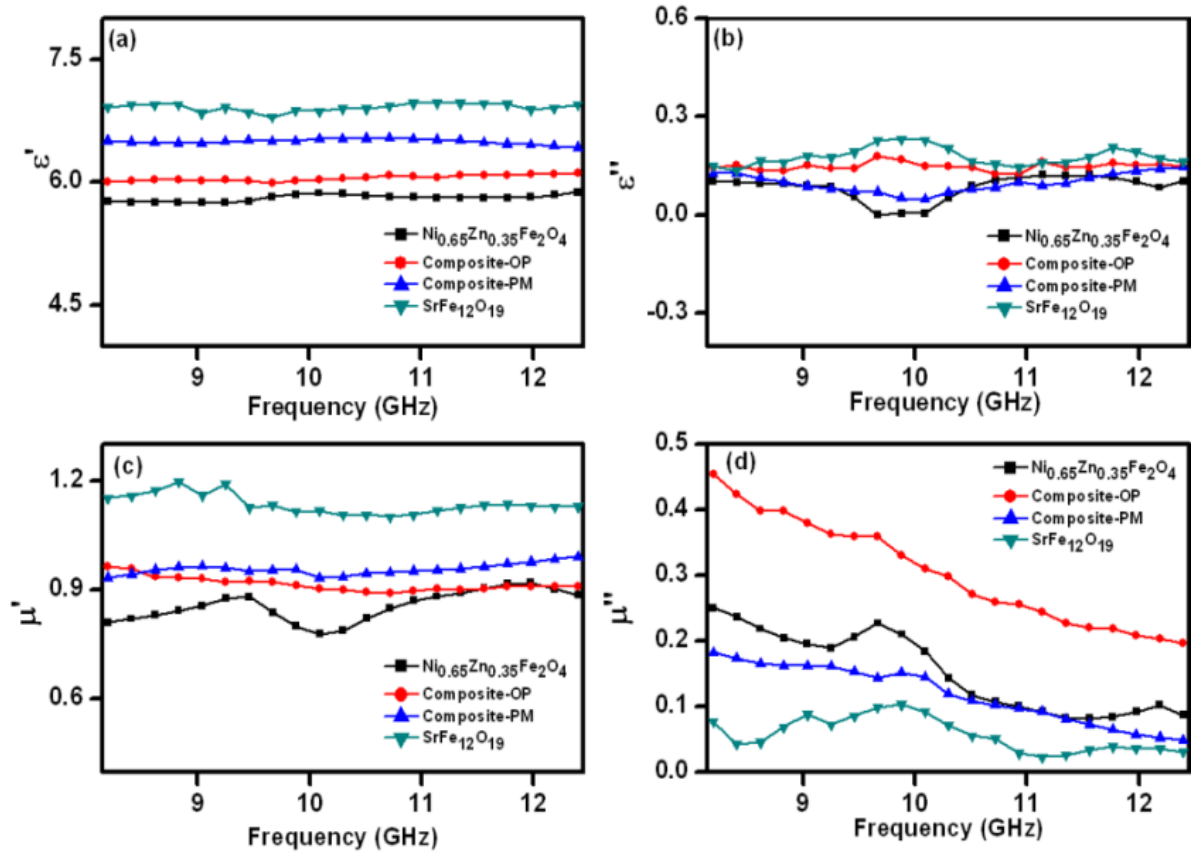
Fig. 5.7 (a) Real ($\varepsilon'$), (b) imaginary ($\varepsilon''$) parts of relative complex permittivity and (c) real ($\mu'$), (d) imaginary ($\mu''$) parts of relative complex permeability of pure $SrFe_{12}O_{19}$, $Ni_{0.65}Zn_{0.35}Fe_2O_4$ nanopowders and $(SrFe_{12}O_{19})_{0.15}$-$(Ni_{0.65}Zn_{0.35}Fe_2O_4)_{0.85}$ nanocomposites prepared by one-pot and physical mixing method.

Refection Loss for nanocomposites and pure ferrite nanopowders with a specimen thickness of 3 mm is shown in Fig. 5.8 (a). The estimated electromagnetic wave absorption values are listed in Table 5.4. It was observed that the composite-OP showed higher reflection loss (~ -16 dB at 9.88 GHz corresponds to ~97.5% absorption) than that of composite-PM (~ -6 dB at 10.09 GHz). Pure hard and soft ferrite nanopowders showed almost negligible reflection loss i.e maximum loss of ~ -6 dB for both. Composite-OP showed ≥ -10 dB reflection loss (i.e. > 90% absorption) over 3.1 GHz (8.2 GHz to 11.3 GHz) frequency range. Fig. 5.8 (b) illustrates the reflection loss vs frequency for one-pot synthesized nancomposite with different thickness of the absorber. The reflection loss was found to be increased with increasing thickness of the sample till 3.5 mm with the shifting of the frequency corresponds to maximum loss towards lower frequency. Reflection loss of ~ -22 dB i.e. > 99% absorption was observed at 8.2 GHz for absorber thickness of 3.5 mm but frequency range corresponds

_____

to reflection loss ≥ -10 dB (means > 90% absorption) becomes narrower in comparison with the specimen thickness of 3 mm.

The improved microwave absorption property of hard-soft ferrite nanocomposites was attributed due to the exchange spin coupling interaction existing between hard and soft ferrite phases.[387, 388, 390, 435]
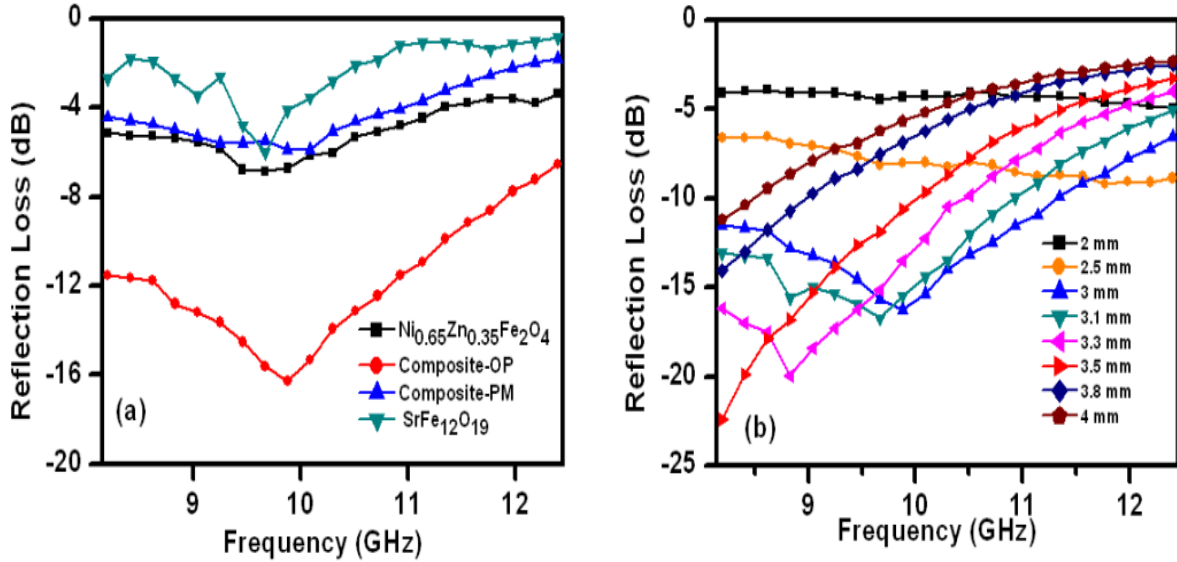


Fig. 5.8 Reflection loss vs. frequency plot for (a) pure $SrFe_{12}O_{19}$, $Ni_{0.65}Zn_{0.35}Fe_2O_4$ nanopowders and $(SrFe_{12}O_{19})_{0.15}$-$(Ni_{0.65}Zn_{0.35}Fe_2O_4)_{0.85}$ nanocomposites prepared by one-pot and physical mixing method and (b) Reflection loss vs. frequency plot for $(SrFe_{12}O_{19})_{0.15}$-$(Ni_{0.65}Zn_{0.35}Fe_2O_4)_{0.85}$ nanocomposites prepared by one-pot method at different absorber thickness.

Table 5.4 Microwave absorption characteristics of pure $SrFe_{12}O_{19}$, $Ni_{0.65}Zn_{0.35}Fe_2O_4$ nanopowders and $(SrFe_{12}O_{19})_{0.15}$-$(Ni_{0.65}Zn_{0.35}Fe_2O_4)_{0.85}$ nanocomposites prepared by one-pot and physical mixing method

| Sample | Minimum RL (dB) | Frequency (GHz) |
|---|---|---|
| $SrFe_{12}O_{19}$-pure | -6.1 | 9.67 |
| $(SrFe_{12}O_{19})_{0.15}$-$(Ni_{0.65}Zn_{0.35}Fe_2O_4)_{0.85}$ (one-pot method) | -16.2 | 9.88 |
| $(SrFe_{12}O_{19})_{0.15}$-$(Ni_{0.65}Zn_{0.35}Fe_2O_4)_{0.85}$ (physical mixing method) | -5.8 | 9.67 |
| $Ni_{0.65}Zn_{0.35}Fe_2O_4$-pure | -6.8 | 9.67 |

_____

## 5.3 Summary of Results

(i)      (SrFe$_{12}$O$_{19}$)$_{1-x}$-(Ni$_{0.65}$Zn$_{0.35}$Fe$_2$O$_4$)$_x$ nanocomposites were successfully synthesized using EDTA precursor based one-pot method where precursor was calcined at 800 °C for 4 h.

(ii)      Thermal decomposition of the precursor was completed at ~450 °C.

(iii)      XRD patterns of (SrFe$_{12}$O$_{19}$)$_{1-x}$-(Ni$_{0.65}$Zn$_{0.35}$Fe$_2$O$_4$)$_x$ nanocomposites, prepared by one-pot method as well as physical mixing method exhibited the diffraction peaks corresponding to both spinel Ni$_{0.65}$Zn$_{0.35}$Fe$_2$O$_4$ and hexagonal SrFe$_{12}$O$_{19}$ phase.

(iv)      In (SrFe$_{12}$O$_{19}$)$_{1-x}$-(Ni$_{0.65}$Zn$_{0.35}$Fe$_2$O$_4$)$_x$ nanocomposites synthesized by OP method, the crystallite size of Ni$_{0.65}$Zn$_{0.35}$Fe$_2$O$_4$ phase was increased from 11 to 33 nm with increasing amount of Ni$_{0.65}$Zn$_{0.35}$Fe$_2$O$_4$ phase in the composite. The same trend was observed for SrFe$_{12}$O$_{19}$ phase and its crystallite size was found to be increased from 22 to 40 nm.

(v)      (SrFe$_{12}$O$_{19}$)$_{1-x}$-(Ni$_{0.65}$Zn$_{0.35}$Fe$_2$O$_4$)$_x$ nanocomposites synthesized by PM method, the crystallite sizes of both spinel and hexagonal phase did not change much with varying amount of Ni$_{0.65}$Zn$_{0.35}$Fe$_2$O$_4$ and SrFe$_{12}$O$_{19}$ phases in the composites and were found to be ~33 nm for Ni$_{0.65}$Zn$_{0.35}$Fe$_2$O$_4$ and ~40 nm for SrFe$_{12}$O$_{19}$. These values were almost same in comparison with the crystallite sizes of pure Ni$_{0.65}$Zn$_{0.35}$Fe$_2$O$_4$and SrFe$_{12}$O$_{19}$.

(vi)      (SrFe$_{12}$O$_{19}$)$_{1-x}$-(Ni$_{0.65}$Zn$_{0.35}$Fe$_2$O$_4$)$_x$ nanocomposites synthesized by PM method, clear segregation of hexagonal SrFe$_{12}$O$_{19}$ nanoparticles and spherical shaped agglomerated Ni$_{0.65}$Zn$_{0.35}$Fe$_2$O$_4$ nanoparticles were observed. Nanocomposites, prepared by one-pot method, almost uniform shaped nanoparticles (average particle size ~60-70 nm) were observed.

(vii)      (SrFe$_{12}$O$_{19}$)$_{1-x}$-(Ni$_{0.65}$Zn$_{0.35}$Fe$_2$O$_4$)$_x$ nanocomposites synthesized by one-pot method, showed single hysteresis loop, signifying hard and soft phases were well exchanged coupled to each other. Whereas, composites-PM exhibited a typical two loop "bee waist" type hysteresis loop, indicating the absence of exchange coupling between hard and soft phase. M$_s$ and H$_c$ values of all the composites prepared by one-pot method were higher than those of the composites prepared by physical mixing method.

_____

(viii)   Nanocomposites synthesized by one-pot method are having only magnetic loss parameter whereas dielectric loss parameter is negligible.

(ix)   $(SrFe_{12}O_{19})_{1-x}$-$(Ni_{0.65}Zn_{0.35}Fe_2O_4)_x$ nanocomposites synthesized by one-pot method showed greater reflection loss (~ -16 dB at 9.88 GHz corresponds to 97.5% absorption) than composite-PM method (~ -6 dB at 9.67 GHz) for absorber thickness of 3 mm. Pure soft and hard ferrite nanopowders showed reflection loss lower than -10 dB (~-7 dB and ~-6 dB respectively).

(x)   $(SrFe_{12}O_{19})_{0.15}$-$(Ni_{0.65}Zn_{0.35}Fe_2O_4)_{0.85}$ nanocomposite synthesized by OP method exhibited reflection loss of ~ -22 dB (i.e. ~99.4% absorption) at 8.2 GHz for absorber thickness of 3.5 mm.

_____

<div align="right">

**Chapter 6**

</div>

# Synthesis and characterization of (BaFe$_{12}$O$_{19}$)$_{1-x}$-(Mn$_{0.2}$Ni$_{0.4}$Zn$_{0.4}$Fe$_2$O$_4$)$_x$ nanocomposites and study of their magnetic and microwave absorption properties

## 6.1 Experimental procedure

### 6.1.1 Materials required

BaCO$_3$, Mn(NO$_3$)$_2$.4H$_2$O, Ni(NO$_3$)$_2$.6H$_2$O, Fe(NO$_3$)$_3$.9H$_2$O, Zn dust, Nitric Acid and Ethylene diamine tetra acetic acid (EDTA) were purchased from Merck, India and used without further purification. Zn(NO$_3$)$_2$ and Ba(NO$_3$)$_2$ were prepared by dissolving Zn dust and BaCO$_3$ respectively in aqueous nitric acid.

### 6.1.2 Synthesis of (BaFe$_{12}$O$_{19}$)$_{1-x}$-(Mn$_{0.2}$Ni$_{0.4}$Zn$_{0.4}$Fe$_2$O$_4$)$_x$ nanocomposites by one-pot method (OP Method)[444]

To prepare (BaFe$_{12}$O$_{19}$)$_{1-x}$-(Mn$_{0.2}$Ni$_{0.4}$Zn$_{0.4}$Fe$_2$O$_4$)$_x$ nanocomposites (with x= 0.85, 0.75, 0.5 and 0.25) using one-pot method stoichiometric amount of aqueous solutions of BaNO$_3$, Mn(NO$_3$)$_2$.4H$_2$O, Ni(NO$_3$)$_2$.6H$_2$O, Zn(NO$_3$)$_2$ Fe(NO$_3$)$_3$.9H$_2$O, and EDTA were mixed in a beaker (Table 6.1) and stirred for 2 h. This reaction mixture was then dried at ~110 °C for 2 h. Black colour floppy carbonaceous material was formed after drying, which referred as precursor powder. Then the precursor powders were calcined at 800 °C for 4 h in air atmosphere to obtain pure (BaFe$_{12}$O$_{19}$)$_{1-x}$-(Mn$_{0.2}$Ni$_{0.4}$Zn$_{0.4}$Fe$_2$O$_4$)$_x$ nanocomposites.

### 6.1.3 Synthesis of (BaFe$_{12}$O$_{19}$)$_{1-x}$-(Mn$_{0.2}$Ni$_{0.4}$Zn$_{0.4}$Fe$_2$O$_4$)$_x$ nanocomposites by physical mixing method (PM Method)

Another set of composite samples with various composition (with x= 0.85, 0.75, 0.5 and 0.25) was prepared by using 'physical mixing' method where pure Mn$_{0.2}$Ni$_{0.4}$Zn$_{0.4}$Fe$_2$O$_4$ and BaFe$_{12}$O$_{19}$ powders were mixed with appropriate weight ratio (Table 6.1) using a mortar pestle. Pure BaFe$_{12}$O$_{19}$ and Mn$_{0.2}$Ni$_{0.4}$Zn$_{0.4}$Fe$_2$O$_4$ nanopowders were prepared separately by using the EDTA- precursor method which has been developed by us.[255, 253] Detail synthesis procedure of pure BaFe$_{12}$O$_{19}$ nanopowders has already been described in Chapter 2, Section 2.1.3.

To prepare $Mn_{0.2}Ni_{0.4}Zn_{0.4}Fe_2O_4$ nanopowder, we have used metal nitrates, such as $Fe(NO_3)_3.9H_2O$, $Ni(NO_3)_2.6H_2O$, $Mn(NO_3)_2.4H_2O$, $Zn(NO_3)_2$ as starting materials and water as solvent. Stoichiometric amounts of metal nitrates were dissolved in distilled water according to the molar compositions as shown in Table 6.1. The aqueous solutions of metal nitrates and EDTA were mixed in a molar ratio of 1: 1 and stirred for 1 h at room temperature using a magnetic stirrer. The pH of the reaction mixture was found to be ~2. Dark brown colored precursors were formed when the reaction mixtures were evaporated to dryness on a hot plate at 125 °C. Partial decomposition of the precursors was observed during drying. The precursor powders were then calcined in air for 2 h at 525 °C to obtain Mn-Ni-Zn ferrite nanopowders.

Table 6.1 Starting materials required for preparation of $(BaFe_{12}O_{19})_{1-x}$-$(Mn_{0.2}Ni_{0.4}Zn_{0.4}Fe_2O_4)_x$ nanocomposites

| Composition | *$Mn^{II}$-nitrate (g) | *Zn dust (g) | *$Ni^{II}$-nitrate (g) | *$Fe^{III}$-nitrate (g) | Ba-Carbonate (g) | *EDTA (g) | **$Mn_{0.2}Ni_{0.4}Zn_{0.4}Fe_2O_4$ (g) | **$BaFe_{12}O_{19}$ (g) |
|---|---|---|---|---|---|---|---|---|
| $Mn_{0.2}Ni_{0.4}Zn_{0.4}Fe_2O_4$-pure | 0.212 | 0.112 | 0.497 | 3.419 | --- | 3.71 | --- | --- |
| $(BaFe_{12}O_{19})_{0.15}$-$(Mn_{0.2}Ni_{0.4}Zn_{0.4}Fe_2O_4)_{0.85}$ | 0.116 | 0.06 | 0.269 | 3.846 | 0.08 | 14.31 | 0.55 | 0.45 |
| $(BaFe_{12}O_{19})_{0.25}$-$(Mn_{0.2}Ni_{0.4}Zn_{0.4}Fe_2O_4)_{0.75}$ | 0.082 | 0.043 | 0.192 | 3.98 | 0.108 | 14.21 | 0.39 | 0.61 |
| $(BaFe_{12}O_{19})_{0.5}$-$(Mn_{0.2}Ni_{0.4}Zn_{0.4}Fe_2O_4)_{0.5}$ | 0.037 | 0.019 | 0.086 | 4.18 | 0.146 | 13.91 | 0.18 | 0.82 |
| $(BaFe_{12}O_{19})_{0.75}$-$(Mn_{0.2}Ni_{0.4}Zn_{0.4}Fe_2O_4)_{0.25}$ | 0.014 | 0.007 | 0.032 | 4.3 | 0.166 | 13.75 | 0.07 | 0.93 |
| $BaFe_{12}O_{19}$-pure | --- | --- | ---- | 4.365 | 0.177 | 13.74 | --- | --- |

*For one-pot method
**For physical mixing method

_____

## 6.2 Results and Discussion

### 6.2.1 Thermal analysis

TGA and DSC analysis were used to investigate the thermal decomposition behavior of precursors, prepared by OP method. A total weight loss of ~95 % was observed when the precursor powder was heated from 30 to 550 °C in air (Fig. 6.1). Initially, ~4 % weight loss occurred in the region of 40 to 100 °C due to loss of moisture from the sample. Then in the temperature range of 200 to 470 °C, ~91 % weight loss was observed. This might be due to the oxidative decomposition of precursor and evolution of $CO_2$ and $NO_x$ gases. This decomposition was also appeared as an exothermic peak at 429 °C in DSC thermogram. No weight loss was observed in TGA when the sample was heated beyond 470 °C. This confirmed the full decomposition of carbonaceous mass of the precursor occurred within 470 °C.
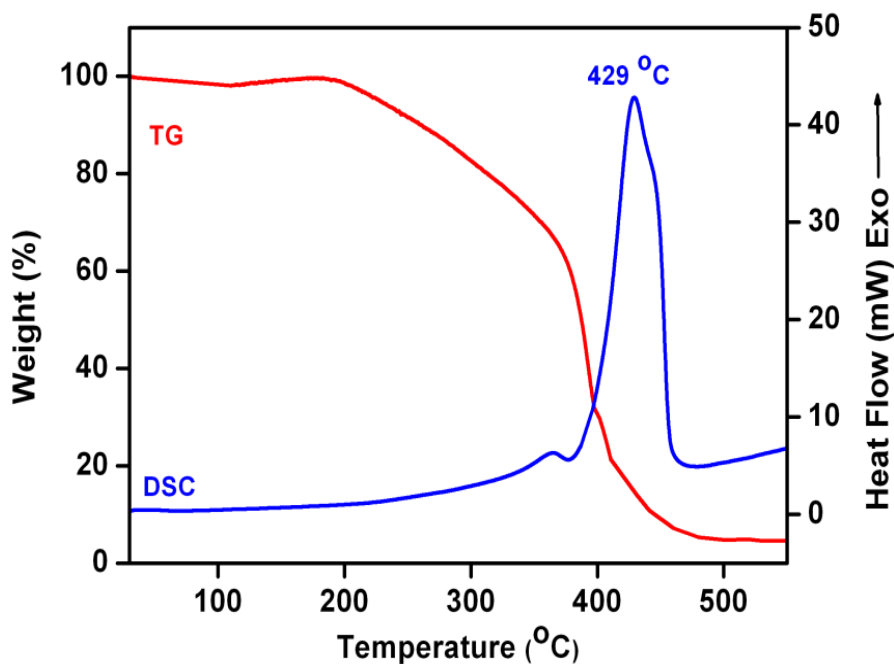


Fig. 6.1 TGA- DSC thermogram of $(BaFe_{12}O_{19})_{0.5}$-$(Mn_{0.2}Ni_{0.4}Zn_{0.4}Fe_2O_4)_{0.5}$ precursor.

### 6.2.2 X-Ray Diffraction analysis

XRD patterns of $(BaFe_{12}O_{19})_{1-x}$-$(Mn_{0.2}Ni_{0.4}Zn_{0.4}Fe_2O_4)_x$ nanocomposites, prepared by one-pot method as well as physical mixing exhibited the diffraction peaks corresponding to both spinel $Mn_{0.2}Ni_{0.4}Zn_{0.4}Fe_2O_4$ [253] and hexagonal $BaFe_{12}O_{19}$ [ICDD 84-0757] phase (Fig. 6.2 (A) and (B)) and indicated the coexistence of both the phases in the composite powders. Any

impurity peak, such as NiO, MnO, ZnO, BaO, $BaCO_3$, $\alpha$-$Fe_2O_3$ etc. within the resolution of the technique was not observed. However, variation in relative intensities of the diffraction peaks was observed for these two types of composites. This might be due to the variation of crystalline size and homogeneous distribution of the spinel and hexagonal phases in the nanocomposites with the method of preparation. The average crystallite sizes of $Mn_{0.2}Ni_{0.4}Zn_{0.4}Fe_2O_4$ and $BaFe_{12}O_{19}$ phases in $(BaFe_{12}O_{19})_{1-x}$-$(Mn_{0.2}Ni_{0.4}Zn_{0.4}Fe_2O_4)_x$ nanocomposites were calculated by X-ray peak-broadening method using Scherrer's equation[437] and listed on Table 6.2. For $Mn_{0.2}Ni_{0.4}Zn_{0.4}Fe_2O_4$, the diffraction peak at $2\theta=$ 35.6º, which corresponds to (311) plane and for $BaFe_{12}O_{19}$, diffraction peak at $2\theta=$ 34.2 º, i.e. (114) plane were used.
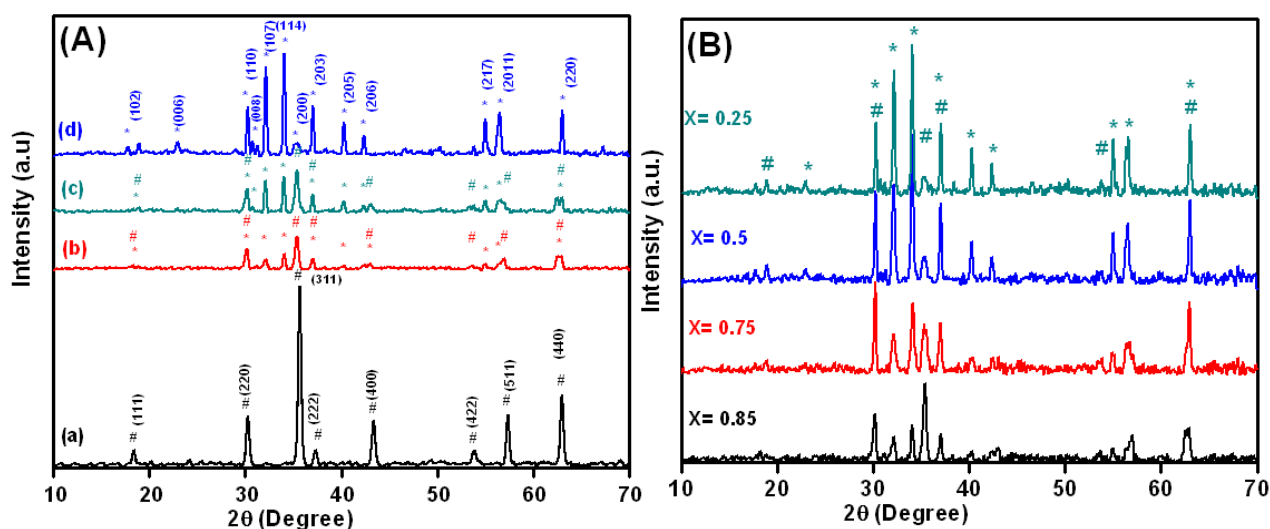


Fig. 6.2 (A) XRD spectra of the (a) pure $Mn_{0.2}Ni_{0.4}Zn_{0.4}Fe_2O_4$, $(BaFe_{12}O_{19})_{0.15}$-$(Mn_{0.2}Ni_{0.4}Zn_{0.4}Fe_2O_4)_{0.85}$ nanocomposites prepared by (b) one-pot, (c) physical mixing methods and (d) $BaFe_{12}O_{19}$ nanopowders, (B) XRD spectra of $(BaFe_{12}O_{19})_{1-x}$-$(Mn_{0.2}Ni_{0.4}Zn_{0.4}Fe_2O_4)_x$ nanocomposites synthesized by one-pot method (#$Mn_{0.2}Ni_{0.4}Zn_{0.4}Fe_2O_4$ and *$BaFe_{12}O_{19}$).

The important feature was that, in $(BaFe_{12}O_{19})_{1-x}$-$(Mn_{0.2}Ni_{0.4}Zn_{0.4}Fe_2O_4)_x$ nanocomposites-OP method, the crystallite size of $Mn_{0.2}Ni_{0.4}Zn_{0.4}Fe_2O_4$ phase was increased from 11 to 19 nm with increasing amount of $Mn_{0.2}Ni_{0.4}Zn_{0.4}Fe_2O_4$ phase in the composite. The same trend was observed for $BaFe_{12}O_{19}$ phase and its crystallite size was found to be increased from 22 to 43 nm. $(BaFe_{12}O_{19})_{1-x}$-$(Mn_{0.2}Ni_{0.4}Zn_{0.4}Fe_2O_4)_x$ nanocomposites -PM method, the crystallite sizes of both spinel and hexagonal phase did not change much with varying amount of $Mn_{0.2}Ni_{0.4}Zn_{0.4}Fe_2O_4$ and $BaFe_{12}O_{19}$ phases in the composites and were found to be ~18 nm for $Mn_{0.2}Ni_{0.4}Zn_{0.4}Fe_2O_4$ and ~43 nm for $BaFe_{12}O_{19}$. These values were almost same in

comparison with the crystallite sizes of pure $Mn_{0.2}Ni_{0.4}Zn_{0.4}Fe_2O_4$ and $BaFe_{12}O_{19}$ nanopowders and indicated that the pure phases retain their individual crystallite sizes in the composites.

Table 6.2 Average crystalline size of $(BaFe_{12}O_{19})_{1-x}$-$(Mn_{0.2}Ni_{0.4}Zn_{0.4}Fe_2O_4)_x$ nanocomposites prepared by one-pot and physical mixing method

| Sample | Crystallite size (nm) | | | |
|---|---|---|---|---|
| | One-Pot synthesis | | Physical mixing synthesis | |
| | *(114)plane | #(311)plane | *(114)plane | #(311)plane |
| $Mn_{0.2}Ni_{0.4}Zn_{0.4}Fe_2O_4$-pure | -- | 19 | -- | -- |
| $(BaFe_{12}O_{19})_{0.15}$-$(Mn_{0.2}Ni_{0.4}Zn_{0.4}Fe_2O_4)_{0.85}$ | 22 | 16 | 43 | 19 |
| $(BaFe_{12}O_{19})_{0.25}$-$(Mn_{0.2}Ni_{0.4}Zn_{0.4}Fe_2O_4)_{0.75}$ | 27 | 14 | 42 | 17 |
| $(BaFe_{12}O_{19})_{0.5}$-$(Mn_{0.2}Ni_{0.4}Zn_{0.4}Fe_2O_4)_{0.5}$ | 34 | 12 | 43 | 16 |
| $(BaFe_{12}O_{19})_{0.75}$-$(Mn_{0.2}Ni_{0.4}Zn_{0.4}Fe_2O_4)_{0.25}$ | 38 | 11 | 45 | 18 |
| $BaFe_{12}O_{19}$-pure | 43 | -- | -- | -- |

* For $BaFe_{12}O_{19}$

# For $Mn_{0.2}Ni_{0.4}Zn_{0.4}Fe_2O_4$

### 6.3.3 TEM and SEM analysis

Nanocomposites prepared by physical mixing and one-pot method showed two distinct types of microstructures when their morphology was investigated by HRTEM (Fig. 6.3). In case of the nanocomposites-PM (Fig. 6.3(d, f, h, j), clear segregation of hexagonal $BaFe_{12}O_{19}$ nanoparticles (average particle size of ~60-70 nm, Fig. 6.3(a)) and spherical shaped agglomerated $Mn_{0.2}Ni_{0.4}Zn_{0.4}Fe_2O_4$ nanoparticles (~20 nm average particle size, Fig. 6.3(b)) were observed. On the contrary, for the nanocomposites, prepared by one-pot method, almost uniform shaped nanoparticles (average particle size ~60-70 nm) were observed (Fig. 6.3(c, e, g, i)). SEM micrographs of the composites also revealed the intimate coexistence of $Mn_{0.2}Ni_{0.4}Zn_{0.4}Fe_2O_4$ and $BaFe_{12}O_{19}$ particles in the composites-OP (Fig. 6.4 (a)) and presence of large $BaFe_{12}O_{19}$ and small $Mn_{0.2}Ni_{0.4}Zn_{0.4}Fe_2O_4$ nanoparticles in the composites-PM (Fig. 6.4 (b)).
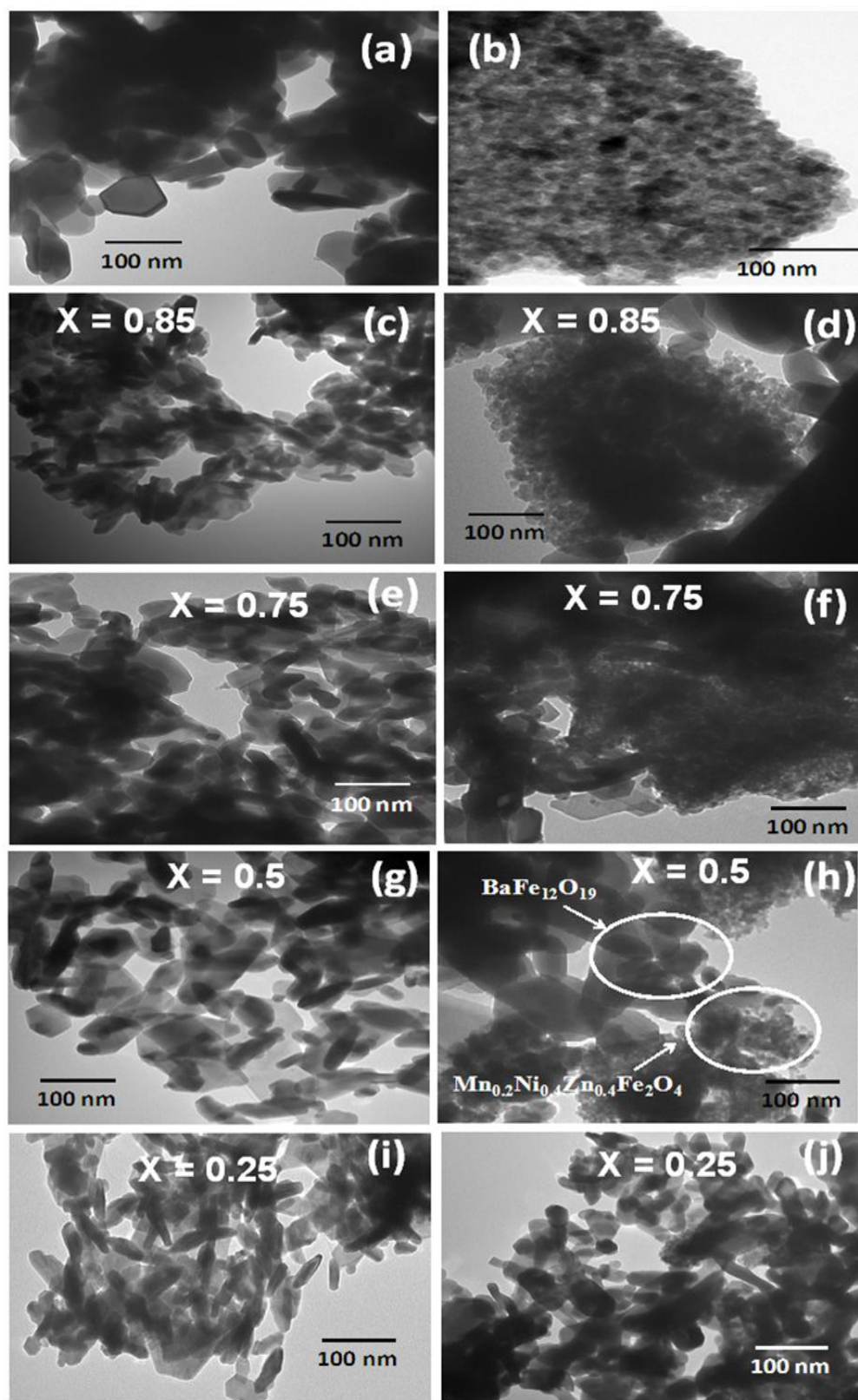
Fig. 6.3 TEM micrographs of (a) pure BaFe$_{12}$O$_{19}$, (b) pure Mn$_{0.2}$Ni$_{0.4}$Zn$_{0.4}$Fe$_2$O$_4$ nanopowders and (BaFe$_{12}$O$_{19}$)$_{1-x}$-(Mn$_{0.2}$Ni$_{0.4}$Zn$_{0.4}$Fe$_2$O$_4$)$_x$ nanocomposites synthesis by (c, e, g, i) one-pot and (d, f, h, j) physical mixing method.
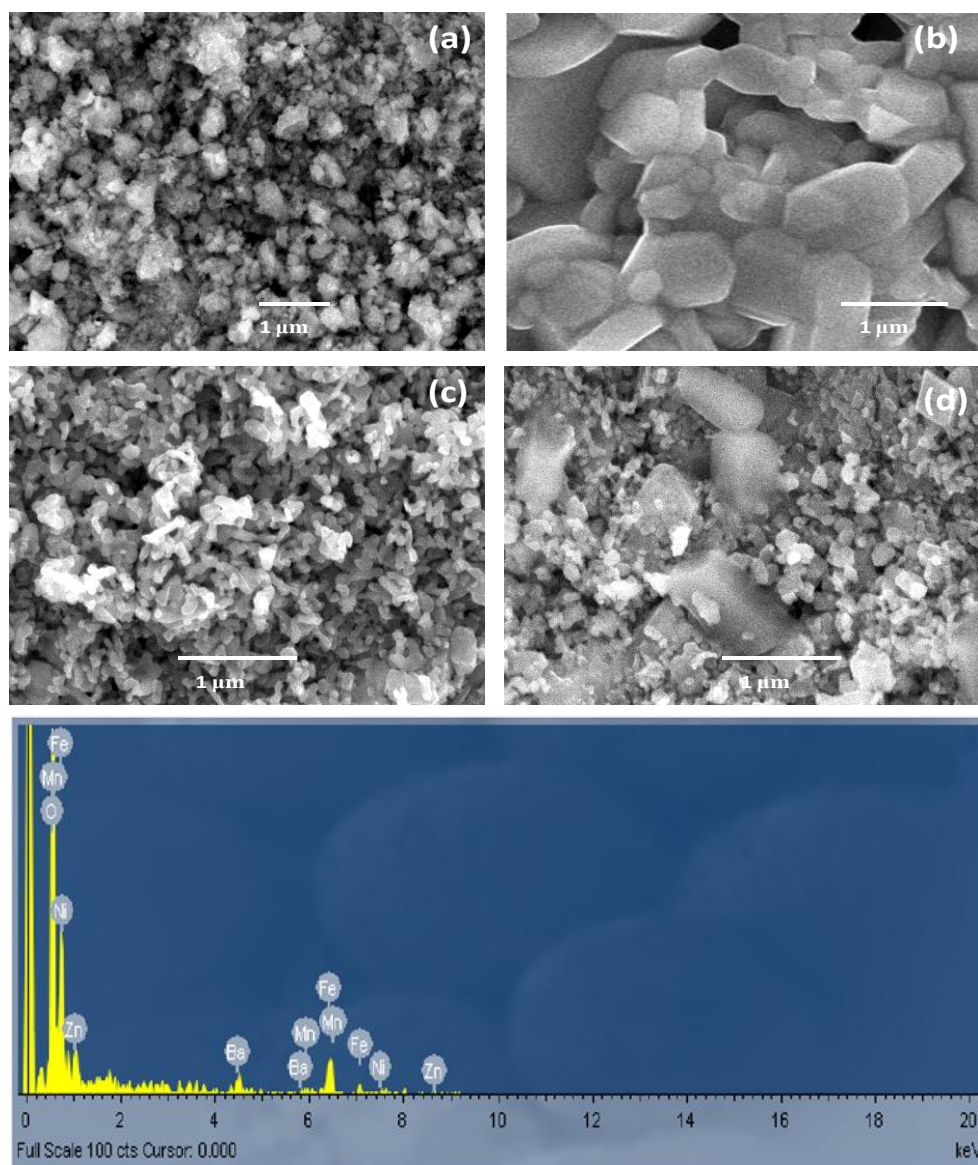
Fig. 6.4 SEM micrographs of (a) pure $Mn_{0.2}Ni_{0.4}Zn_{0.4}Fe_2O_4$, (b) Pure $BaFe_{12}O_{19}$ and $(Mn_{0.2}Ni_{0.4}Zn_{0.4}Fe_2O_4)_{0.5}$-$(BaFe_{12}O_{19})_{0.5}$ nanocomposites prepared by (c) one-pot, (d) physical mixing method and (e) EDX spectra of $(BaFe_{12}O_{19})_{0.5}$-$(Mn_{0.2}Ni_{0.4}Zn_{0.4}Fe_2O_4)_{0.5}$ nanocomposite prepared by one-pot method.

Electron microscopic analysis clearly shows that, the nanocomposites synthesized by one-pot method possess better homogeneous mixing of $Mn_{0.2}Ni_{0.4}Zn_{0.4}Fe_2O_4$ and $BaFe_{12}O_{19}$ phase than the composites prepared by physical mixing method. This difference in morphology of the samples may play important role in the magnetic and microwave absorption properties of the nanocomposites. EDX analysis (Fig. 4(c)) of final nanocomposite indicated the presence of all the elements (e.g. Mn, Ni, Zn, Fe, Ba and O).

_____

### 6.3.4 Magnetic measurements

VSM was used to measure the room temperature magnetization behaviours of (BaFe$_{12}$O$_{19}$)$_{1-x}$-(Mn$_{0.2}$Ni$_{0.4}$Zn$_{0.4}$Fe$_2$O$_4$)$_x$ nanocomposites prepared by OP and PM method and shown in Fig. 6.5.
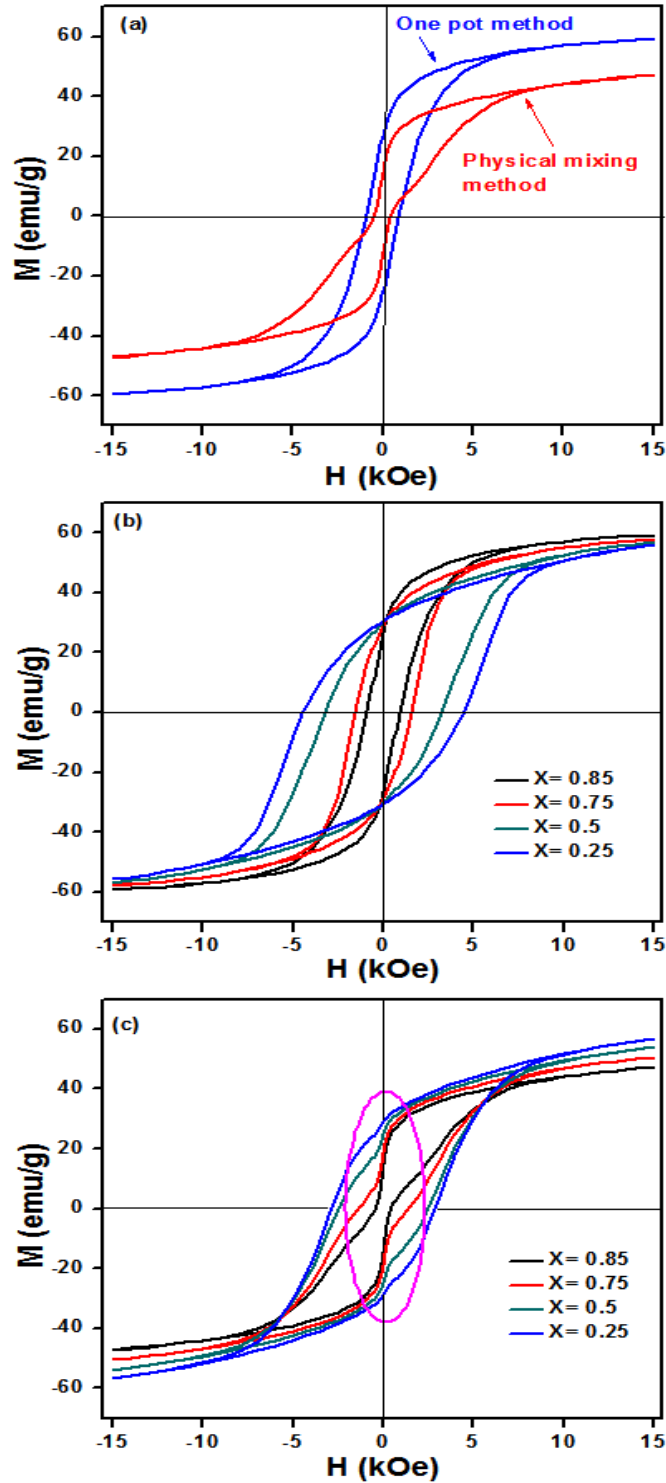


Fig. 6.5 Room temperature hysteresis loops for (a) (BaFe$_{12}$O$_{19}$)$_{0.15}$-(Mn$_{0.2}$Ni$_{0.4}$Zn$_{0.4}$Fe$_2$O$_4$)$_{0.85}$ nanocomposite prepared by one-pot and physical mixing method and (BaFe$_{12}$O$_{19}$)$_{1-x}$-(Mn$_{0.2}$Ni$_{0.4}$Zn$_{0.4}$Fe$_2$O$_4$)$_x$ nanocomposite prepared by (b) one-pot, (c) physical mixing method.

The most important observation was that, composites-OP, showed single hysteresis loop, signifying hard and soft phases were well exchanged coupled to each other. Whereas, composites-PM exhibited a typical two loop "bee waist" type hysteresis loop, indicating the absence of exchange coupling between hard and soft phase (Fig.6.5(a)).[387, 431-433] Fig. 6.5 (b) also reflects that all the composition of $(NiFe_2O_4)_x$-$(BaFe_{12}O_{19})_{1-x}$ showed single hysteresis loop for composites synthesized by OP-method whereas two loop hysteresis for nanocomposites-PM (Fig. 6.5 (c)). Hence, $(BaFe_{12}O_{19})_{1-x}$-$(Mn_{0.2}Ni_{0.4}Zn_{0.4}Fe_2O_4)_x$ nanocomposites, prepared by one-pot method, though possessed crystallographycally two phase behaviour but demonstrated magnetically good single phase behaviour. Coercivity ($H_c$) values of the nanocomposites prepared by both the methods increased with increasing hard ferrite phase (i.e. $BaFe_{12}O_{19}$) content in the composite (Table 6. 3).

Table 6.3 $M_s$ and $H_c$ values of the $(BaFe_{12}O_{19})_{1-x}$-$(Mn_{0.2}Ni_{0.4}Zn_{0.4}Fe_2O_4)_x$ nanocomposites prepared by one-pot and physical mixing method

| Sample | One-pot synthesis | | Physical mixing synthesis | | Theoretical $M_s$ without exchange coupling (emu/g) |
|---|---|---|---|---|---|
| | $H_c$ (Oe) | $M_s$ (emu/g) | $H_c$ (Oe) | $M_s$ (emu/g) | |
| $Mn_{0.2}Ni_{0.4}Zn_{0.4}Fe_2O_4$-pure | 61.1 | 39.1 | -- | -- | -- |
| $(BaFe_{12}O_{19})_{0.15}$-$(Mn_{0.2}Ni_{0.4}Zn_{0.4}Fe_2O_4)_{0.85}$ | 923 | 59.3 | 459 | 47.1 | 46.9 |
| $(BaFe_{12}O_{19})_{0.25}$-$(Mn_{0.2}Ni_{0.4}Zn_{0.4}Fe_2O_4)_{0.75}$ | 1577 | 57.6 | 1391 | 50.4 | 51.2 |
| $(BaFe_{12}O_{19})_{0.5}$-$(Mn_{0.2}Ni_{0.4}Zn_{0.4}Fe_2O_4)_{0.5}$ | 3207 | 56.9 | 2466 | 53.9 | 53.45 |
| $(BaFe_{12}O_{19})_{0.75}$-$(Mn_{0.2}Ni_{0.4}Zn_{0.4}Fe_2O_4)_{0.25}$ | 4450 | 55.8 | 2839 | 56.8 | 55.37 |
| $BaFe_{12}O_{19}$-pure | 4914 | 56.5 | -- | -- | -- |

For the nanocomposites-OP, initial incorporation of $BaFe_{12}O_{19}$ phase caused enhancement of saturation magnetization ($M_s$) values which was due to the spring exchange coupling between hard and soft magnetic phases. However, subsequent increase of $BaFe_{12}O_{19}$ content in the $(BaFe_{12}O_{19})_{1-x}$-$(Mn_{0.2}Ni_{0.4}Zn_{0.4}Fe_2O_4)_x$ nanocomposites (i.e., with increasing (1-x) values) did not affect much on $M_s$ value. Whereas, in case of composites-PM, $M_s$ values were increased with increasing amount of $BaFe_{12}O_{19}$. $M_s$ and $H_c$ values of all the composites prepared by one-pot method were higher than those of the composites prepared by physical mixing method. These facts indicate that hard and soft ferrite phases are sufficiently exchanged coupled to each other in the composites prepared by one-pot method.

Theoretically calculated values of $M_s$ of the composites (when hard and soft phases are not exchange coupling) using equation 2.1, were found to be almost matching with the experimentally obtained values of the composites prepared by physical mixing method (Table 6.3), which clearly indicates the absence of spin exchange coupling between hard and soft ferrite phases in the composites-PM.

### 6.3.5 Microwave absorption study

Microwave absorption behavior of $(BaFe_{12}O_{19})_{1-x}$-$(Mn_{0.2}Ni_{0.4}Zn_{0.4}Fe_2O_4)_x$ nanocomposites with different compositions (x= 0.85, 0.75, 0.5, 0.25) synthesized by one-pot method were investigated. Loss tangent vs. frequency were plotted to understand the particular loss mechanism for each composite and shown in Fig. 6.6 (a) and (b). The dielectric and magnetic loss tangents can be expressed as $\tan\delta_\varepsilon = \varepsilon''/\varepsilon'$ and $\tan\delta_\mu = \mu''/\mu'$, respectively. Fig. 6.6 (b) shows that these composites are having only magnetic loss parameter whereas dielectric loss parameter is negligible (Fig. 6.6 (a)). Reflection loss was calculated using equation (1.4 and 1.5) and plotted against frequency for different $(BaFe_{12}O_{19})_{1-x}$-$(Mn_{0.2}Ni_{0.4}Zn_{0.4}Fe_2O_4)_x$ nanocomposites (x= 0.85, 0.75, 0.5, 0.25) synthesized by OP method for thickness 3 mm (Fig. 6.6 (c)). In RL vs frequency plot, the dip of the curves were designated for maximum absorption i.e. minimum RL. It was observed that, with decreasing value of x (i.e. increasing $BaFe_{12}O_{19}$ content in the composite) maximum absorption was decreases. As the composite, having composition $(BaFe_{12}O_{19})_{0.15}$-$(Mn_{0.2}Ni_{0.4}Zn_{0.4}Fe_2O_4)_{0.85}$, exhibited minimum reflection loss ($\sim$ -15dB) i.e. maximum absorption compare to other composites, so this composition has been chosen for further studies and its microwave absorption properties were compared with the composite prepared by PM method as well as pure $Mn_{0.2}Ni_{0.4}Zn_{0.4}Fe_2O_4$ and $BaFe_{12}O_{19}$.

_____
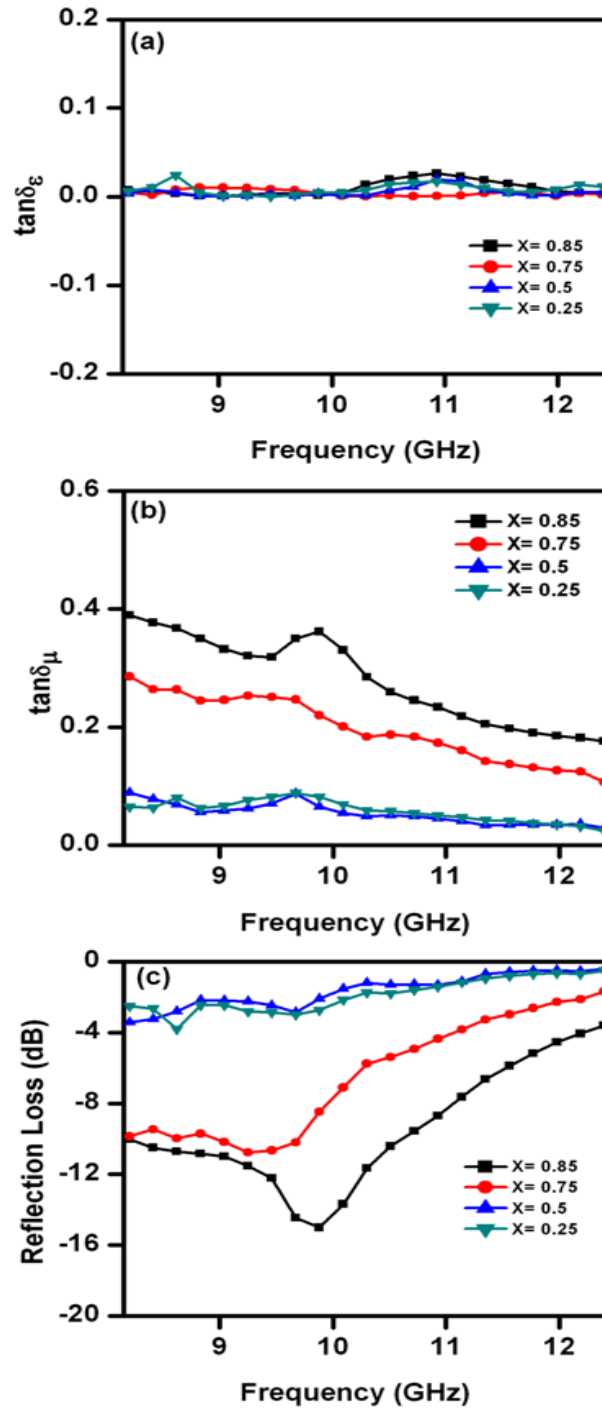


Fig. 6.6 (a) Loss Tangent of relative complex permittivity (tan$\delta_\varepsilon$), (b) Loss Tangent of relative complex permeability (tan$\delta_\mu$) and (c) Reflection loss vs. frequency plot (BaFe$_{12}$O$_{19}$)$_{1-x}$-(Mn$_{0.2}$Ni$_{0.4}$Zn$_{0.4}$Fe$_2$O$_4$)$_x$ nanocomposites synthesized by one-pot method.

The real and imaginary permittivity (Fig. 6.7(a). and (b)) and permeability (Fig. 6.7 (c) and (d)) for the nanocomposites synthesized by both the methods, pure BaFe$_{12}$O$_{19}$ and Mn$_{0.2}$Ni$_{0.4}$Zn$_{0.4}$Fe$_2$O$_4$ nanopowders were plotted as a function of frequency in the X-band range (8.2- 12.4 GHz).
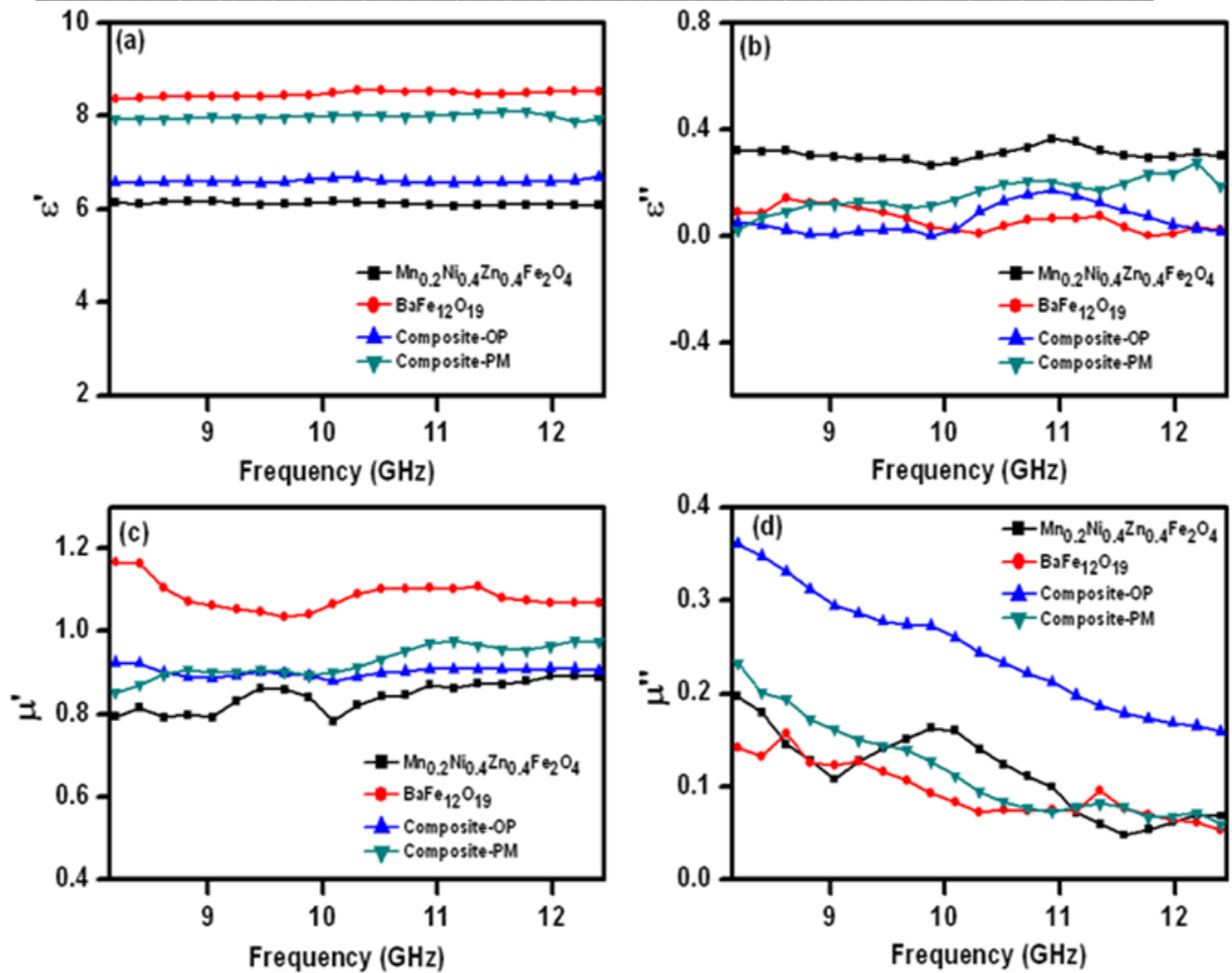
Fig. 6.7 (a) Real (ε'), (b) imaginary (ε") parts of relative complex permittivity and (c) real (μ'), (d) imaginary (μ") parts of relative complex permeability of pure BaFe$_{12}$O$_{19}$, Mn$_{0.2}$Ni$_{0.4}$Zn$_{0.4}$Fe$_2$O$_4$ nanopowders and (BaFe$_{12}$O$_{19}$)$_{0.15}$-(Mn$_{0.2}$Ni$_{0.4}$Zn$_{0.4}$Fe$_2$O$_4$)$_{0.85}$ nanocomposites prepared by one-pot and physical mixing method.

It was observed that, over the entire frequency range, ε′ values remained almost constant. Both nanocomposites ε′ value was in between the values of pure BaFe$_{12}$O$_{19}$ and Mn$_{0.2}$Ni$_{0.4}$Zn$_{0.4}$Fe$_2$O$_4$ (Fig. 6.7(a)). The imaginary dielectric parameter (ε″) values remained almost constant except a broad peak appeared in the range of 9.88 GHz to 12.4 GHz for the composite-OP (Fig. 6.7(b)). The intrinsic, electric dipole polarization and interfacial polarization are mainly responsible for this kind of behavior.[4] The real permeability (μ′) values of composite and pure nanopowders remained almost constant throughout the entire frequency range (Fig. 6.7 (c)). The imaginary permeability (μ″) values (Fig. 6.7 (d)) showed a decreasing tendency from 8.2 GHz to 12.4 GHz for both the nanocomposites and pure ferrites, however, maximum imaginary permeability was observed for the composite synthesized by one-pot method.

106

_____

Refection Loss for nanocomposites as well as pure ferrite nanopowders was calculated for absorber thickness 3 mm (Fig. 6.8 (a)). The estimated electromagnetic wave absorption values are listed in Table 6.4.
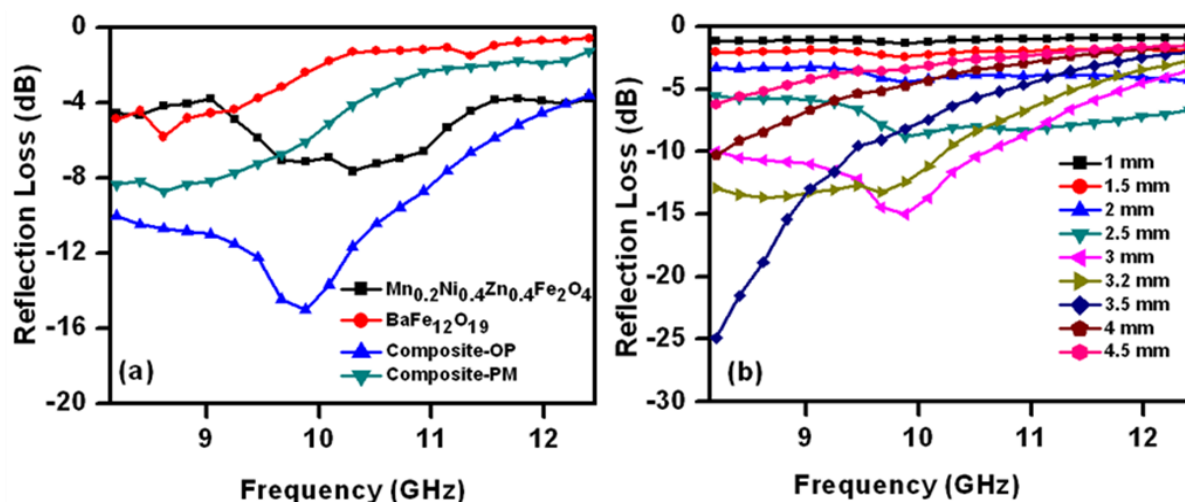


Fig. 6.8 Reflection loss vs. frequency plot for (a) pure BaFe$_{12}$O$_{19}$, Mn$_{0.2}$Ni$_{0.4}$Zn$_{0.4}$Fe$_2$O$_4$ nanopowders and (BaFe$_{12}$O$_{19}$)$_{0.15}$-(Mn$_{0.2}$Ni$_{0.4}$Zn$_{0.4}$Fe$_2$O$_4$)$_{0.85}$ nanocomposites prepared by one-pot and physical mixing method and (b) Reflection loss vs. frequency plot for (BaFe$_{12}$O$_{19}$)$_{0.15}$-(Mn$_{0.2}$Ni$_{0.4}$Zn$_{0.4}$Fe$_2$O$_4$)$_{0.85}$ nanocomposites prepared by one-pot method at different specimen thickness.

In Fig. 6.8 (a), it was observed that, composite-OP method showed greater reflection loss (~ -15 dB at 9.88 GHz corresponds to ~96.84% absorption) than composite-PM method (~ -8.7 dB at 8.62 GHz). Pure hard and soft ferrite nanopowders showed reflection loss lower than -10dB (~-7 dB and ~-6 dB respectively). For composite-OP method showed >10 dB reflection loss (i.e. > 90% absorption) over the frequency range of 8.2 GHz to 10.6 GHz. Fig. 6.8 (b) illustrates the reflection loss vs frequency for one-pot synthesized nancomposites with different thickness of the absorber. The reflection loss was found to be increased with increasing thickness of the sample till 3.5 mm with the shifting of the frequency corresponds to maximum loss towards lower frequency. Reflection loss of ~ -25 dB (i.e. > 99% absorption) was observed at 8.2 GHz for absorber thickness of 3.5 mm but frequency range corresponds to reflection loss > -10 dB (means > 90% absorption) becomes narrower than the specimen thickness of 3 mm. The RL value of -20 dB is equivalent to 99% absorption, which is considered as the satisfactory microwave absorption.

Table 6.4 Microwave absorption characteristics of pure BaFe$_{12}$O$_{19}$, Mn$_{0.2}$Ni$_{0.2}$Zn$_{0.4}$Fe$_2$O$_4$ nanopowders and (BaFe$_{12}$O$_{19}$)$_{0.15}$-(Mn$_{0.2}$Ni$_{0.4}$Zn$_{0.4}$Fe$_2$O$_4$)$_{0.85}$ nanocomposites prepared by one-pot and physical mixing method

| Sample | Minimum RL (dB) | Frequency (GHz) |
|---|---|---|
| BaFe$_{12}$O$_{19}$-pure | -5.8 | 8.62 |
| (BaFe$_{12}$O$_{19}$)$_{0.15}$-(Mn$_{0.2}$Ni$_{0.4}$Zn$_{0.4}$Fe$_2$O$_4$)$_{0.85}$ (one-pot method) | -15 | 9.88 |
| (BaFe$_{12}$O$_{19}$)$_{0.15}$-(Mn$_{0.2}$Ni$_{0.4}$Zn$_{0.4}$Fe$_2$O$_4$)$_{0.85}$ (physical mixing method) | -8.7 | 8.62 |
| Ni$_{0.65}$Zn$_{0.35}$Fe$_2$O$_4$-pure | -7.6 | 10.3 |

## 6.3 Summary of Results

(i)    (BaFe$_{12}$O$_{19}$)$_{1-x}$-(Mn$_{0.2}$Ni$_{0.4}$Zn$_{0.4}$Fe$_2$O$_4$)$_x$ nanocomposites were successfully synthesized using EDTA precursor based one-pot method where precursor was calcined at 800 °C for 4 h.

(ii)    Thermal decomposition of the precursor was complete at ~470 °C.

(iii)    XRD patterns of (BaFe$_{12}$O$_{19}$)$_{1-x}$-(Mn$_{0.2}$Ni$_{0.4}$Zn$_{0.4}$Fe$_2$O$_4$)$_x$ nanocomposites, prepared by one-pot method exhibited the diffraction peaks corresponding to both spinel Mn$_{0.2}$Ni$_{0.4}$Zn$_{0.4}$Fe$_2$O$_4$ and hexagonal BaFe$_{12}$O$_{19}$ phase.

(iv)    In (BaFe$_{12}$O$_{19}$)$_{1-x}$-(Mn$_{0.2}$Ni$_{0.4}$Zn$_{0.4}$Fe$_2$O$_4$)$_x$ nanocomposites synthesized by OP method, the crystallite size of Mn$_{0.2}$Ni$_{0.4}$Zn$_{0.4}$Fe$_2$O$_4$ phase was increased from 11 to 19 nm with increasing amount of Mn$_{0.2}$Ni$_{0.4}$Zn$_{0.4}$Fe$_2$O$_4$ phase in the composite. The same trend was observed for BaFe$_{12}$O$_{19}$ phase and its crystallite size was found to be increased from 22 to 43 nm.

(v)    (BaFe$_{12}$O$_{19}$)$_{1-x}$-(Mn$_{0.2}$Ni$_{0.4}$Zn$_{0.4}$Fe$_2$O$_4$)$_x$ nanocomposites synthesized by PM method, the crystallite sizes of both spinel and hexagonal phase did not change much with varying amount of Mn$_{0.2}$Ni$_{0.4}$Zn$_{0.4}$Fe$_2$O$_4$ and BaFe$_{12}$O$_{19}$ phases in the composites and were found to be ~18 nm for Mn$_{0.2}$Ni$_{0.4}$Zn$_{0.4}$Fe$_2$O$_4$ and ~43 nm for BaFe$_{12}$O$_{19}$. These values were almost same in comparison with the crystallite sizes of pure Mn$_{0.2}$Ni$_{0.4}$Zn$_{0.4}$Fe$_2$O$_4$ and BaFe$_{12}$O$_{19}$.

(vi)    Nanocomposites synthesized by PM method, clear segregation of hexagonal BaFe$_{12}$O$_{19}$ nanoparticles and spherical shaped agglomerated Mn$_{0.2}$Ni$_{0.4}$Zn$_{0.4}$Fe$_2$O$_4$ nanoparticles were observed. Nanocomposites, prepared by one-pot method,

almost uniform shaped nanoparticles (average particle size ~60-70 nm) were observed.

(vii) Nanocomposites-OP, showed single hysteresis loop, signifying hard and soft phases were well exchanged coupled to each other. Whereas, composites-PM exhibited a typical two loop "bee waist" type hysteresis loop, indicating the absence of exchange coupling between hard and soft phase. $M_s$ and $H_c$ values of all the composites prepared by one-pot method were higher than those of the composites prepared by physical mixing method.

(viii) Nanocomposites synthesized by one-pot method are having only magnetic loss parameter whereas dielectric loss parameter is negligible

(ix) Nanocomposite-OP showed greater reflection loss (~ -15 dB at 9.88 GHz corresponds to ~96.84% absorption) than composite-PM method (~ -8.7 dB at 8.62 GHz) for absorber thickness of 3 mm. Pure hard and soft ferrite nanopowders showed reflection loss lower than -10dB (~-7 dB and ~-6 dB respectively).

(x) (BaFe$_{12}$O$_{19}$)$_{0.15}$-(Mn$_{0.2}$Ni$_{0.4}$Zn$_{0.4}$Fe$_2$O$_4$)$_{0.85}$ nanocomposite synthesized by OP method exhibited reflection loss of ~ -25 dB (i.e. > 99.7% absorption) at 8.2 GHz for absorber thickness of 3.5 mm.

_____

<div align="right">

**Chapter 7**

</div>

# Synthesis and characterization of (SrFe$_{12}$O$_{19}$)$_{1-x}$-(Mn$_{0.2}$Ni$_{0.4}$Zn$_{0.4}$Fe$_2$O$_4$)$_x$ nanocomposites and study of their magnetic and microwave absorption properties

## 7.1 Experimental procedure

### 7.1.1 Materials required

Sr(NO$_3$)$_2$, Mn(NO$_3$)$_2$.4H$_2$O, Ni(NO$_3$)$_2$.6H$_2$O, Fe(NO$_3$)$_3$.9H$_2$O, Zn dust, Nitric Acid and Ethylene diamine tetra acetic acid (EDTA) were purchased from Merck, India and used without further purification. Zn dust was dissolved in aqueous nitric acid to get Zn(NO$_3$)$_2$.

### 7.1.2 Synthesis of (SrFe$_{12}$O$_{19}$)$_{1-x}$-(Mn$_{0.2}$Ni$_{0.4}$Zn$_{0.4}$Fe$_2$O$_4$)$_x$ nanocomposites by one-pot method (OP Method)[445]

To prepare (SrFe$_{12}$O$_{19}$)$_{1-x}$-(Mn$_{0.2}$Ni$_{0.4}$Zn$_{0.4}$Fe$_2$O$_4$)$_x$ nano-composites (with x= 0.85, 0.75, 0.5 and 0.25) using one-pot method stoichiometric amount of aqueous solutions of Sr(NO$_3$)$_2$, Mn(NO$_3$)$_2$.4H$_2$O, Ni(NO$_3$)$_2$.6H$_2$O, Zn(NO$_3$)$_2$, Fe(NO$_3$)$_3$.9H$_2$O and EDTA were mixed in a beaker (Table 7.1) and stirred for 2 h. This reaction mixture was then dried at ~110 °C for 2 h. Black colour floppy carbonaceous material was formed after drying, which referred as precursor powder. Then the precursor powders were calcined at 800 °C for 4 h in air atmosphere to obtain desire (SrFe$_{12}$O$_{19}$)$_{1-x}$-(Mn$_{0.2}$Ni$_{0.4}$Zn$_{0.4}$Fe$_2$O$_4$)$_x$ nanocomposites.

### 7.1.3 Synthesis of (SrFe$_{12}$O$_{19}$)$_{1-x}$-(Mn$_{0.2}$Ni$_{0.4}$Zn$_{0.4}$Fe$_2$O$_4$)$_x$ nanocomposites by physical mixing method (PM Method)

Another set of composite samples with various composition (with x= 0.85, 0.75, 0.5 and 0.25) was also prepared by using 'physical mixing' method where pure Mn$_{0.2}$Ni$_{0.4}$Zn$_{0.4}$Fe$_2$O$_4$ and SrFe$_{12}$O$_{19}$ powders were mixed with appropriate weight ratio (Table 7.1) using a mortar pestle. Pure SrFe$_{12}$O$_{19}$ and Mn$_{0.2}$Ni$_{0.4}$Zn$_{0.4}$Fe$_2$O$_4$ nanopowders were prepared separately by using the EDTA- precursor method which has been developed by us.[253, 441] Detail Synthesis

110

procedure for pure $SrFe_{12}O_{19}$ and $Mn_{0.2}Ni_{0.4}Zn_{0.4}Fe_2O_4$ nanopowders has been described in Chapter 3, Section 3.1.3 and Chapter 6, Section 6.1.3 respectively.

Table 7.1 Starting materials required for synthesis of $(SrFe_{12}O_{19})_{1-x}$-$(Mn_{0.2}Ni_{0.4}Zn_{0.4}Fe_2O_4)_x$ nanocomposites

| Composition | *$Mn^{II}$-nitrate (g) | *$Zn$ dust (g) | *$Ni^{II}$-nitrate (g) | *$Fe^{III}$-nitrate (g) | $Sr^{II}$-nitrate (g) | *EDTA (g) | #$Mn_{0.2}Ni_{0.4}Zn_{0.4}Fe_2O_4$ (g) | #$SrFe_{12}O_{19}$ (g) |
|---|---|---|---|---|---|---|---|---|
| $Mn_{0.2}Ni_{0.4}Zn_{0.4}Fe_2O_4$-Pure | 0.212 | 0.112 | 0.497 | 3.419 | -- | 3.71 | -- | -- |
| $(SrFe_{12}O_{19})_{0.15}$-$(Mn_{0.2}Ni_{0.4}Zn_{0.4}Fe_2O_4)_{0.85}$ | 0.119 | 0.062 | 0.275 | 3.93 | 0.088 | 14.69 | 0.56 | 0.44 |
| $(SrFe_{12}O_{19})_{0.25}$-$(Mn_{0.2}Ni_{0.4}Zn_{0.4}Fe_2O_4)_{0.75}$ | 0.085 | 0.045 | 0.197 | 4.11 | 0.119 | 14.53 | 0.4 | 0.6 |
| $(SrFe_{12}O_{19})_{0.5}$-$(Mn_{0.2}Ni_{0.4}Zn_{0.4}Fe_2O_4)_{0.5}$ | 0.038 | 0.02 | 0.089 | 4.35 | 0.163 | 14.47 | 0.18 | 0.0.82 |
| $(SrFe_{12}O_{19})_{0.75}$-$(Mn_{0.2}Ni_{0.4}Zn_{0.4}Fe_2O_4)_{0.25}$ | 0.015 | 0.007 | 0.034 | 4.49 | 0.186 | 14.36 | 0.07 | 0.93 |
| $SrFe_{12}O_{19}$-Pure | -- | -- | -- | 4.57 | 0.199 | 14.38 | -- | -- |

\* One-pot Synthesis,

\# Physical mixing synthesis

## 7.2 Results and Discussion

### 7.2.1 Thermal analysis

TGA and DSC analysis were employed to examine the thermal decomposition behavior of precursors, prepared by OP method. Thermogram of precursor powder (Fig. 7.1) revealed that a total weight loss of ~98 % took place when the precursor powder was heated from 30 to 550 °C in air. At first stage, ~3 % weight loss occurred in the region of 40 to 100 °C due to loss of moisture from the precursor. Then, ~95 % weight loss was observed in the temperature range of 190 to 415 °C, which might be due to the oxidative decomposition of precursor and evolution of $CO_2$ and $NO_x$ gases. This decomposition was also reflected in DSC thermogram as an exothermic peak at 414 °C. No weight loss was observed in TGA

_____

when the sample was heated beyond 450 °C. This confirmed the full decomposition of carbonaceous mass of the precursor occurred within 450 °C.
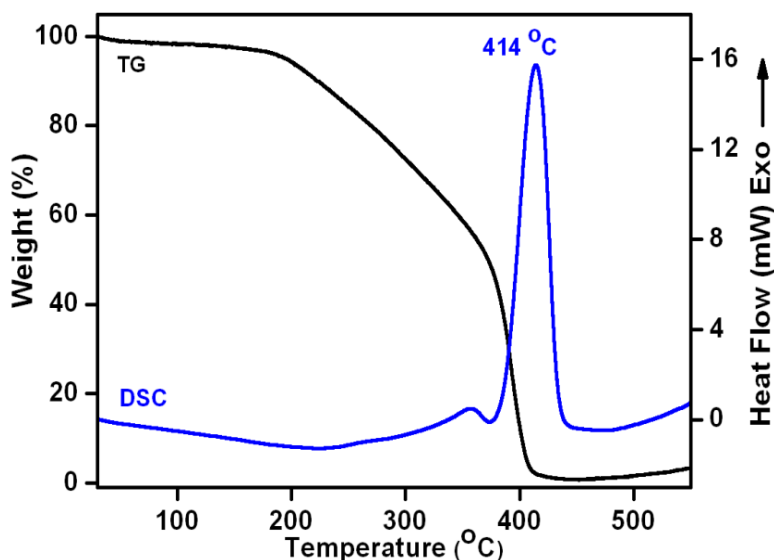


Fig. 7.1 TGA- DSC thermogram of (SrFe$_{12}$O$_{19}$)$_{0.5}$-(Mn$_{0.2}$Ni$_{0.4}$Zn$_{0.4}$Fe$_2$O$_4$)$_{0.5}$ precursor.

## 7.2.2 X-Ray Diffraction analysis

Powder X-ray diffraction (XRD) was carried out to study the phases present in the nanocomposites. XRD patterns of (SrFe$_{12}$O$_{19}$)$_{1-x}$-(Mn$_{0.2}$Ni$_{0.4}$Zn$_{0.4}$Fe$_2$O$_4$)$_x$ nanocomposites prepared by both the methods, exhibited the diffraction peaks corresponding to both spinel Mn$_{0.2}$Ni$_{0.4}$Zn$_{0.4}$Fe$_2$O$_4$ [253] and hexagonal SrFe$_{12}$O$_{19}$ [ICDD 80-1198] phase (Fig. 7.2 (A) and (B)). The XRD patterns confirmed the coexistence of both the phases in the composite powders. Any impurity peak, such as NiO, MnO, ZnO, SrO, SrCO$_3$, α-Fe$_2$O$_3$ etc. within the resolution of the technique was not observed. However, difference in relative intensities of the diffraction peaks was observed for these two types of composites. This might be due to the fact that, homogenous distribution of the spinel and hexagonal phases, present in the nanocomposites, vary with the synthesis route. The average crystallite sizes of Mn$_{0.2}$Ni$_{0.4}$Zn$_{0.4}$Fe$_2$O$_4$ and SrFe$_{12}$O$_{19}$ phases in (SrFe$_{12}$O$_{19}$)$_{1-x}$-(Mn$_{0.2}$Ni$_{0.4}$Zn$_{0.4}$Fe$_2$O$_4$)$_x$ nanocomposites were calculated by X-ray peak-broadening method using Scherrer's equation[437] and listed on Table 7.2. The significant feature was that, in (SrFe$_{12}$O$_{19}$)$_{1-x}$-(Mn$_{0.2}$Ni$_{0.4}$Zn$_{0.4}$Fe$_2$O$_4$)$_x$ composites-OP, the crystallite size of Mn$_{0.2}$Ni$_{0.4}$Zn$_{0.4}$Fe$_2$O$_4$ phase was increased from 10 to 19 nm with increasing amount of Mn$_{0.2}$Ni$_{0.4}$Zn$_{0.4}$Fe$_2$O$_4$ phase in the composite. The same trend was observed for SrFe$_{12}$O$_{19}$ phase and its crystallite size was increased from 26 to 40 nm. In case of (SrFe$_{12}$O$_{19}$)$_{1-x}$-(Mn$_{0.2}$Ni$_{0.4}$Zn$_{0.4}$Fe$_2$O$_4$)$_x$ composites-PM,

_____

the crystallite sizes of both spinel and hexagonal phase did not vary with varying amount of $Mn_{0.2}Ni_{0.4}Zn_{0.4}Fe_2O_4$ and $SrFe_{12}O_{19}$ phases in the composites and was found to be ~19 nm for $Mn_{0.2}Ni_{0.4}Zn_{0.4}Fe_2O_4$ and ~40 nm for $SrFe_{12}O_{19}$. These values were approximately same with the crystallite sizes of pure $Mn_{0.2}Ni_{0.4}Zn_{0.4}Fe_2O_4$ and $SrFe_{12}O_{19}$ nanopowders which imply that the pure phases retain their individual crystallinity in the composites.
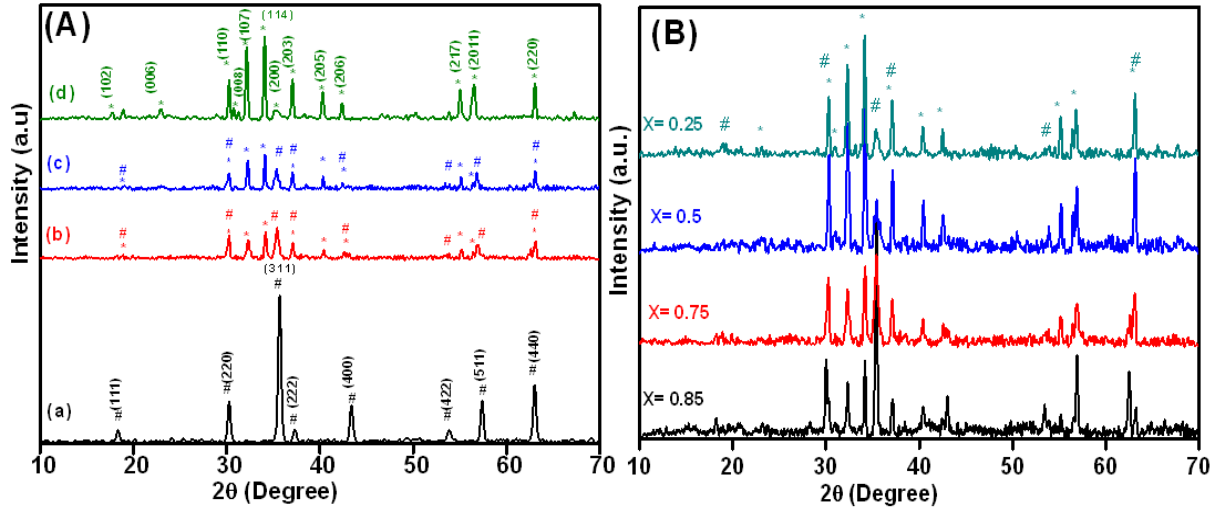


Fig. 7.2 (A) XRD spectra of the (a) pure $Mn_{0.2}Ni_{0.4}Zn_{0.4}Fe_2O_4$, $(SrFe_{12}O_{19})_{0.25}$-$(Mn_{0.2}Ni_{0.4}Zn_{0.4}Fe_2O_4)_{0.75}$ nanocomposites prepared (b) one-pot, (c) physical mixing methods, and (d) pure $SrFe_{12}O_{19}$ nanopowders (B) XRD spectra of $(SrFe_{12}O_{19})_{1-x}$-$(Mn_{0.2}Ni_{0.4}Zn_{0.4}Fe_2O_4)_x$ nanocomposites synthesized by one-pot method (#$Mn_{0.2}Ni_{0.4}Zn_{0.4}Fe_2O_4$ and * $SrFe_{12}O_{19}$).

Table 7.2 Average crystalline size of $(SrFe_{12}O_{19})_{1-x}$-$(Mn_{0.2}Ni_{0.4}Zn_{0.4}Fe_2O_4)_x$ nanocomposites prepared by one-pot and physical mixing method

| Sample | Crystallite size (nm) | | | |
|---|---|---|---|---|
| | One-Pot synthesis | | Physical mixing synthesis | |
| | *(114)plane | #(311)plane | *(114)plane | #(311)plane |
| $Mn_{0.2}Ni_{0.4}Zn_{0.4}Fe_2O_4$-Pure | -- | 19 | -- | -- |
| $(SrFe_{12}O_{19})_{0.15}$-$(Mn_{0.2}Ni_{0.4}Zn_{0.4}Fe_2O_4)_{0.85}$ | 26 | 17 | 39 | 16 |
| $(SrFe_{12}O_{19})_{0.25}$-$(Mn_{0.2}Ni_{0.4}Zn_{0.4}Fe_2O_4)_{0.75}$ | 30 | 16 | 42 | 18 |
| $(SrFe_{12}O_{19})_{0.5}$-$(Mn_{0.2}Ni_{0.4}Zn_{0.4}Fe_2O_4)_{0.5}$ | 34 | 16 | 41 | 21 |
| $(SrFe_{12}O_{19})_{0.75}$-$(Mn_{0.2}Ni_{0.4}Zn_{0.4}Fe_2O_4)_{0.25}$ | 36 | 10 | 40 | 20 |
| $SrFe_{12}O_{19}$-Pure | 40 | -- | -- | -- |

* For $SrFe_{12}O_{19}$, # For $Mn_{0.2}Ni_{0.4}Zn_{0.4}Fe_2O_4$

_____

### 7.2.3 TEM and SEM analysis

During analysis on morphology of two different types of nanocomposites (prepared by PM and OP method) by HRTEM (Fig. 7.3) two distinct types of microstructures were observed.
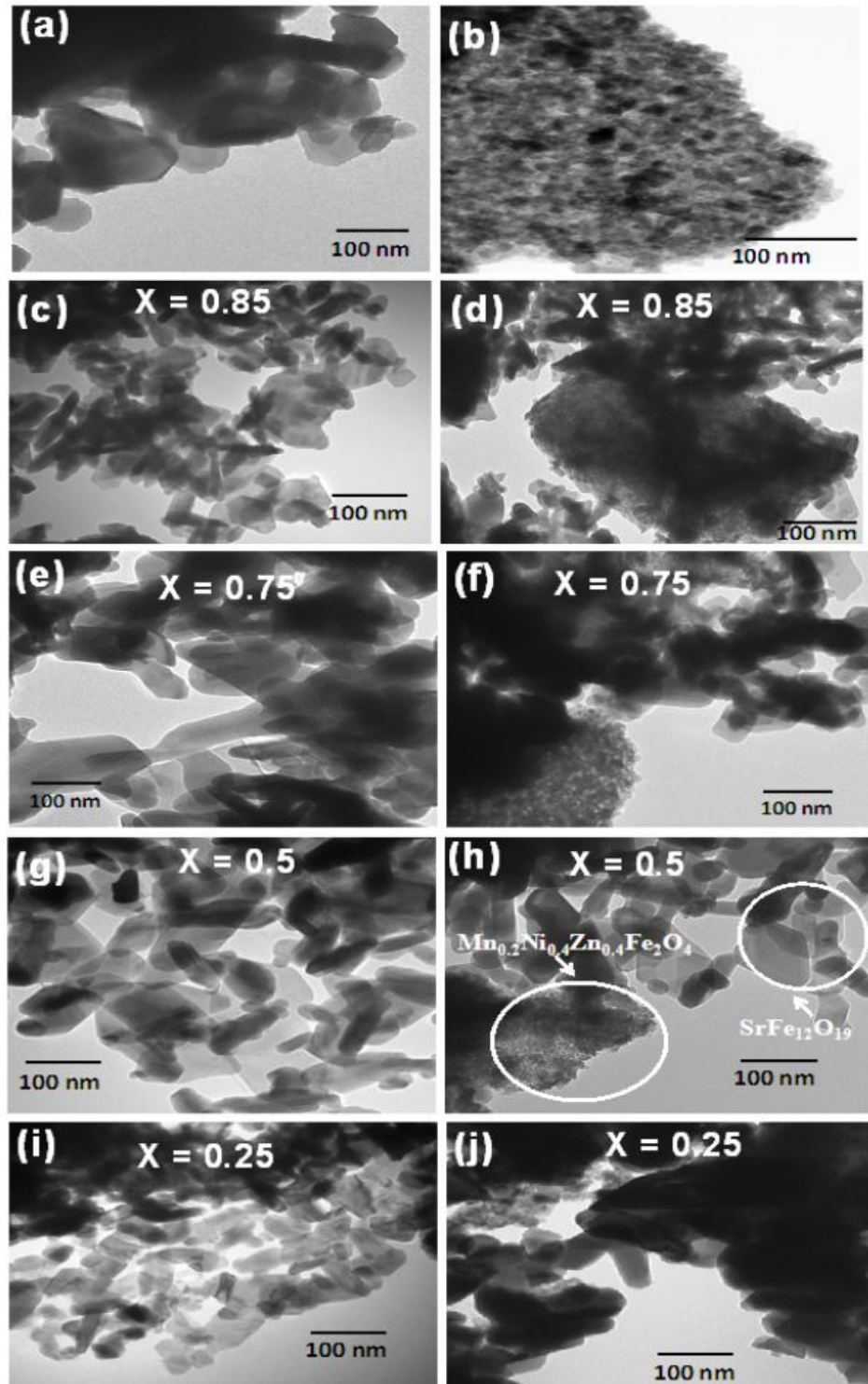


Fig. 7.3 TEM micrographs of (a) pure SrFe$_{12}$O$_{19}$, (b) pure Mn$_{0.2}$Ni$_{0.4}$Zn$_{0.4}$Fe$_2$O$_4$ nanopowders and (SrFe$_{12}$O$_{19}$)$_{1-x}$-(Mn$_{0.2}$Ni$_{0.4}$Zn$_{0.4}$Fe$_2$O$_4$)$_x$ nanocomposites synthesis by (c, e, g, i) one-pot and (d, f, h, j) physical mixing method.

_____

In case of composites-OP, almost regular shaped nanoparticles (average particle size ~60-70 nm) were observed (Fig. 7.3(c, e, g, i)). On the contrary, in composites-PM (Fig. 7.3(d, f, h, j), clear separation of Mn$_{0.2}$Ni$_{0.4}$Zn$_{0.4}$Fe$_2$O$_4$ phase, having spherical shaped agglomerated nanoparticles (~20 nm average particle size, Fig. 7.3(b)) and hexagonal SrFe$_{12}$O$_{19}$ nanoparticles (average particle size of ~50-70 nm, Fig.7.3(a)) were present.

SEM micrographs (Fig.7. 4 (c and (d)) of the samples also revealed the intimate coexistence of both Mn$_{0.2}$Ni$_{0.4}$Zn$_{0.4}$Fe$_2$O$_4$ and SrFe$_{12}$O$_{19}$ particles in the composites-OP (Fig. 7.4 (c)) and presence of large SrFe$_{12}$O$_{19}$ (Fig. 7.4(b)) and small Mn$_{0.2}$Ni$_{0.4}$Zn$_{0.4}$Fe$_2$O$_4$ particles (Fig. 7.4(a)) in the composites-PM (Fig. 7.4 (d)). EDX analysis (Fig. 4(e)) of final nanocomposite indicated the presence of all the elements (e.g. Mn, Ni, Zn, Fe, Sr and O).
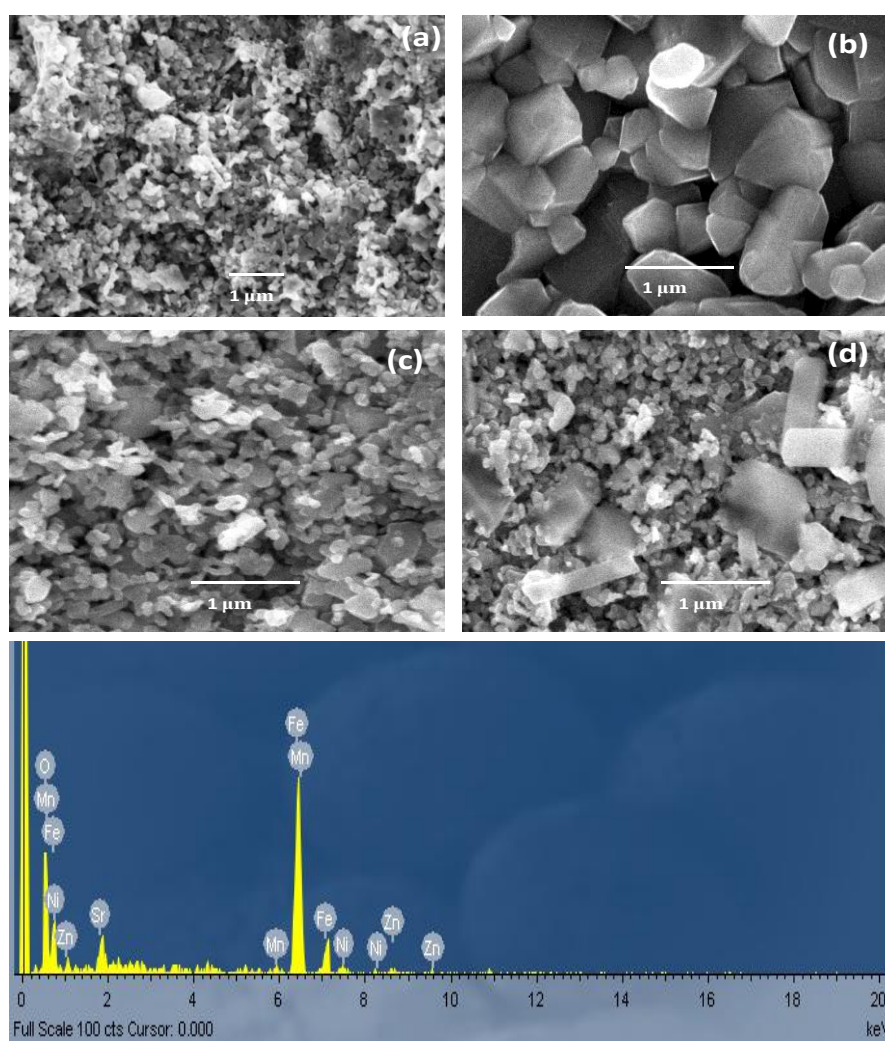


Fig. 7.4 SEM micrographs of (a) pure Mn$_{0.2}$Ni$_{0.4}$Zn$_{0.4}$Fe$_2$O$_4$, (b) Pure SrFe$_{12}$O$_{19}$ and (SrFe$_{12}$O$_{19}$)$_{0.5}$-(Mn$_{0.2}$Ni$_{0.4}$Zn$_{0.4}$Fe$_2$O$_4$)$_{0.5}$ nanocomposites prepared by (c) one-pot, (d) physical mixing method and (e) EDX spectra of (SrFe$_{12}$O$_{19}$)$_{0.5}$-(Mn$_{0.2}$Ni$_{0.4}$Zn$_{0.4}$Fe$_2$O$_4$)$_{0.5}$ nanocomposite prepared by one-pot method.

It was obvious from electron microscopic analysis that, better homogeneous mixing of hard and soft ferrite phases achieved in the nanocomposites, synthesized by one-pot method, than the composites prepared by physical mixing method. This dissimilarity in morphology of the composites may influence the magnetic and microwave absorption properties of the nanocomposites.

### 7.2.4 Magnetic measurements

The room temperature magnetization behaviours of (SrFe$_{12}$O$_{19}$)$_{1-x}$-(Mn$_{0.2}$Ni$_{0.4}$Zn$_{0.4}$Fe$_2$O$_4$)$_x$ nanocomposites prepared by two different methods (OP and PM method) were measured by VSM with an applied field of 15 kOe and shown in Fig.7. 5. The most significant observation was that, composites-OP showed single hysteresis loop, demonstrating hard and soft phases were well exchanged coupled to each other. Whereas, composites-PM exhibited a typical two loop "bee waist" type hysteresis loop, suggesting the absence of exchange coupling between hard and soft phase.[387, 431-433] Fig. 7.5 (b) also reflects that all the composition of (NiFe$_2$O$_4$)$_x$-(SrFe$_{12}$O$_{19}$)$_{1-x}$ showed single hysteresis loop for composites synthesized by OP-method whereas two loop hysteresis for nanocomposites-PM (Fig. 7.5 (c)). Hence, (SrFe$_{12}$O$_{19}$)$_{1-x}$-(Mn$_{0.2}$Ni$_{0.4}$Zn$_{0.4}$Fe$_2$O$_4$)$_x$ nanocomposites, prepared by one-pot method, though exhibited crystallographycally two phase behaviour but showed magnetically good single phase behaviour.

It was also noticed that, coercivity (H$_c$) values of the nanocomposites prepared by both the methods increased with increasing hard ferrite (i.e. SrFe$_{12}$O$_{19}$) content in the sample (Table. 3). For the composites-OP, initial inclusion of SrFe$_{12}$O$_{19}$ phase caused improvement of saturation magnetization (M$_s$) which was due to the spring exchange coupling between hard and soft magnetic phases. However, successive increment of SrFe$_{12}$O$_{19}$ content in the (SrFe$_{12}$O$_{19}$)$_{1-x}$-(Mn$_{0.2}$Ni$_{0.4}$Zn$_{0.4}$Fe$_2$O$_4$)$_x$ nanocomposites (i.e., with increasing (1-x) values) did not influence much on M$_s$. Whereas, in case of composites-PM, M$_s$ value was increased with increasing amount of SrFe$_{12}$O$_{19}$. M$_s$ and H$_c$ values of all the composites prepared by one-pot method were greater than those of the composites prepared by physical mixing method. These facts indicate that hard and soft ferrite phases are well exchanged coupled to each other in the composites prepared by one-pot method. Theoretically calculated values of M$_s$ of the composites (when hard and soft phases are not exchange coupling) using equation 2.1, were

almost matching with the experimentally obtained values of the composites prepared by physical mixing method (Table 7.3).
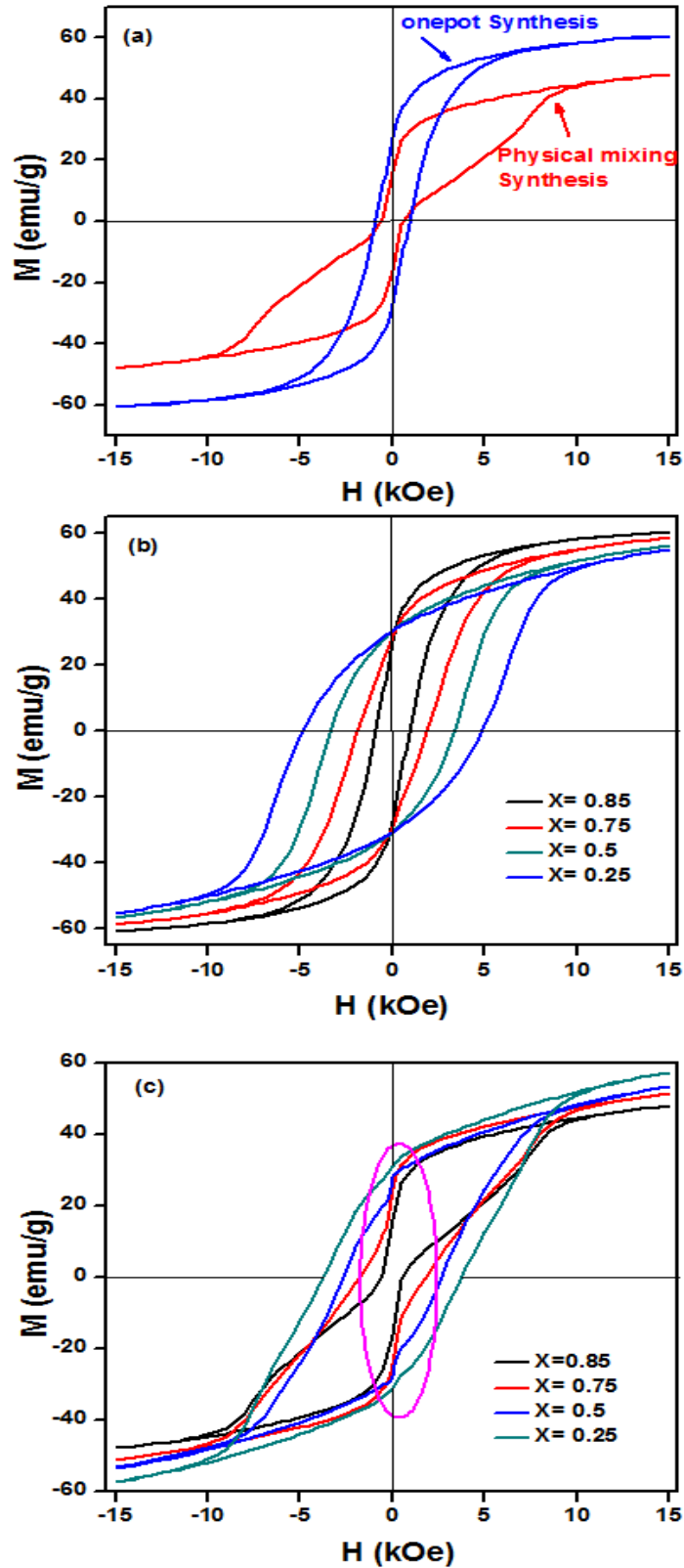


Fig. 7.5 Room temperature hysteresis loops for (a) $(SrFe_{12}O_{19})_{0.15}$-$(Mn_{0.2}Ni_{0.4}Zn_{0.4}Fe_2O_4)_{0.85}$ nanocomposite prepared by one-pot and physical mixing method and $(SrFe_{12}O_{19})_{1-x}$-$(Mn_{0.2}Ni_{0.4}Zn_{0.4}Fe_2O_4)_x$ nanocomposite prepared by (b) one-pot, (c) physical mixing method.

117

_____

Table 7.3 $M_s$ and $H_c$ values of the $(SrFe_{12}O_{19})_{1-x}$-$(Mn_{0.2}Ni_{0.4}Zn_{0.4}Fe_2O_4)_x$ nanocomposites prepared by one-pot and physical mixing method

| Sample | One-pot synthesis | | Physical mixing synthesis | | Theoretical $M_s$ without exchange coupling (emu/g) |
|---|---|---|---|---|---|
| | $H_c$ (Oe) | $M_s$ (emu/g) | $H_c$ (Oe) | $M_s$ (emu/g) | |
| $Mn_{0.2}Ni_{0.4}Zn_{0.4}Fe_2O_4$-Pure | 61 | 39.1 | -- | -- | -- |
| $(SrFe_{12}O_{19})_{0.15}$-$(Mn_{0.2}Ni_{0.4}Zn_{0.4}Fe_2O_4)_{0.85}$ | 910 | 60.6 | 581 | 47.8 | 47.2 |
| $(SrFe_{12}O_{19})_{0.25}$-$(Mn_{0.2}Ni_{0.4}Zn_{0.4}Fe_2O_4)_{0.75}$ | 1912 | 58.4 | 1792 | 51.1 | 50.2 |
| $(SrFe_{12}O_{19})_{0.5}$-$(Mn_{0.2}Ni_{0.4}Zn_{0.4}Fe_2O_4)_{0.5}$ | 3350 | 56.3 | 2687 | 53.4 | 54.3 |
| $(SrFe_{12}O_{19})_{0.75}$-$(Mn_{0.2}Ni_{0.4}Zn_{0.4}Fe_2O_4)_{0.25}$ | 4840 | 55.1 | 3746 | 57.3 | 56.3 |
| $SrFe_{12}O_{19}$-Pure | 5866 | 57.6 | -- | -- | -- |

## 7.2.5 Microwave absorption study

Microwave absorption behavior of $(SrFe_{12}O_{19})_{1-x}$-$(Mn_{0.2}Ni_{0.4}Zn_{0.4}Fe_2O_4)_x$ nanocomposites with different compositions (x= 0.85, 0.75, 0.5, 0.25) synthesized by one-pot method were studied. Loss tangent vs. frequency were plotted to understand the particular loss mechanism involved for each composite and shown in Fig. 7.6 (a) and (b). The dielectric and magnetic loss tangents can be expressed as $tan\delta_\varepsilon = \varepsilon''/ \varepsilon'$ and $tan\delta_\mu = \mu''/ \mu'$, respectively. Fig. 7.6 (b) revealed that these composites are having only magnetic loss parameter whereas the dielectric loss parameter is negligible (Fig. 7.6 (a)). Reflection loss was calculated using equation (1.4 and 1.5) and plotted against frequency for different $(SrFe_{12}O_{19})_{1-x}$-$(Mn_{0.2}Ni_{0.4}Zn_{0.4}Fe_2O_4)_x$ nanocomposites (x= 0.85, 0.75, 0.5, 0.25) synthesized by OP method for thickness 3 mm (Fig. 7.6 (c)). In Reflection Loss vs. frequency plot, the dip of the curves was designated for minimum RL indicating maximum absorption. It was observed that, with decreasing the value of x (i.e. increasing $SrFe_{12}O_{19}$ content in the composite) maximum absorption was also decreased. As the composite having composition $(Mn_{0.2}Ni_{0.4}Zn_{0.4}Fe_2O_4)_{0.85}$-$(SrFe_{12}O_{19})_{0.15}$ exhibited minimum reflection loss (~ -15 dB) i.e. maximum absorption compare to other composites, so we have selected this composition for further studies and the absorption properties are compared with the composite prepared by PM method as well as pure $Mn_{0.2}Ni_{0.4}Zn_{0.4}Fe_2O_4$ and $SrFe_{12}O_{19}$.
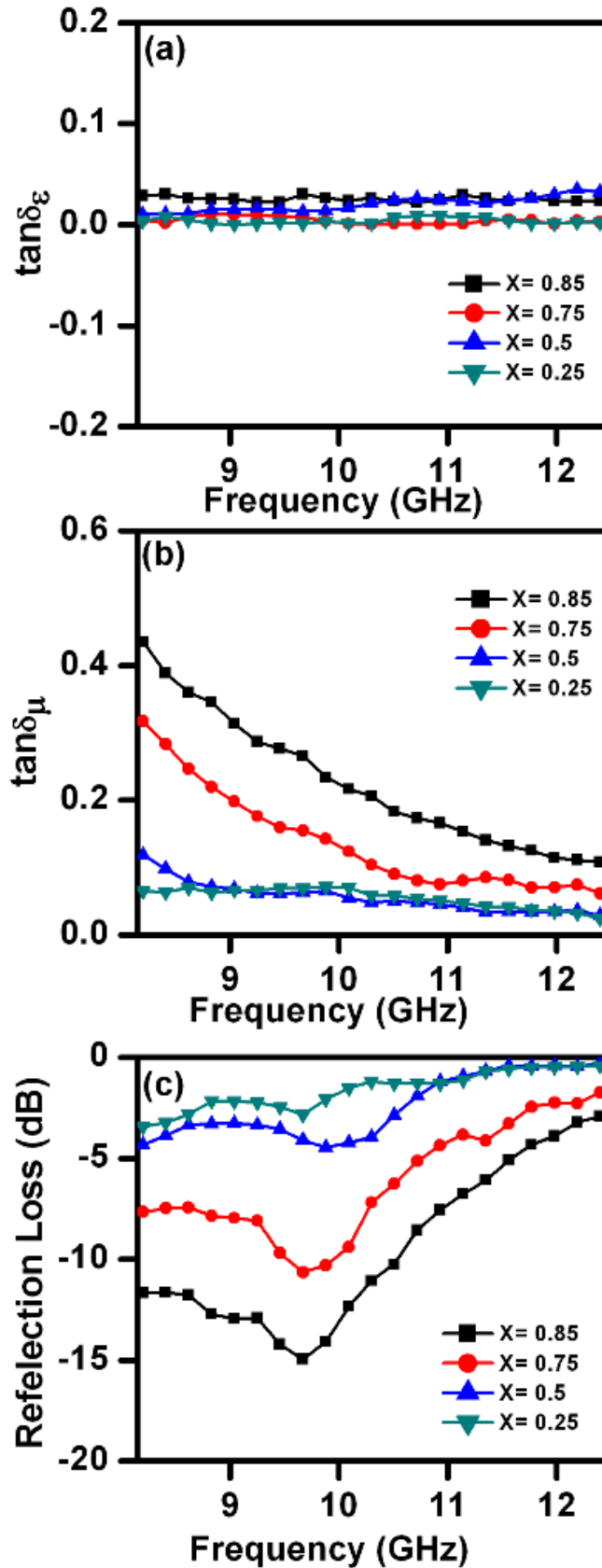
Fig. 7.6 (a) Loss Tangent of relative complex permittivity (tan$\delta_\varepsilon$), (b) Loss Tangent of relative complex permeability (tan$\delta_\mu$) and (c) Reflection loss vs. frequency plot (SrFe₁₂O₁₉)₁₋ₓ-(Mn₀.₂Ni₀.₄Zn₀.₄Fe₂O₄)ₓ nanocomposites synthesized by one-pot method.

_____

The real and imaginary permittivity (Fig. 7.7 (a). and (b)) and permeability (Fig. 7.7 (c) and (d)) for the nanocomposites synthesized by both the methods, pure SrFe$_{12}$O$_{19}$ and Mn$_{0.2}$Ni$_{0.4}$Zn$_{0.4}$Fe$_2$O$_4$ nanopowders were plotted as a function of frequency in the X-band range (8.2-12.4 GHz). It was observed that, ε′ values remained almost constant over the entire frequency range. Nanocomposites synthesized by one-pot method showed higher ε′ value than the composite prepared by physical mixing method as well as pure SrFe$_{12}$O$_{19}$ and Mn$_{0.2}$Ni$_{0.4}$Zn$_{0.4}$Fe$_2$O$_4$ nanopowders (Fig. 7.7(a)). The imaginary dielectric parameter (ε″) values remained nearly constant for both composites as well as pure hard and soft ferrite nanopowders (Fig. 7.7 (b)). The real permeability (μ′) values of both the composite and pure nanopowders remained almost constant in the complete frequency range of X-band (Fig. 7.7 (c)). The imaginary permeability (μ″) values (Fig. 7.7 (d)) showed a decreasing tendency from 8.2 GHz to 12.4 GHz for both the nanocomposites and pure ferrites, however, maximum imaginary permeability was observed for the composite synthesized by one-pot method.
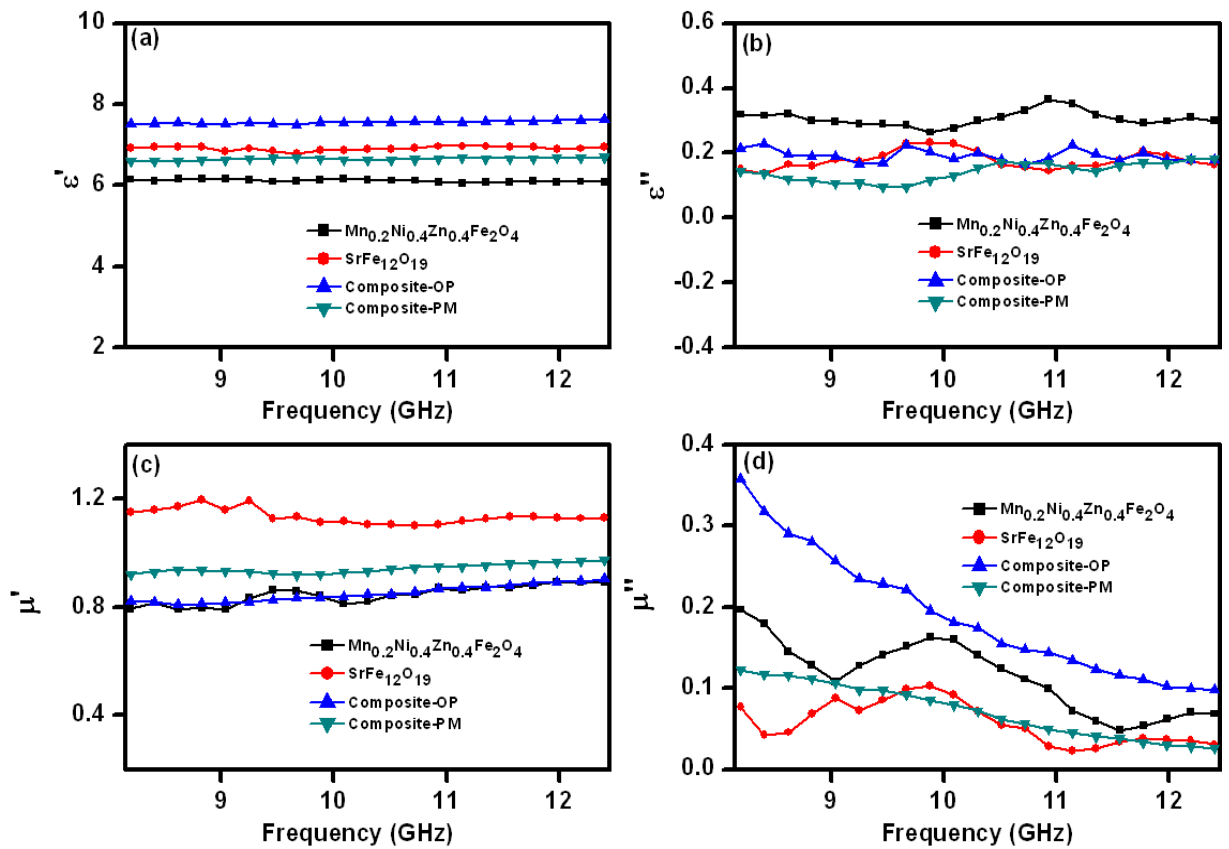


Fig. 7.7 (a) Real (ε'), (b) imaginary (ε") parts of relative complex permittivity and (c) real (μ'), (d) imaginary (μ") parts of relative complex permeability of pure Mn$_{0.2}$Ni$_{0.4}$Zn$_{0.4}$Fe$_2$O$_4$, SrFe$_{12}$O$_{19}$ nanopowders and (SrFe$_{12}$O$_{19}$)$_{0.15}$-(Mn$_{0.2}$Ni$_{0.4}$Zn$_{0.4}$Fe$_2$O$_4$)$_{0.85}$ nanocomposites prepared by one-pot and physical mixing method.

_____

Refection Loss for nanocomposites as well as pure ferrite nanopowders was calculated for absorber thickness 3 mm and shown in Fig. 7.8 (a). The estimated electromagnetic wave absorption values are listed in Table 7.4. From Fig. 7.8 (a), it was observed that the composite-OP showed greater reflection loss (~ -15 dB at 9.67GHz corresponds to ~96.84% absorption) compare to the composite-PM (~ -4 dB at 9.46 GHz). Pure hard and soft ferrite nanopowders showed reflection loss lower than -10dB (~ -6 dB and ~ -8 dB respectively).Composite-OP showed >10 dB reflection loss (i.e. > 90% absorption) over frequency range of 8.2 GHz to 10.53 GHz. Fig. 7.8 (b) illustrates the reflection loss vs. frequency for one-pot synthesized nancomposite with different thickness of the absorber. The reflection loss was found to be increased with increasing thickness of the absorber till 3.5mm with the shifting of the frequency corresponds to maximum loss towards lower frequency. Reflection loss of ~ -28 dB i.e. 99.84% absorption was observed at 8.2 GHz for absorber thickness of 3.5 mm but frequency range corresponds to reflection loss $\geq$ -10 dB (means > 90% absorption) becomes narrower than the specimen thickness of 3 mm. The RL value of -20 dB is equivalent to 99% absorption, which is considered as the satisfactory microwave absorption.
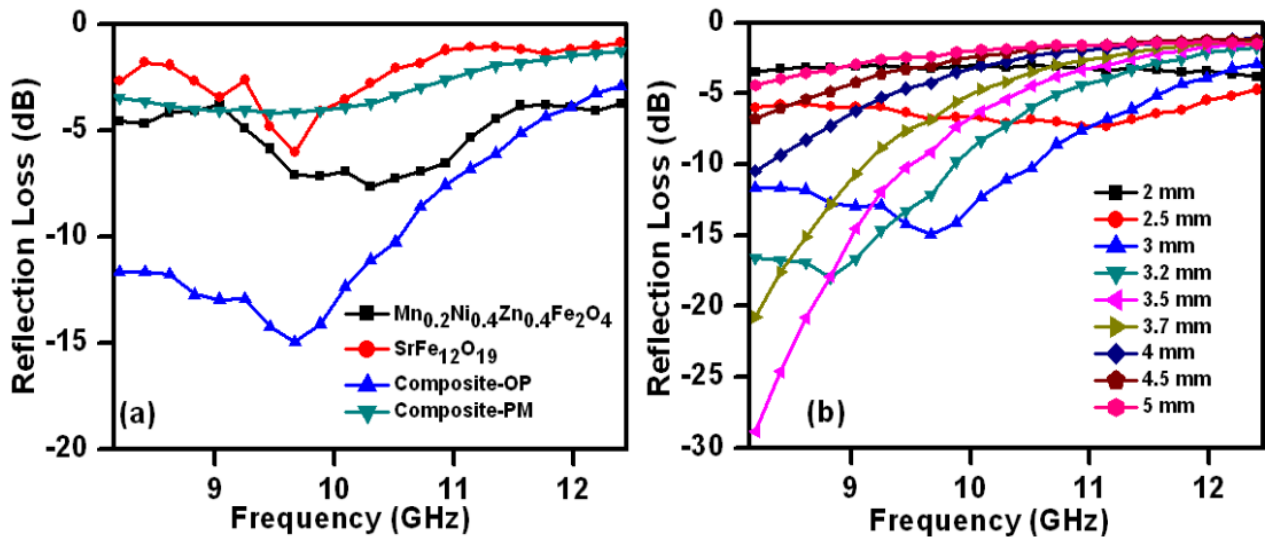


Fig. 7.8 Reflection loss vs. frequency plot for (a) pure $Mn_{0.2}Ni_{0.4}Zn_{0.4}Fe_2O_4$, $SrFe_{12}O_{19}$ nanopowders and $(SrFe_{12}O_{19})_{0.15}$-$(Mn_{0.2}Ni_{0.4}Zn_{0.4}Fe_2O_4)_{0.85}$ nanocomposites prepared by one-pot and physical mixing method and (b) Reflection loss vs. frequency plot for $(SrFe_{12}O_{19})_{1-x}$-$(Mn_{0.2}Ni_{0.4}Zn_{0.4}Fe_2O_4)_x$ nanocomposites prepared by one-pot method at different specimen thickness.

_____

Table 7.4 Microwave absorption characteristics of pure SrFe$_{12}$O$_{19}$, Mn$_{0.2}$Ni$_{0.4}$Zn$_{0.4}$Fe$_2$O$_4$ nanopowders and (SrFe$_{12}$O$_{19}$)$_{0.15}$-(Mn$_{0.2}$Ni$_{0.4}$Zn$_{0.4}$Fe$_2$O$_4$)$_{0.85}$ nanocomposites prepared by one-pot and physical mixing method

| Sample | Minimum RL (dB) | Frequency (GHz) |
|---|---|---|
| SrFe$_{12}$O$_{19}$-Pure | -6.01 | 9.67 |
| (SrFe$_{12}$O$_{19}$)$_{0.15}$-(Mn$_{0.2}$Ni$_{0.4}$Zn$_{0.4}$Fe$_2$O$_4$)$_{0.85}$ (one-pot method) | -14.95 | 9.67 |
| (SrFe$_{12}$O$_{19}$)$_{0.15}$-(Mn$_{0.2}$Ni$_{0.4}$Zn$_{0.4}$Fe$_2$O$_4$)$_{0.85}$ (physical mixing method) | -4.2 | 9.46 |
| Mn$_{0.2}$Ni$_{0.4}$Zn$_{0.4}$Fe$_2$O$_4$-Pure | -7.64 | 10.3 |

## 7.3 Summary of Results

(i) (SrFe$_{12}$O$_{19}$)$_{1-x}$-(Mn$_{0.2}$Ni$_{0.4}$Zn$_{0.4}$Fe$_2$O$_4$)$_x$ nanocomposites were successfully synthesized using EDTA precursor based one-pot method where precursor was calcined at 800 °C for 4 h.

(ii) Thermal decomposition of the precursor was complete at ~450 °C.

(iii) XRD patterns of (SrFe$_{12}$O$_{19}$)$_{1-x}$-(Mn$_{0.2}$Ni$_{0.4}$Zn$_{0.4}$Fe$_2$O$_4$)$_x$ nanocomposites, prepared by one-pot method exhibited the diffraction peaks corresponding to both spinel Mn$_{0.2}$Ni$_{0.4}$Zn$_{0.4}$Fe$_2$O$_4$ and hexagonal SrFe$_{12}$O$_{19}$ phase.

(iv) In (SrFe$_{12}$O$_{19}$)$_{1-x}$-(Mn$_{0.2}$Ni$_{0.4}$Zn$_{0.4}$Fe$_2$O$_4$)$_x$ nanocomposites synthesized by OP method, the crystallite size of Mn$_{0.2}$Ni$_{0.4}$Zn$_{0.4}$Fe$_2$O$_4$ phase was increased from 10 to 19 nm with increasing amount of Mn$_{0.2}$Ni$_{0.4}$Zn$_{0.4}$Fe$_2$O$_4$ phase in the composite. The same trend was observed for SrFe$_{12}$O$_{19}$ phase and its crystallite size was found to be increased from 26 to 40 nm.

(v) (SrFe$_{12}$O$_{19}$)$_{1-x}$-(Mn$_{0.2}$Ni$_{0.4}$Zn$_{0.4}$Fe$_2$O$_4$)$_x$ nanocomposites synthesized by PM method, the crystallite sizes of both spinel and hexagonal phase did not change much with varying amount of Mn$_{0.2}$Ni$_{0.4}$Zn$_{0.4}$Fe$_2$O$_4$ and SrFe$_{12}$O$_{19}$ phases in the composites and were found to be ~20 nm for Mn$_{0.2}$Ni$_{0.4}$Zn$_{0.4}$Fe$_2$O$_4$ and ~40 nm for SrFe$_{12}$O$_{19}$. These values were almost same in comparison with the crystallite sizes of pure Mn$_{0.2}$Ni$_{0.4}$Zn$_{0.4}$Fe$_2$O$_4$ and SrFe$_{12}$O$_{19}$.

(vi) Nanocomposites synthesized by PM method, clear segregation of hexagonal SrFe$_{12}$O$_{19}$ nanoparticles and spherical shaped agglomerated Mn$_{0.2}$Ni$_{0.4}$Zn$_{0.4}$Fe$_2$O$_4$

_____

nanoparticles were observed. Nanocomposites, prepared by one-pot method, almost uniform shaped nanoparticles (average particle size ~60-70 nm) were observed.

(vii) Nanocomposites-OP, showed single hysteresis loop, signifying hard and soft phases were well exchanged coupled to each other. Whereas, composites-PM exhibited a typical two loop "bee waist" type hysteresis loop, indicating the absence of exchange coupling between hard and soft phase. M$_s$ and H$_c$ values of all the composites prepared by one-pot method were higher than those of the composites prepared by physical mixing method.

(viii) Nanocomposites synthesized by one-pot method are having only magnetic loss parameter whereas dielectric loss parameter is negligible

(ix) Nanocomposite-OP showed greater reflection loss (~ -15 dB at 9.67 GHz corresponds to ~96.84% absorption) than composite-PM method (~ -4.2 dB at 9.46 GHz) for absorber thickness of 3 mm. Pure hard and soft ferrite nanopowders showed reflection loss lower than -10dB (~-7 dB and ~-6 dB respectively).

(x) (SrFe$_{12}$O$_{19}$)$_{0.15}$-(Mn$_{0.2}$Ni$_{0.4}$Zn$_{0.4}$Fe$_2$O$_4$)$_{0.85}$ nanocomposite synthesized by OP method exhibited reflection loss of ~ -28 dB (i.e. > 99.84% absorption) at 8.2 GHz for absorber thickness of 3.5 mm.

_____

<div align="right">

**Chapter 8**

</div>

## Conclusions and future scope of work

### 8.1 Conclusions

Based on the results obtained (which have been discussed in Chapter 2 to Chapter 7) following conclusions have been drawn:

1. In the present research work, ethylenediaminetertaacetic acid (EDTA) precursor based one-pot method has been developed for synthesis of hard-soft ferrite nanocomposites. This synthesis method is referred as 'one-pot' method because formation of both hard and soft ferrite phases occurred simultaneously in the same reaction mixture. This method is a versatile one and capable of producing variety of ferrite nanocomposites such as $(NiFe_2O_4)_x$-$(BaFe_{12}O_{19})_{1-x}$, $(NiFe_2O_4)_x$-$(SrFe_{12}O_{19})_{1-x}$, $(Ni_{0.65}Zn_{0.35}Fe_2O_4)_x$-$(BaFe_{12}O_{19})_{1-x}$, $(Ni_{0.65}Zn_{0.35}Fe_2O_4)_x$-$(SrFe_{12}O_{19})_{1-x}$, $(Mn_{0.2}Ni_{0.4}Zn_{0.4}Fe_2O_4)_x$-$(BaFe_{12}O_{19})_{1-x}$, $(Mn_{0.2}Ni_{0.4}Zn_{0.4}Fe_2O_4)_x$-$(SrFe_{12}O_{19})_{1-x}$.

2. In this synthesis method, the chelating agent (EDTA) plays a critical role. It not only prevents the segregation or intermittent precipitation of metal ions from solution during evaporation but also helps the formation of a fluffy, voluminous, porous, carbon-rich precursor. During decomposition of precursor, nascent metal oxides form, which are basically small atomic clusters with proper chemical homogeneity, embedded into the precursor. These nascent metal oxides when calcined at 800 °C produce desired composite powders. During thermal decomposition, precursors produce gases (such as $CO_2$, $NO_x$) that help to dissipate the heat of combustion and thus inhibit the sintering of fine particles during the process to produce nanocomposites.

3. The advantages this method offers are (i) requirement of comparatively lower calcination temperature (ii) no impurity phases present in the final product (iii) use of cheap metal nitrates and EDTA as starting materials and water as solvent, instead of expensive metal complexes or delicate reagents or organic solvents, help in reduction

_____

of the processing cost (iv) no corrosive regents like NaOH is required (v) no elaborate or expensive reaction set up is required (vi) chemical composition of the final products can easily be controlled. The simplicity of the process, its cost-effectiveness and capability of producing various types of ferrite nanoparticle make this method attractive.

4. In any step of this synthesis method filtration or washing was not involved so, there was no chance to lose any metal ions from the composites. EDX analysis of the final nanocomposites also revealed that all the metal ions are present in the composites. Hence, the final compositions of the composites are according to the molar compositions of the metal ions taken in the first step of the synthetic method.

5. XRD patterns of hard-soft ferrite nanocomposites, prepared by one-pot as well as physical mixing method exhibited the diffraction peaks corresponding to both spinel soft and hexagonal hard phase. Any impurity peak within the resolution of the technique was not observed.

6. In hard-soft ferrite nanocomposites synthesized by one-pot method, the crystallite size soft and hard phase was varied with variation of amount of soft and hard phase in the composite. Whereas, nancomposites synthesized by physical mixing method the crystallite sizes remains almost same as pure hard and soft ferrite.

7. Electron microscopic analysis clearly shows that, the nanocomposites synthesized by one-pot method possess better homogeneity than the composites prepared by physical mixing method. In case of the nanocomposites synthesized by physical mixing method, clear segregation of hexagonal hard phase (average particle size of ~60-70 nm) and spherical shaped agglomerated soft phase (~20 nm average particle size) were observed. On the contrary, for the nanocomposites, prepared by one-pot method, almost uniform shaped nanoparticles (average particle size ~60-70 nm) were observed.

8. Nanocomposites synthesized by one-pot method, showed single hysteresis loop, signifying hard and soft phases were well exchanged coupled to each other. Whereas, composites synthesized by physical mixing method exhibited a typical two loop "bee waist" type hysteresis loop, indicating the absence of exchange coupling between hard

_____

and soft phase. $M_s$ and $H_c$ values of all the composites prepared by one-pot method were higher than those of the composites prepared by physical mixing method.

9. Nanocomposites, synthesized by one-pot method, exhibited superior microwave absorption property than that of nanocomposites synthesized by physical mixing method and both pure hard and soft ferrite. In one-pot synthesis method, as both the phases are grown together from a single reaction mixture, intimate co-existence of nanosized hard and soft ferrite phases were observed. This fact leads to sufficient exchange coupling between hard and soft ferrite phases in these nanocomposites which finally influence the magnetic and microwave absorption properties.

10. Among all the synthesized nanocomposites, $(SrFe_{12}O_{19})_{0.15}$-$(Mn_{0.2}Ni_{0.4}Zn_{0.4}Fe_2O_4)_{0.85}$ nanocomposite synthesized by OP method exhibited reflection loss of ~ -28 dB (i.e. > 99.84% absorption) at 8.2 GHz for absorber thickness of 3.5 mm.

11. Simple method of preparation, superior magnetic and microwave absorption properties make these nanocomposites potential candidates for application in next generation permanent magnets as well as radar absorbing materials.

## 8.2 Limitations of the developed chemical method

However, the two main limitations of the developed methods are:

(i) These methods are not suitable for synthesizing metallic nanoparticles or nanopowders that contain metal ions in lower/unstable oxidation state.

(ii) These methods are not appropriate to synthesize metal nitrides.

## 8.4 Future scope of work

1. Detail investigation on microstructure, magnetic and microwave absorption properties with variation of sintering temperature.

2. Fabrication of flexible coating materials consists of hard-soft ferrite nanocomposites and polymer/rubber for suitable radar absorbing materials (RAM) for defence stealth application.

# References

**1.** E. C. Snelling, *Soft Ferrites Properties and Applications*, Iliffe Book Ltd., London (**1969**).

**2.** J. Smit and H. P. J. Wijn, *Ferrites Physical Properties of Ferrimagnetic Oxidea in Relation to Their Technical Applications,* Philips Technical Library, Eindhoven (**1959**).

**3.** Ü. Özgür, Y. Alivov and H. Morkoç, *J. Mater. Sci: Mater. Electron.* 20, 789 (**2009**).

**4.** A-H. Lu, E. L. Salabas and F. Schüth, *Angew. Chem. Int. Ed.* 46, 1222 (**2007**).

**5.** J. K. Oh and J. M. Park, *Prog. Polym. Sci.* 36, 168 (**2011**).

**6.** T. K. Indira and P. K. Lakshmi, *Int. J. Pharm . Sci. Nanotechnol.* 3, 1035 (**2010**).

**7.** E. Umut, in *Modern Surface Engineering Treatments* edited M. Aliofkhazraei, InTech, Rijeka, Ch. 8, p. 186 (**2013**).

**8.** A. G. Roca, R. Costo, A. F Rebolledo, S. Veintemillas-Verdaguer, P. Tartaj,.T. González-Carreño, M. P. Morales and C. J. Serna, *J. Phys. D: Appl. Phys.* 42, 224002 (**2009**).

**9.** S. Laurent, D. Forge, M. Port, A. Roch, C. Robic, L.Vander Elst and R. N. Muller, *Chem. Rev.* 108, 2064 (**2008**).

**10.** A. S. Teja and P-Y. Koh, *Prog. Cryst. Growth Charact. Mater.* 55, 22 (**2009**).

**11.** P. Pant, S. Bhuvaneswari and N. N. Ghosh, *Recent Patents Nanotechnol.* 2, 8 (**2008**).

**12.** N. N. Ghosh, in *Powder Engineering, Technology and Applications*, edited J. M. Barker, Nova Science Publishers, New York, Ch. 7, p.197 (**2011**).

**13.** M. Sugimoto, *J. Am. Ceram. Soc.* 82, 269 (**1999**).

**14.** C. D. Owens, *Proc. IRE.* 44, 1234 (**1956**).

**15.** H. P. J. Wijn in *Proceedings of the International Conference on Ferrites*, Edited Y. Hoshino, S. Iida and M. Sugimoto. University of Tokyo Press, Tokyo, p. xix. (**1971**)

**16.** S. Hilpert, *Ber. Dtsch. Chem. Ges.* 42, 2248 (**1909**).

**17.** S. Hilpert and A. Wille, *Z. Phys. Chem. B*. 18, 291 (**1932**).

**18.** S. Hilpert and A. Lindner, *Z. Phys. Chem. B*. 22, 395 (**1933**).

**19.** S. Hilpert and R. Schweinhagen, *Z. Phys. Chem. B*. 31, 1 (**1935**).

**20.** S. Hilpert, German Pat. Nos. 226, 347 (**1909**).

**21.** S. Hilpert, German Pat. Nos. 227, 787 (**1909**).

**22.** Y. Kato and T. Takei, *J. Inst. Electr. Eng. Jpn.* 53, 408 (**1933**).

**23.** T. Takei, T. Yasuda and S. Ishihara, *Electrotech. J.* 4, 75 (**1940**).

**24.** Y. Kato and T. Takei, Japan Pat. No. 110,822 (**1932**).

**25.** Y. Kato and T. Takei, U.S. Pat. No. 1,976,230 (**1934**).

**26.** Y. Kato and T. Takei, U.S. Pat. No. 1,997,193 (**1935**).

**27.** Y. Kato and T. Takei, Japan Pat. No. 98,844 (**1932**).

**28.** L. Néel, Ann. Phys. (Paris) 3, 137 (**1948**).

**29.** L. Snoek, Physica (Holland) 3, 463 (**1936**).

**30.** J. L. Went, G. W. Ratenau, E. W. Gorter and G. W. van Oosterhout, *Philips Tech. Rev.* 13, 194 (**1951**).

**31.** G. H. Jonker, H. P. J. Wijn and P. B. Braum, *Philips Tech. Rev.* 18, 145 (**1956/1957**).

**32.** C. L. Hogan, *Bell. Syst. Tech. J.* 31, 1 (**1952**).

**33.** E. Allbers-Schoenberg, *J. Appl. Phys.* 25, 152 (**1954**).

**34.** J. F. Dillion Jr., E. M. Gyorgy and J. P. Remeika, *Phys. Rev. Lett.* 22, 643 (**1969**).

**35.** M. Camras, U.S. Pat. No. 2,694,656 (**1954**).

**36.** M. M. Hessien, M. Radwan and M. M. Rashad, *J. Anal. Appl. Pyrolysis.* 78, 282 (**2007**).

**37.** R. C. Pullar, *Prog. Mater. Sci.* 57, 1191 (**2012**).

**38.** Y. J. Shin and J. H.Oh, *IEEE Trans. Magn.* 29, 3437 (**1993**).

**39.** M. Kaiser, *J. Alloys Compd.* 468, 15 (**2009**).

**40.** S. D. Bhame and P. A. Joy, *J. Am. Ceram. Soc.* 91, 1976 (**2008**).

**41.** D. Sakellari, V. Tsakaloudi, E. K. Polychroniadis and V. Zaspalisw, *J. Am. Ceram. Soc.* 91, 366 (**2008**).

**42.** N. Sivakumar, A. Narayanasamy, N. Ponpandianb and G. Govindaraj, *J. Appl. Phys.* 101, 084116 (**2007**).

**43.** P. Yadoji, R. Peelamedu, D. Agrawal and R. Roy, *Mater. Sci. Eng. B.* 98, 269 (**2003**).

**44.** A. A.Sattar, H. M. El-Sayed, K. M. El-Shokrofy and M. M. El-Tabey, *J. Mater. Sci.* 42, 149 (**2007**).

**45.** A. K. M. A. Hossain, T. S. Biswas, S. T. Mahmud, T. Yanagida , H. Tanaka and T. Kawai, *J. Magn. Magn. Mater.* 321, 81 (**2009**).

**46.** A. Yourdkhani, S. A. S. Ebrahimi and H. R. Koohdar, *J. Alloys Compd.* 470, 561 (**2009**).

**47.** V. G. Patil, S. E. Shirsath, S. D. More, S. J. Shukla and K.M. Jadhav, *J. Alloys Compd.* 488, 199 (**2009**).

**48.** P. N. Vasambekar, C. B. Kolekar and A. S. Vaingankar, *J. Mater. Sci: Mater. Electron.* 10, 667 (**1999**).

**49.** J-P Zhou, L. Lv and X-Z Chen, *J. Ceram. Process. Res.* 11, 263 (**2010**).

**50.** S. B. Waje, M. Hashim, W. D. W. Yusoff and Z. Abbas, *J. Appl. Sci. Res.* 5. 1440, (**2009**).

**51.** S. B. Waje, M. Hashim, W. D. W. Yusoff and Z. Abbas, *Appl. Surf. Sci.* 256, 3122 (**2010**).

**52.** Y. C. Wang, J. Ding, J. H. Yin, B. H. Liu, J. B. Yi and S. Yu, *J. Appl. Phys.* 98, 124306 (**2005**).

**53.** C. N. Chinnasamya, A. Narayanasamya, N. Ponpandian, R. J. Joseyphus, B. Jeyadevan, K. Tohji and K. Chattopadhyay, *J. Magn. Magn. Mater.* 238, 281 (**2002**).

**54.** G. Nabiyouni, M. J. Fesharaki, M. Mozafari and J. Amighian, *Chin. Phys. Lett.* 27, 126401 (**2010**).

**55.** V. Šepelák, I. Bergmann, A. Feldhoff, P. Heitjans, F. Krumeich, D. Menzel, F. J. Litterst, S. J. Campbell and K. D. Becker, *J. Phys. Chem. C.* 111, 5026 (**2007**).

**56.** M. A. A. Bhuiyan, S. M. Hoque and S. Choudhury, *J. Bangladesh Acad* . Sci. 34, 189 (**2010**).

**57.** A. A.Sattar, H. M. El-Sayed, K. M. El-Shokrofy and M. M. El-Tabey, *J. Mater. Eng. Perform.* 14, 99 (**2005**).

**58.** H. S. Woon, K. P. Lim, N. Puteri, R. Rozaimah and C.Y. Tan, *Am. J. Eng. Appl. Sci.* 2, 580 (**2009**).

**59.** M. Y. Salunkhe and D. K. Kulkarni, *J. Magn. Magn. Mater.* 279, 64 (**2004**).

**60.** P. Hernández-Gómez, C. Torres, C. de Francisco, J. M. Muñoz, O. Alejos, J. I. Iñiguez and V. Raposo, *J. Magn. Magn. Mater.* 272- 276, e1843 (**2004**).

**61.** S. A. S. Ebrahimi, A. Kianvash, C. B. Ponton and I. R. Harris, *Ceram. Int.* 26, 379 (**2000**).

**62.** P. Sharma, R. A. Rocha, S. N. de Medeiros and A. Paesano Jr., *J. Alloys Compd.* 443, 37 (**2007**).

**63.** B. S. Zlatkov, M. V. Nikolic, O. Aleksic, H. Danninger and E. Halwax, *J. Magn. Magn. Mater.* 321, 330 (**2009**).

**64.** H. Sözeri, *J. Magn. Magn. Mater.* 321, 2717 (**2009**).

**65.** G. Benito, M. P. Morales, J. Requena, V. Raposo, M. Vázquez and J. S. Moya, *J. Magn. Magn. Mater.* 234, 65 (**2001**).

**66.** A. Verma and R. Chatterjee, *J. Magn. Magn. Mater.* 306, 313 (**2006**).

**67.** J. J. Suh and Y. H. Han, *J. Am. Ceram. Soc.* 85, 765 (**2003**).

**68.** A. Verma, T. C. Goel, R. G. Mendiratta and M. I. Alam, *Mater. Sci. Eng. B.* 60, 156 (**1999**).

**69.** A. Tavakoli, M. Sohrabi and A. Kargari, *Chem. Pap.* 61, 151 (**2007**).

**70.** W. Chang, G. Skandan, S. C. Danforth, B. H. Kear and H. Hahn, *Nanostruc. Mater.* 4, 507 (**1994**).

**71.** H. O. Pierson, *Handbook of Chemical Vapor Deposition: Principles, Technology, and Applications*, William Andrew Inc, New York (**1999**).

**72.** C. Powell, J. Oxley and J. Blocher, *Vapor Deposition*, John Wiley & Sons, New York, (**1966**).

---

**73.** W. Chang, G. Skandan, H. Hahn, S. C. Danforth and B. H. Kear, *Nanostruc. Mater.* 4 345 (**1994**).

**74.** S. Pignard, H. Vincent, J. P. Sénateur, *Thin Solid Films.* 350, 119 (**1999**).

**75.** W. Kern and V. Bam, in *Thin Film Processes* edited J. Vossen and W. Kern, Academic Press, New York, (**1978**).

**76.** T. Maruyama and T. Kanagawa, *J. Electrochem. Soc.* 143, 1675 (**1996**).

**77.** K. Shalini, G. N. Subbanna, S. Chandrasekaran and S. A. Shivashankar, *Thin Solid Films.* 424, 56 (**2003**).

**78.** S. Park, S. Lim and H. Choi, *Chem. Mater.* 18, 5150 (**2006**).

**79.** H. Itoh, T. Uemura, H. Yamaguchi and S. Naka, *J. Mater. Sci.* 24, 3549 (**1989**).

**80.** A. G. Fitzgeralda and R. Engin, *Thin Solid Films.* 20, 317 (**1974**).

**81.** D. B. Chrisey and G. K. Hubler, *Pulsed laser deposition of thin films*, Wiley, New York (**1994**).

**82.** M. S. Rafique, M. Khaleeq-ur-Rahman, Saif-ur-Rehman, S. Anjum, M. S. Anwar, K. A. Bhatti, S. Saeed and M. S. Awan, *Vacuum* 82, 1233 (**2008**).

**83.** R. Alexandrescu, I. Morjan, I. Voicu, F. Dumitrache, L. Albu, I. Soare and G. Prodan, *Appl. Surf. Sci.* 248, 138 (**2005**).

**84.** O. Bomati-Miguel, L. Mazeina, A. Navrotsky and S. Veintemillas-Verdaguer, *Chem. Mater.* 20, 591 (**2008**).

**85.** M. Sorescu, L. Diamandescu, R. Swaminathan, M. E. McHenry and M. Feder, *J. Appl. Phys.* 97, 10G105 (**2005**).

**86.** D. Lisjak, K. Bobzin, K. Richardt, M. Bégard, G. Bolelli, L. Lusvarghi, A. Hujanen, P. Lintunen, M. Pasquale, E. Olivetti, M. Drofenik and T. Schläfer, *J. Eur. Ceram. Soc.* 29, 2333 (**2009**).

**87.** R. Swaminathan, J. Woods, S. Calvin, J. Huth and M. E. McHenry, *Adv. Sci. Technol.* 45, 2337 (**2006**).

**88.** G. Dixit, j. P. Singh, R. C. Srivastava, H. M. Agrawal, R. J. Choudhary and A. Gupta, Indian. *J. Pure. Ap. Phy.* 48, 287 (**2010**).

**89.** A-K. Axelsson, M. Valant, L. Fenner, A. S. Wills and N. M. Alford, *Thin Solid Films.* 517, 3742 (**2009**).

**90.** H. Zhang, W. W. Wang, H. Li, S. Meng and D. Li, *Mater. Lett.* 62, 1230 (**2008**).

**91.** D. Predoi, V. Kuneser and G. Filoti, *Romanian Rep. Phys.* 56, 373 (**2004**).

**92.** T. P. Raming, A. J. A. Winnubst, C. M. van Kats and A. P. Philipse, *J. Colloid.Interf. Sci.* 249, 346 (**2002**).

**93.** M. E. Mendoza, F. Donado, R. Silva, M. A. Perez and J. L. Carrillo, *J. Phys. Chem. Solids.* 66, 927 (**2005**).

**94.** S. S. Nair, S. Rajesh, V. S. Abraham, M. R. Anantharaman and V. P. N. Nampoori, J. *Magn. Magn. Mater.* 305, 28 (**2006**).

**95.** I. H. Gul, W. Ahmed and A. Maqsood, *J. Magn. Magn. Mater.* 320, 270 (**2008**).

**96.** B. P. Rao, O. Caltun, W. S. Cho, C. O. Kim and C. G. Kim, *J. Magn. Magn. Mater.* 310, e812 (**2007**).

**97.** M. Banerjee, N. Verma and R Prasad, *J.Mater. Sci.* 42, 1833 (**2007**).

**98.** O. Suwalka, R. K. Sharma, S. Varkey, N. Lakshmi and K. Venugopalan, *J. Magn. Magn. Mater.* 313, 198 (**2007**).

**99.** S. Modak, M. Ammar, F. Mazaleyrat, S. Das and P. K. Chakrabarti, *J. Alloys Compd.* 473, 15 (**2009**).

**100.** R. Boistelle and J. P. Astier, *J. Cryst. Growth* 90, 14 (**1988**).

**101.** T. Sugimoto, *Chem. Eng. Technol.* 26, 3 (**2003**).

**102.** H -C. Schwarzer and W. Peukert, *Chem. Eng. Commun.* 191, 580 (**2004**).

**103.** X. Shihong, S. Wenfeng, Y. Jian, C. Mingxia and S. Jianwei, *Chin. J. Chem. Eng.* 15, 190 (**2007**).

**104.** H. C. Shin, K. D. Jung, S. H. Han, J. W. Kim and S. C. Choi, *J. Ceram. Process. Res.* 4, 30 (**2003**).

**105.** M. Maletin, E. G. Moshopoulou and V. V. Srdic, *Phys. Stat. Sol. A.* 205, 1831 (**2008**).

**106.** M. Thomas and K. C. George, *Indian. J. Pure. Ap. Phy.* 47,81 (**2009**).

**107.** J. B. Silva, W. de Brito and N. D. S. Mohallem, *Mater. Scie.Eng. B.* 112, 182 (**2004**).

**108.** V. Kumar, A. Rana, M. S. Yadav and R. P. Pant, *J. Magn. Magn. Mater.* 320, 1729 (**2008**).

**109.** K. Maaz, A. Mumtaza, S. K. Hasanain and A. Ceylan, *J. Magn. Magn. Mater.* 308, 289 (**2007**).

**110.** K. Jainae, K. Sanuwong, J. Nuangjamnong, N. Sukpirom and F. Unob, *Chem. Eng. J.* 160, 586 (**2010**).

**111.** Y. Chen, M. Ruan, Y.F. Jiang, S.G. Cheng and W. Li, *J. Alloys Compd.* 493, L36 (**2010**).

**112.** Y. Cedeño-Mattei and O. Perales-Pérez, *Microelectr.* J. 40, 673 (**2009**).

**113.** M. Veverka, P. Veverka, O. Kaman, A. Lančok, K. Závěta,E. Pollert, K.Knížek, J. Boháček, M. Beneš, P.Kašpar, E.Duguet and S. Vasseur, *Nanotechnology* 18, 345704 (**2007**).

**114.** D. Biswal, B. N. Peeples,C. Peeples and A. K. Pradhan, J. *Magn. Magn. Mater.* 345, 1 (**2013**).

**115.** C. Venkataraju, G. Sathishkumar, K. Sivakumar, *J. Alloys Compd.* 498, 203 (**2010**).

**116.** M. N. Ashiq, M. J. Iqbal and I. H. Gul, *J. Alloys Compd.* 487, 341 (**2009**).

**117.** M. M. Hessien, M. M. Rashad, M. S. Hassan and K. El-Barawy, *J. Alloys Compd.* 476, 373 (**2009**).

**118.** J. F. Wang, C. B. Ponton, I. R. Harris, *J. Magn. Magn. Mater.* 242–245, 1464 (**2002**).

**119.** A. Ataie and S. Heshmati-Manesh, *J. Eur. Ceram. Soc.* 21, 1951 (**2001**).

**120**. A. Drmota, M. Drofenik and A. Žnidaršič, *Ceram. Int.* 38, 973 (**2012**).

**121.** A. Calleja, E. Tijero, B. Martinez, S. Pifiol, F. Sandiumenge and X. Obradors, *J. Magn. Magn. Mater.* 196-197, 293 (**1999**).

**122.** K. K. Mallick, P. Shepherd and R. J. Green, *J. Eur. Ceram. Soc.* 27, 2045 (**2007**).

**123.** H -F. Yu, *J. Magn. Magn. Mater.* 341, 79 (**2013**).

**124.** E. Hoseinkhani, M. Mehdipour and H. Shokrollahi, *J. Electron. Mater.* 42, 739 (**2013**).

**125.** Darja Lisjak and Miha Drofenik, *J. Eur. Ceram. Soc.* 27, 4515 (**2007**).

**126.** P. Shepherd, K. K. Mallick and R. J. Green, *J. Magn. Magn. Mater.* 311, 683 (**2007**).

**127.** K. S. Moghaddam and A. Ataie, *J. Alloys Compd.* 426, 415 (**2006**).

**128**. A. Ataie, S. Heshmati-Manesh and H. Kazempour, *J. Mater. Sci.* 37, 2125 (**2002**).

**129.** P. E. Garcia-Casillas, A. M. Beesley, D. Bueno, J. A. Matutes-Aquino and C. A. Martinez, *J. Alloys Compd.* 369, 185 (**2004**).

**130.** M. M. Rashad and I. A. Ibrahim, *J. Magn. Magn. Mater.* 323, 2158 (**2011**).

**131.** G. A. El-Shobaky, A. M. Turky, N. Y. Mostafa and S. K. Mohamed, *J. Alloys Compd.* 493, 415 (**2010**).

**132.** C. Venkataraju, G. Sathishkumar, K. Sivakumar, *J. Magn. Magn. Mater.* 322, 230 (**2010**).

**133.** X. Q. Liu, S. W. Tao and Y. S. Shen, *Sens. Actuators A.* 40, 161 (**1997**).

**134.** K. Kojima, M. Miyazaki, F. Mizukami and K. Maeda, *J. Sol-Gel Sci. Technol.* 8, 77 (**1997**).

**135.** U. T. Lam, R. Mammucari, K. Suzuki and N. R. Foster, *Ind. Eng. Chem. Res.* 47, 599 (**2008**).

**136.** C. Cannas, D. Gatteschi, A. Musinu, G. Piccaluga and C. Sangregorio, *J. Phys. Chem. B.* 102, 7721 (**1998**).

**137.** G. Ennas, A. Musinu, G. Piccaluga, D. Zedda, D. Gatteschi, C. Sangregorio, J. L. Stanger, G. Concas, G. Spano, *Chem. Mater.* 10, 495 (**1998**).

**138.** G. M. da Costa, E. De Grave, P. M. A. de Bakker and R. E. Vandeberghe, *J. Solid State Chem.* 113, 405 (**1994**).

**139.** A. Ataie and A. Mali, *J. Electroceram.* 21,357 (**2008**).

**140.** P. Sivakumar, R. Ramesh, A. Ramanand, S. Ponnusamy and C. Muthamizhchelvan, *Mater. Res. Bull.* 46, 2204 (**2011**).

**141.** L. Li, G. Li, R. L. Smith, Jr. and H. Inomata, *Chem. Mater.* 12, 3705 (**2000**).

**142.** Z. H. Zhou, J. M. Xue, J. Wang, H. S. O. Chan, T. Yu and Z. X. Shen, *J. Appl. Phys.* 91, 6015 (**2002**).

**143.** A. Mehri, S. A. S. Ebrahimi, H. Abdizadeh and H. Khanmohammadi, *J. Supercond. Nov. Magn.* 25, 2743 (**2012**).

**144.** M. H. Habibi and A. H. Habibi, *J Therm Anal Calorim.* 113, 843 (*2013*).

**145.** Z. Liu, H -Y. Xu, X. Liu, W –C. Liu. and Y Li, *Adv. Mater. Res.* 550-553, 329 (**2012**).

**146.** J. Akl, T. Ghaddar, A. Ghanem and H. El-Rassy, *J. Mol. Catal. A-Chem.* 312, 18 (**2009**).

**147.** E. V. Gopalan, P. A. Joy, I. A. Al-Omari, D. S. Kumar,Y. Yoshida, M. R. Anantharaman, *J. Alloys Compd.* 485, 711 (**2009**).

**148.** M. George, S. S. Nair, K A Malini, P. A. Joy and M. R. Anantharaman, *J. Phys. D: Appl. Phys.* 40, 1593 (**2007**).

**149.** J -G. Lee, J. Y. Park and C. S. Kim, *J. Mater. Sci.* 33, 3965 (**1998**).

**150.** M. Sivakumar, S. Kanagesan, K. Chinnaraj, R. Suresh Babu and S. Nithiyanantham, J. *Inorg. Organomet. Polym.* 23, 439 (**2013**).

**151.** M. Popovici, C. Savii, D. Niznansky, J. Subrt, J. Bohacek, D. Becherescu, C. Caizer, C. Enach and C. Ionescu,. *J. Optoelectron. Adv. Mater.* 5, 251 (**2003**).

**152.** S. Zahi, M. Hashim and A. R. Daud, *J. Magn. Magn. Mater.* 308, 177 (**2007**).

**153.** J. Azadmanjiri, Mater. *Chem. Phys.* 109, 109 (**2008**).

**154.** M. Zhang, Q. C Liu, Z. F. Zi, Y. Q. Dai, X. B. Zhu, Y. P. Un And J. M. Dai, *Sci. China. Tech. Sci.* 56, 13 (**2013**).

**155.** M. Rahimi, P. Kameli, M. Ranjbar, H. Hajihashemi and H. Salamati, *J. Mater. Sci.* 48, 2969 (**2013**).

**156.** 156. H –F. Yu and H-Y. Lin, *J. Magn. Magn. Mater.* 283, 190 (**2004**).

**157.** L. Junliang, Z. Yanwei, G. Cuijing, Z. Wei and Y. Xiaowei, *J. Eur. Ceram.Soc.* 30, 993 (**2010**).

**158.** G. Xu, H. Ma, M. Zhong, J. Zhou, Y. Yue and Z. He, *J. Magn. Magn. Mater.* 301, 383 (**206**).

**159.** M. Mozaffari, M. Taheri and J. Amighian, *J. Magn. Magn. Mater.* 321, 1285 (**2009**).

**160.** L. Junliang, Z. Yanwei, S. Xiaodong, G. Cuijing and Z. Wei, *J. Cryst. Growth.* 311, 2363 (**2009**).

**161.** G. Mu, X. Pan, N. Chen, K. Gan and M. Gu, *Mater. Res. Bull.* 43, 1369 (**2008**).

**162.** L. Junliang, Z. Wei, G. Cuijing and Z. Yanwei, *J. Alloys Compd.* 479, 863 (**2009**).

**163.** W. Zhong, W. Ding, Y. Jiang, N. Zhang, J. Zhang, Y. Du and Q. Yan, *J. Am. Ceram. Soc.* 80, 3258 (**1997**).

**164.** H. Zhan, M. Wu, X. Yao and L. Zhang, *Rare Metals* 22,125 (**2003**).

**165.** M. G. Hasab, S. A. S. Ebrahimi and A. Badiei, *J. Non-Cryst. Solids* 353, 814 (**2007**).

**166.** M. G. Hasab, S. A. S. Ebrahimi and A. Badiei, *J. Magn. Magn. Mater.* 310, 2477 (**2007**).

**167.** P. C. A. Brito, R. F. Gomes, J. G. S. Duque and M. A. Macêdo, *Physica B* 384, 91 (**2006**).

**168.** S. Alamolhoda, S. A. S. Ebrahimi and A. Badiei, *J. Magn. Magn. Mater.* 303, 61 (**2006**).

**169.** D.Chen and R. Xu, *Mater. Res. Bull.* 33, 1015 (**1998**).

**170.** C. Burda, X. Chen, R. Narayanan and M.A. El-Sayed, *Chem. Rev.* 105, 1025 (**2005**).

**171.** S. E. Kushnir, A. I. Gavrilov, P. E. Kazin, A. V. Grigorieva, Y. D. Tretyakov and M. Jansen, *J. Mater. Chem.* 22, 18893 (**2012**).

**172.** L. Chen, Y. Shen and J. Bai, *Mater. Lett.* 63, 1099 (**2009**).

173. D. E. Zhang, X. Zhang, X. M. Ni, J. M. Song and H. G. Zheng, *J. Magn. Magn. Mater.* 305, 68 (**2006**).

**174.** X. Shen, Y. Wang, X. Yang, Y. Xia , J. Zhuang and P. Tang, *Trans. Nonferrous Met. Soc. China* 19, 1588 (**2009**).

**175.** Q. Liu, H. Huang, L. Lai, J. Sun, T. Shang, Q. Zhou and Z. Xu, *J. Mater. Sci.* 44, 1187 (**2009**).

**176.** Y. Li, R. Yi, A. Yan, L. Deng, K. Zhou and X. Liu, *Solid State Sci.* 11, 1319 (**2009**).

**177.** W. Jiang, Z. Cao, R. Gu, X. Ye, C. Jiang and X. Gong, *Smart Mater. Struct.* 18, 125013 (**2009**).

**178.** X –J. Xu, L –H. Zhou, Q -G Zhai, and C-Z. Lu, *J. Am. Ceram. Soc.* 90, 1959 (**2007**).

**179.** S. Komarneni, M. C. D'Arrigo, C. Leonelli, G. C. Pellacani and H Katsuki, *J. Am. Ceram. Soc.* 81, 3041 (**1998**).

**180.** M. Cao, T. Liu, S. Gao, G. Sun, X. Wu, C. Hu and Z. L. Wang, *Angew. Chem. Int. Ed.* 44, 2 (**2005**).

**181.** H.-W. Wang and S.-C. Kung, *J. Magn. Magn. Mater.* 270, 230 (**2004**).

**182.** X. Li, Q. Li, Z. Xia and W. Yan, *J. Alloys Compd.* 458, 558 (**2008**).

**183.** X. Liu, G. Qiu, A. Yan, Z. Wang and X. Li, *J. Alloys Compd.* 433, 216 (**2007**).

**184.** X. Zhang and Q. Li, *Mater. Lett.* 62, 988 (**2008**).

___

**185.** S. Verma, P. A. Joy, Y. B. Khollam, H. S. Potdar and S. Deshpande, *Mater. Lett.* 58, 1092 (**2004**).

**186.** C. Upadhyay, D. Mishra, H. C. Verma, S. Anand and R. P. Das, *J. Magn. Magn. Mater.* 260, 188 (**2003**).

**187.** C.-S. Hwang and N.-C. Wang ,Mater. *Chem. Phys.* 88, 258 (**2004**).

**188.** X. Li and G. Wang. *J. Magn. Magn. Mater.* 321, 1276 (**2009**).

**189.** T. Sato, K. Sue, W. Suzuki, M. Suzuki, K. Matsui, Y. Hakuta, H. Hayashi, K. Arai, S. Kawasaki, A. Kawai-Nakamura and T. Hiaki, *Ind. Eng. Chem. Res.* 47, 1855 (**2008**).

**190.** X. Tanga,R. Y. Hong, W. G. Feng and D. Badami, *J. Alloys Compd.* 562, 211 (**2013**).

**191.** A. C. F. M. Costa, A. M. D. Leite, H. S. Ferreira, R. H. G. A. Kiminami, S. Cavac and L. Gama, *J. Eur. Ceram. Soc.* 28, 2033 (**2008**).

**192.** J. Jasinski, K. E. Pinkerton, I. M. Kennedy and V. J. Leppert *Sens. Actuators, B Chem.* 109, 19 (**2005**).

**193.** A. C. F. M. Costa, E. Tortella, M. R. Morelli and R. H. G. A. Kiminami, *J. Magn. Magn. Mater.* 256, 174 (**2003**).

**194.** R. V. Mangalaraja, S. T. Lee, S. Ananthakumar, P. Manohar and C. P. Camurri, *Mater. Sci. Eng. A.* 476, 234 (**2008**).

**195.** Y.-P. Fu, K.-Y. Pan and C.-H. Lin, *Mater. Lett.* 57, 291 (**2002**).

**196.** C.-C. Hwang, T.-Y. Wu, J. Wan and J.-S. Tsai, *Mater. Sci. Eng. B.* 111, 49 (**2004**).

**197.** L. Gama, A. P. Diniz, A. C. F. M. Costa, S. M. Rezende, A. Azevedoa and D. R. Cornejoc, *Physica B* 384, 97(**2006**).

**198.** A. C. F. M. Costa, R. T. Lula, R. H. G. A. Kiminami, L. F. V. Gama, A. A. de Jesus and H. M. C. Andrade, *J. Mater. Sci.* 41, 4871 (**2006**).

**199.** J. Y. Patil, M. S. Khandekar,I. S. Mulla and S. S. Suryavanshi, *Curr. Appl. Phys.* 12, 319 (**2012**).

**200.** A. B. Salunkhe, V. M. Khot, M. R. Phadatare and S. H. Pawar, *J. Alloys Compd.* 514, 91 (**2012**).

**201.** T. Prabhakaran and J. Hemalatha, *J. Alloys Compd.* 509, 7071 (**2011**).

**202.** M. S. Khandekar, R. C. Kambale, J. Y. Patil, Y. D. Kolekar and S. S. Suryavanshi, *J. Alloys Compd.* 509, 1861 (**2011**).

**203.** S. Castro, M. Gayoso and C. Rodríguez, *J. Solid State Chem.* 134, 227 (**1997**).

**204.** S. Albuquerque, J. D. Ardisson and W. A. A. Macedo, *J. Appl. Phys.* 87, 4352 (**2000**).

**205.** C. Caizer and M. Stefanescu, *J. Phys. D. Appl. Phys.* 35, 3035 (**2002**).

**206.** Y. X. Pang and X. J. Bao, *J. Mater. Chem.* 12, 3699 (**2002**).

**207.** V. Pillai, P. Kumar, M. J. Hou, P. Ayyub and D. O. Shah, *Adv. Colloid. Interfac.* 55, 241 (**1995**).

**208.** P. Tartaj and L. C. De Jonghe, *J. Mater. Chem.* 10, 2786 (**2000**).

**209.** I. Capek, *Adv. Colloid. Interfac.* 110, 49 (**2004**).

**210.** P. Xu, X. Han and M. Wang, *J. Phys. Chem. C.* 111, 5866 (**2007**).

**211.** H. Zhu, X. Gu, D. Zuo, Z. Wang, N.Wang and K. Yao, *Nanotechnology* 19, 405503 (**2008**).

**212.** D. Makovec and M. Drofenik, *J Nanopart. Res.* 10, 131 (**2008**).

**213.** D. Makovec, A. Kodre, I. Arčon and M. Drofenik, *J Nanopart. Res.* 11, 1145 (**2009**).

**214.** D. O. Yener and H. Giesche, *J. Am. Ceram. Soc.* 84, 1987 (**2001**).

**215.** A –T. Ngo and M –P. Pileni, *Adv. Mater.* 12, 276 (**2000**).

**216.** X. Cao and L. Gu, *Nanotechnology* 16, 180 (**2005**).

**217.** M. Han, C. R. Vestal and Z. J. Zhang, *J. Phys. Chem. B.* 108, 583 (**2004**).

**218.** C. P. L. Rubinger, D. X. Gouveia, J. F. Nunes, C. C. M. Salgueiro, J. A. C. Paiva, M. P. F. Graça, P. André and L. C. Costa, *Microw. Opt. Techn. Let.* 49, 1341 (**2007**).

**219.** A. Scano, G. Ennas, F. Frongia, A. L. Barbera, M. A. López-Quintela, G. Marongiu, G. Paschina, D. Peddis, M. Pilloni and C. Vázquez-Vázquez, *J. Nanopart. Res.* 13, 3063 (**2011**).

**220.** S. Thakur, S. C. Katyal and M. Singh, *J. Magn. Magn. Mater.* 321, 1 (**2009**).

**221.** L. Satyanarayana, K. M. Reddy and S. V. Manorama, *Mater. Chem. Phys.* 82, 21 (**2003**).

**222.** A. R. Buenoa, M. L. Gregori and M.C.S. Nóbrega *Mater. Chem. Phys.* 105, 229 (**2007**).

**223.** R. C. Chikate, K-W. Jun and C. V. Rode, *Polyhedron* 27, 933 (**2008**).

**224.** M. Iijima, K. Sato, K. Kurashima, T. Ishigaki and H. Kamiya, *Powder Technol.*181, 45 (**2008**).

**225.** S. H. Keluskar, R. B. Tangsali, G .K. Naik and J. S. Budkuley, *J. Magn.Magn. Mater.* 305, 296 (**2006**).

**226.** D. Zhang X. J. , Zhang, X. M. Nia, J. M. Song and H. Zheng, *J. Magn. Magn. Mater.* 305, 68 (**2006**).

**227.** S. A. Ghodake, U. R. Ghodake, S. R. Sawant, S. S. Suryavanshi and P.P. Bakare, *J. Magn. Magn. Mater.* 305, 110 (**2006**).

**228.** A. Verma, O. P. Thakur, C. Prakash, T. C. Goel and R. G. Mendiratta *Mater. Sci. Eng. B.* 116, 1 (**2005**).

**229.** J. M. Yang and F. S. Yen, *J. Alloys Compd.* 450, 387 (**2008**).

**230.** M. Mouallem-Bahout, S. Bertrand and O. Pena, *J. Solid State Chem.* 178, 1080 (**2005**).

**231.** M. M. Mallapur, P. A. Shaikh, R. C. Kambale, H. V. Jamadar, P. U. Mahamuni and B.K. Chougule, *J. Alloys Compd.* 479, 797 (**2009**).

**232.** P. Pant, B. D. Naik and N. N. Ghosh, *Mater. Technol. Adv. Perform. Mater.* 24, 213 (**2009**).

**233.** N. N. Ghosh and P. P. Sarangi, in *Nanomaterials: Properties, Preparation and Processes* edited. V. Cabral and R. Silva, Nova Publishers, New York (**2010**), ch 10, p367.

**234.** P. P. Sarangi, B. Naik and N. N. Ghosh, *Powder Technol.* 192, 245 (**2009**).

**235.** P. P. Sarangi, S. R. Vadera, M. K. Patra and N. N. Ghosh, *Powder Technol.* 203, 348 (**2010**)**.**

**236.** P. P. Sarangi, S. R. Vadera, M. K. Patra, C. Prakash, R. Selvin and N. N. Ghosh, *Integr. Ferroelectr.* 116, 1 (**2010**).

**237.** R. M. Mohamed, M. M.Rashad, F. A.Haraz and W. Sigmund, *J.Magn. Magn. Mater.* 322, 2058 (*2010*).

**238.** X. Tang, B. Y. Zhao and K. A. Hu, *J. Mater. Sci.* 41 3867 (**2006**).

**239.** S -G. Kim, W -N. Wang, T. Iwaki, A. Yabuki and K. Okuyama, *J. Phys. Chem. C.* 111, 10175 (**2007**).

**240.** A. K. Singh, T. C. Goel and R.G. Mendiratta, *Solid State Commun.* 125 121 (**2003**).

**241.** A. Verma, M. I. Alam, R. Chatterjee,T. C. Goel, R. G. Mendiratta, *J. Magn. Magn. Mater.* 300, 500 (**2006**).

**242.** J. S. Jang, P. H. Borse, J. S. Lee, O –S. Jung, C.-R. Cho, E. D. Jeong, M. G. Ha, M. S. Won and H. G. Kim, *Bull. Korean Chem. Soc.* 30, 1738 (**2009**).

**243.** M. Gharagozlou, *J. Alloys Compd.* 486, 660 (**2009**).

**244.** E. Manova, D. Paneva, B. Kunev, C. Estournès, E. Rivière, K. Tenchev, A. Léaustic and I. Mitov, *J. Alloys Compd.* 485, 356 (**2009**).

**245.** A. Ataie and S.E. Zojaji, *J. Alloys Compd.* 431, 331 (**2007**).

**246.** R.K.Tiwary, S. P. Narayan and O. P.Pandey, *J. Min. Met.* 44 B, 91 (**2008**).

**247.** J. Yu, S.Tang , L. Zhai, Y. Shi and Y. Du, *Physica B.* 404, 4253 (**2009**).

**248.** S. Maensiri, C. Masingboon, B. Boonchom and S. Seraphin, *Scripta Mater.* 56 797 (**2007**).

**249.** K. V. P. M. Shafi, Y. Koltypin, A. Gedanken, R. Prozorov, J. Balogh, J. Lendvai and I. Felner, *J. Phys. Chem. B.* 101, 6409 (**1997**).

**250.** M. Sivakumar, A. Gedanken, W. Zhong, Y. W. Du, D. Bhattacharya,Y. Yeshurun and I. Felner, *J. Magn. Magn. Mater.* 268, 95 (**2004**).

___

**251.** I. Perelshtein, N. Perkas, S. Magdassi, T. Zioni, M. Royz, Z. Maor and A. Gedanken, *J Nanopart. Res.* 10, 191 (**2008**).

**252.** A. Rajput, S. Hazra and N. N. Ghosh, *J. Exp. Nanosci.* 8, 629 (**2013**).

**253.** S. Hazra, M. K. Patra, S. R .Vadera and N. N. Ghosh, *Optoelectron. Adv. Mater.- Rapid Commun.* 6, 451 (**2012**).

**254.** A. Rajput, S. Hazra, B. N. Krishna, P. Chavali, S. Datla and N. N. Ghosh, *Particuology* 9, 243 (**2011**).

**255.** A. Rajput, S. Hazra, G. F. Fernando and N. N. Ghosh, *Synth. React. Inorg. Met.-Org. Nano-Metal Chem.* 41, 1114 (**2011**).

**256.** P. P. Sarangi, S. R. Vadera, M. K. Patra and N. N. Ghosh, *J. Optoelectron. Adv. Mater.* 12, 1279 (**2010**).

**257.** P. P. Sarangi, B. Naik, S. R. Vadera, M. K. Patra, C. Prakash and N. N. Ghosh, *Mater. Technol. Adv. Perform. Mater.* 24 , 97 (**2009**).

**258.** P. P. Sarangi, S. R. Vadera, M. K. Patra, C. Prakash and N. N. Ghosh, *J. Am. Ceram. Soc.* 92, 2425 (**2009**).

**259.** P. P. Sarangi, B. Naik and N. N. Ghosh, *J. Am. Ceram. Soc.* 91, 4145 (**2008**).

**260.** N. N. Ghosh and P. P. Sarangi, In *Combustion Synthesis Novel Routes to Novel Materials*, edited M. Lacner, Bentham Science Publishers, Sharjah (**2010**), Ch. 10 p. 123.

**261.** S. Hazra, M. K. Patra, S. R. Vadera and N. N. Ghosh, *J. Am. Ceram. Soc.* 95, 60 (**2012**).

**262.** D. K. Kim, M. Mikhaylova, Y. Zhang and M. Muhammed, *Chem. Mater.* 15, 1617 (**2003**).

**263.** C. L. Lin, C. F. Lee and W. Y. Chiu, *J. Colloid Interface Sci.* 291, 411 (**2005**).

**264.** L. E. Euliss, S. G. Grancharov, S. O'Brien, T. J. Deming, G. D. Stucky, C. B. Murray and G. A. Held, *Nano Lett.* 3, 1489 (**2003**).

**265.** X. Liu, Y. Guan, Z. Ma and H. Liu, *Langmuir* 20, 10278 (**2004**).

**266.** R. Hong, N. O. Fischer, T. Emrick and V. M. Rotello, *Chem. Mater.* 17, 4617 (**2005**).

**267.** M. Kim, Y. Chen, Y. Liu and X. Peng, *Adv. Mater.* 17, 1429 (**2005**).

**268.** R. Krishna, E.Titus, R. Krishna, N. Bardhan, D. Bahadur and J.Gracio, *J. Nanosci. Nanotechnol.* 12, 6645 (**2012**).

**269.** S. Vaidya, A. Kar, A. Patra and A. K. Ganguli, *Rev. Nanosci. Nanotechnol.* 2, 106 (**2012**).

**270.** Z. P. Xu, Q. H. Zeng, G. Q. Lu and A. B. Yu, *Chem. Eng. Sci.* 61, 1027 (**2006**).

**271.** H. Lee, E. Lee, D. K. Kim, N. K. Jang, Y. Y. Jeong and S. Jon, *J. Am. Chem. Soc.* 128, 7383 (**2006**).

**272.** S. Mohapatra, N. Pramanik, S. Mukherjee, S. K. Ghosh and P. Pramanik, *J. Mater. Sci.* 42, 7566 (**2007**).

**273.** L. Zhou, J. Yuan and Y. Wei, *J. Mater. Chem.* 21, 2823 (**2011**).

**274.** D. L. Ma, T. Veres, L. Clime, F. Normandin, J. W. Guan, D. Kingston and B. Simard, *J. Phys. Chem. C.* 111, 1999 (**2007**).

**275.** J. P. Ge, T. Huynh, Y. X. Hu and Y. D. Yin, *Nano Lett.* 8, 931 (**2008**).

**276.** G. Y. Liu, H. Wang, X. L. Yang and L. Y. Li, *Eur. Polym. J.* 45, 2023 (**2009**).

**277.** T. N. Narayanan, A. P. Reena Mary, P. K. Anas Swalih, D. SakthiKumar, D. Makarov, M. Albrecht, J. Puthumana, A. Anas, and M. R. Anantharaman, *J. Nanosci. Nanotechnol.* 11, 1958 (**2011**).

**278.** S. J. Guo, S. J. Dong and E. K. Wang, *Chem.–Eur. J.* 15, 2416 (**2009**).

**279.** I. Y. Goon, L. M. H. Lai, M. Lim, P. Munroe, J. J. Gooding and R. *Amal, Chem. Mater.* 21, 673 (**2009**).

**280.** X. Le Guével, E. Prinz, R. Müller, R. Hempelmann and M. Schneider, *J. Nanopart. Res.* 14,727 (**2012**).

**281.** F. Carlá, G. Campo, C, Sangregorio, A, Caneschi,C, de Julián Fernández and L. I. Cabrera, *J Nanopart. Res.* 15, 1813 (**2013**).

**282.** H. Y. Jung, J. H. Park, S. Hwang and J. Kwak, *J. Biomed. Nanotechnol.* 9, 901 (**2013**).

**283.** M. Kooti, S. Saiahia and H. Motamedi, *J. Magn. Magn. Mater.* 333, 138 (**2013**).

**284.** M. H. Sousa, F. A. Tourinho, J. Depeyrot, G. J. da Silva and M. C. F. L. Lara, *J. Phys. Chem. B.* 105, 1168 (**2001**).

**285.** Y. A. Barnakov, M. H. Yu and Z. Rosenzweig, *Langmuir* 21, 7524 (**2005**).

**286.** S. H. Im, T. Herricks, Y. T. Lee, Y. Xia, *Chem. Phys. Lett.* 40, 19 (**2005**).

**287.** P. I. Girginova, A. L. Daniel-da-Silva, C. B. Lopes, P. Figueira, M. Otero, V. S. Amaral, E. Pereira and T. Trindade, *J. Colloid Interface Sci.* 345, 234 (**2010**).

**288.** K. R. Hurley, Y –S. Lin, J. Zhang,S. M. Egger and C. L. Haynes, *Chem. Mater.* 25, 1968 (**2013**).

**289.** H. M. Joshi, M. De. F. Richter, J. He. P. V. Prasad and V. P. Dravid, *J. Nanopart. Res.* 15, 1448 (**2013**).

**290.** X. Liu, Z. Ma, J. Xing and H. Liu, *J. Magn. Magn. Mater.* 270, 1 (**2004**).

**291.** Y. Zhu, F. Y. Jiang, K. Chen, F. Kang and Z. K. Tang, *J. Sol-Gel Sci. Technol.* 66, 180 (**2013**).

**292.** K. Can, M. Ozmen and M. Ersoz, *Colloids Surf. B.* 71, 154 (**2009**).

_____

**293.** Z. Zhang, L. Song, J. Dong, D. Guo, X. Du, B. Cao, Y. Zhang, N. Gu and X. Mao, *J. Nanopart. Res.* 15, 1659 (**2013**).

**294.** H. R. Shaterian and M. Aghakhanizadeh, *Catal. Sci. Technol.* 3, 425 (**2013**).

**295.** P. F.Wang, H. X. Jin, M. Chen, D. F. Jin, B.Hong, H. L. Ge, J. Gong, X. L. Peng,H. Yang, Z. Y. Liu and X. Q. Wang. *J. Nanomater.* 2012, 1 (**2012**).

**296.** P. Dai, W. Yuxia, M. Wu and Z. Xu, Micro. *Nano. Lett.* 7, 219 (**2012**).

**297.** H –L.Hsu, R. Selvin, J –W. Cao, L. S. Roselin and M. Bououdina, *Sci. Adv. Mater.* 3, 939 (**2011**).

**298.** S. Yamamoto, R. Fujita, K. Sanada and N. Horiishi, U.S. Pat. No. 4828916 (**1989**).

**299.** H. Nakamura, H. Machida, M. Tanaka, A. Watada, F. Omi and N. Koinuma, U.S. Pat. No. 4670322 (**1987**).

**300** H. Machida, H. Nakamura, F. Omi, A. Watada and Y. Kaneko, U.S. Pat. No. 4788095 (**1988**)

**301.** H. Nakamura, H. Machida, M. Tanaka, A. Watada, F. Omi and N. Koinuma, U.S. Pat. No. 4670323 (**1987**).

**302.** H. Kobayashi, H. Machida and M. Tanaka, U.S. Pat. No. 4544602 (**1985**).

**303.** T. Ito, T. Ido, H. Takeuchi, M. Hashimoto, T. Maeda and M. Awa, U.S. Pat. No. 4578313 (**1986**).

**304.** J. L. Davis, U.S. Pat. No. 5695877 (**1997**).

**305.** D. W. Johnson Jr., J. Thomson Jr. and R. B. Van Dover, U.S. Pat. No. 6716488 (**2004**).

**306.** S. Kitahata and M. Kishimoto, U.S. Pat. No. 4677024 (**1987**).

**307.** S. Matsumoto and K. Fukai, U.S. Pat. No. 4042516 (**1977**).

**308.** O. Kobayashi, O. Yamada, K. Honda and S. Kawasaki, U.S. Pat. No. 6296791 (**2001**).

**309.** H. Togane, U.S. Pat. No. 4846987 (**1989**).

**310.** O. Kubo, T. Ido, T. Nomura and T. Maeda, U.S. Pat. No. 4493874 (**1985**).

**311.** H. Hibst, U.S. Pat. No. 4680130 (**1987**).

**312.** A. S. Patil and L. E. Netherton, U.S. Pat. No. 4292294 (**1981**).

**313.** A. Goldman and A.M. Laing, U.S. Pat. No. 4097392 (**1978**).

**314.** Y. Hong, H. S. Jung and P. R. Taylor, U.S. Pat. No. 6599608 (**2003**).

**315.** B. B. Yu and A. Goldman, U.S. Pat. No. 4372865 (**1983**).

**316.** Y. Watanabe and S. Isoyama, U.S. Pat. No. 4120807 (**1978**).

**317.** E. Kurita, H. Kurokawa and K. Fujioka, US 5336421 (**1994**).

**318.** M. Hashiuchi, A. Oyama and T. Yamanishi, U.S. Pat. No.5356712 (**1994**).

**319.** P. Rudolf, W. Steck, W. Sarnecki and C. Jaeckh, U.S. Pat. No. 4259368 (**1981**).

**320.** H. Hibst, P. Rudolf and H. Jakusch, U.S. Pat. No. 4764300 (**1988**).

**321.** K. Mori, M. Kawabata, M. Kunishige, N. Horiishi and K. Toda, U.S. Pat. No. 4992191 (**1991**).

**322.** H, Yamamoto, U.S. Pat. No. 5055322 (**1991**).

**323.** L. M. Scott and G. D. Rexroat, U.S. Pat. No. 4683167 (**1987**).

**324.** K. Takadete, U.S. Pat. No. 20050068122 (**2005**).

**325.** K. Sakashita and Y. Iwahashi, U.S. Pat. No. 4975214 (**1990**).

**326.** C. H. Lu, U.S. Pat. No. 4192902 (**1980**).

**327.** N. Nagai, N. Horiishi, M. Kiyama and T. Takada, U.S. Pat. No. 4561988 (**1985**).

**328.** N. Nagai, N. Horiishi, M. Kiyama and T. Takada, U.S. Pat. No. 4548801 (**1985**).

**329.** L. O. Jones, U.S. Pat. No. 4042518 (**1977**).

**330.** R. Schmidberger and H. Franke, U.S. Pat. No. 4336242 (**1982**).

**331.** P. Tartaj, M. D. Morales, S. Veintemillas-Verdaguer, T. Gonzalez-Carreno and C.J. Serna, *J. Phys. D: Appl. Phys.* 36, R182 (**2003**).

**332.** J. S. Kim, T. J. Yoon, B. G. Kim, S. J. Park, H. W. Kim, K. H. Lee, S. B. Park, J. K. Lee and M. H. Cho, *Toxicolo. Sci.* 89, 338 (**2006**).

**333.** P. Tartaj, M. P. Morales, T. Gonzalez-Carreno, S. Veintemillas-Verdaguer and C. J. Serna, *J. Magn. Magn. Mater.* 290, 28 (**2005**).

**334.** S. Nigam, K. C.Barick and D. Bahadur, *J. Magn. Magn.Mater.* 323, 237 (**2011**).

335. K -J. Lee, J. H. An, J -R.Chun, K -H.Chung, W −Y.Park, J −S. Shin, D −H. Kim and Y. Y. Bahk, *J. Biomed. Nanotechnol.* 9, 1071 (**2013**).

**336.** C. Sun, J. S. H. Lee and M. Zhang, *Adv. Drug Deliver. Rev.* 60, 1252 (**2008**).

**337.** M. Babic, D. Horak, P. Jendelova, K. Glogarova, V. Herynek, M. Trchova, K. Likavcanova, P. Lesny, E. Pollert, M. Hajek and E. Sykova, *Bioconjugate Chem.* 20, 283 (**2009**).

**338.** J. Khandare and T. Minko, *Prog. Polym. Sci.*31, 359 (**2006**).

**339.** N. Nishiyama and K. Kataoka, *Adv. Polym. Sci.* 193, 67 (**2006**).

**340.** J.K. Oh, D. I. Lee and J. M. Park, *Prog. Polym. Sci.* 34, 1261 (**2009**).

**341.** A. K. Gupta and M. Gupta, *Biomaterials* 26, 3995 (**2005**).

**342.** S. Mornet, S. Vasseur, F. Grasset and E. Duguet, *J. Mater. Chem.* 14, 2116 (**2004**).

**343.** M. Gonzales-Weimuller, M. Zeisberger and K. M. Krishnan, *J. Magn. Magn. Mater.* 321,1947 (**2009**).

**344.** P. M. Zélis, G. A. Pasquevich, S. J. Stewart, M. B. F. van Raap, J. Aphesteguy, I. J. Bruvera, C. Laborde,.B. Pianciola, S. Jacobo and F. H. Sánchez, *J. Phys. D: Appl. Phys.* 46, 125006 (**2013**).

**345.** D –H. Jang, Y –I. Lee, K –S. Kim, E –S. Park, S –C. Kang, T –J. Yoon and Y -H.Choa, *J. Nanosci. Nanotechnol.* 13, 6098 (**2013**).

**346.** R. Ramesh, S. Ponnusamy and C. Muthamizhchelvan, *Sci. Adv. Mater.* 5, 1250 (**2013**).

**347.** S. Mornet, S. Vasseur, F. Grasset, P. Verveka, G. Goglio, A. Demourgues, J. Portier, E. Pollert, E. Duguet, *Prog. Solid State Chem.* 34, 237 (**2006**).

**348.** M. Jeun, Y. J. Kim, K. H. Park, S. H. Paek and S. Bae, *J. Nanosci. Nanotechnol.* 13, 5719 (**2013**).

**349.** T. Neuberger, B. Schopf, H. Hofmann, M. Hofmann, B. von Rechenberg, *J. Magn. Magn. Mater.* 293, 483 (**2005**).

**350.** E. Mazario, N. Menéndez, P. Herrasti, M. Cañete, V. Connord and J. Carrey, J. *Phys. Chem. C.* 117, 11405 (**2013**).

**351.** N. Lee and T. Hyeon, *Chem. Soc. Rev.* 41, 2575 (**2012**).

**352.** A. K. A. Silva, C. Wilhelm, J. Kolosnjaj-Tabi, N. Luciani and F. Gazeau, *Pharm. Res.* 29, 1392 (**2012**).

**353.** N. Lee, H. R. Cho, M. H. Oh, S. H. Lee, K. Kim, B. H. Kim, K. Shin, T –Y. Ahn, J. W. Choi, Y –W. Kim, S. H. Choi and T. Hyeon, *J. Am. Chem. Soc.* 134, 10309 (**2012**).

**354.** P. Kucheryavy, J. He, V. T. John, P. Maharjan, L. Spinu, G. Z. Goloverda,and V. L. Kolesnichenko, *Langmuir* 29, 710 (**2013**).

**355.** B. Zhang, B. Yang,C. Zhai,B. Jiang and Y. Wu, *Biomaterials* 34, 5843 (**2013**).

**356.** N. Ahmed, C. Jaafar-Maalej, M. M. Eissa, H. Fessi and A.Elaissari, *J. Biomed. Nanotechnol.* 9, 1579 (**2012**).

**357.** A. S. Wadajkar, J. U. Menon and K. T.Nguyen, *Rev. Nanosci. Nanotechnol.* 1, 284 (**2012**).

**358.** A. Kleinauskas, J –K.Kim, G –H. Choi, H –T. Kim, K. Røe and P. Juzenas, *Rev. Nanosci. Nanotechnol.* 1, 271 (**2012**).

**359.** S. Smitha, V. S. Haseena, T. N. Narayanan, A. P. R. Mary, P. M. Ajayan, J. Puthumana, A. A. Aziz, R. R. Aburto, S. A. Mani, P. A. Joy and M. R. Anantharaman, *Mater. Express.* 2, 265 (**2012**).

**360.** J. Fan, Y. Tan, L. Jie, X. Wu, R. Yu and M. Zhang, *Stem Cell Res. Ther.* 4, 44 (**2013**).

**361.** I. Safarik and M. Safarikova, *Biomagn. Res. Technol.* 2, 7 (**2004**).

**362.** S. Giri, B. G. Trewyn, M. P. Stellmaker and V. S.-Y. Lin, *Angew. Chem. Int. Ed.* 117, 5166 (**2005**).

**363.** B -H. Lai,C –H. Chang, C -C. Yeh and D -H. Chen, *Sep. Purif. Technol.* 108, 83 (**2013**).

**364.** A. I. Carrillo, E. Serrano, R. Luque and J. García-Martínez, *Appl. Catal. A.* 453, 383 (**2013**).

**365.** K. S. Lee, R. M. Anisur, K. W. Kim, W. S. Kim, T -J. Park, E. J. Kang and I. S. Lee, *Chem. Mater.* 24,682 (**2012**).

**366.** K. K. Senapati, S. Roy, C. Borgohain and P. Phukan, *J. Mol. Catal. A: Chem.* 352, 128 (**2012**).

**367.** A. Dandia, R. Singh, J. Joshi and S. Maheshwari, *Eur. Chem. Bull.* 2, 825 (**2013**).

**368.** K. Swapna, S. N. Murthy, and Y. V. D. Nageswar, *Eur. J. Org. Chem.* 2011, 1940 (**2011**).

**369.** D. Wang, L. Salmon, J. Ruiz and Didier Astruc, *Chem. Commun.* 49, 6956 (**2013**).

**370.** A. S. Singh, U. B. Patil and J. M. Nagarkar, *Catal. Commun.* 35, 11 (**2013**).

**371.** S. Park, I. S. Lee and J. Park, *Org. Biomol. Chem.* 11, 395 (**2013**).

**372.** J. Mondal, T. Sen and A. Bhaumik, *Dalton Trans.* 41, 6173 (**2012**).

**373.** B. Sahoo, S. K. Sahu, S. Nayak, D. Dhara and P. Pramanik, *Catal. Sci. Technol.* 2, 1367 (**2012**).

**374.** D. K. Kim, M. S. Toprak, M. Mikhaylova, Y. S. Jo, S. Savage and H. B. Lee, *Solid State Phenom.* 165, 99 (**2003**).

**375.** A. V. Lopatin, N. E. Kazantseva, N. Yu, O. A. Kazantsev, J. Dyakonova, A. Vil and P. Saha, *J. Commun. Technol. Electron.* 53, 487 (**2008**).

**376.** K. A. Malini, M. R. Anantharaman and A. Gupta, *Bull. Mater. Sci.* 27, 361 (**2004**).

**377.** B. Kiskan, A. L. Demirel, O. Kamer and Y. Yagci, *J. Polym. Sci., Part A: Polym. Chem.* 46, 6780 (**2008**).

**378.** M. R. Anantharaman, K. A. Malini, S. Sindhu, E. M. Mohammed, S. K. Date, S. D. Kulkarni, P. A. Joy and P. Kurian, *Bull. Mater. Sci.* 24, 623 (**2001**).

**379.** J. Jiang, L. H. Ai and L. Y Liu. *Mater. Lett.* 64, 888 (**2010**).

**380.** T. H. Ting and K. H. Wu, *J. Magn. Magn. Mater.* 322, 2160 (**2010**).

**381.** J. Deng, X. Ding, W. Zhang, Y. Peng, J. Wang, X. Long, P. Li and A. S. C. Chan, *Polymer* 43, 2179 (**2002**).

**382.** P. Xu, X. Han, J. Jiang, X. Wang, X. Li and A. Wen, *J. Phys. Chem. C.* 111, 12603 (**2007**).

**383.** A. B. Rajput, S. J. Rahaman, M. K. Patra, S. R. Vadera, G. Sarkhel, and N. N. Ghosh, *Polym-Plast. Technol. Eng.* 52, 1097 (**2013**).

**384.** A. B. Rajput., M. Sharifi , H. V. Pol, M. K. Patra, S. R. Vadera, P. M. Singru and N. N. Ghosh, *J. Nanosci. Lett.* 3, 26 (**2013**).

**385.** A. B. Rajput, S. J. Rahaman, G. Sarkhel, M. K. Patra, S. Vadera, P. M. Singru, Y. Yagci and N. N. Ghosh, *J. Appl. Polym. Sci.* 128, 3726 (**2013**).

**386.** E. F. Kneller and R. Hawig, *IEEE Trans. Magn.* 27, 3588 (**1991**).

**387.** X. Shen, F. Song, J. Xiang, M. Liu, Y. Zhu and Y. Wang, *J. Am. Ceram. Soc.* 95, 3863 (**2012**).

**388.** S. Tyagi, H. B. Baskey, R. C. Agarwala, V. Agarwala and T. C. Shami, *Ceram. Int.* 37, 2631 (**2011**).

**389.** J. R. Liu, M. Itoh and K. Machida, *Appl. Phys. Lett.* 88, 062503 (**2006**).

**390.** N. Chen, G. Mu, X. Pan, K. Gan and M. Gu, *Mater. Sci. Eng. B.* 139, 256 (**2007**).

**391.** T. Maeda, S. Sugimoto, T. Kagotani, N. Tezuka K. Inomata, *J. Magn. Magn. Mater.* 281, 195 (**2004**).

**392.** R. W. Gao, W. C. Feng, H. Q. Liu, B. Wang, W. Chen and G. B. Han, *J. Appl. Phys.* 94, 664 (**2003**).

**393.** M. Zong, Y. Huang,Y. Zhao, X. Sun, C. Qu, D. Luo and Jiangbo, *RSC Adv.* 3, 23638 (**2013**).

**394.** Y. Sun, F. Xiao, X. Liu, C. Feng and C. Jin, *RSC Adv.* 3, 22554 (**2013**).

**395.** S. Hazra and N.N. Ghosh, *J. Nanosci Nanotechnol.* 14, 1983 (**2014**).

**396.** R. S. Meena, S. Bhattachrya and R. Chatterjee, *Mater. Des.* 31, 3220 (**2010**).

**397.** R. S. Meena, S. Bhattachrya and R. Chatterjee, *Mater. Sci. Eng., B.* 171, 133 (**2010**).

**398.** R. S. Meena, S. Bhattachrya and R. Chatterjee, *J. Magn. Magn. Mater.* 322, 1923 (**2010**).

**399.** R. Ji, C. Cao, Z. Chen, H. Zhai and J. Bai, *J. Mater. Chem. C.* 2, 5944 (**2014**).

**400.** R. Valenzuela, S. Ammar, F. Herbst, R. Ortega-Zempoalteca, *Nanosci. Nanotechnol. Lett.* 3, 598 (**2011**).

**401.** X. P. Shao, B. Dai, X. W. Zhang and Y. J. Ma, *J. Nanosci. Nanotechnol.* 12, 1122 (**2012**).

**402.** H. Liu, X. Meng, X. Yang, M. Jing, X. Shen and M. Dong, *J. Nanosci. Nanotechnol.* 14, 2878 (**2014**).

**403.** X. Yang, M. Jing, X. Shen, X. Meng, M. Dong, D. Huang and Y. Wang, *J. Nanosci. Nanotechnol.* 14, 2419 (**2014**).

**404.** S. Choopani, N. Keyhan, A. Ghasemi, A. Sharbati and R. S. Alam, *Mater. Chem. Phys.* 113, 717 (**2009**).

**405.** M. Asgharia, A. Ghasemi, E. Paimozd and A. Morisako, *Mater. Chem. Phys.* 143, 161 (**2013**).

**406.** L. G. Yan, J. B. Wang, X. H. Han, Y. Ren, Q. F. Liu and F. S. Li, *Nanotechnology* 21, 095708 (**2010**).

**407.** R. C. Pullar, J. D. Breeze and N. M. Alford, *J. Am. Ceram.Soc.* 88, 2466 (**2005**).

**408.** X. H. Guo, Y. H. Deng, D. Gu, R. C. Che and D. Y. Zhao, *J. Mater. Chem.* 19, 6706 (**2009**).

**409.** X. L. Dong, X. F. Zhang, H. Huang and F. Zuo, *Appl. Phys. Lett.* 92, 013127 (**2008**).

**410.** W. L. Song, M. S. Cao, Z. L. Hou, J. Yuan and X. Y. Fang, *Scripta Mater.* 61, 201 (**2009**).

**411.** P. Bhattacharya, S. Dhibar and C. K. Das, *Polym-Plast Technol.* 52, 892 (**2013**).

**412.** Q. Ling, J. Sun, Q. Zhao and Q. Zhou, *Polym-Plast Technol.* 49, 481 (**2010**).

**413.** V. Gupta, M. K. Patra, A. Shukla, L. Saini, S. Songara, R. Jani, S. R. Vadera and N. Kumar, *J. Nanopart. Res.* 14, 1271 (**2012**).

**414.** H. Targhagh and R. Fazaeli, *Nanosci. Nanotechnol. Lett.* 6, 295 (**2014**).

**415.** G. Hatui and C. K. Das, *J. Nanosci. Nanotechnol.* 12, 8034 (**2012**).

**416.** X. Gui, K. Wang, A. Cao, J. Wei, R. Lv, F. Kang, Q. Shu, Y. Jia and D. Wu, *J. Nanosci. Nanotechnol.* 10, 1808 (**2010**).

**417.** G. Ma, B. Hao, L. Li, K. Chen, Y. He, R. Qiao, J. Li and Y. Ding, *Sci. Adv. Mater.* 6, 298 (**2014**).

**418.** H. Chen, J. Liu, J. Zhang and R. Che, *Nanosci. Nanotechnol. Lett.* 5, 191 (**2013**).

**419.** S. Deka, P. A. Joy and A. P.Kumar, *Sci. Adv. Mater.* 1, 262 (**2009**).

**420.** V. Gupta, M. K. Patra, A. Shukla, L. Saini, S. Songara, R. Jani, S. R. Vadera and N. Kumar, *Sci. Adv. Mater.* 6, 1196 (**2014**).

**421.** S. B. Narang, C. Singh, Y. Bai and I. S. Hudiara, *Mater. Chem. Phys.* 111, 225 (**2008**).

**422.** P. Bhattacharya, S. Dhibar, G. Hatui, A. Mandal, T. Das and C. K. Das, *RSC Adv.* 4, 17039 (**2014**).

**423.** A. Ghasemi, A. Hossienpour, A. Morisako, A. Saatchi and M. Salehi, *J. Magn. Magn. Mater.* 302, 429 (**2006**).

**424.** A. Ghasemi, A. Hossienpour, A. Morisako, X. X. Liu and A. Ashrafizadeh, *Mater. Des.* 29, 112 (**2008**).

**425.** D. Goll, M. Seeger and H. Kronmuller, *J. Magn. Magn. Mater.* 185, 49 (**1998**).

**426.** H. W. Kwon, I. C. Jeong, A. S. Kim, D. H. Kim, S. Namkung, T. S. Jang and D. H. Lee, *J .Magn. Magn. Mater.* 304, e219 (**2006**).

**427.** J. S. Jiang, J. E. Pearson, Z. Y. Liu, B. Kabius, S. Trasobares, D. J. Miller, S. D. Bader, D. R. Lee, D. Haskel, G. Srajer and J. P. Liu, *J. Appl. Phys.* 97, 10K311 (**2005**).

**428.** J. P. Liu, Y. Liu, R Skomaski and D. J. Sellmyer, *J. Appl. Phys.* 85, 4812 (**1999**).

**429.** C. Sudakar, G. N. Subbanna and T. R. N. Kutty, *J. Appl. Phys.* 94, 6030 (**2003**).

**430.** M. Pal, S. Bid, S. K. Pradhan, B. K. Nath, D. Das and D. Chakravorty, *J. Magn. Magn. Mater.* 269, 42 (**2004**).

**431.** F. Song, X. Shen, M. Liu and J. Xiang, *J. Colloid. Interf. Sci.* 354, 413 (**2011**).

**432.** D. Roy and P. S. A. Kumar, *J. Appl. Phys.* 106, 073902 (**2009**).

**433.** D. Roy, C. Shivakumara and P. S. A. Kumar, *J. Magn. Magn .Mater.* 321, L11 (**2009**).

**434.** K. W. Moon, S. G. Cho, Y. H. Choa, K. H. Kim and J. Kim, *Phys. Stat. Sol. (a).* 204, 4141 (**2007**).

**435.** T. Xie, L. Xu and C. Liu, *RSC Adv.* 3, 15856 (**2013**).

**436.** N. Yoshiyuoi and S. Kunihiro, *IEEE Trans Microwave Eng Theory Technol.* 19, 65 (**1971**).

**437.** B. D. Cullity, *Elements of X-ray Diffraction*, Addison-Wesley, New York (**1978**).

**438.** R. N. Das, A. Pathak and P. Pramanik, *J. Am. Ceram. Soc.* 81, 3357 (**1998**).

**439.** S. M. A. Radmanesh and S. A. S. Ebrahimi, *J. Supercond. Nov. Magn.* 26, 2411 (**2013**).

**440.** A. Xia, S. Ren, C. Zuo, L. Zhang, M. Xie, Y. Deng, R. Wu, W. Xu, C. Jin and X. Liu, *RSC Adv.* 4, 18885 (**2014**).

**441.** S. Hazra, B. K. Ghosh, M. K. Patra, R. K. Jani, S. R. Vadera and N. N. Ghosh, *J. Nanosci. Nanotechnol.* (Accepted for publication) (doi:10.1166/jnn.2015.10491) (**2014**).

**442.** S. Hazra, B. K. Ghosh, M. K. Patra, R. K. Jani, S. R. Vadera and N. N. Ghosh, *Powder Technol.* (Revised manuscript submitted, Manuscript Id: POWTEC-D-14-01004R1) (**2014**).

**443.** S. Hazra, B. K. Ghosh, H. R. Joshi, M. K. Patra, R. K. Jani, S. R. Vadera and N. N. Ghosh**,** Microwave absorption and Magnetic properties of $(SrFe_{12}O_{19})_{1-x}$-$(Ni_{0.65}Zn_{0.35}Fe_2O_4)_x$ nanocomposites prepared by a Novel One-pot Synthetic Method, (**Manuscript under preparation**).

**444.** S. Hazra, B. K. Ghosh, H. R. Joshi, M. K. Patra, R. K. Jani, S. R. Vadera and N. N. Ghosh**,** *RSC. Adv.* 4, 45715 (**2014**).

**445.** S. Hazra, B. K. Ghosh, M. K. Patra, R. K. Jani, S. R. Vadera and N. N. Ghosh, A Novel 'One-Pot' Synthetic Methodology for preparation of $(SrFe_{12}O_{19})_{1-x}$-$(Mn_{0.2}Ni_{0.4}Zn_{0.4}Fe_2O_4)_x$ nanocomposites and their Microwave absorption and Magnetic properties, (**Manuscript under preparation**).

## List of Publications:

**International Journals:**

1. S. Hazra, M. K. Patra, S. R. Vadera and N. N. Ghosh, A novel but simple 'one-pot' synthetic route for preparation of $(NiFe_2O_4)_x$-$(BaFe_{12}O_{19})_{1-x}$ nanocomposites, *Journal of the American Ceramic Society* 95, 60-63 (2012).

2. S. Hazra and N.N. Ghosh, Preparation of Nanoferrites and Their Applications, *Journal of Nanoscience and Nanotechnology* 14, 1983-2000 (2014).

3. S. Hazra, B. K. Ghosh, H. R. Joshi, M. K. Patra, R. K. Jani, S. R. Vadera and N. N. Ghosh, Development of a Novel 'One-Pot' Synthetic Method for Preparation of $(Mn_{0.2}Ni_{0.4}Zn_{0.4}Fe_2O_4)_x$-$(BaFe_{12}O_{19})_{1-x}$ nanocomposites and Study of their Microwave Absorption and Magnetic Properties, *RSC Advances* 4, 45715-45725 (2014).

4. S. Hazra, B. K. Ghosh, M. K. Patra, R. K. Jani, S. R. Vadera and N. N. Ghosh, 'One-Pot' Synthetic Method for preparation of $(NiFe_2O_4)_x$-$(SrFe_{12}O_{19})_{1-x}$ nanocomposites and their Microwave absorption properties, *Journal of Nanoscience and Nanotechnology* (Accepted) (doi:10.1166/jnn.2015.10491) (2014).

5. S. Hazra, B. K. Ghosh, M. K. Patra, R. K. Jani, S. R. Vadera and N. N. Ghosh, A Novel 'One-Pot' Synthetic Method for Preparation of $(Ni_{0.65}Zn_{0.35}Fe_2O_4)_x$-$(BaFe_{12}O_{19})_{1-x}$ nanocomposites and Study of their Microwave absorption and Magnetic properties, *Powder Technology.* (Revised manuscript submitted, Manuscript Id: POWTEC-D-14-01004R1) (2014).

6. S. Hazra, B. K. Ghosh, H. R. Joshi, M. K. Patra, R. K. Jani, S. R. Vadera and N. N. Ghosh, Microwave absorption and Magnetic properties of $(SrFe_{12}O_{19})_{1-x}$-$(Ni_{0.65}Zn_{0.35}Fe_2O_4)_x$ nanocomposites prepared by a Novel One-pot Synthetic Method, (Manuscript under preparation).

7. S. Hazra, B. K. Ghosh, M. K. Patra, R. K. Jani, S. R. Vadera and N. N. Ghosh, A Novel 'One-Pot' Synthetic Methodology for preparation of $(SrFe_{12}O_{19})_{1-x}$-$(Mn_{0.2}Ni_{0.4}Zn_{0.4}Fe_2O_4)_x$ nanocomposites and their Microwave absorption and Magnetic properties, (Manuscript under preparation).

8. S. Hazra, M. K. Patra, S. R. Vadera and N. N. Ghosh, Preparation of $Mn_{0.2}Ni_xZn_{(0.8-x)}Fe_2O_4$ nanopowders by using a novel EDTA precursor method and their microstructute,

DC resistivity and magnetic properties, *Optoelectronics and Advanced Materials – Rapid Communications* 6, 451- 455 (2012).

9. A.Rajput, S. Hazra and N. N. Ghosh, Synthesis and characterization of pure single-phase CoFe$_2$O$_4$ nanopowder via a simple aqueous solution based EDTA-precursor route, *The Journal of Experimental Nanoscience* 8, 629-639 (2013).

10. A. B. Rajput, S. Hazra, N. B. Krishna, P. Chavali, S. Datla and N. N. Ghosh, Preparation of NiFe$_2$O$_4$ nanopowder via EDTA precursor and study of its properties, *Particuology* 10, 29-34 (2012).

11. A. B. Rajput, S. Hazra, G. F. Fernando and N. N. Ghosh, Synthesis of single-phase barium hexaferrite nanopowder via a novel EDTA- precursor based route and its DC resistivity and magnetic property, *Synthesis and Reactivity in Inorganic, Metal-Organic, and Nano-Metal Chemistry* 41, 1114-1121 (2011).

12. B. K. Ghosh, S. Hazra, B. Naik and N. N. Ghosh**,** Preparation of Ru nanocatalysts supported on SBA-15 and their Excellent Catalytic Activity towards Decolorization of Various Dyes, *Journal of Nanoscience and Nanotechnology* (Accepted) (2014).

13. B. K. Ghosh, S. Hazra, B. Naik and N. N. Ghosh, Preparation of Cu nanoparticle loaded SBA-15 and their Excellent Catalytic Activity in Reduction of Variety of Dyes, *Powder Technology* (Accepted) (2014).

14. B. Sarma, D. Dhar Purkayastha, S. Hazra, L. Gogoi, C. R. Bhattacharjee, N. N. Ghosh and J. Rout, Biosynthesis of fluorescent gold nanoparticles using an edible freshwater red alga, Lemanea fluviatilis (L.) C.Ag. and antioxidant activity of biomatrix loaded nanoparticles, *Bioprocess and Biosystems Engineering* (Accepted, DOI 10.1007/s00449-014-1233-2) (2014).

15. S. Hazra, S. Balaji, M. Banerjee, A. Ganguly, .N. N. Ghosh**,** A. Chatterjee, A PEGylated-Rhodamine based sensor for "turn-on" fluorimetric and colorimetric detection of Hg$^{2+}$ ions in aqueous media, *Analytical Methods* 6, 3784-3790 (2014).

16. B. Sarma, D. Dhar Purkayastha, S. Hazra, L. Gogoi, C. R. Bhattacharjee, N. N. Ghosh and J. Rout, Biosynthesis of gold nanoparticles using a freshwater green alga, Prasiola crispa, *Materials Letters* 116, 94-97 (2014).

17. B. Naik, S. Hazra, P. Muktesh, V. S. Prasad and N. N. Ghosh, A Facile Method for Preparation of Ag Nanoparticle Loaded MCM-41 and Study of its Catalytic Activity for Reduction of 4- Nitrophenol *Science of Advanced Materials, A Special Issue on*

*"Advanced Materials for Catalytic Applications"* 3, 1025-1030 (2011).

18. B. Naik, S. Hazra, V. S. Prasad and N. N. Ghosh, Synthesis of Ag nanoparticles within the pores of SBA-15: an efficient catalyst for reduction of 4-nitrophenol, *Catalysis Communications* 12, 1104-1108 (2011).

**Conferences:**

1. B. Naik, S. Hazra, and N. N. Ghosh, "Synthesis of Ag/TiO2 Nanoparticle Loaded Mesoporous $SiO_2$ and $Al_2O_3$ Catalysts and Study of their Catalytic Properties" The Sixth *International Symposium on Nanoporous Materials*, Banff, Canada, August 21-24, 2011.

2. A. B. Rajput, S.Choudhury, S.Hazra and N. N. Ghosh "Preparation and Characterization of Pure Single-Phase $ZnFe_2O_4$ Nanopowder via a Simple Aqueous Solution Based EDTA-Precursor Method" In *International Conference on Emerging Technologies: Micro to Nano 2013 (ETMN-2013)* February 23-24, 2013, BITS Pilani, K. K. Birla Goa Campus, India,

3. N. N. Ghosh, A. B.Rajput, S.Hazra, P. M.Singru, S. R.Vadera, M. K.Patra and H. V. Pol "Preparation, characterization and properties of flexible magnetic nanocomposite sheets of MNPs-polybenzoxazine-LLDPE". In *International Conference on Emerging Technologies: Micro to Nano 2013 (ETMN-2013)*. February 23-24, 2013, BITS Pilani, K. K. Birla Goa Campus, India,

4. S. Hazra, M. K. Patra, S. R. Vadera and N. N. Ghosh[*] "A Novel Aqueous Solution Based 'One-Pot' Synthetic Route for Preparation of Soft-Hard Ferrite Nanocomposites Having High Saturation Magnetization and High Coercivity Value" *International Union of Materials Research Societies – International Conference in Asia – 2013 (IUMRS-ICA-2013)* during December 16-20, 2013 at INDIAN INSTITUTE OF SCIENCE in Bangalore, India.

5. N. N. Ghosh, A. B. Rajput, S. Hazra, S. R. Vadera, M. K. Patra and H. V. Pol "Preparation of Flexible Magnetic Nanocomposite Sheets Composed of Magnetic Nanoparticles- Polybenzoxazine –LLDPE" *International Union of Materials Research Societies – International Conference in Asia – 2013 (IUMRS-ICA-2013)* during December 16-20, 2013at INDIAN INSTITUTE OF SCIENCE in Bangalore, India.

6. S. Hazra, B. K. Ghosh, M. K. Patra, R. K. Jani, S. R. Vadera and N. N. Ghosh "A novel

aqueous solution based 'one-pot' synthetic route for preparation of hard-soft ferrite nanocomposites having enhance magnetic and microwace absorption property" *INDO- UK INTERNATIONAL WORKSHOP ON ADVANCED MATERIALS AND THEIR APPLICATIONS IN NANOTECHNOLOGY (AMAN 2014)* BITS Pilani, KK Birla Goa campus May 17- 19th 2014 Page no: 151

7. B. K. Ghosh, S. Hazra, B. Naik and N. N. Ghosh "Preparation of Cu nanoparticle loaded SBA-15 and their Excellent Catalytic Activity in Reduction of Variety of Dyes" *INDO- UK INTERNATIONAL WORKSHOP ON ADVANCED MATERIALS AND THEIR APPLICATIONS IN NANOTECHNOLOGY (AMAN 2014)* BITS Pilani, KK Birla Goa campus May 17- 19th 2014 Page no: 154

8. S. Hazra, H. Joshi, A. Ahuja, B. K. Ghosh and N. N. Ghosh "Development of a simple aqueous solution based chemical method for synthesis of mesoporous $TiO_2$." *INDO- UK INTERNATIONAL WORKSHOP ON ADVANCED MATERIALS AND THEIR APPLICATIONS IN NANOTECHNOLOGY (AMAN 2014)* BITS Pilani, KK Birla Goa campus May 17- 19th 2014 Page no: 157

9. D. Dhar Purkayastha, S. Kairi, S. Hazra, N. N. Ghosh and C. R. Bhattacharjee "Surfactant-assisted low-temperature thermal decomposition of copper(II) acetylacetonate as an access to copper nanoparticles" *INDO- UK INTERNATIONAL WORKSHOP ON ADVANCED MATERIALS AND THEIR APPLICATIONS IN NANOTECHNOLOGY (AMAN 2014)* BITS Pilani, KK Birla Goa campus May 17- 19th 2014 Page no: 149

# BIO-DATA OF CANDIDATE

**Personal details:**

| | |
|---|---|
| **Name** | Subhenjit Hazra |
| **Date of Birth** | 12-08-1985 |
| **Education** | M.Sc. (Organic Chemistry) |
| | Assam University, Silchar (2009). |
| | B.Sc. (Chemistry) |
| | Syamsundar Collage, University of Burdwan, (2007). |
| **Email** | hazra.sj2009@gmail.com |

**Scholarships and Awards:**

1. Junior Research Fellowship, from the "Defence Research & Development Organisation" (DRDO), May 2010-April 2012.
2. Senior Research Fellowship, from the "Defence Research & Development Organisation" (DRDO), April 2012-March 2013.
3. Senior Research Fellowship, from the "Council of Scientific and Industrial Research" (CSIR), April 2013-till date.

**Publications during Ph.D Programme:**

Listed in Appendix I.

## BIO-DATA OF SUPERVISOR

| | |
|---|---|
| **Name** | Dr. Narendra Nath Ghosh |
| **Current Position** | Associate Professor |
| | Department of Chemistry |
| | Birla Institute of Technology and |
| | Science-Pilani, K. K. Birla, Goa Campus |
| | City: Zuarinagar, State: Goa-403726, India. |
| **Date of Birth**: | 01-01-1970 |
| **Education** | Ph. D. (Chemistry): IIT-Kharagpur (1999). |
| | M Sc (Chemistry): 1$^{st}$ Class-IIT-Kharagpur (1994). |
| **Areas of Research** | (i) Nonmaterial's (Chemical Synthesis Methodologies, Characterizations and Applications in Catalysis, Sensors, separations etc). |
| | (ii) Mesoporous Materials (particularly catalysts). |
| | (iii) Nanocomposite (polymer-fiber, polymer-ceramic), polymer (polybenzoxazine, epoxy). |

**No. of Sponsored Research Projects**

**(i) As PI:** 09 (DST-UKIERI, DRDO, DST, BRNS)

**(ii) As Co-PI:** 04

**No. of International journal Publications** 62

**No. of International conference proceedings** 14

**No. of Invited Book Chapter** 5

**No. of Invited Talks** 11

**Honors/Awards/Recognition**

1. Visiting Scientist Fellowship Award by "The Scientific and Technological Research Council of Turkey (TUBITAK)" 2006, 2009.

2. Member Expert in Chemistry for selection of candidates for Commonwealth Scholarship., UK Nominated by Ministry of Human Resource Development, Government of India.

3. Best Poster paper award "A Simple Chemical Technique for Synthesis of High Surface Area Mesoporous Silica Matrix and Iron-Oxide Incorporated Silicates" International Congress of Environmental Research (ICER 08) 2008.

4. Invited as Chairperson (for NANO-O9 and NANO-11 Sessions) in the 16th International Conference on Composites or Nano Engineering, ICCE-16, July 20-26, 2008 in Kunming, China.

5. Travel Grant Awards received from Indian National Science Academy, New Delhi, BITS- Pilani, Rajasthan, CSIR New Delhi, DST New Delhi. Appendix III.

6. Outstanding Scientist of 21st Century medal: Cambridge UK 2005.

7. Honorary appointment to the Research Board of Advisors of "The American Biographical Institute", USA. 2003.

8. Eminent Scientists of Today Medal by International Biographical Center Cambridge, U.K, 2002.

9. Biography has published in several Who's Who in Science and Engineering from USA, UK.

10. The Royal Academy Of Engineering for Research Exchanges with China And India-Short Award for 2010.

11. Receives a prestigious research grant under the DST UKIERI Thematic Partnership Scheme.

**Reviewer of International Journals**:

Thin Solid Films, Materials research Society, USA, Journal of the American Ceramic Society, Macromolecular Symposia, Journal of Surface Coating and Technology, Powder Technology, Journal of Microporous and Mesoporous Materials, International Journal of the Physical Sciences, Journal of Experimental nanoscience, Catalysis communications, Journal of Magnetism and Magnetic materials, Journal of Electroceramics, Composite Interface, Synthesis and Reactivity in Inorganic, Metal-Organic, and Nano-Metal Chemistry, Journal of applied Polymer Science, Matreials Chemistry and Physics etc.